



Finite element simulation of multi-layer repair welding and experimental investigation of the residual stress fields in steel welded components

Ardeshir Sarmast¹ · Jan Schubnell¹ · Majid Farajian²

Received: 1 June 2021 / Accepted: 21 February 2022 / Published online: 14 April 2022
© International Institute of Welding 2022

Abstract

In this work, the effect of multi-pass repair welding for removing a fatigue crack on the residual stress fields of GMA-welded S355J2+N and S960QL structural steel T-joints was investigated. Two scenarios were considered, a fatigue crack smaller than half of the plate thickness, and a fatigue crack larger than half of the plate thickness. Samples were first welded in a T-joint structure; then, cracks were created on their weld toes by cyclic loading; after that, the cracks were machined at one or two sides of the plate, depending on the crack length, and finally, the sample was repaired by two-pass welding on each machined area. Longitudinal and transverse residual stresses were measured by the X-ray diffraction method. A 2D thermo-metallurgical-mechanical finite element model was developed for each sample to estimate the residual stress fields through the weldments. The results show that, regardless of the alloy or repairing in one or two sides, the repair welding increases the magnitude of the residual stresses compared to the initial weld, but the alloys show different behaviors during the process. In S960QL samples, during repair welding of one weld toe, the residual stress evolutions in previously welded areas that are not subjected to the repair welding occur due to the morphological changes in the phases and expansions and contractions, while for S355J2N samples, the expansions and contractions are mainly responsible for these changes.

Keywords Repair welding · Residual stress · Structural steel · Thermo-metallurgical-mechanical simulation · Finite element method

1 Introduction

Repair welding is widely used in various industries to either remove imperfections or increase the endurance of welded components when they reach their final service life. During arc repair welding processes, as the arc passes on the specimen, the material melts and solidifies. The transient thermal history of the weldment causes microstructural evolutions and thermal expansions and contractions [1]. These expansions and contractions during repair welding cause strains,

which lead to the formation of residual stress in the component. The resulting residual stress could be more detrimental than the welding residual stress, because of higher levels of constraint on the repair welded specimens [1, 2]. Song and Dong [3] stated that the dominance of residual stresses in repair welds is so high that the initial welding-induced residual stresses could be neglected during the repair welding simulation. Owing to the wide variety of welding processes, these residual stresses could be different in different components, even when the geometry is the same [4]. These residual stresses could be added to the pre-existing residual stresses in the material and also to the service loads and negatively affect its integrity and performance [5]. Therefore, understanding the residual stress evolutions during repair welding turned to be a key factor for an accurate, successful design. Several researchers have worked on the subject in recent years. For instance, Charkhi and Akbari [6] developed a three-dimensional finite element thermo-mechanical model to study the effect of pre-heating on the residual stress modification of repair welded A106-B carbon steel and S304

Recommended for publication by Commission XIII—Fatigue of Welded Components and Structures

✉ Majid Farajian
Farajian@slv-duisburg.de

¹ Fraunhofer Institute for Mechanics of Materials IWM,
Freiburg, Germany

² GSI Gesellschaft Für Schweißtechnik International mbH,
Duisburg, Germany

stainless steel pipes. They found the effect of preheating significant in controlling the residual stresses in the component. In another work, Elcoate et al. [7] investigated the effect of short and long multi-layer repair welding and also inter-pass temperature on the residual stress of a stainless steel pipe utilizing a thermo-mechanical model. They concluded that the inter-pass temperature has a dominant effect on the magnitude of the residual stresses. They also observed high magnitude tensile residual stress in the axial direction close to the welded area in short repair samples. Salerno et al. [8] validated a 3D FE model to predict the residual stress fields in a repair welded titanium plate. They highlighted that the interaction between the pre-existing residual stresses in the component and repair welding-induced residual stresses is still unclear. Jiang et al. [9] investigated the effect of repair welding depth on the longitudinal and transverse residual stress distribution in various sections of a 316L stainless steel component by neutron diffraction and finite element methods. They developed a 3D sequentially coupled thermo-mechanical model utilizing a double ellipsoid heat source and isotropic and kinematic strain hardening models. They concluded that, due to the increase in the number of repair passes, the deeper the repair welding is, the higher the residual stress in the specimen will be.

Despite the widespread application of the repair welding and its dominant effect on the lifetime of the component, the subject is barely investigated. Because of this reason and the complex nature of residual stresses during repair welding, the effect of repair welding on the residual stress redistribution through the welded components is not completely clear yet. The fact that the residual stresses in various weldments could be different depending on the welding process parameters such as welding current, voltage and speed, the alloy and molten material behavior, clamping method, and level makes the situation even more complicated [10]. One important case is the repair welding of the structural steels due to the fatigue crack formation. This happens, especially in the structures like cranes or bridges that reach their lifetime. Repair welding these structures could make higher levels of the residual stresses that could be added to the service loads and cause early failure of the structure, which in the case of bridges and cranes can cause irreparable damages.

Therefore, this study aims towards investigating the effect of repair welding on residual stress and distortion of steel

structures that are subjected to repair welding due to the formation of the fatigue cracks. In this regard, two commonly used structural steel, S355J2+N in normalized condition and quenched and tempered S960QL alloy, were welded in a T-joint structure by gas metal arc welding (GMAW) process. Two cases of fatigue crack formation were considered, one with the crack length smaller and another with the crack length larger than the plate thickness. Then depending on the crack length, the samples were repaired on one and two sides. X-Ray diffraction method was employed to measure the residual stresses through the components. Also, the cross-section of the weldments was observed under the optical microscope, and the hardness of the weld material and surrounding area was measured. To study the residual stress distribution in the whole sample and not only in one section, 2D finite element thermomechanical-mechanical models were also developed utilizing SYSWELD software to calculate the thermal contours, phase transformations, and residual stresses of the weldments. The models were validated with the experiments. JMatPro v10 software was deployed to develop the material model for the simulation. The material model also was calibrated with the tensile tests at room and elevated temperatures.

2 Experimental procedure

Two stiffeners with the dimensions of $170 \times 50 \times 10 \text{ mm}^3$ were welded in a T-joint structure on both sides of a plate with dimensions of $170 \times 370 \times 10 \text{ mm}^3$ by the gas metal arc welding (GMAW) process. Two different steel, one, structural steel S355J2+N in the normalized condition and the other, high strength quenched and tempered S960QL were deployed as the base material. Both the stiffener and plate were from the same material. G4Si1 filler material with 1.2-mm diameter was utilized for welding of S355J2+N samples, and X90-IG (Mn_2NiCrMo) wire with 1-mm diameter was used for S960QL samples, according to DIN EN 757. The chemical composition of the alloys and filler materials is presented in Table 1. The chemical composition of the base materials was measured by spectral analysis and the chemical composition of the filler materials was taken from the manufacturer datasheet. During welding of all samples, M21-ArC-18 was used as the shielding gas with a flow rate of 15–18 l/min to protect the hot area from reacting with the air. S960QL samples are susceptible

Table 1 Chemical composition of the alloys and filler metals

Material	C	Al	Cr	Cu	Mn	Mo	Nb	Ni	Si	Ti	V	P	S	Fe
S355J2+N	0.16	0.032	0.04	0.015	1.46	0.007	0.014	0.035	0.168	0.0123	0.008	0.0106	0.0051	Bal
G4Si1	0.08	0	0	0	1.65	0	0	0	1	0	0	0	0	Bal
S960QL	0.156	0.057	0.196	0.013	1.24	0.608	0.013	0.083	0.206	0.0003	0.0465	0.0096	0.0018	Bal
X90-IG	0.1	0	0.35	0	1.8	0.6	0	2.3	0.8	0	0	0	0	Bal

to hot cracking; therefore, they were locally preheated before welding to temperatures between 80 and 150°C, according to SEW088 guideline [11] by a flame torch. The hot cracking is not the case for the S355J2+N samples, and they were welded without preheating.

Two possible scenarios were considered for the fatigue crack formation. First, the crack length is lower than half of the plate thickness, which could be repaired by one side machining and repair welding. Second, the length of the crack is larger than half of the plate thickness. In this case, the material removal shall be performed by three fourth of the plate thickness from one side, repair welding on this side, and machining of the plate on the opposite side of the crack and repair welding. To create cracks with different sizes for the study, the specimens were loaded on a resonance-frequency machine RUMUL 150 K (Russenberger Prüfmaschinen AG, Neuhausen am Rheinfall, Switzerland). A sinusoidal 4-point bending load was imposed on the sample. To analyze the Δf , a-correlation for different load levels, a beach mark test was carried out utilizing four specimens. Shutdown criterion of $\Delta f = 0.2$ was used for crack generation on one-side repair samples ($a < t/2$), and $\Delta f = 1.2$ was used as the criterion for the double-side repair samples ($a > t/2$). Figure 1 shows

the setup used for the creation of the cracks. To be sure the crack only initiates on one weld, the other three welds were mechanically treated by high-frequency mechanical impact (HFMI). The samples were tested by penetrant testing (PT) and magnetic-particle testing (MT) to make sure the crack with the desired depth was created. More details about the NDT tests and fatigue crack removal from weldments can be found in another publication of ours [12].

After crack creation, they were removed by manual machining. PT and MT were utilized to be sure that the crack was completely removed. The GMAW process was also used for the repair welding. The lag time between welding and repairing of S960QL samples was selected as the temperature of samples was 100°C. Table 2 shows the welding parameters of initial and repair welding. For all welds, the quality class B according to DIN EN ISO 5817:2014–6 was reached. During the whole welding process, type K NiCr-Ni class 1 thermocouples with a wire diameter of 0.1 mm were employed, according to EN 60,584, to record the temperature history of the weldments. Figure 2 shows the location of the thermocouples and the sequence of the process. Five thermocouples were used in total for recording the temperature history of each sample with a 1-mm distance from one another (Fig. 3).

Fig. 1 Setup for the crack creation

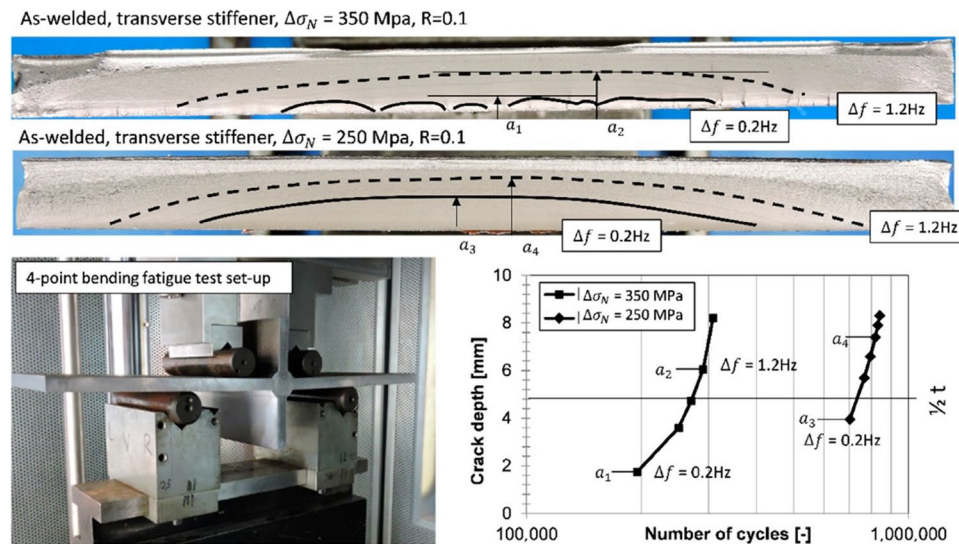


Table 2 Welding parameters

Sample	Current (A)	Voltage (V)	Speed (mm/s)	Heat input (J/mm)	Efficiency
S355J2+N — initial weld	247	29.4	6.65	1092.22	0.9
S355J2+N — repair, root pass	212	42	7.69	1157.52	0.6*
S355J2+N — repair, cover pass	222	42	6.45	1445.22	0.6
S960QL — initial weld	216	29.4	5	1270.08	0.7
S960QL — repair, root pass	215	42	7.69	1173.9	0.9
S960QL — repair, cover pass	220	42	5.56	1663.2	0.7

*For the double-side repair welded sample, the arc (thermal) efficiency of the root pass on the first side is considered to be 0.9

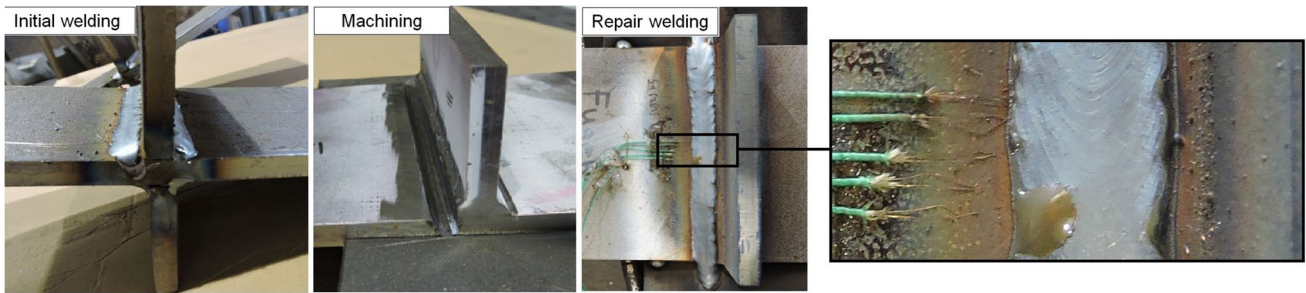


Fig. 2 The sequence of initial welding, machining and repair welding

To study the residual stresses, an X-ray diffraction instrument with a mobile diffractometer type XSTRESS G3 was deployed. The measurements were carried out from the weld toe through the base material in longitudinal and transverse directions by Cr-K α radiation at the ferritic (211) lattice plane. The penetration of the X-ray was around 5 μm . In the transverse direction, the stiffeners restricted the tilt angle of the diffractometer; thus, the measurements were done only in one tilt direction with 7 tilt angles, from 0 to 45°. In the longitudinal direction, which was free for the movement of the goniometer, 15 tilt angles were deployed to do the measurement, from -45 to 45°. Figure 4 shows the configuration of the diffractometer against the sample. The $\sin \psi^2$ -method [13] was used for the residual stress measurement, assuming an even residual stress state for the transverse direction. For the calculation of the residual stresses from the diffraction results, the elastic constants of $E=210$ GPa and $v=0.3$ were used, where E is Young's modulus, and v is Poisson's ratio.

3 Modeling

To calculate the thermal contours and the residual stress fields, six different two-dimensional thermo-metallurgical-mechanical models for initial weld and one-side and double-side repair welded S355J2+N and S960QL components were developed in the SYSWELD software. Due to the negligible effect of the mechanical stresses on the temperature fields and solid-state phase transformations [14], the thermal and metallurgical models were fully coupled to each other and sequentially coupled to the mechanical models.

3.1 Thermal modeling

To handle the thermal calculations, the conduction equation was used as the governing equation and convection and radiation were considered the boundary conditions [14]:

$$\rho C_p \frac{\partial T}{\partial t} = \nabla(k\nabla T) + Q \quad (1)$$

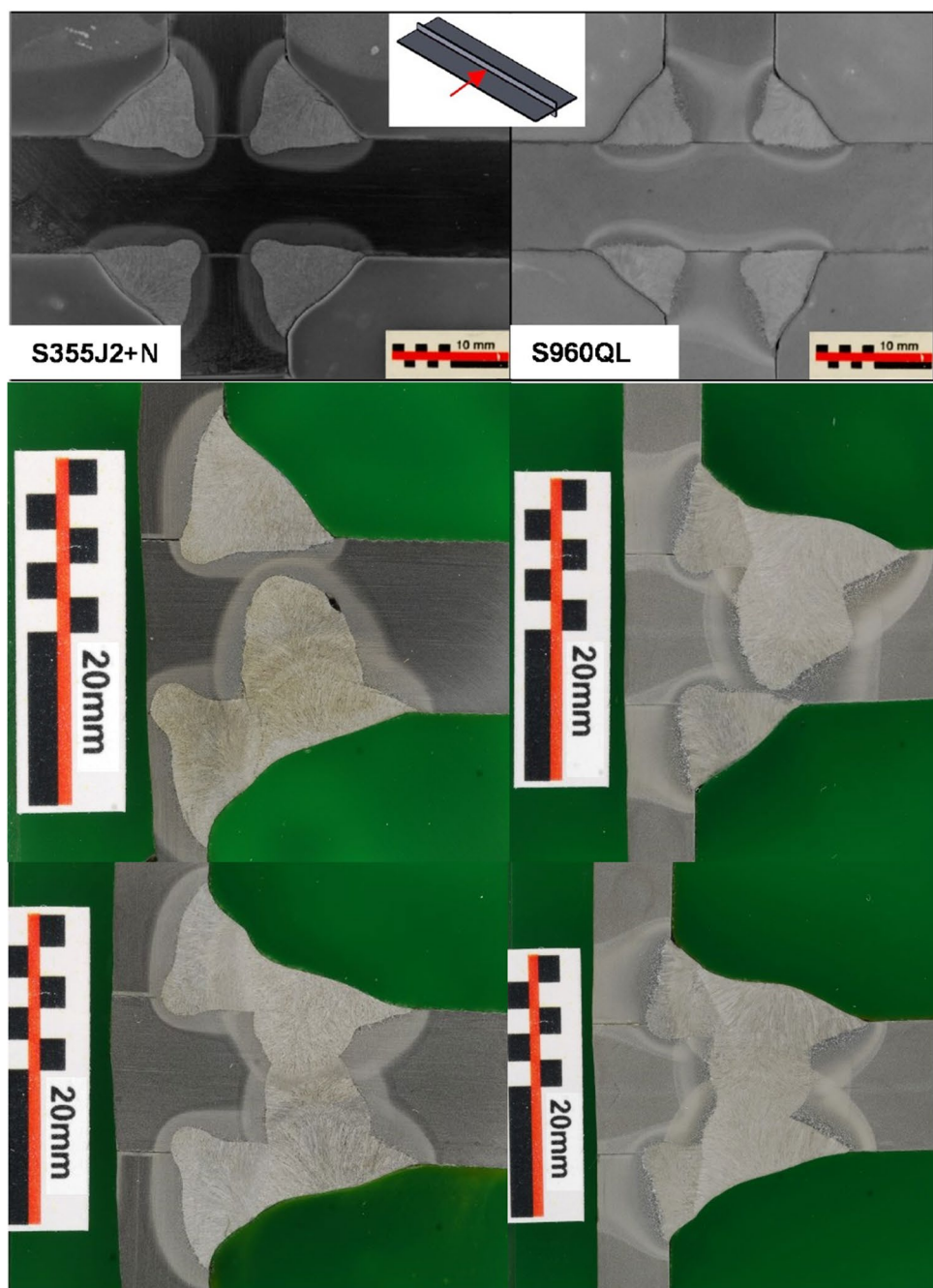
$$k \frac{\partial T}{\partial t} = -h(T - T_a) - \sigma \epsilon (T^4 - T_a^4) \quad (2)$$

where ρ is the density, C_p is the specific heat, T is the temperature, t is time, k is the thermal conductivity, Q represents the heat input from the heat source, h is the heat conduction coefficient, T_a is the ambient temperature, σ is Stefan-Boltzmann constant, and ϵ is the emissivity. To increase the accuracy of the calculations, the density, thermal conductivity, and specific heat of the alloys were considered to be temperature- and phase-dependent. Figure 5 shows the material properties used in the thermo-metallurgical-mechanical simulations. The properties of the base materials and filler metals of S960QL samples were modeled by the JMatPro-v10 software. SYSWELD database was used for the material properties of S355J2+N base material, and the relevant filler material properties were modeled by JMatPro v10. The calculated material properties were calibrated with the tensile tests on the base material at various temperatures. Due to the fluid flow characteristics of the weld pool, its thermal conductivity is significantly higher than that of the liquid material under quasi-static conditions [15]. To consider the stirring effects of the weld pool, the thermal conductivity of the liquid material was considered to be a characteristic of the welding process and assumed three times higher than that of the base material at room temperature. In all models, the emissivity and the heat transfer coefficient were taken as 0.3 and 8 W/m²K, respectively.

Another boundary condition of the thermal model is the heat input from the welding torch. According to the observed melt pool, the double ellipsoid equation developed by Goldak et al. [16] was deployed to simulate the imposed heat from the heat source. To estimate the weld pool shape and thermal history of the weldments more precisely, conical distribution along the weld pool depth was taken with double ellipsoid distribution on the surface.

$$q(x, y, z) = \frac{6\sqrt{3}f_f Q}{ab_f c\pi\sqrt{\pi}} \exp\left(\frac{-3x^2}{a^2} + \frac{-3[y + v(\tau - t)]^2}{b_f^2} + \frac{-3z^2}{c^2}\right) \quad (3)$$

Fig. 3 Residual stress measurement by XRD



$$q(x, y, z) = \frac{6\sqrt{3}f_r Q}{ab_r c \pi \sqrt{\pi}} \exp\left(-\frac{3x^2}{a^2} + \frac{-3[y + v(\tau - t)]^2}{b_r^2} + \frac{-3z^2}{c^2}\right) \quad (4)$$

In these equations, f_f and f_r are the heat fractions of the front and rear portions of the heat source; a , b_f , b_r , and c are the geometrical parameters of the double ellipsoid function; x , y , and z are the coordinates; τ is the lag factor; t is the time; Q represents the welding heat input which is defined as ηVI in arc welding processes, where η is the arc efficiency, V is the welding voltage, and I is the arc current. The arc

efficiency of an arc welding process depends on many factors such as the shielding gas, the current polarity, and the arc length [17, 18]. According to reported values for the arc efficiency of the GMAW process in literature [19–22], values shown in Table 2 were taken as the arc efficiency in the models. The geometrical parameters of the double ellipsoid equation, arc efficiency, convection coefficient, emissivity, and melt pool conductance were considered variables. The values of the variables were determined through the validation process of the thermal model with the temperature recorded by thermocouples and the melt pool dimensions.



Fig. 4 Residual stress measurement by XRD

3.2 Metallurgical modeling

Metallurgical models are responsible for the calculation of microstructural evolutions. Microstructural evolutions consist of grain growth, solidification, solid-state phase transformations, precipitation evolution, etc. [23]. In the employed alloys in this study, the controlling microstructural feature, which defines the mechanical properties of the specimen, is the solid-state phase transformation. The fraction of the final phases and their morphology define the final material properties that determine the performance of the product. Steel alloys undergo a series of diffusion-controlled and diffusionless transformations during the heating and cooling cycles of welding. Austenite is the key phase during the metallurgical simulation of steels. All phase transformations go toward or out of this phase. The equilibrium phase fraction of the austenite phase determines whether this phase forms or dissolves. During heating of the alloy, as the temperature rises, the

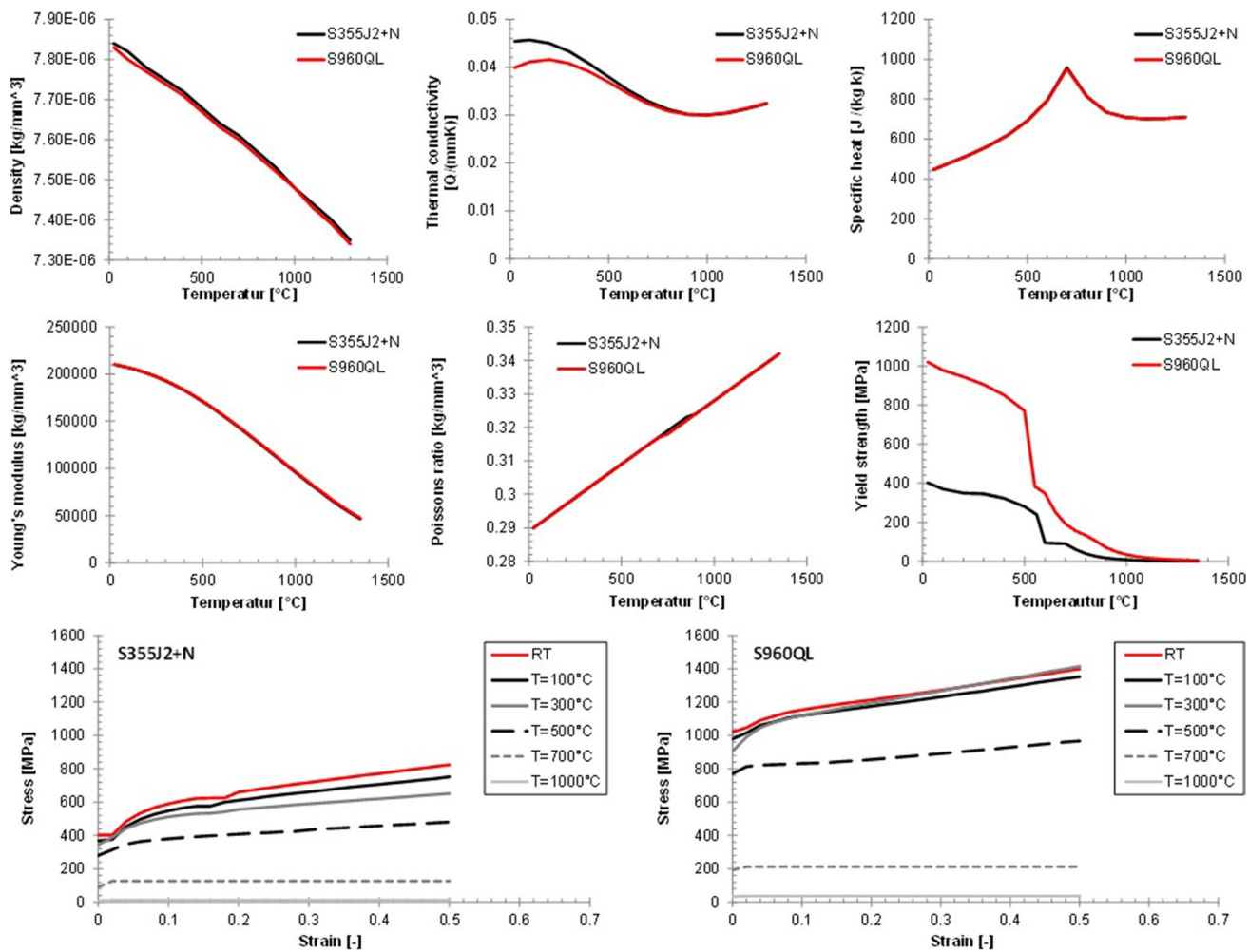


Fig. 5 Thermo-physical and mechanical properties of S355J2+N and S960QL alloys employed in the models

equilibrium austenite phase fraction gradually increases and pre-existing phases transform to the austenite. During the cooling, on the other hand, the equilibrium austenite phase fraction decreases by decreasing the temperature and depending on the cooling rate the austenite phase dissolves to ferrite (α), pearlite (P), bainite (B), martensite (M), or a combination of them. Figure 6 shows the flowchart of the phase transformation used in this study.

The formation of the austenite phase from all these phases is diffusion-controlled and so are the transformations of austenite to ferrite, pearlite, and bainite phases. The austenite to martensite transformation, however, is a diffusionless phenomenon. To estimate the diffusion-controlled phase formations, the equation developed by Leblond and Devaux [24] was utilized:

$$\dot{X} = \frac{X_{eq}(T) - X}{\tau(T)} \quad (5)$$

where X is the phase proportion, X_{eq} is the equilibrium phase proportion, τ represents the time after that X reaches 1, and T is the temperature. The equation contains two functions of the temperature, $X_{eq}(T)$ and $\tau(T)$. The former changes between 0 and 1 and the latter is always positive; otherwise, X would not tend towards X_{eq} . For the diffusionless austenite to martensite transformation, Koistinen-Marburger equation [25] was utilized:

$$X_M = (1 - \exp(-b_{KM}(T_{ms} - T)))X_\gamma \quad T < T_{ms} \quad (6)$$

where X_γ is the austenite phase proportion available at the start of the martensite transformation, T is the temperature to reach, T_{ms} is the martensite start temperature, and b_{KM} is a material-dependent coefficient.

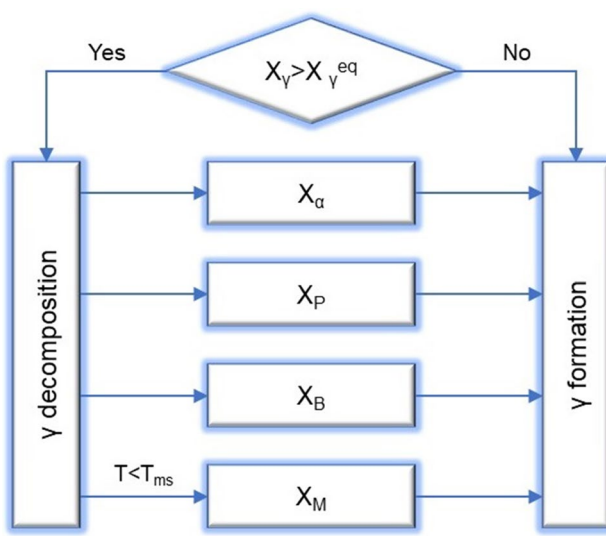


Fig. 6 Schematic of metallurgical simulation

The constant values of the abovementioned equations were extracted from the continuous cooling transformation (CCT) diagram of the alloys, which was calculated by JMatPro software (Version 10) based on the interpolation from the Thermtech Database [26]. The Austenitization temperature (AC3) and the initial grain size are the input of the calculation. The AC3 was estimated according to the empirical formulation proposed by Trzaska [27] based on the chemical composition of the base materials, given in Table 1. The average grain size was estimated according to ASTM E112 – 13 (2017) that was 20 μm for S355J2+N, and 9 μm for S960QL samples. Figure 7 shows the calculated CCT diagram of the alloys calculated by JMatPro compared to the data taken from ZTU-Atlas [28].

The parameters of Leblond and Koistinen-Marburger equations were also calibrated with the JMatPro software package. For S355J2+N alloy, the martensite start temperature was 420 °C, and b_{KM} was 0.01428. These values for the S960QL alloy were 404 °C and 0.0208, respectively. Leblond parameters were selected according to the CCT diagrams (Fig. 7).

3.3 Mechanical modeling

By having the thermal contours and phase proportions of the samples in hand, stress fields can be calculated. The principle of minimum potential energy on an elastic–plastic material can be used [29]:

$$\delta\pi = \int (d\sigma)^T \delta d\epsilon dV - \int (dF)^T \delta du fS = 0 \quad (7)$$

Here, $d\sigma$ and $d\epsilon$ are the vectors of the stress and strain increments, respectively; dF is the surface traction vector, and du is the displacement vector. Also, the constitutive equation was deployed during the mechanical simulation [30]:

$$\sigma = D\epsilon^e \quad (8)$$

where D is the stiffness matrix of the material. The strain vector in welding can be decomposed to several elements including elastic strain tensor (ϵ^e), plastic strain tensor (ϵ^p), thermal strain tensor (ϵ^{th}), visco-plastic strain tensor (ϵ^{vp}), creep strain tensor (ϵ^c), metallurgical strain tensor (ϵ^{tr}), and transformation plasticity strain tensor (ϵ^{tp}). In the mechanical simulation of welding, in addition to the elastic and thermal strain tensors, at least one plastic strain tensor must be considered to calculate the residual stress fields [31]. Because of the negligible effect of creep and visco-plastic strains during welding, they were removed from the total strain equation [32]:

$$\epsilon = \epsilon^e + \epsilon^p + \epsilon^{th} + \epsilon^{tr} + \epsilon^{tp} \quad (9)$$

Thermal and metallurgical strains are briefly known as thermal strain and were calculated by [33]:

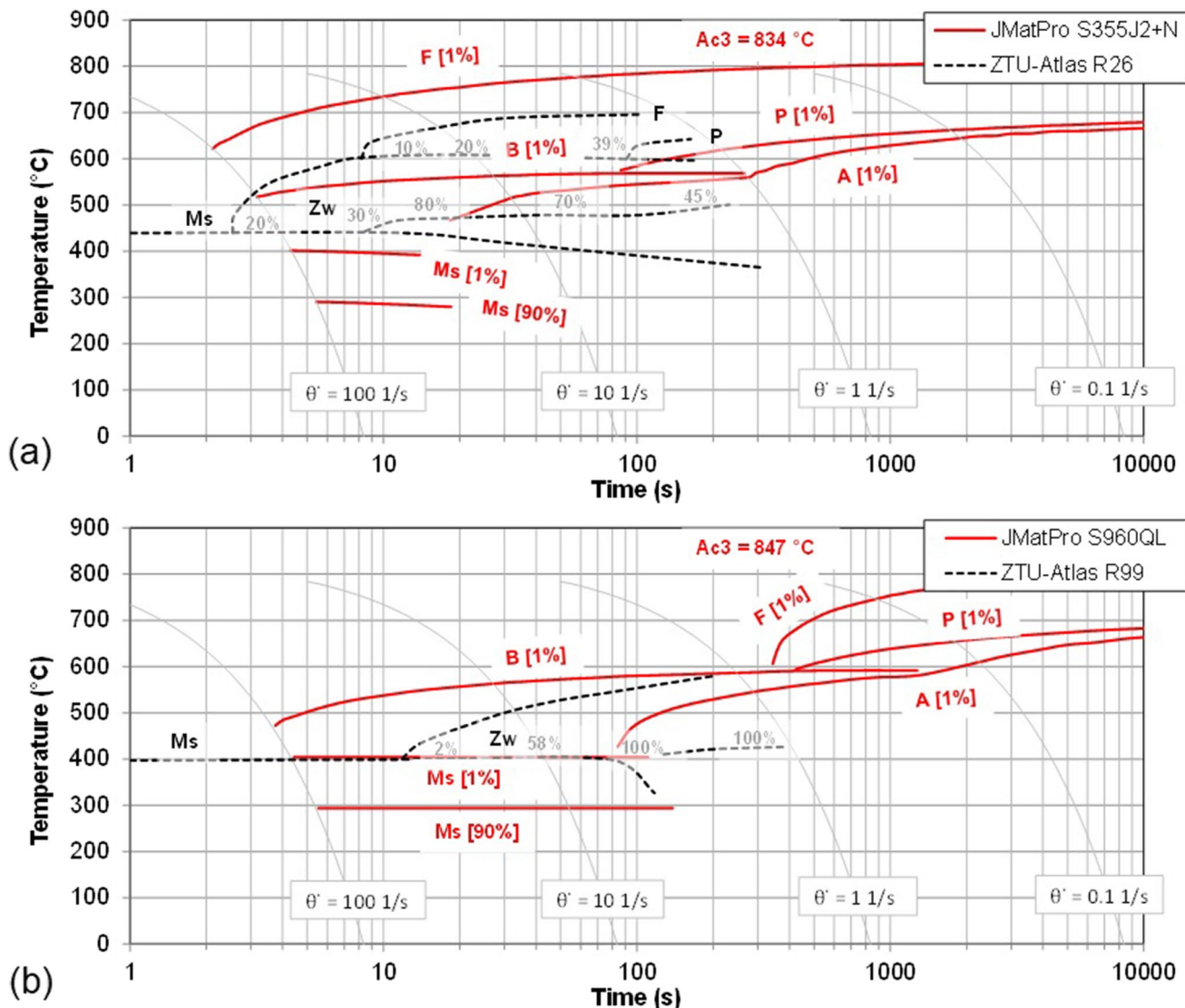


Fig. 7 CCT diagram of a S355J2+N and b S960QL sample calculated by JMatPro and reference values from ZTU-Atlas [28]

$$\varepsilon^{th} = \sum X_i \varepsilon_i^{th}(T) \quad (10)$$

where X_i is the fraction of phase i , and $\varepsilon_i^{th}(T)$ is the thermal strain of phase i at temperature T . The transformation plasticity strain was calculated by [33]:

$$\dot{\varepsilon}^{tp} = -\frac{3}{2} k \times h \left(\frac{\bar{\sigma}}{\sigma_y} \right) \times S \times \ln(x) \times \dot{x} \quad (11)$$

where k is the coefficient of the transformation plasticity, h is a non-linear function for the applied stress, x is the fraction of the hardener phase, S is the strain deviator, $\bar{\sigma}$ is the equivalent stress, and σ_y is the yield stress of the material.

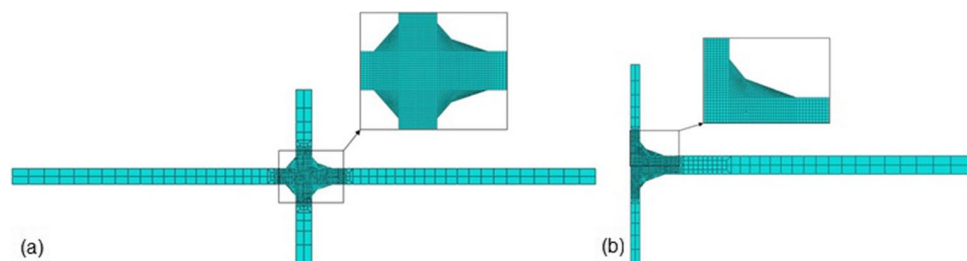
Since the welds on both sides of the stiffener in S960QL samples were deposited simultaneously, half of the sample was considered in the modeling. The implemented meshing

system for both thermo-metallurgical and mechanical models is presented in Fig. 8. Non-uniform meshing system was employed to reduce the calculation time. To make sure of the calculation accuracy, a mesh sensitivity analysis was carried out. Also, to consider machining and depositing of the filler material, the elements activation and deactivation method were implemented.

4 Results and discussion

Figure 9 shows the cross-section of the initial weld, one-side repair welded, and double-side repair welded S355J2+N samples, also the temperature history of a point on the surface in the HAZ 2-mm away from the weld toe during the initial welding and the complete thermal cycle of repair

Fig. 8 The meshing system used in thermo-metallurgical-mechanical model of a S355J2+N and b S960QL sample



welding of S355J2+N sample. Owing to the conical heat distribution in the weld pool depth, the predicted weld pool shape and dimensions are in good agreement with the measured values. As can be seen, the actual cooling rate of the weldment is lower than the estimated value. One reason is that during 2D modeling the heating of the sample in farther cross-sections due to welding is not being considered. The convection through the cooler material causes higher heat sinks which result in faster cooling of the specimen. The model was validated using the thermocouple measurements and weld pool dimensions of the base weld and then used for the simulation of the repair welds.

Figure 10 shows the measured and estimated cross-sections and also the temperature–time curve for initial welding and repair welding of the S960QL sample. In this sample, however, the modeled and measured cooling rates are almost the same. During the welding of S960QL alloy, the sample was preheated to 100°C locally at the weld location by a torch. While during the modeling of the process, the initial temperature of the whole sample was considered to be 100°C. It means that, in practice, there was a temperature gradient in the transverse direction of the sample, which

causes higher heat sinks in the weldments compared to the model. Considering this fact and the effect of neglecting the heating of the farther sections in 2D modeling, the estimated and measured values are closer to one another compared to the S355J2+N sample. It should be noted that, in the repair welding thermal history of both alloys, the side that temperature was measured is the second repair weld, and therefore, the last temperature peaks show the melting at the vicinity of the measurement area.

Fatigue crack usually initiates at the weld toe of a T-joint, therefore, this study focuses on the residual stress evolution at the weld toe of the weldments. To validate the mechanical models, estimated values were compared to the measured ones for the initial welding. Since only half of the tilt angles were used for the transverse residual stress measurement, only measured longitudinal residual stresses were used for the model validation. Figure 11 shows the distribution of the longitudinal residual stresses from 1.5 mm away from the weld toe to the base material of the initial welds. The predicted and measured residual stress profiles are almost the same, but there is a slight difference between their magnitudes. During the production of the specimens, samples

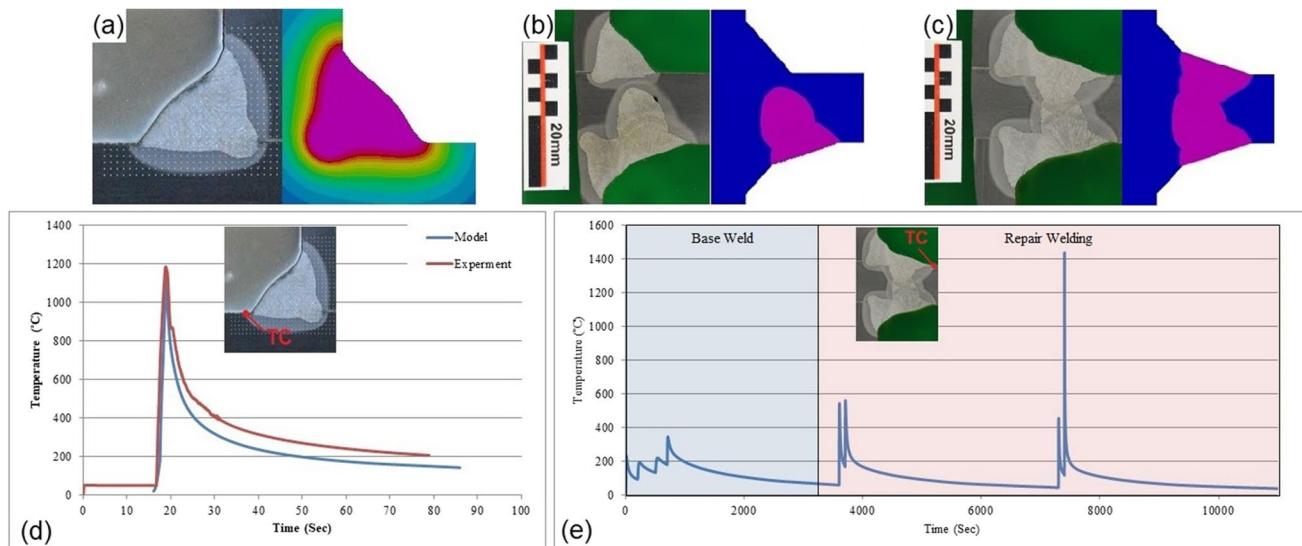


Fig. 9 a Weld pool cross-section of initial weld, b weld pool cross-section of one-side repair welded, c weld pool cross-section of double-side repair welded, d temperature history of the initial weld, and e temperature history of double-side repair welded of S355J2+N sample

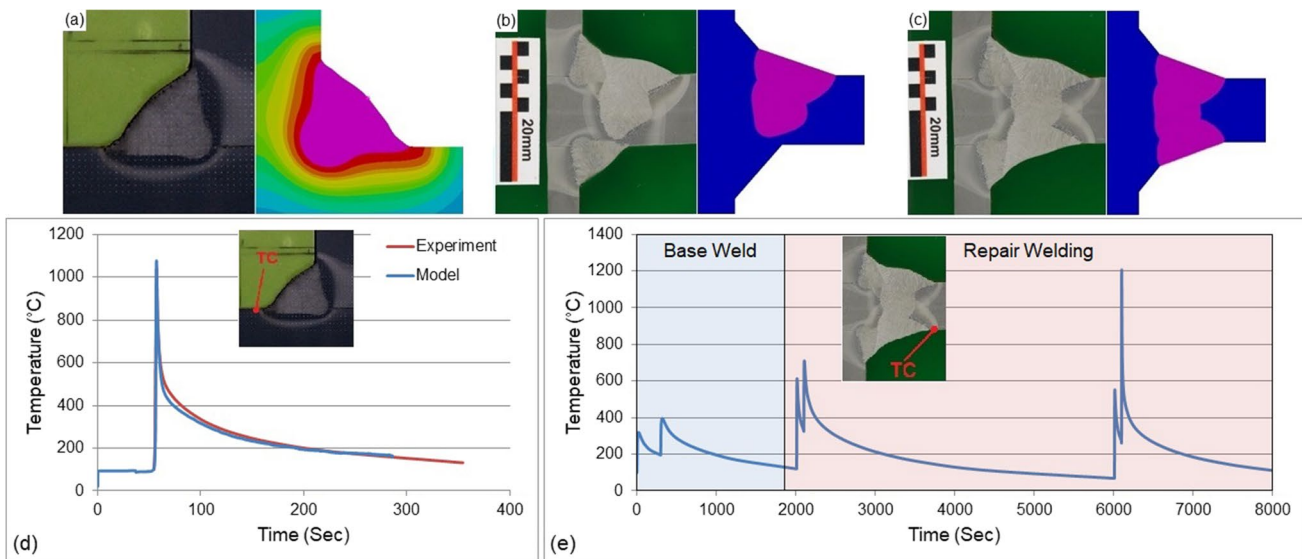


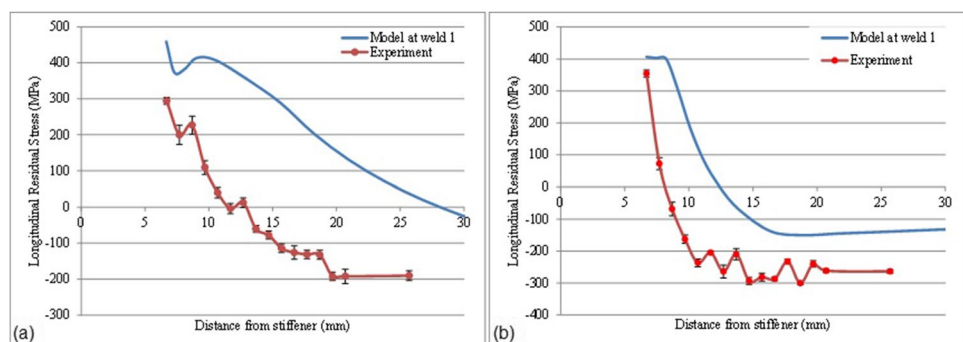
Fig. 10 **a** Weld pool cross-section of initial weld, **b** weld pool cross-section of one-side repair welded, **c** weld pool cross-section of double-side repair welded, **d** temperature history of the initial weld, and **e** temperature history of double-side repair welded S960QL sample

were blasted after welding. Blasting of the samples introduces compressive residual stresses on the surface of the specimens. As mentioned in the experimental procedure, the XRD measurement focuses on a few micrometers underneath the surface. Therefore, the actual residual stress of the as-welded samples should be higher than the measured values. As can be seen in this figure, despite the higher strength of the S960QL alloy, its weldments show a smaller area of tensile stresses. The thermal conductivities of the materials are very close, and the welding parameters of both samples are almost the same. This difference is the effect of the preheating of the S960QL sample. Due to preheating of S960QL weldments, the temperature gradient is smaller and lower levels of tensile stresses are observed.

Figure 12 illustrates the residual stress evolution through the whole sample during initial welding and repair welding of the S355J2 + N sample in longitudinal and transverse directions. The numbers show the sequence of welding. In the double-side repair welded sample, repair welding was first carried out in weld toe of weld 4 and

then weld 1. Residual stress in both directions significantly increased by repairing the components. At the weld toe of the initial weld, one-side repair weld, and double-side repair weld of S355J2 + N, the longitudinal residual stresses are 460 MPa, 586 MPa, and 719 MPa, respectively. The maximum transverse residual stresses on the surface of the initial weld, one-side repair welded, and double-side repair welded samples are 74 MPa, 389 MPa, and 324 MPa, respectively. Initial welding creates compressive transverse residual stress at all weld toes, while repair welding transforms it to the tensile residual stress. Although the longitudinal residual stress increases by proceeding with the repair welding, the transverse residual stress reduces a little after repair welding on two sides of the plate. To look at the evolution of residual stress of the alloy at the weld toe of each weld more precisely, Fig. 13 shows the residual stress distribution from the weld toe to the base metal of S355J2 + N. It is worth mentioning that the locations of the weld toe of weld 1 and 4 changes after repair welding and corresponding residual stresses were

Fig. 11 Numerical and experimental longitudinal residual stresses from 1.5 mm from the weld toe to the base material of **a** S355J2 + N and **b** S960QL sample



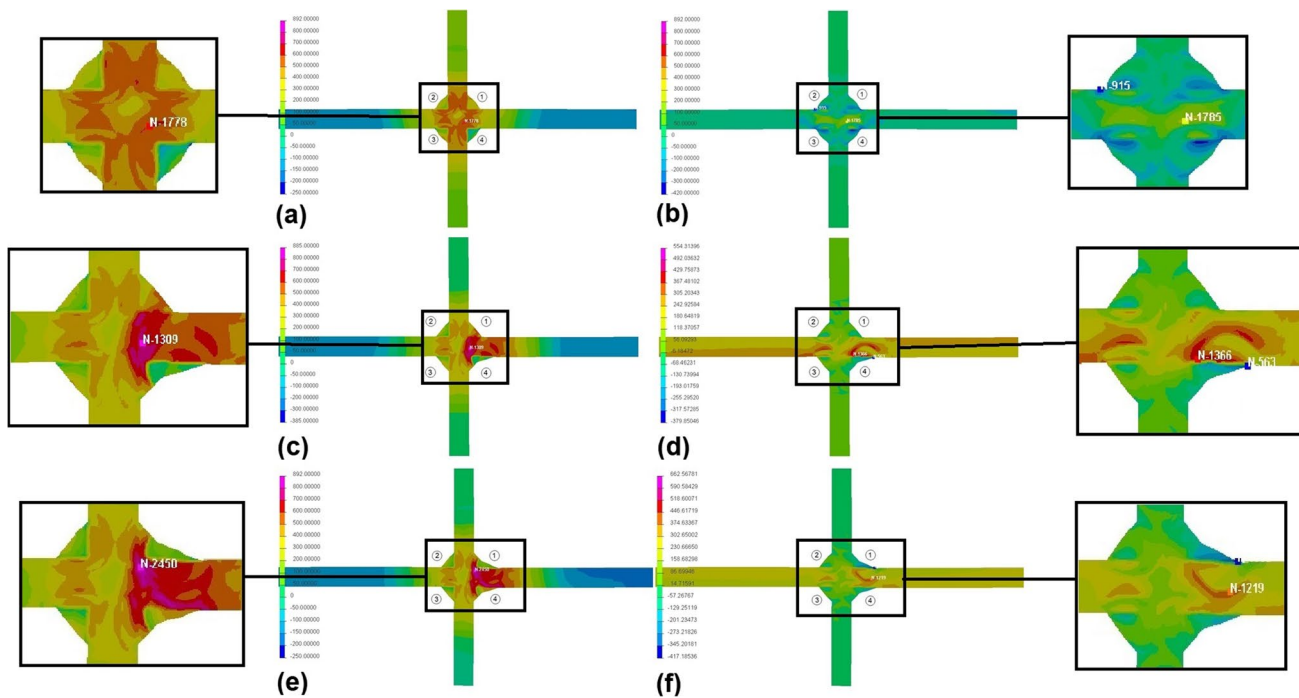


Fig. 12 **a** Residual stress distribution in a longitudinal direction of initial weld, **b** transverse direction of initial weld, **c** longitudinal direction of one-side repair welding, **d** transverse direction of one-

side repair welding, **e** longitudinal direction of double-side repair welding, and **f** transverse direction of double-side repair welding of S355J2+N sample

measured at the new weld toes. As can be seen, after initial welding, the residual stresses of welds are not the same. Welding on the back of the plate (weld 3 and 4) increases the residual stress on the top side of the plate (weld 1 and 2), which has already been welded. $T-t$ diagrams of the weldments (Fig. 9), show that welding on the back of the

plate increases the temperature of the weld toes on the top of the plate to temperatures lower than 600 °C. These temperatures are not high enough to accelerate the stress relief of the specimen. In contrast, it causes higher temperature gradients in the component, which contribute to the formation of higher residual stress. Due to the same

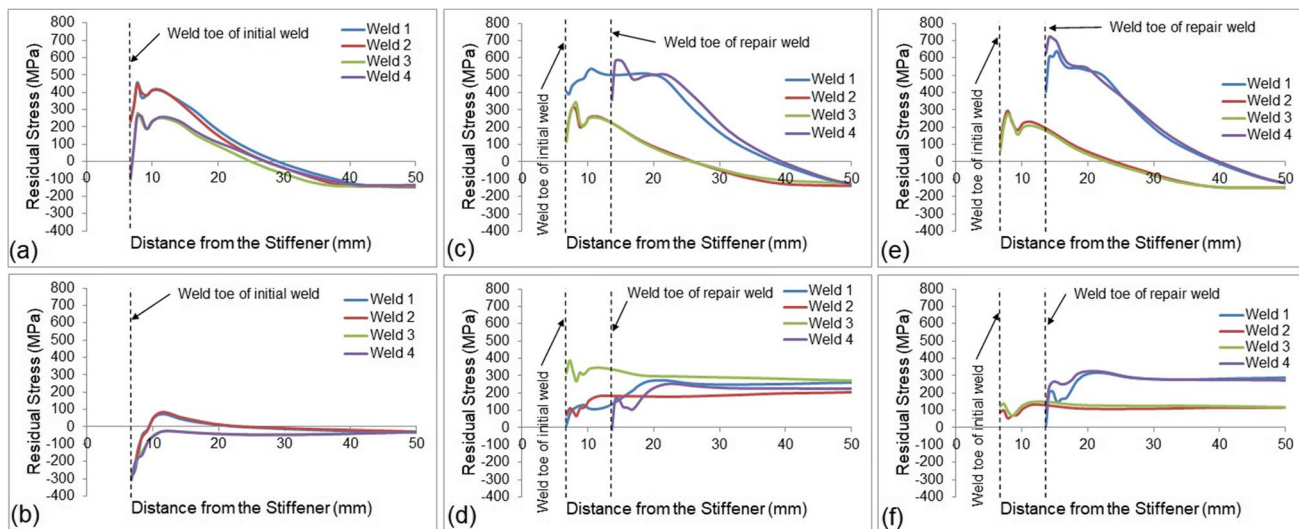


Fig. 13 **a** The surface residual stress distribution from weld toe through base material of S355J2+N sample in a longitudinal direction of initial weld, **b** transverse direction of initial weld, **c** longitu-

dinal direction of one-side repair welded, **d** transverse direction of one-side repair welded, **e** longitudinal direction of double-side repair welded, and **f** transverse direction of double-side repair welded

reason, repair welding on one side of the plate (weld 4) increases the residual stress of that side and the other side of the plate (weld 1). Continuation of the repair process on the second side of the plate (weld 1) increases the residual stress on both repaired weld toes to higher magnitudes. Looking at the other side of the stiffener (welds 2 and 3), which were not subjected to the repair welding, reveals that first repair welding (weld 4) decreases the longitudinal residual stress of weld 2, while increasing the transverse residual stress of weld 3. The second repair welding (weld 1) likewise decreases the residual stress of weld 3, but more slightly, and does not increase the residual stress of weld 2 significantly. The temperature changes on the weld toes of welds 2 and 3 are not high enough to either activate the solid-state phase transformations or release the residual stresses. The only reason for these changes is the balance of the residual stresses at these weld toes due to the changes in the residual stress of the surrounding area.

It is evident in Fig. 13 that the maximum value of the longitudinal residual stress almost in all welds happens in the close vicinity of the weld toe. But for the transverse direction, the maximum value is normally away from the weld toe. Nonetheless, the residual stress values at all weld toes are high, and taking the stress concentration effect at the weld toe into account, they could contribute to an early failure of the component.

Figure 14 shows the proportion of the phases at the weld toes of all the welds after double-side repair welding of the S355J2+N sample. It should be noted that the weld toes of welds 1 and 4 belong to the repair welds; thus, the phase transformation for the initial welds at these corners is not evident. No phase transformation happens in a given weld toe due to welding of the other corners of the T-joint. It was also expected considering the fact that the maximum temperature of a given weld toe is lower than the critical temperature for the solid-state transformations during welding of the other corners. The model suggests that the microstructure of all weld toes consists of Bainite and Martensite, although the proportion of the phases is different at different weld toes. Figure 15 shows the microstructure of the specimen in this region, which consists of bainite and martensite. According to the figure, the hardness of the weld toe of the other side of the plate did not change significantly during repair welding of the opposite side, showing that there was no considerable change in the phase morphologies. All these results prove that the changes in the residual stress of other weld toes during repair welding of one weld toe are due to expansions and contractions at these areas.

Figures 16 and 17 show the residual stress evolution in the longitudinal and transverse directions during initial welding, one-side, and double-side repair welding of the S960QL sample. As can be seen, the magnitude of the

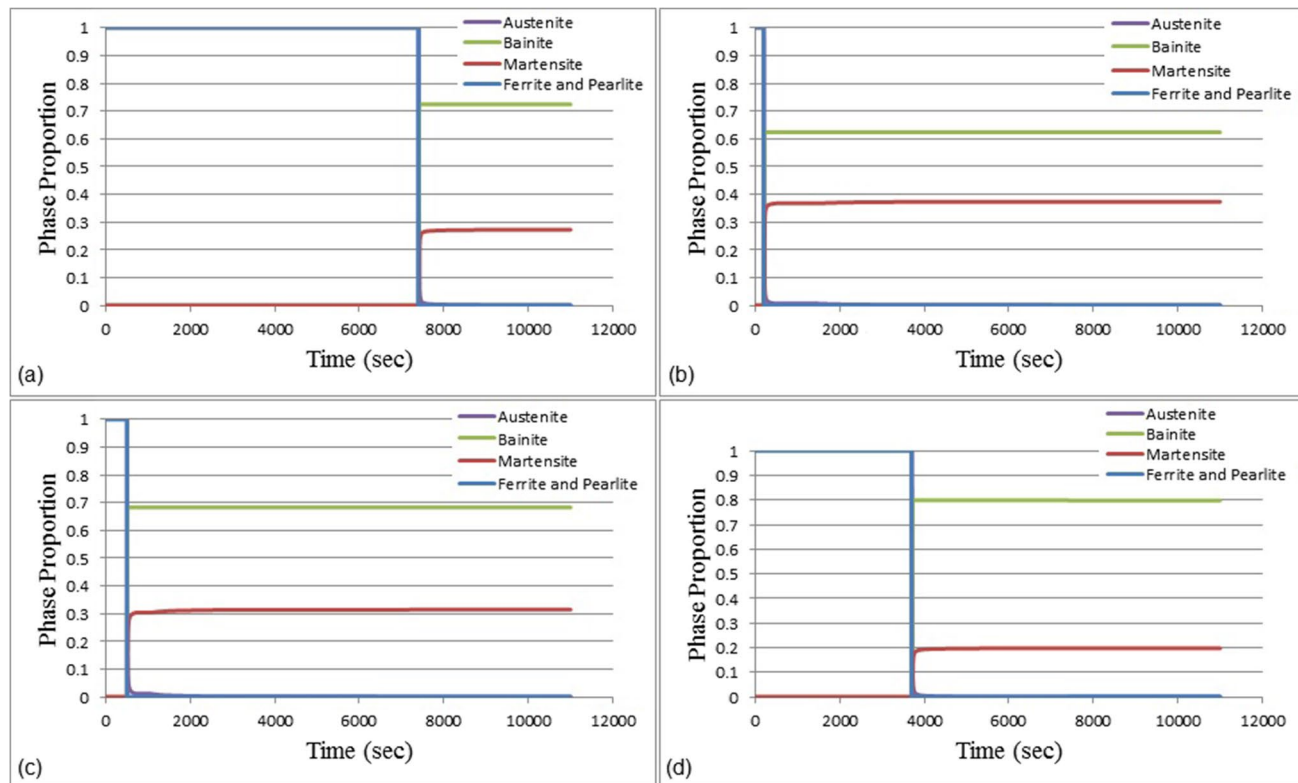


Fig. 14 Phase proportions at weld toe of **a** weld 1, **b** weld 2, **c** weld 3, and **d** weld 4 of S355J2+N sample

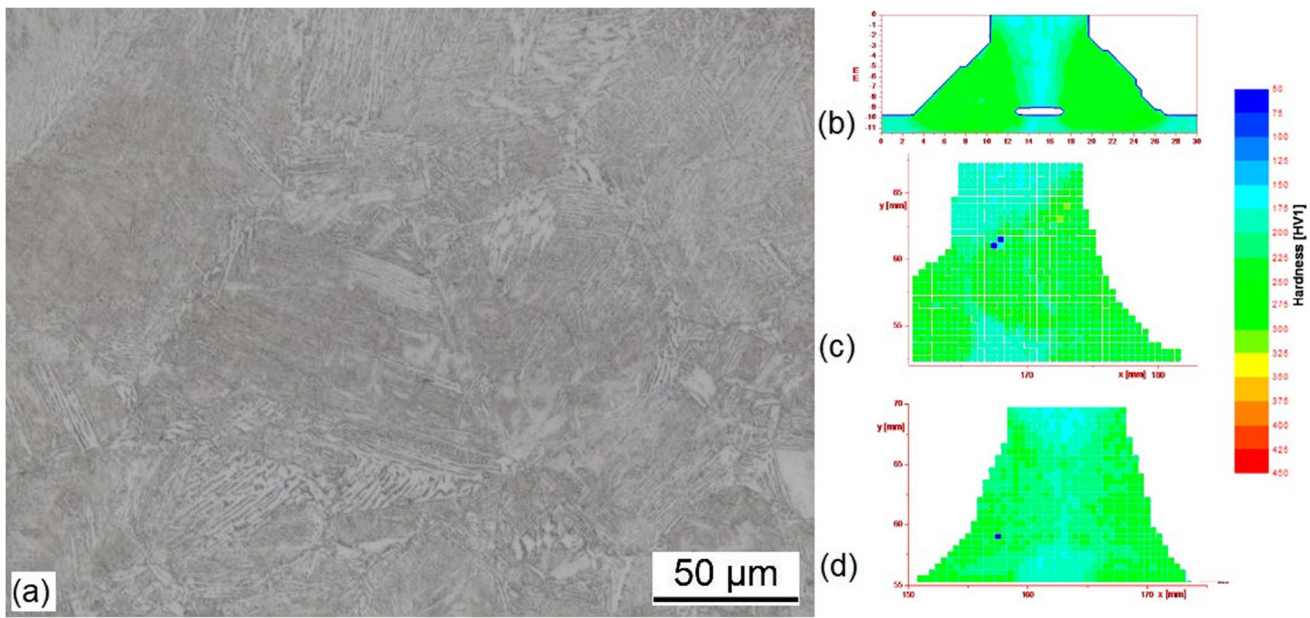


Fig. 15 **a** Microstructure of the weld toe, **b** hardness of the sample after initial welding, **c** hardness of the sample after one-side repair welding, and **d** hardness of the sample after double-side repair welding of S355J2+N sample

residual stress in both directions increases after repair welding compared to the initial weld, regardless of repairing on one or two sides. But after double-side repair welding, longitudinal and transverse residual stresses are reduced compared to one-side repair welding. As can be seen in the results of the metallurgical simulation (Fig. 18), there is no phase transformation on the other weld toes during repair welding. Checking the temperature contours of the specimens approves that the temperature of the other welds does not reach the austenitization temperature of the alloy. Therefore, during repair welding, the phase transformations are limited to the repaired area and its adjacent material. Looking at the microstructure and hardness of the specimen at the weld toe (Fig. 19) reveals that the microstructure of the weld toe consists of bainite phase only, which is in agreement with the model. But a closer look at the hardness values after repair welding shows that, although there was no phase transformation in the area, the temperature was high enough to change the morphology of the phases. The change in the morphology of the bainite phase reduced its hardness that contributes to decreasing the yield strength of the material and deformation in lower stresses. Furthermore, by moving from the weld toe to the base material, the hardness first decreases then increases. The same happens to the residual stresses of the regions. The region with lower strength yields sooner and shows lower residual stress magnitude. With the same logic, the region with higher strength yields at higher stresses and shows higher levels of residual stress. As can be seen in Fig. 17, the maximum longitudinal residual stress happens away from the weld toe, while

the maximum value in the transverse direction is at or in the direct vicinity of the weld toe. The magnitude of the residual stress in both directions at the weld toe is almost the same. Considering the stress concentration at the weld toe, these values could be even more critical than the higher values in HAZ far away from the weld toe. In conclusion, the morphological changes in the phases and contractions and expansions together are responsible for the residual stress evolutions in the repair welded S960QL sample. It is worth mentioning that the highest residual stress values are inside the components, but since the fatigue crack initiates from the surface of the specimen, they are not studied here.

5 Conclusion

Residual stress evolutions during repair welding of a fatigue crack in S355J2N and S960QL structural steel T-joints have been studied through experimentation and numerical models. The results show that repair welding increases the magnitude of residual stress in the components in transverse and longitudinal directions compared to the initial weld. The residual stress at the weld toe of all initial welds increased regardless of the location of welding. The alloys show different responses to the repair welding on the opposite side of the plate. Double-side repair welding of the S355J2+N component reduced the level of transverse residual stress at weld toes while the longitudinal residual stress increased at all weld toes. In the S960QL sample, on the other hand, the magnitude of

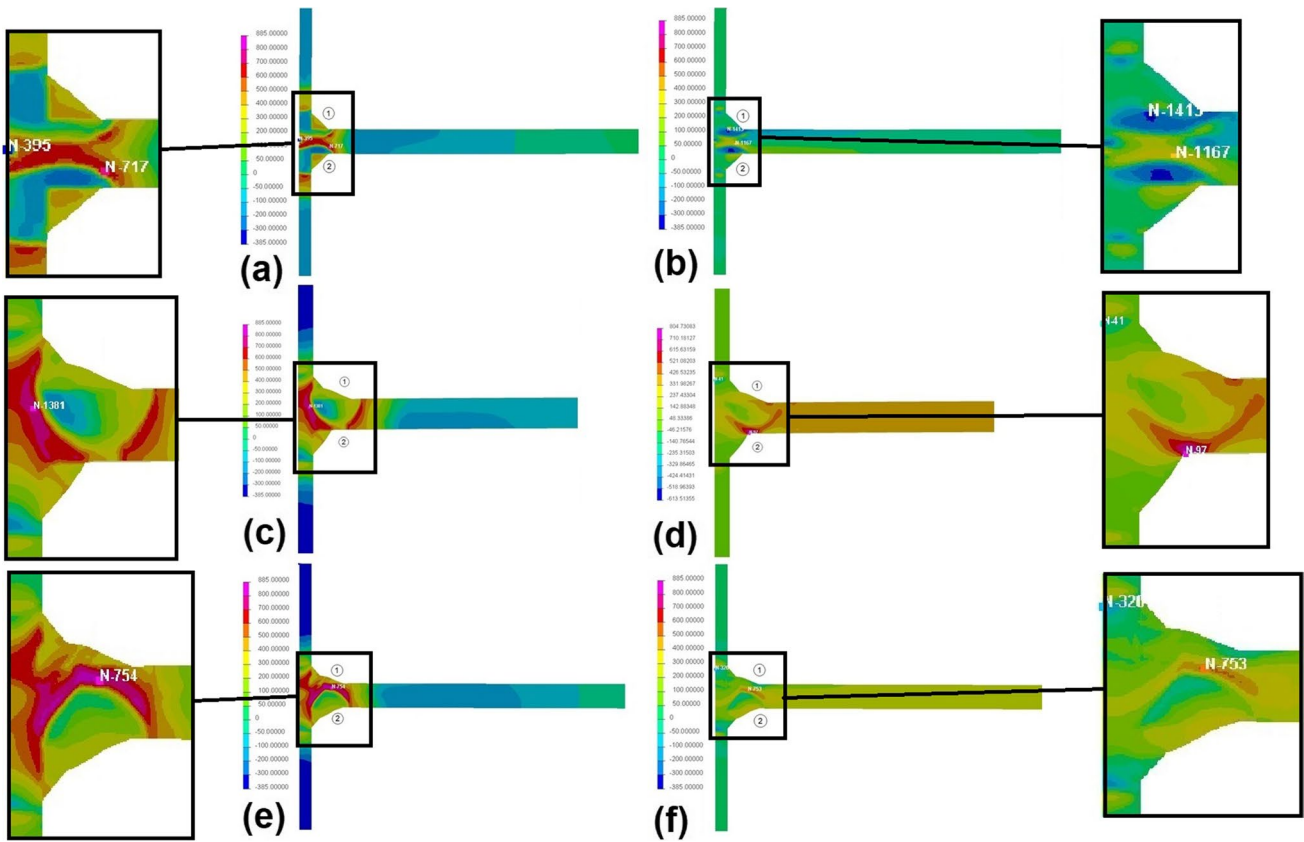


Fig. 16 Residual stress distribution in **a** longitudinal direction of initial weld, **b** transverse direction of initial weld, **c** longitudinal direction of one-side repair welding, and **d** transverse direction of one-side

repair weld, **e** longitudinal direction of two-side repair weld, and **f** transverse direction of two-side repair weld of S960QL sample

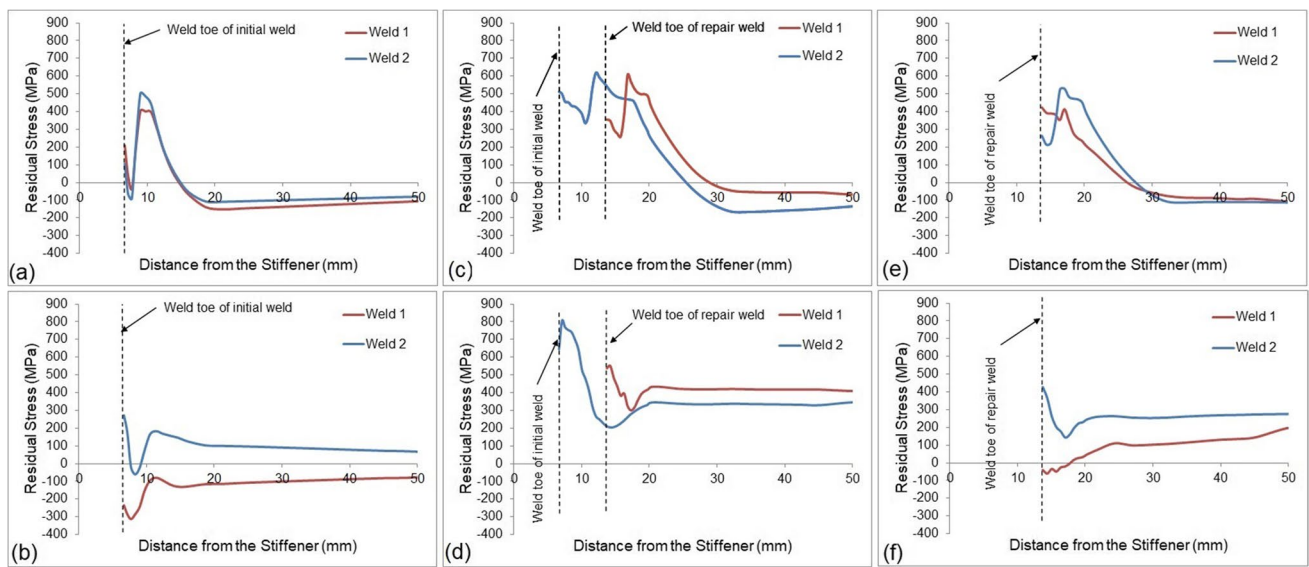


Fig. 17 The surface residual stress distribution from weld toe through base material of S960QL sample in **a** longitudinal direction of initial weld, **b** transverse direction of initial weld, **c** longitudinal direction

of one-side repair welding, **d** transverse direction of one-side repair welding, **e** longitudinal direction of two-side repair weld, and **f** transverse direction of two-side repair weld

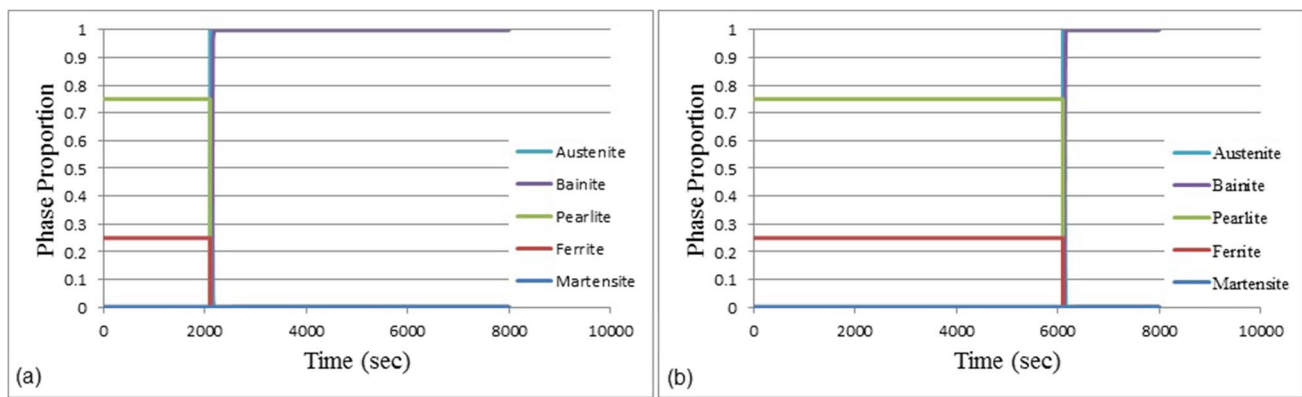


Fig. 18 Phase proportions at weld toe of **a** weld 1 and **b** weld 2 of S960QL sample

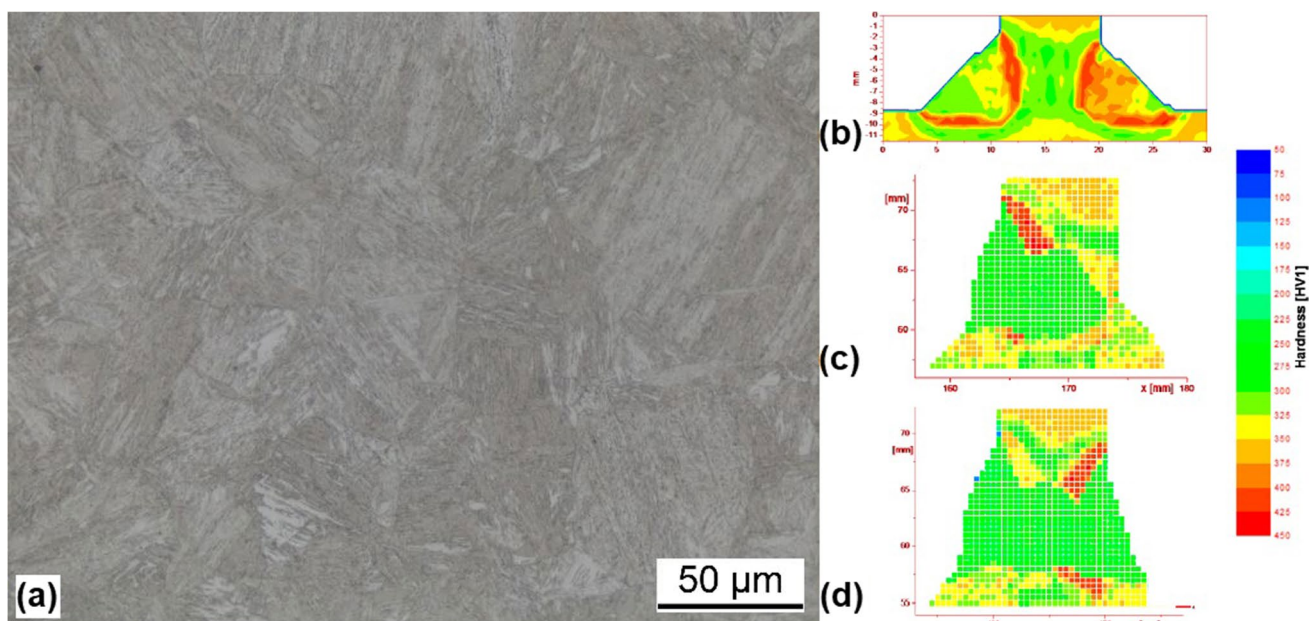


Fig. 19 **a** Microstructure close to the weld toe, **b** hardness of the sample after initial welding, **c** hardness of the sample after one-side repair welding, and **d** hardness of the sample after double-side repair welding of S355J2+N sample

residual stresses in both directions decreased after double-side repair welding compared to the residual stress of the one-side repair welding. Furthermore, repair welding does not necessarily cause maximum residual stresses in the repaired area. The results show that the magnitude of the residual stresses in both directions of the S355J2+N sample is higher on the weld toe of the weld on the opposite side of the stiffener. Repair welding causes phase transformations only at and in the vicinity of the repaired area but changes the distribution and magnitude of the residual stresses through the whole component. Although, there are morphological changes in the Bainite phase in the HAZ of the S960QL sample after double-side repair welding compared to the one-side repair welding. These

morphological changes are not evident in the S355J2+N sample. The reason for the evolution of the residual stresses in the locations far from the repaired area in the S355J2+N sample, therefore, is the expansion and contraction leading to an inhomogeneous plastic deformation of the material through the weldment. While in the S960QL sample, the morphological changes also contribute to the residual stress evolution in addition to the expansion and contraction.

Declarations

Conflict of interest The authors declare no competing interest.

References

1. Goldak J, Asadi M (2014) Challenges in validation of computational weld mechanics code to compute residual stress and distortion in welds. *J Press Vessel Technol Trans ASME* 136:1–8. <https://doi.org/10.1115/1.4024458>
2. Dong P (2018) On repair weld residual stresses and significance to structural integrity. *Weld World* 62:351–362. <https://doi.org/10.1007/s40194-018-0554-1>
3. Song S, Dong P (2017) Residual stresses at weld repairs and effects of repair geometry. *Sci Technol Weld Join* 22:265–277. <https://doi.org/10.1080/13621718.2016.1224544>
4. Unsworth D, Driver RG, Li L (2020) Measurement and prediction of residual stresses in welded girders. *J Constr Steel Res* 169:106007. <https://doi.org/10.1016/j.jcsr.2020.106007>
5. Farajian M, Nitschke-Pagel T, Siegela D (2014) Welding residual stress behavior in tubular steel joints under multiaxial loading. *HTM J Heat Treat Mater* 69:6–13. <https://doi.org/10.3139/105.110208>
6. Charkhi M, Akbari D (2019) Experimental and numerical investigation of the effects of the pre-heating in the modification of residual stresses in the repair welding process. *Int J Press Vessel Pip* 171:79–91. <https://doi.org/10.1016/j.ijpvp.2019.02.006>
7. Elcoate CD, Dennis RJ, Bouchard PJ, Smith MC (2005) Three dimensional multi-pass repair weld simulations. *Int J Press Vessel Pip* 82:244–257. <https://doi.org/10.1016/j.ijpvp.2004.08.003>
8. Salerno G, Bennett CJ, Sun W, Becker AA (2017) Residual stress analysis and finite element modelling of repair-welded titanium sheets. *Weld World* 61:1211–1223. <https://doi.org/10.1007/s40194-017-0506-1>
9. Jiang W, Luo Y, Wang BY et al (2015) Neutron diffraction measurement and numerical simulation to study the effect of repair depth on residual stress in 316L stainless steel repair weld. *J Press Vessel Technol Trans ASME* 137:1–12. <https://doi.org/10.1115/1.4028515>
10. Withers PJ (2007) Residual stress and its role in failure. *Reports Prog Phys* 70:2211–2264. <https://doi.org/10.1088/0034-4885/70/12/R04>
11. SEW 088 Guideline (2017) Supplementary Sheet 1 to SEW 088: Weldable Fine Grain Steels: Guidelines for Processing, Particular for Fusion Welding, Cold Cracking During Welding, Determining Appropriate Minimum Preheating, DIN German Institute for Standardization. Berlin, Germany
12. Schubnell J, Ladendorf P, Sarmast A et al (2021) Fatigue performance of high- and low-strength repaired welded steel joints. *Metals (Basel)* 11:293
13. Macherauch E, Müller P (1961) Das $\sin^2\psi$ Verfahren von Röntgenographische Eigenspannungen. *Z angew Phys* 13:305–312
14. Goldak JA, Akhlaghi M (2005) Computational welding mechanics. Springer Science+Business Media, Inc., 233 Spring Street, New York
15. De A, DebRoy T (2004) A smart model to estimate effective thermal conductivity and viscosity in the weld pool. *J Appl Phys* 95:5230–5240. <https://doi.org/10.1063/1.1695593>
16. Goldak J, Chakravarti A, Bibby M (1984) A new finite element model for welding heat sources. *Metall Trans B* 15:299–305
17. Grong ØY (1997) Metallurgical modelling of welding, 2nd edn. The Institute of Materials, London
18. Gourd LM (1995) Principles of welding technology, 3rd edn. Edward Arnold, London
19. Aarbogh HM, Hamide M, Fjær HG et al (2010) Experimental validation of finite element codes for welding deformations. *J Mater Process Technol* 210:1681–1689. <https://doi.org/10.1016/j.jmatprotoc.2010.05.014>
20. Bajpe T, Chelladurai H, Ansari MZ (2016) Mitigation of residual stresses and distortions in thin aluminium alloy GMAW plates using different heat sink models. *J Manuf Process* 22:199–210. <https://doi.org/10.1016/j.jmapro.2016.03.011>
21. Goyal VK, Ghosh PK, Saini JS (2009) Analytical studies on thermal behaviour and geometry of weld pool in pulsed current gas metal arc welding. *J Mater Process Technol* 209:1318–1336. <https://doi.org/10.1016/j.jmatprotoc.2008.03.035>
22. Schenk T, Richardson IM, Kraska M, Ohnimus S (2009) Modeling buckling distortion of DP600 overlap joints due to gas metal arc welding and the influence of the mesh density. *Comput Mater Sci* 46:977–986. <https://doi.org/10.1016/j.commatsci.2009.05.003>
23. Lindgren L-E (2007) Computational welding mechanics: thermo-mechanical and microstructural simulations. Woodhead Publishing, Cambridge, London
24. Leblond JB, Devaux J (1984) A new kinetic model for anisothermal metallurgical transformations in steels including effect of austenite grain size. *Acta Metall* 32:137–146. [https://doi.org/10.1016/0001-6160\(84\)90211-6](https://doi.org/10.1016/0001-6160(84)90211-6)
25. Koistinen DP (1959) A general equation prescribing the extent of the austenite-martensite transformation in pure iron-carbon alloys and plain carbon steels. *Acta Metall* 7:59–60
26. Saunders N, Miodownik P (1998) CALPHAD (Calculation of Phase Diagrams): A Comprehensive Guide, 1st ed. Elsevier Science Ltd, Langford Lane, Kidlington, Oxford
27. Trzaska J (2016) Calculation of critical temperatures by empirical formulae. *Arch Metall Mater* 61:981–986. <https://doi.org/10.1515/am-2016-0167>
28. Seyffarth P, Meyer B, Scharff A (2018) Großer Atlas Schweiß-ZTU-Schaubilder, 2nd ed. DVS Media GmbH, Dusseldorf
29. Belytschko T, Liu WK, Moran B, Elkhodary KI (2014) Nonlinear finite elements for continua and structures, 2nd ed. John Wiley & Sons, Ltd, Hoboken
30. Sarmast A, Serajzadeh S (2019) The influence of welding polarity on mechanical properties, microstructure and residual stresses of gas tungsten arc welded AA5052. *Int J Adv Manuf Technol* 105:3397–3409. <https://doi.org/10.1007/s00170-019-04580-7>
31. Lindgren LE (2001) Finite element modeling and simulation of welding. part 2: Improved material modeling. *J Therm Stress* 24:195–231. <https://doi.org/10.1080/014957301300006380>
32. Hamelin CJ, Muránsky O, Smith MC et al (2014) Validation of a numerical model used to predict phase distribution and residual stress in ferritic steel weldments. *Acta Mater* 75:1–19. <https://doi.org/10.1016/j.actamat.2014.04.045>
33. Hemmesi K, Farajian M, Boin M (2017) Numerical studies of welding residual stresses in tubular joints and experimental validations by means of x-ray and neutron diffraction analysis. *Mater Des* 126:339–350. <https://doi.org/10.1016/j.matdes.2017.03.088>

Publisher's note Springer Nature remains neutral with regard to jurisdictional claims in published maps and institutional affiliations.



Use of adhesives in repair of cracks in ship structures

R. C. Allan, J. Bird & J. D. Clarke

To cite this article: R. C. Allan, J. Bird & J. D. Clarke (1988) Use of adhesives in repair of cracks in ship structures, Materials Science and Technology, 4:10, 853-859, DOI: [10.1179/mst.1988.4.10.853](https://doi.org/10.1179/mst.1988.4.10.853)

To link to this article: <http://dx.doi.org/10.1179/mst.1988.4.10.853>



Published online: 18 Jul 2013.



Submit your article to this journal 



Article views: 28



View related articles 



Citing articles: 9 View citing articles 

Overview

Use of adhesives in repair of cracks in ship structures

The structures of modern warships frequently contain significant quantities of aluminium alloy: a material especially prone to fatigue induced cracking. The satisfactory repair of such cracks is often vital if the fighting efficiency of a warship is to be maintained properly and would usually be carried out by welding. The welding of aluminium and its alloys is often difficult and onboard is further complicated by the necessity to remove inflammable linings, cables, and items of equipment to reduce the fire risk and provide access for the repair. Consequently, repair welds are often carried out from the most accessible side and are seldom full penetration. The finished weld is invariably little more than a sealant with a fatigue life inferior to that of the original plate. Initiation of further cracking in the repair weld can be prevented by adhesively bonding a reinforcement across the weld to provide a strength at least as good as that of the original plate and a stiffness sufficient to prevent the onset of further cracking. The use of adhesively bonded steel and carbon fibre patches in typical ship applications are described and the factors governing patch design, methods of surface preparation to ensure good bond durability in a marine environment, and choice of adhesives are discussed.

MST/834

R. C. Allan
J. Bird
J. D. Clarke

© 1988 The Institute of Metals. Manuscript received 24 December 1987; in final form 5 February 1988. The authors are with the Admiralty Research Establishment, Dunfermline, Fife, Scotland. An earlier version of this paper was presented at the conference 'Structural adhesives in engineering' held at the University of Bristol on 2-4 July 1986 and organised by The Institution of Mechanical Engineers.

Introduction

Aluminium has been used in the shipbuilding industry for many years: from special applications such as liquid methane tanks for the Methane Pioneer and others to the deck and superstructure construction in merchant ships such as Oriana,¹ Canberra,² and Queen Elizabeth II. The superstructures and deckhouses in those vessels were made entirely of aluminium, whereas other vessels, such as the United States, had composite superstructures with aluminium attached to steel beams and stiffeners.

Aluminium has also been used in the decks and superstructures of warships: the Iranian destroyers built by Vickers in the 1960s, the Van Trompe Class destroyers of The Netherlands Navy, the FFG1, FFG7, and others of the US Navy, and recently the Type 21 frigates of the Royal Navy. There have also been proposals for all aluminium warships, but no such ship has yet been built.³

Aluminium is attractive to a designer in that it has a density and a modulus which are both one-third that of steel and a specific strength greater than that of steel. Thus, in addition to weight saving, it has the advantage that for a given strain the applied stress will be one-third that of steel, enabling long continuous superstructures to be designed without the need for expansion joints.

When designing a ship, the superstructure can be regarded as contributing to the strength of the hull girder or otherwise. However, even if the superstructure is not designed to contribute to the longitudinal strength of the ship, it will develop significant stress during hull bending. In addition, design features and stress concentrations can significantly increase the local stress level. Thus, special care must be taken in design to limit the stress in the aluminium superstructure, subject to the full hull bending moment.

The combination of induced stress and stress concentrations often results in fatigue damage in long aluminium superstructures attached to conventional steel hulls (Fig. 1). Although this can be alleviated by use of an expansion joint, this is not a complete solution as this only tends to concentrate the stresses elsewhere, often with more serious consequences, such as the fatigue failure of longitudinal stiffeners in deckheads (Fig. 2).

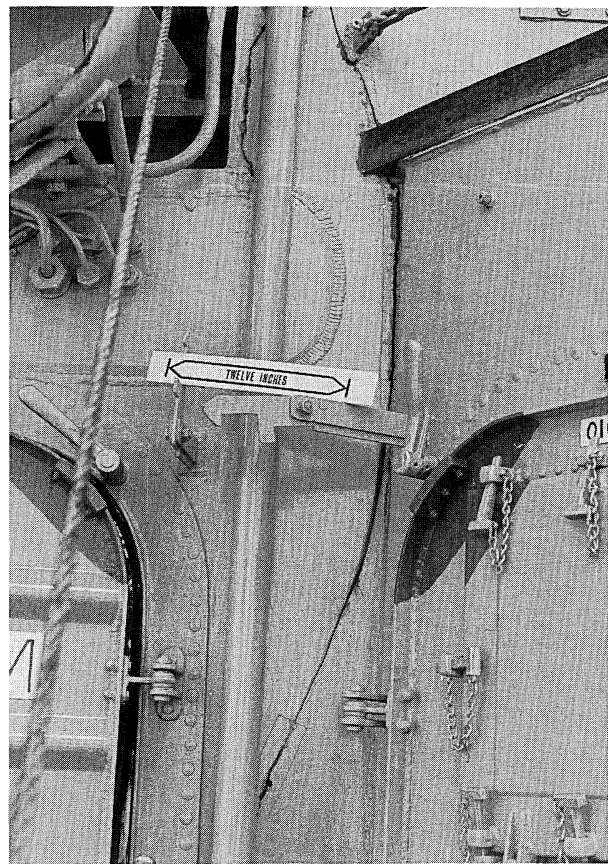
It is obvious that large cracks must be repaired to maintain the structural strength and prevent ingress of sea water to sensitive areas. However, if welding is used, the fatigue performance will be inferior to that of the original aluminium plate (Fig. 3).⁴ For weld repair, services may have to be stripped out below decks to prevent damage, particularly to electrical cables. Also, because of the difficulties of aluminium weld repair in a shipyard, the quality of the repair is likely to be poor. Thus, however the weld repair is carried out future performance will be inferior to that of the original structure.

Where fatigue cracking occurs, the problem results from insufficient material being available to maintain the strain induced stress at an acceptable level. This could be solved by either replacing the original plating with thicker plate, which would increase the superstructural weight, or by locally strengthening the structure with a material of higher modulus.^{5,6} This action would locally reduce the applied strain and thus the imposed stress in the aluminium, thereby reducing the likelihood of fatigue damage.

High modulus materials such as steel or carbon fibre would suffice depending on application and environment, although boron fibres might also be considered. These materials could be bonded to the aluminium plate in sufficient thickness to achieve the required reduction in stress level, the patch being tapered to avoid imposing a local stress concentration at the patch boundary.

The use of adhesively bonded patches to repair structures has been examined by many investigators and their use has increased dramatically over recent years. Adhesively bonded repairs of ship structures are invariably extremely cost effective because they can be carried out from the most accessible side and require no stripping out of equipment etc. from compartments in the immediate vicinity of the area to receive the patch. Where it is possible to repair cracks without the necessity to remove equipment this is done; the reinforcement is added for cosmetic purposes, but the weld will have little or no penetration and virtually no strength.

Unfortunately, the analytical techniques that have been devised for the design of patches are more applicable to the thinner structures used in aircraft. However, there are sufficient similarities with the repair of aircraft and reinforcement of other structures such as bridges⁷⁻⁹ to



1 Typical crack in aluminium alloy superstructure

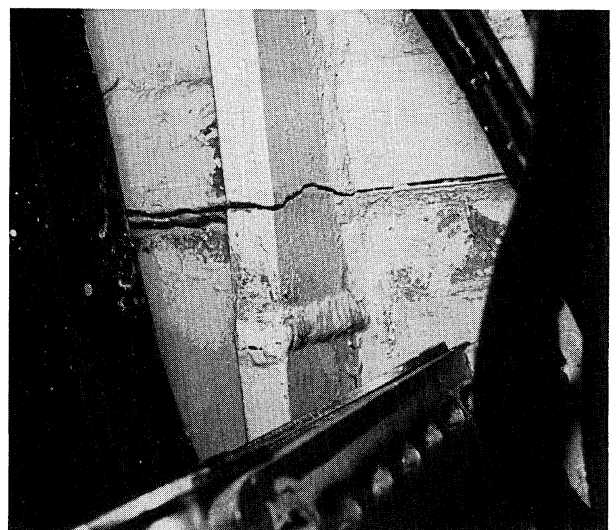
encourage the use of adhesively bonded patches in ship repair, although there are particular restraints which must be observed.

In the present paper, the work carried out at ARE (Dunfermline) to determine the strength of steel and carbon patches applied to aluminium plate material and the application of the technique to the repair of aluminium decks in Type 21 frigates of the Royal Navy are described and the performance of these patches in service is discussed.

Design considerations

The most serious cracking experienced in warships has usually been caused by the stress arising from vertical bending of the hull girder resulting from wave action. This produces alternating compressive and tensile stresses in the deck and bottom structure in the longitudinal direction. Since the bottom structure is relatively free of stress concentrations, most of the cracking occurs in the decks: at openings, at ends of superstructure sections, or at changes in deck plating thickness, and nearly always initiates in a welded joint.

During its life a warship will experience about 3×10^7 wave encounters. Most of these will be of small wave height and the resultant stresses will be correspondingly small, but there will be a reducing number of higher stresses. Measurements on warships at sea by ARE (Dunfermline) have shown that the probability distribution of the maximum stress in each wave encounter over a long period is approximately exponential. Analytical methods are available for calculating the fatigue damage for a particular welded joint configuration and probability



2 Example of deckhead cracking

distribution of stress range.¹⁰ It is usually assumed that the fatigue curve can be represented by

$$N_f = A(\Delta\sigma)^{-b} \quad \dots \dots \dots \quad (1)$$

where N_f is the number of cycles to failure, $\Delta\sigma$ is the stress range, and A and b are empirical constants. For most joints in steel and aluminium $b \approx 3$.

If the cumulative probability distribution of stress range is given by

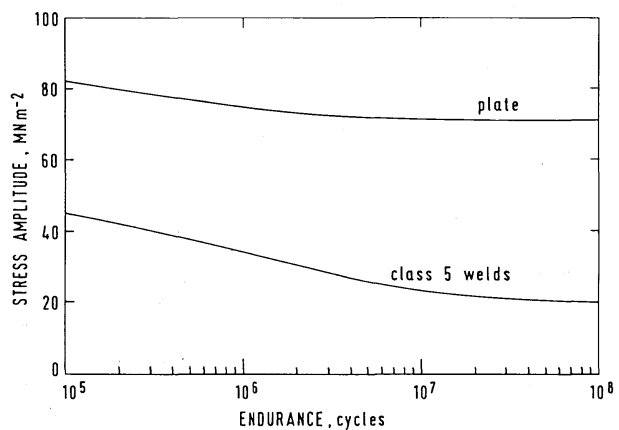
$$P(\Delta\sigma) = \exp(-\alpha\Delta\sigma/\Delta\sigma_0) \quad \dots \dots \dots \quad (2)$$

where $\Delta\sigma_0$ is the maximum stress range expected in a ship life corresponding to a probability of exceedance per wave encounter of $1/\alpha$, then the Palmgren-Miner damage accumulation law gives the following expression for the fatigue usage D in a ship life

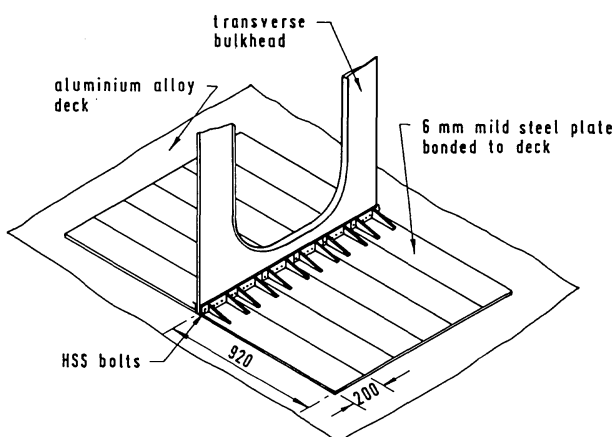
$$D = \sum \frac{N_i}{N_{f(i)}} = \frac{\alpha N_L b!}{A} (\Delta\sigma_0)^b \quad \dots \dots \dots \quad (3)$$

where N_L is the number of cycles in a ship life. There are a number of additional stress cycles resulting from hull vibrations following impacts between the hull and the sea surface, but the correction required for these is generally fairly small. Crack initiation is assumed to occur when the value of D is of the order of 1.0.

If the contributions to D from different parts of the fatigue curve are examined for typical welded joints and loading configurations, it is found that most damage



3 Fatigue design curve for N8 aluminium alloy



4 Repair of internal deck of frigate using bonded steel patches joined by bolting through bulkhead

results from the midrange (i.e. 10^4 – 10^5 cycles) of the fatigue curve.

It can be seen from equation (3) that the fatigue life of a joint is proportional to $(\Delta\sigma)^b$, so that for $b = 3$ the life can be doubled for a stress reduction of only about 20%. If a patch is bonded over a repaired weld and the patch is long enough and the adhesive thin enough for there to be insignificant shear in the region of the weld, then transverse sections can be assumed to remain plane under load. The longitudinal stress in the plate next to the weld σ_1 is then given by

$$\sigma_1 = \frac{\sigma_0}{1 + (E_2 t_2 / E_1 t_1)} \quad \dots \dots \dots \quad (4)$$

where σ_0 is the stress in the plate in the absence of the patch reinforcement, E_1 and E_2 are the elastic moduli of the plate and patch respectively, and t_1 and t_2 are the thicknesses of the plate and patch respectively.

In this relationship, it is assumed that the adhesive carries an insignificant longitudinal load and that the supporting structure (stiffeners and bulkheads) effectively eliminates bending effects.

For internal applications, where sea water corrosion and differential expansion effects resulting from temperature fluctuations are not a problem, steel patches have been used successfully on aluminium decks. For such patches, $E_2/E_1 = 3.0$. If the patch thickness were, say, half the original plate thickness, the plate stress would be reduced to a factor 0.4 times the original value giving a factor of 15.6 increase in fatigue life. In practice, such large increases in fatigue strength are not possible for a number of reasons. The fatigue strength of the repaired weld is never as good as the original and very often has a large area of lack of fusion internally. Therefore, it is not possible to grind down the weld bead without losing a large fraction of the weld metal and the patch has had to be recessed to accommodate the weld bead. The adhesive does reduce the load carried by the patch to some extent, and the fatigue strength of the adhesive is a governing factor. If the deck is not flat, e.g. at a transition in plate thickness where both stepped steel patches and laminated carbon fibre patches have been used, the step increases the flexibility of the patch and reduces its effectiveness. Nevertheless, despite these factors, a substantial improvement in fatigue life can still be obtained.

An alternative approach is to use patches without a repair weld, then, provided the patch is strong enough, the governing factor is the fatigue strength of the adhesive joint. This can be improved by the choice of adhesive and the reduction of stress concentration at the end of the patch as discussed below.

In some instances, cracking has occurred close to, and on both sides of, a transverse bulkhead. Then, to avoid cracking at the bulkhead, the patches on either side have had to be joined by bolting through the bulkhead, thus obtaining a continuous load path (Fig. 4). The steel patches were applied as longitudinal strips 200 mm wide for ease of handling.

Surface preparation

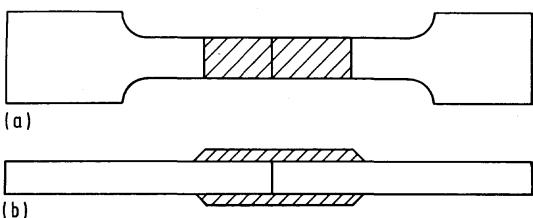
The method chosen for preparing aluminium alloy surfaces for bonding must achieve strong durable bonds. The use of flammable or corrosive liquids is not generally acceptable onboard ship. The use of organic degreasing agents entails considerable fire risk, since their vapours can be drawn into ventilation systems and spread throughout the ship. Also to be avoided are aggressive chemicals which can penetrate cracks and other openings to attack and damage wiring and equipment contained within the ship structure. Chemical paint strippers have also been known to degrade adhesive bonds, even though every effort has been made to remove all traces of the stripper from surfaces to be bonded.

Therefore, the preparation of adherend surfaces onboard ship is limited to simple degreasing using a commercial low toxicity solvent such as Genklene (1:1:1 trichlorethane) applied by wiping with lint free cloths, followed by grit blasting with 60/80 size alumina grit to produce a clean, bare metal surface.

A freshly grit blasted surface of aluminium and its alloys is very active and extremely susceptible to contamination from atmospheric moisture, dust, and grease which can adversely affect the performance of the bonded joint. To reduce the possibility of contamination to a minimum as short a time as possible should elapse between grit blasting and adhesive application. Large areas are more conveniently prepared in stages to minimise the time taken between surface preparation and application of adhesive. This is especially so where large carbon fibre patches are involved, although, as a consequence, the first ply of the laminate to be laid will contain several butt joints. Provided generous overlaps are used at the joints, no significant loss of strength and stiffness of the finished patch should occur, because all subsequent plies can usually be laid in continuous lengths. Both steel and carbon fibre patches are finished with a 10:1 taper at the ends to reduce stress concentration.

Bond durability greater than that offered by simple degreasing and grit blasting is especially desirable for marine bonded joints and might be achieved using alternative methods of surface preparation. Phosphoric acid anodising, for example, is well established in the aircraft industry as a proven method of surface preparation leading to the formation of strong durable adhesive joints in aluminium alloys. Combining the phosphoric acid with colloidal silica to form a gel is one method of making the process more manageable, but after anodising there remains a considerable quantity of aggressive chemical to be completely and safely removed – a not inconsiderable task if the restraints imposed onboard ship are to be observed.

Previous work¹¹ has demonstrated that γ -glycidoxypropyltrimethoxysilane (Union Carbide A187 silane) can be used as a coupling agent on grit blasted aluminium alloy surfaces with the effect of increasing the durability of structural adhesive joints. Application of a 1 or 5 vol.-% aqueous solution of A187 silane results in a slight improvement in initial joint strength and considerably increased durability of joints immersed in water when compared with untreated joints.

*a* central weldment; *b* outer weldment

5 Specimen used in bond strength test

Silane priming of grit blasted surfaces is very convenient to use onboard ship and, although without the same reputation as phosphoric acid anodising, is still capable of producing more than adequate joint durability to meet the surface requirement.

Some adhesives incorporate silane in their formulation, but for ship application experience has shown that it is better to apply the silane in a separate process. This has the advantage of direct control and when applied very quickly after grit blasting helps to seal a highly active aluminium alloy surface.

Patch material and adhesives

For ship repairs, two patch materials of modulus higher than that of the usual marine aluminium alloy have been found to work well. The choice of patch material has been largely governed by situation, patch area, and the relative flatness of the area to be patched.

Mild steel patches are cheap, readily fashioned, and well suited for patching interior surfaces well away from weatherdecks. The plating used for steel patches is typically 6 mm thick and can usually be persuaded by the strategic application of pressure from weights and shoring to accommodate slight undulations in, say, a deck surface, to achieve thin bondlines. Where variations in a surface are of a very minor nature, the use of a gap filling adhesive will suffice. All the repairs involving steel patches carried out so far on HM ships have been with Permabond E04 or E32, which are both cold setting, gap filling, epoxy adhesives.

Less flat areas, especially those containing changes in plate thickness and curved surfaces, are more conveniently reinforced with patches of carbon fibre composite laminated directly onto a ship structure using cold setting epoxy resin. A typical carbon fibre patch consists of eight plies of unidirectional woven roving of 340 g m^{-2} nominal mass laminated with Ciba-Geigy 1927 epoxy resin and

hardener. The resin has a low initial viscosity enabling easy penetration of the carbon fibre and bonds well to the aluminium alloy plating of a ship superstructure.

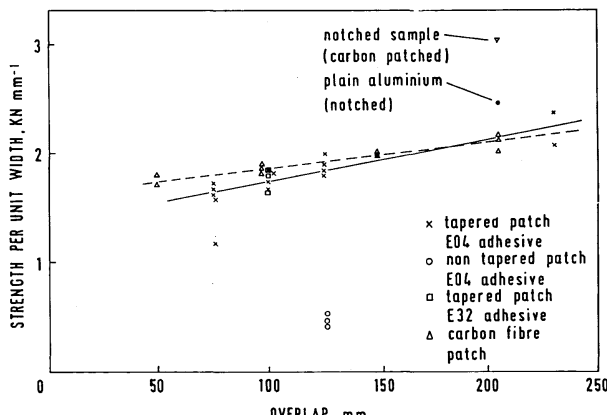
There is a particular problem in that if, in the presence of water, the aluminium alloy is in electrical contact with the carbon fibre of the patch, severe stress corrosion of the metal may occur leading to serious loss of bond strength. Although the carbon fibre in a laminated patch is effectively sealed and electrically isolated from the metal structure by the resin matrix, a moisture barrier of 0.15 mm thick aluminium foil is bonded over the patch to overlap it by about 100 mm all round. The aluminium foil is in turn protected by two plies of 300 g m^{-2} chopped strand glass laminate finished with a heavy epoxy resin flow coat.

Bond strength

Estimates of bond strength were made using aluminium alloy samples of the type shown in Fig. 5. Steel patches were bonded with either Permabond E04 or E32 epoxy adhesives. Fully cured, preformed carbon fibre patches laminated with Ciba-Geigy 1927 epoxy resin were bonded to the aluminium using Permabond F241 acrylic adhesive. In all cases, the patch material was attached to both sides of the sample to ensure axiality of stressing when the samples were tested to failure in tension.

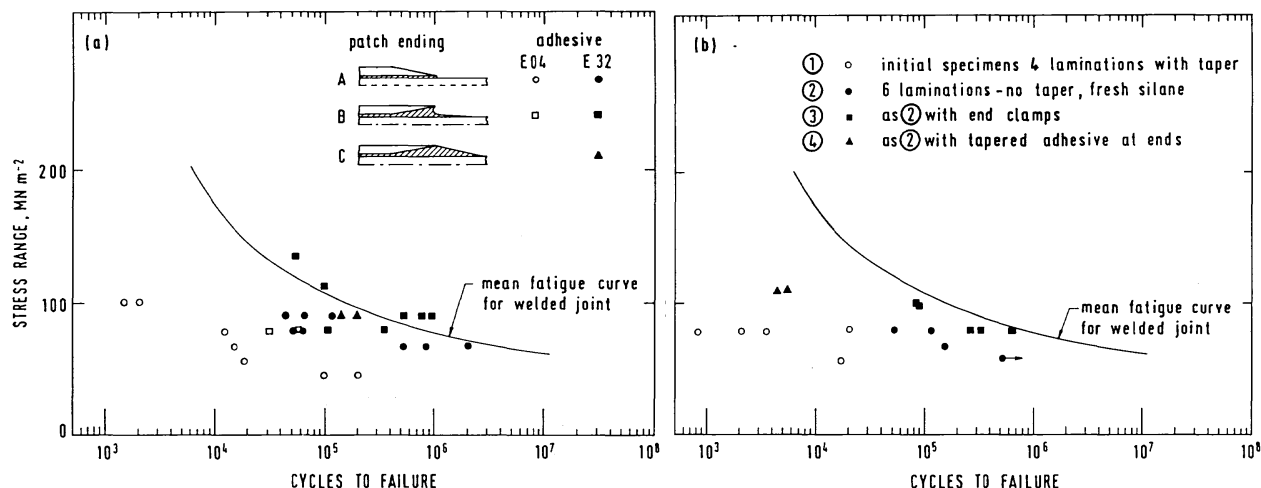
Using E04 adhesive and steel patches, the bond strength can be shown to vary in relation to the overlap (Fig. 6). The samples were all made by patching across abutting aluminium ends. To have some uniformity in expressing the failure load, the failure load per unit width is reported rather than the failure load per overlap area. The former method will give a better indication of any increase in strength. A number of the samples were tested without tapering the ends of the patches and the effective decrease of the failure stress due to the stress concentration at the patch ends can be judged (Fig. 6). Similar results are reported for the E32 adhesive in comparison with the strength of E04 provided the base material is correctly prepared.

The carbon fibre patches used in the tests were either laminated directly onto the suitably prepared aluminium test coupons using 1927 resin or laid-up previously as a separate patch, fully cured, and finally bonded to the testpiece using F241 adhesive. In all cases, patches with tapered ends were used. It can be seen that the strength of the carbon fibre patch is similar to that of the steel patch for the range of overlap tested. Also, in a number of cases, as an alternative to patching abutting aluminium ends, notched aluminium samples were used. The average failure stress for these samples (Fig. 6) is less than for the additive failure stress of carbon patched abutting aluminium and plain aluminium samples alone.



6 Effect of overlap on bond strength

To compare adhesives and joint designs, fatigue tests have been carried out on welded joints reinforced with patches and patched unwelded joints. The plate material in each case was 8 mm N8 aluminium alloy and the patches were either 5 mm steel or unidirectional carbon fibre with 4 or 6 laminations. The completed specimens (similar to those used for static strength, Fig. 5) were 700 mm long, 75 mm wide at the grips, with a radius transition to a uniform 50 mm over the central 300 mm. The patch width was also



a effect of patch geometry and adhesive type; b effect of taper, number of laminations, and clamping

7 Fatigue strength of a bonded steel-aluminium joints and b CFRP patched specimens

50 mm and the patch overlap was 100 mm each side in all cases (i.e. 200 mm patch length).

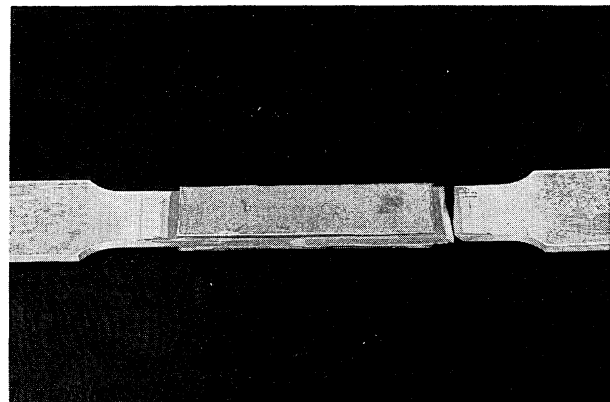
Although in practice patches applied to ships have been on one side only, the test specimens were patched on both sides to avoid bending effects. They were also tested in cyclic tension to avoid bending by buckling under compression. This is considered to be a more severe test (in terms of fatigue life for a given stress range) than the actual situation of compression-tension cycling. A minimum stress/maximum stress ratio R of 0.1 was used throughout and the test frequency was limited to 1 Hz to avoid heating effects. The steel patches had a 10:1 taper over the first 50 mm of each end to reduce the stress concentration at the ends. These were originally bonded with the longer flat surface in contact with the plate. Then, following the results reported by Adams and Wake,¹² it was decided to invert the patches, since the increased adhesive at the ends would be more effective in reducing the stress concentration. In each case the bond thickness over the central region was 0.08 ± 0.03 mm. Also, Lees¹³ has suggested that Permabond E32 should have a better fatigue life than E04 which had been used in the early tests and in ship repairs. Both these improvements were effective as can be seen in Fig. 7a, in which results for unwelded butt jointed specimens can be compared with the mean curve obtained for welded butt joints. The results are plotted in terms of tensile stress in the aluminium to enable direct comparison to be made with the weld for a typical plate thickness, but it must be borne in mind that the fatigue strength of the adhesive joint will be a function of the shear loading on the bond and so will vary with plate thickness.

The change from E04 to E32 adhesive increases the fatigue life by about an order of magnitude and the use of inverted patches gives a further increase of about a factor 4. Standard bonding procedure with inverted patches produces a profile approximating to that shown for type B in Fig. 7a. An attempt was made to improve this by adding further adhesive after the original bond had set and profiling to give a smooth taper (type C). This did not have the desired effect, since the adhesive cracked at the point of maximum thickness and the life was less than that of the specimens without this additional taper. Static testing gave a similar difference. A type C specimen failed at 83 kN compared with 90 and 91 kN for two type B specimens. Admittedly only three type C specimens were tested, but the results do suggest that the strength of type C joints is significantly lower than that of type B. Stress analyses are being carried out to investigate this difference and it is hoped to define the optimum taper configuration.

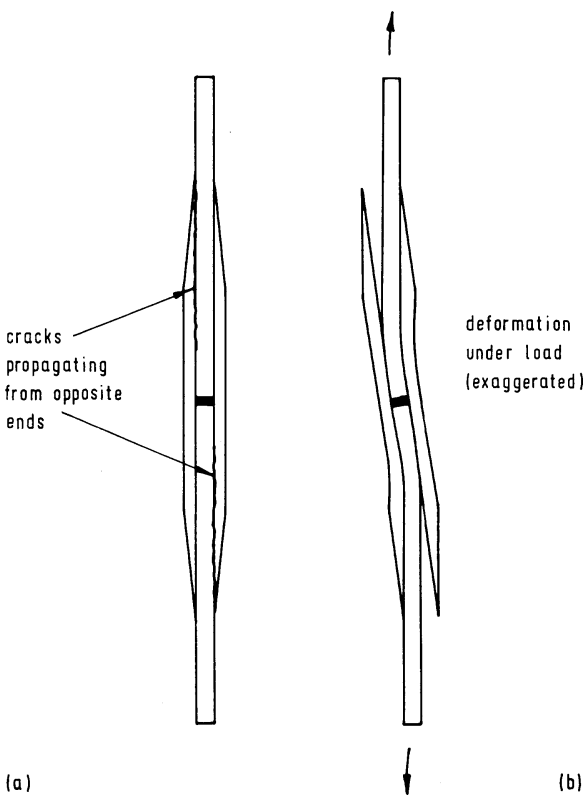
However, the type B patches with E32 adhesive appear adequate for double sided repairs to 8 mm plate, since most of the results lie above the weld fatigue curve and one specimen failed in the aluminium alloy at the end of the adhesive taper (Fig. 8).

The steel patched weld reinforcement specimens gave similar results, with inverted patches and E32 adhesive being the most successful. Most of the specimens failed in the aluminium at the start of the 37 mm radius of the width transition at an endurance of 3–4 times the mean value for a weld. However, it was possible for the patch reinforcement to have a detrimental effect on the fatigue life of the weld if the fatigue strength of the bond was inadequate. This occurred in some cases using E04 adhesive without an adhesive taper to reduce the stress concentration. The bond failure tended to initiate at opposite ends of the two patches, as illustrated in Fig. 9. This form of failure, once initiated, was maintained by the bending of the specimen which increased the peel stresses at the cracked ends. Fatigue failure ultimately occurred in the heat affected zone of the weld under the increasing direct stress as the reinforcement was reduced, plus the additional bending introduced by the asymmetry of the remaining reinforcement. This form of failure is less likely to occur in a ship because of the supporting structure, but the possibility must be borne in mind.

The CFRP specimens were produced by laminating directly onto the aluminium following the same procedure used for ship repairs. For some specimens a taper was



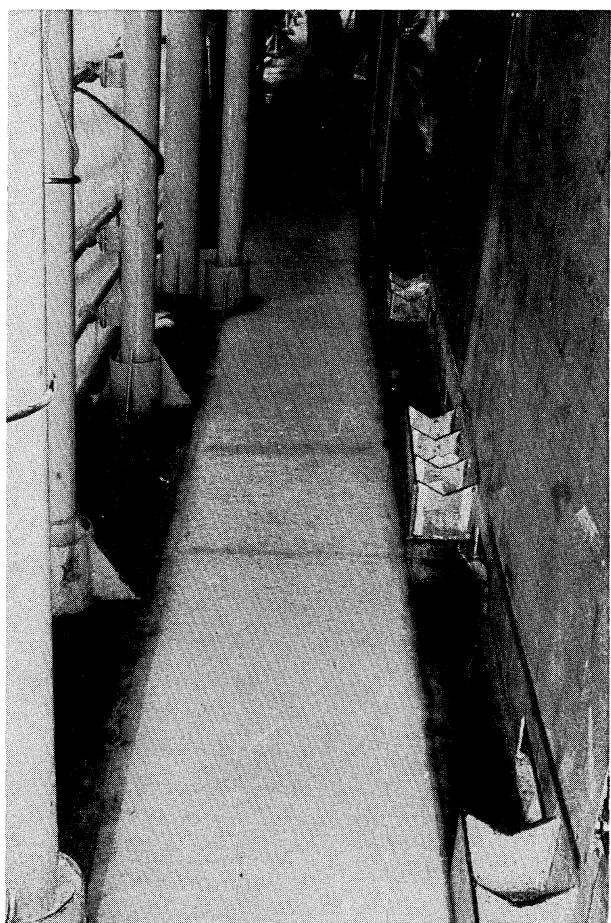
8 Steel patch specimen which failed by fatigue of aluminium



9 Typical mode of failure by fatigue

introduced by making successive laminations approximately 10 mm shorter. Again, both butt joints and welded specimens were tested. Initial results were disappointing. Butt joints failed at lifetimes two orders of magnitude lower than that of the weld. It was later found that improved results could be obtained for both welded and unwelded specimens if fresh silane were used for each batch. A further improvement was obtained with end clamps to produce compressive stresses in the adhesive at the ends of the patch. The clamps were bolted to the aluminium outside the patch area. The bolts had to be highly torqued so that the compressive stress generated in the aluminium prevented crack initiation from the bolt hole. An attempt was also made to improve the fatigue strength by building up an epoxy layer over the region of the ends of the patch before laminating so that the stress was relieved at the end in a manner similar to the type C steel patch specimens. These did not give a significant improvement since a crack initiated fairly rapidly normal to the plate surface at the position of maximum adhesive thickness. This then turned and propagated along the bondline to the aluminium plate. Again it is probable that finite element analysis could be used to derive an improved geometry. Results are shown in Fig. 7b in terms of the nominal stress range in the aluminium.

It can be seen that the clamped specimens are only just below the weld curve. For the CFRP reinforced weld specimens, clamped patches and unclamped patches bonded with fresh silane gave lifetimes 3–10 times that of a butt weld. Therefore, the endurance of these specimens was similar to the E32 bonded steel patches, although none of the CFRP specimens failed in the aluminium. Failure was by propagation of cracks along the bondline in a manner similar to that illustrated for steel specimens in Fig. 9. CFRP patches have proved satisfactory in ship repairs where the overlap was large, but when space is limited and the patches have to be small it appears that inverted taper steel patches bonded with E32 adhesive would be the best choice.



10 Example of deck repair using large CFRP (carbon fibre reinforced plastic) patch

Conclusions

The use of adhesives for attaching high modulus patch materials to aluminium structures has been shown to be a useful technique where the correct surface preparation has enabled the development of adequate adhesive strength.

It has been possible successfully to use large carbon fibre patches on deck structures (Fig. 10) to accommodate both an undulating surface and changes in deck height. Where samples have been tested with short overlaps the steel patches have been shown to have a superior fatigue strength to carbon fibre patches. This could be related to the properties of the adhesive. For bonded steel patches Permabond E32 adhesive has been shown to give a better fatigue life than E04 adhesive.

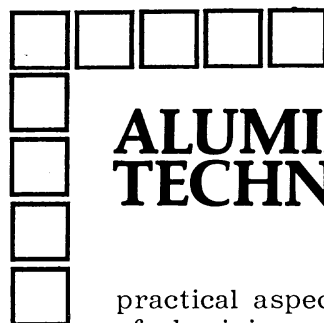
In some instances, it may be possible to use aluminium patches in place of steel, where thermal effects are a problem, provided the aluminium is thick enough to take the load.

Tapered patches have been found to be superior both for static strength and fatigue behaviour. Tapering the adhesive is more effective than tapering the patch. It would be possible to reinforce areas within an as-built structure to reduce their sensitivity to crack initiation.

The fatigue strength of patched simple butt joints has been shown to be as good as that of patched welded joints. Therefore, it may be possible to use patching without first carrying out a weld repair.

References

1. L. REDSHAW: in Proc. Symp. on 'Welding in shipbuilding'; 1962, Abington, Cambridge, The Welding Institute.
2. F. St. M. BRIERLY: *Light Met.*, April 1960.
3. C. H. POHLER, A. B. STAVOURY, J. E. BEACH, and F. F. BORRIELLO: *Nav. Eng. J.*, Oct. 1979, **91**, (5), 33.
4. 'The structural use of aluminium', British Standard Code of Practice CP 118.
5. A. A. BAKER: *Composites*, 1978, **9**, (1), 11.
6. B. DAVIS: 'Strengthening of Brinsworth Road Bridge' (Design and assembly with engineering adhesives), Cranfield Institute of Technology, 1983.
7. K. B. ARMSTRONG: in Proc. SAMPE Conf. on 'Engineering with composites', London, Mar. 1983.
8. K. W. ALLAN, S. Y. T. CHAN, and K. B. ARMSTRONG: *Int. J. Adhes. Adhes.*, 1982, **2**, (4), 239.
9. A. A. BAKER: *Compos. Struct.*, 1984, **2**, 153-181.
10. W. H. MUNSE, T. W. WILBUR, M. L. TELLALIAN, K. NICOLL, and K. WILSON: 'Fatigue characterisation of fabricated ship details for design', US Ship Structure Committee Report SSC 318, 1983.
11. W. A. DUKES, R. A. GLEDHILL, and A. J. KINLOCK: Preprints of 'Organic coatings and plastics', (ACS Philadelphia Meeting), Vol. 35, (1), p. 546.
12. R. D. ADAMS and W. C. WAKE: 'Structural adhesive joints in engineering'; 1984, London, Elsevier Applied Science Publishers.
13. W. A. LEES: personal communication, Permabond Adhesives Ltd, Eastleigh, Hants., 1984.



ALUMINIUM TECHNOLOGY '86

practical aspects and the principles of aluminium alloys, including aerospace, architecture, electronic discs, packaging and transport.

SUBJECT AREAS

- the aluminium industry: Overview delivered at the Plenary Session
- primary technology
- treatment of the melt
- casting technology
- deformation processing
- texture analysis
- recrystallisation
- corrosion and quench sensitivity
- aluminium-lithium alloys
- properties of aluminium alloys
- welding and brazing technology
- alloys for specific applications
- formability
- process modelling
- rapid solidification technology
- composites
- advances in equipment and control: melting and casting
- advances in equipment and control: deformation and processing

BOOK 391 280x210mm 850pp ISBN 0 904357 85 6 Casebound Published 1986

PRICE:

UK: £59.50 Overseas: US\$125.00 (Institute of Metals members deduct 20%)

Orders with remittance, quoting membership no. where applicable, to:

THE INSTITUTE OF METALS
Subscriber Services Department
1 Carlton House Terrace
London SW1Y 5DB

Tel. 01-839 4071 Telex 8814813



WELD REPAIR FOR FATIGUE-CRACKED JOINTS IN STEEL BRIDGES BY APPLYING LOW TEMPERATURE TRANSFORMATION WELDING WIRE

C. Miki, T. Hanji and K. Tokunaga

ABSTRACT

When repairing fatigue damage by welding, the fatigue strength of cracked joints needs to be restored and also improved to prevent the reoccurrence of cracks. In this study, a new welding wire called low temperature transformation (LTT) welding wire, which enables the introduction of compressive residual stresses around a weld bead and the reduction of weld deformation, was applied to the weld repair. Its applicability was investigated by fatigue tests with compact tension specimens and a plate girder specimen. The compact tension specimens revealed that compressive residual stresses introduced by LTT welding wire have positive effects on crack initiation and propagation behaviour. The plate girder specimen indicated that the fatigue lives of cracked joints are restored and also improved by weld repair with LTT welding wire. Therefore, weld repair with LTT welding wire makes it possible to improve the fatigue strength of cracked joints.

IIW-Thesaurus keywords: Fatigue cracks; Low temperature; Transformation; Consumables; Repair; Residual stresses; Welded joints.

1 Introduction

Bolted splices are widely used in steel structures as repair and retrofitting methods for fatigue damage [1], in which additional steel plates are attached to cracked parts with bolts to reduce acting stress. The bolted splice can be a powerful retrofitting method. However, when considering its working speed, it is not always efficient for relatively minor fatigue damage. Besides, the bolted splice cannot be applied to some fatigue cracks because of limited workspace around them.

One of the proper repair methods for minor fatigue damage can include gouging and re-welding. Weld repair will be the more cost-efficient solution and will shorten the work period, compared with the conventional bolted splice method, because no additional members such as splice plates are required. However, with weld repair, there is the possibility of inducing weld defects or residual deformation which may reduce the fatigue strength of repaired joints. In previous research on weld repair [2, 3], it has been presented that the fatigue strength of repaired joints, which depends on weld quality, can recover to the same level as the initial conditions, if cracks are completely removed. That means, even though cracked joints are restored to the initial condition with sound weld repairs, cracks will reoccur in repaired parts because the fatigue strength

of cracked joints is originally low in most of the cases. Therefore, after conventional weld repair, the fatigue strength of repaired joints must be improved by post-weld treatments [4], or stresses acting on repaired joints must be reduced by bolted splices in order to prevent the reoccurrence of cracks.

Recently, there have been studies on the improvement of fatigue strength by the use of a newly-developed welding wire, known as low transformation temperature (LTT) welding wire [5-9]. LTT welding wire enables the introduction of compressive residual stress in the vicinity of the weld bead and the reduction of weld residual deformation, which leads to the increase of fatigue strength without any post-weld treatment. Considering these advantages, previous research has attempted to use LTT welding wire in the repair of fatigue cracks initiated from welded joints, and demonstrated the possibility that weld repair through the use of LTT welding wire can restore and also increase the fatigue strength of repaired joints [10].

In this study, the efficiency of weld repair via the use of LTT welding wire was investigated in detail. Crack propagation behaviour and redistribution of residual stress in a compressive residual stress field introduced by LTT welding wire were examined, then a plate girder specimen repaired by LTT welding wire was tested to reveal the fatigue strength of the repaired girder.

2 Fatigue crack behaviour

in a compressive residual stress field introduced by weld repair

2.1 Test specimens and loading methods

The configurations and dimensions of a specimen are shown in Figure 1. Compact tension (CT) specimens were made of steel plates with 9.0 mm thickness. The mechanical properties and chemical compositions of the material are given in Table 1. A 3.0 mm-long and 0.15 mm-wide notch was machined from the specimen as a trigger of crack initiation. After fatigue cracks originated from the notch and propagated to about 20 mm in length, they were gouged as illustrated in Figure 2 and repaired by welding. This type of crack and groove shape were adopted, on the assumption that weld repair was to be applied to stop holes drilled at the crack tip in actual steel structures.

The mechanical properties and chemical compositions of the welding wire are given in Table 2. The welding condition is given in Table 3. In this study, TIG welding was employed because it is more suited to weld repair than other welding methods. Three specimens were tested

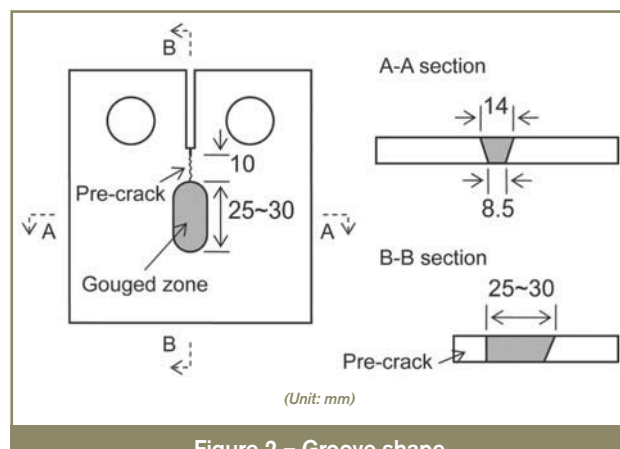


Figure 2 – Groove shape

Table 3 – Weld repair condition for CT specimen

Current [A]	Voltage [V]	Speed [cm/min]	Heat input [J/cm]
130	10~11	20.5	4 185

overall. Two were repaired using LTT welding wire and one with conventional welding wire. The specimens were clamped and welded as shown in Figures 3 and 4. Welding sequences were almost the same, but the resulting weld layers were slightly different among the specimens, as illustrated in Figure 5.

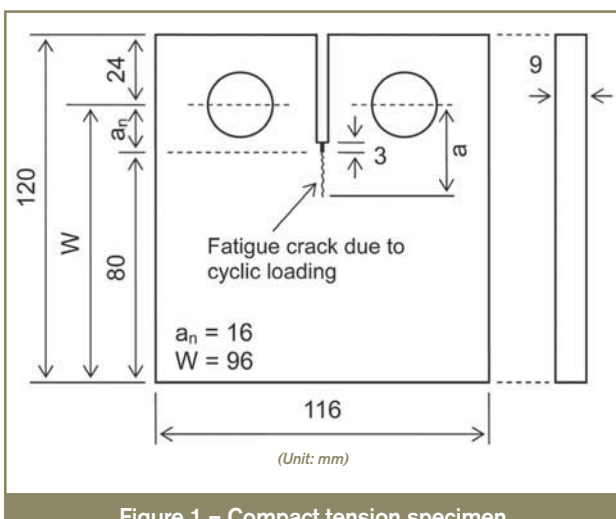


Figure 1 – Compact tension specimen

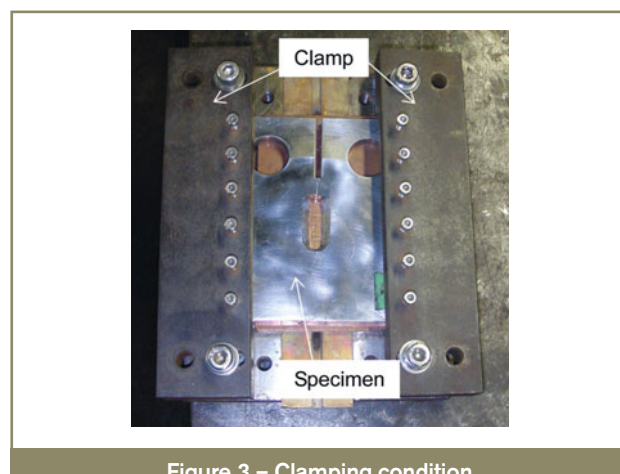


Figure 3 – Clamping condition

Table 1 – Mechanical properties and chemical compositions of material for CT specimen

Yield strength [MPa]	Tensile strength [MPa]	Elongation [%]	Chemical composition [%]								
			C	Si	Mn	P	S	Cu	Ni	Cr	Mo
439	556	25	0.15	0.38	1.53	0.01	0.002	0.03	0.03	0.01	0.001

Table 2 – Mechanical properties and chemical compositions of welding wire for CT specimen

Welding wire	Yield strength [MPa]	Tensile strength [MPa]	Ms [°C]	Chemical composition [%]							
				C	Si	Mn	P	S	Cu	Cr	Ni
LTT	808	852	350	0.055	0.17	0.25	0.007	0.004	—	—	10
Conventional	470	570	600	0.09	0.25	0.65	0.006	0.002	0.31	0.61	0.6

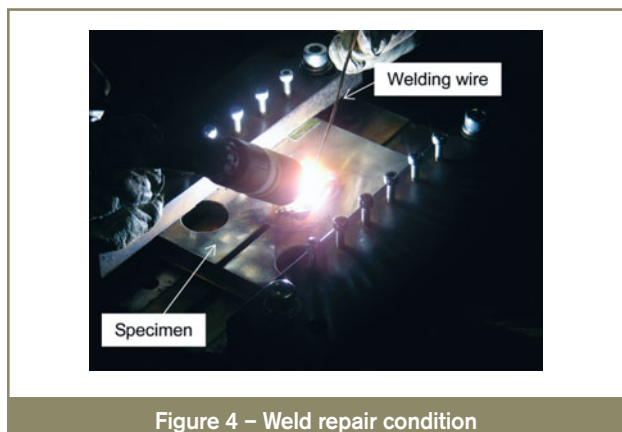


Figure 4 – Weld repair condition

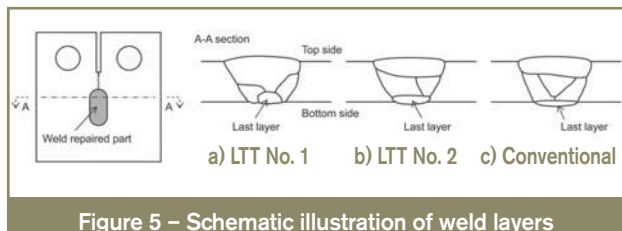


Figure 5 – Schematic illustration of weld layers

Sinusoidal wave with the frequency of 15 Hz to 20 Hz was used in the test. The details of testing procedures are described in 2.3.

42

2.2 Initial distribution of residual stress and its redistribution due to crack growth

2.2.1 Residual stress measurement methods

Residual stress, introduced by weld repair, and its redistribution due to crack propagation, were measured by strain gauges attached to the specimen surface, based on previous experiments [11]. The location of the gauges is shown in Figure 6. Initial residual stress distributions can be obtained from released strains by sectioning after specimen rupture. And, by subtracting the strain released due to crack propagation, measured periodically during the test, from the initial distribution, redistributed residual

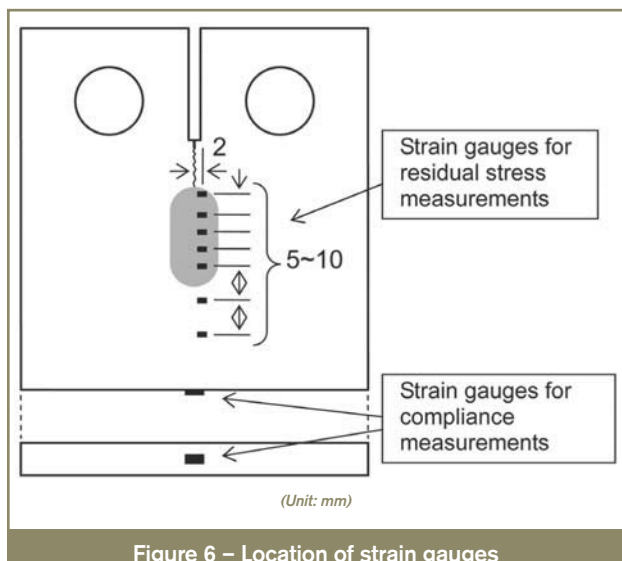


Figure 6 – Location of strain gauges

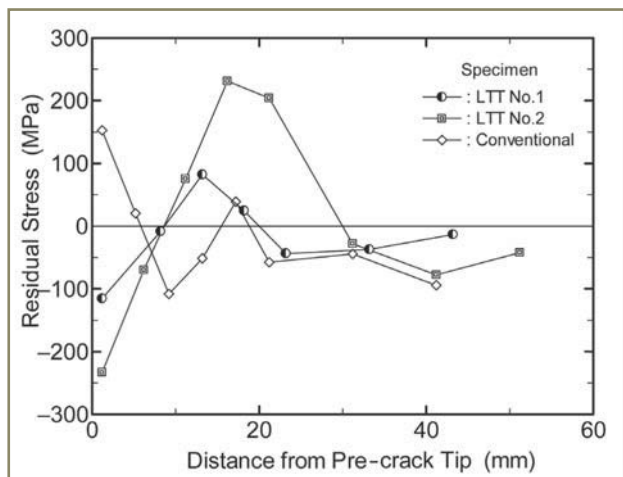


Figure 7 – Initial residual stress distribution

stress can be calculated. At the same time that strain measurements were taken during the test, fatigue crack growth was also observed on both specimen surfaces, using a digital camera with 10-power magnifying lens.

In the specimen repaired by using conventional welding wire, the experiment could not be continued due to an unexpected crack, initiated from a corner of a rectangular slit. While the cause of this phenomenon is unexplained, it might be a case specific to CT-type specimens which have a single-edge crack and low constraint around the slit. This issue will need to be investigated in detail in the future. Therefore, this specimen was artificially cut along the expected crack path, and only initial residual stress distribution was measured by using the same sectioning method.

2.2.2 Measurement results

Figure 7 shows the initial residual stress distribution measured on the top side of each specimen. Abscissa means the distance from the tip of the pre-crack in the crack propagation direction. It can be found that compressive residual stress is introduced around the tip of the specimen repaired with LTT welding wire, while tensile residual stress occurs in the specimen repaired with conventional welding wire. Furthermore, the magnitude of the compressive residual stress varies between the LTT specimens, which may be affected by differences in the weld layers.

Figure 8 indicates the redistribution behaviour of residual stress in the LTT specimen. The coordinate system is the same as in Figure 7. A solid line represents the initial distribution, and broken lines represent the distributions in some crack lengths. The residual stress distributions are different between the top and bottom sides because of multi-layer welding. According to previous research [11], in the case of a crack originating in a tensile residual stress field, residual stress near the crack tip remains tense after crack propagation, due to its redistribution. Similar redistribution behaviour has been reported when a crack occurs in a compressive residual stress field, that is,

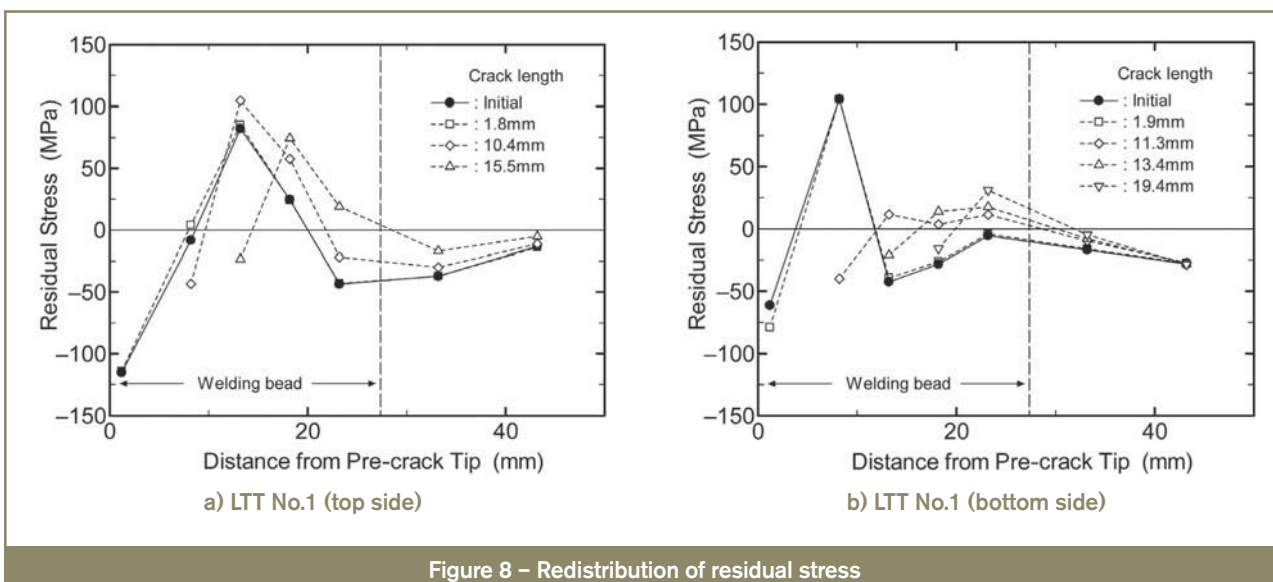


Figure 8 – Redistribution of residual stress

residual stress around the crack tip is redistributed to be compressed by crack growth [12]. In the graph, the same tendency as in the previous study [12] can be observed. The compressive residual stresses act at the crack tip in every crack length, due to the redistribution of the residual stress.

2.3 Fatigue crack initiation and propagation behaviour

Fatigue crack initiation and propagation were observed during the tests, and the effect of compressive residual stresses introduced by weld repair on the cracking behaviour was investigated.

2.3.1 Experimental procedures

In order to detect crack occurrence in the specimen before and after repair, a tip of the notch or the pre-crack was photographed by a digital camera at certain cycles on both surfaces. If the crack could not be observed in images before several millions of loading cycles, the test was suspended and re-started after increasing the load range. Similar procedures were repeated until the crack could be detected at the tip. In this study, crack initiation life was defined as the number of cycles when the crack of 1.0 mm length was found. The loading conditions when the crack was first detected were 1.4~14.0 kN, 1.2~14.0 kN and 1.5~15.0 kN in the specimens before repair, 1.95~19.5 kN in LTT No. 1 specimen, 1.96~19.6 kN in LTT No. 2 specimen.

In the specimens before repair, crack propagation tests were conducted with a limiting reduction rate in stress intensity factor to a value proposed in ASTM E647-08 [13]. The test was launched after growing the crack to at least 2 mm, and crack size measurements were made at intervals recommended by ASTM, that is, a minimum crack extension size was 0.25 mm [13]. The crack growth was measured on both sides from images taken by the digital camera. In the repaired specimen, the crack propagation

tests were performed under the same loading conditions as the crack initiation tests. Crack size measurements followed ASTM recommendations [13].

At the same time as the crack measurement, crack closure loads were also measured by the unloading elastic compliance method [14]. A strain gauge for the compliance method was attached as shown in Figure 6.

2.3.2 Crack initiation life

Generally, in notched specimens, the maximum stress range at the notch tip $\Delta\sigma_{\max}$ can be expressed in the following equation, supposing that the notch-tip radius is extremely small in comparison with the notch length [15].

$$\Delta\sigma_{\max} = \frac{2}{\sqrt{\pi}} \frac{\Delta K}{\sqrt{\rho}} \quad (1)$$

where

ρ is the radius of the notch tip and

ΔK is the stress intensity factor range calculated by assuming a notch as a fatigue crack.

The stress intensity factor range for a CT specimen can be calculated with the following equations,

$$\Delta K = \frac{\Delta P}{t\sqrt{W}} f(\alpha) \quad (2a)$$

$$f(\alpha) = \frac{(2+\alpha)}{(1-\alpha)^{3/2}} (0.886 + 4.64\alpha - 13.32\alpha^2 + 14.72\alpha^3 - 5.6\alpha^4) \quad (2b)$$

where

ΔP is the applied load range,

t is the plate thickness of the specimen and

$\alpha = a/W$, a and W are given in Figure 1.

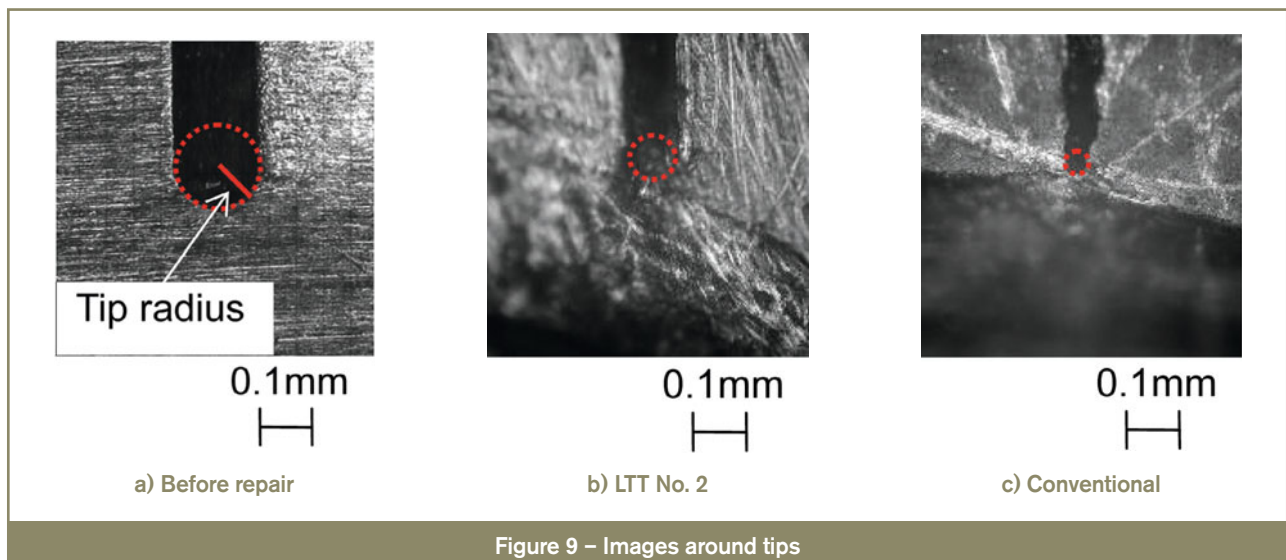


Figure 9 – Images around tips

According to Equation (1), a parameter of the stress intensity factor range, divided by the square root of the notch-tip radius, may be one of the predominant factors in fatigue crack initiation of notched specimens. This has been verified in previous experiments [16, 17]. Therefore, this study tried to correlate the crack initiation life of the specimen to the maximum stress range calculated from the stress intensity factor range and the notch tip radius.

44

The tip radius was measured with an optical microscope in advance of the experiment. Example images around the tip are indicated in Figure 9, and the measurements are summarized in Table 4. The tip radii of the specimens repaired with LTT welding wire are larger than that repaired with conventional welding wire. The reason for such may be as follows: repaired portions with LTT welding wire expand near room temperature during the cooling process, encouraging the opening of the crack. On the other hand, portions repaired using conventional welding wire cool down, with shrinkage occurring around room temperature, causing the crack to close. The measured tip radii can support the expansion and shrinkage at repaired portions. As a result of the expansion during the cooling process of the LTT-repaired portions, compressive residual stress could be introduced in the vicinity of the pre-crack tip, as shown in Figure 7.

The test results are presented in Figure 10 in terms of the maximum stress range calculated by Equation (1) versus the crack initiation life. As mentioned above, the crack initiation life is the number of cycles to the crack length of 1.0 mm. In the graph, a curve proposed by Barsom [16] is also shown in reference to the relationship. It was obtained from experiments where a notch-tip radius was 0.2 mm and the crack initiation life was defined as the

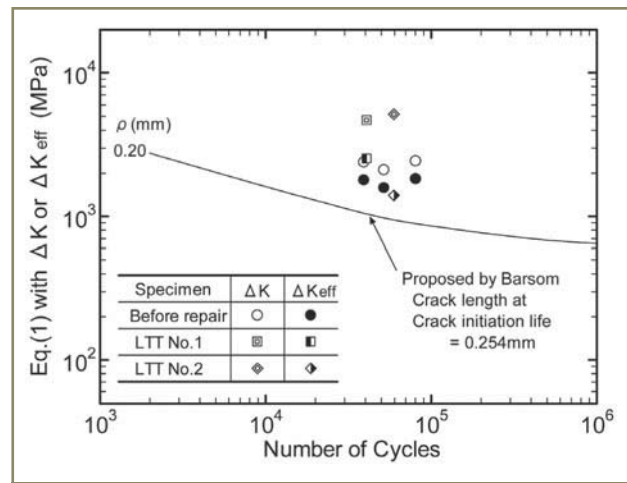


Figure 10 – Crack initiation life

number of cycles to 0.254 mm crack length. The results after repair are located higher than before repair. It means that a higher intensity of stress was required to generate cracks in the repaired specimen than in the specimen before repair. These differences in the maximum stress range for crack initiation may be caused by compressive residual stress due to the weld repair and the differences in yield strength of materials. In this study, further discussion was carried out from the viewpoint of crack closure by compressive residual stresses as described below.

2.3.3 Crack propagation behaviour

The relationships between the crack growth rate and the stress intensity factor range are indicated in Figure 11. The mean design curve proposed by the Japanese Society of Steel Construction [18] is also shown. The crack propagation behaviour differs in every specimen. The results of

Table 4 – Measurements of tip radius

Specimen	Before repair (machined notch)	LTT welding wire		Conventional welding wire
		No. 1	No. 2	
Tip radius [mm]	0.079	0.051	0.040	0.027

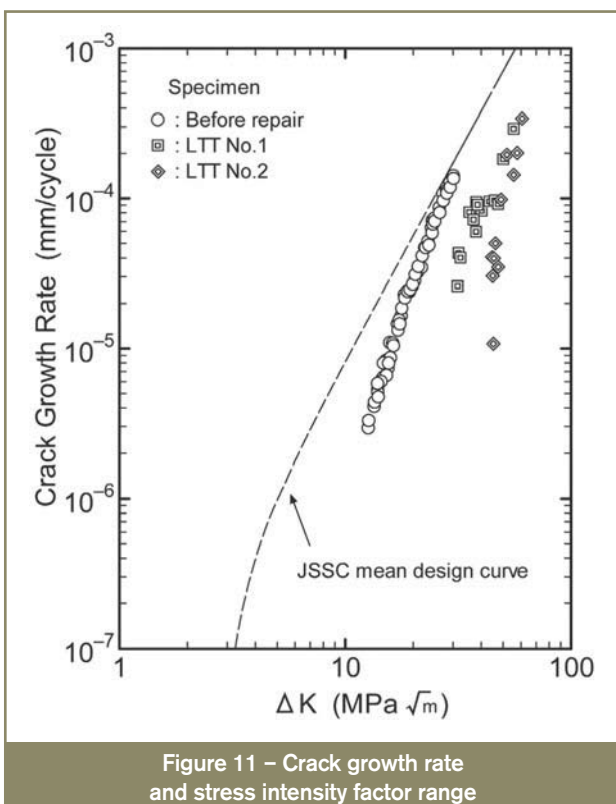


Figure 11 – Crack growth rate and stress intensity factor range

the repaired specimen lie on the right side of the results before repair, which indicates that the crack growth rate was declined by the weld repair. Also, there are slight differences between the repaired specimens due to the magnitude of the initial compressive residual stress at pre-crack tips shown in Figure 7.

2.3.4 Crack closure

Previous research has indicated that residual stress can affect crack closure behaviour and, consequently, change crack propagation characteristics when a crack runs in residual stress fields [19, 20]. In this study, the test results were discussed further in view of the crack closure behaviour.

Crack opening ratio U , which is a ratio between the load range while the crack opens and the entire load range, is calculated with the following equation,

$$U = \frac{P_{\max} - P_{cl}}{\Delta P} = \frac{\Delta K_{eff}}{\Delta K} \quad (3)$$

where

P_{\max} is the maximum value of the applied load,

P_{cl} is the load at which the crack opens under cyclic loading and

ΔK_{eff} is the effective stress intensity factor range defined by Elber [21].

Here, it is assumed that the portion of the cycle that is below the crack opening point does not contribute to fatigue crack growth because there is no change in crack-tip strain during the cyclic loading of a closed crack.

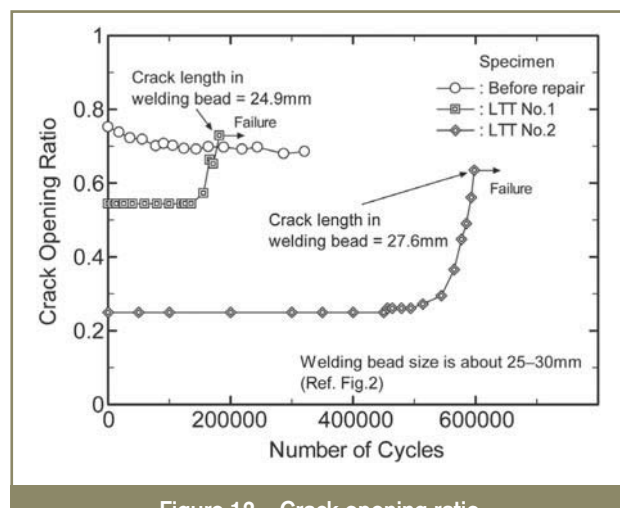


Figure 12 – Crack opening ratio

The crack opening ratio is correlated with the number of cycles in Figure 12. Abscissa is the number of cycles after the crack was detected, which means the cycles for crack propagation. The results demonstrate that the crack tip before repair is almost open over the entire load range, while less than half of the entire load range contributes to crack growth in the LTT-repaired portions. It can be assumed that these differences in the crack opening ratio lead to the differences in the crack initiation and propagation behaviour before and after repair, as shown in Figures 10 and 11. Therefore, the test results were rearranged by using the effective stress intensity factor range calculated with Equation (3).

Rearranged results are shown in Figures 10 and 13, respectively. In aspects of crack initiation and propagation, the test results before and after repair have good

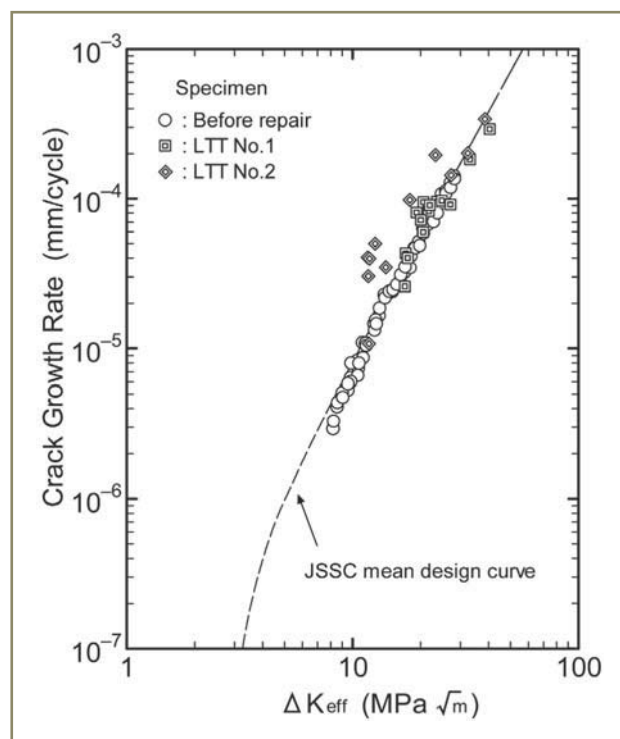


Figure 13 – Crack growth rate and effective stress intensity factor range

agreement with each other. Consequently, it can be confirmed that compressive residual stress introduced by weld repair with LTT welding wire has an influence on crack initiation and propagation behaviour. That means, even in actual structures, if cracks could be repaired by any welding with the introduction of compressive residual stresses, the fatigue life of repaired joints could be improved, as compared to that before repair.

In the next section, the effectiveness of the weld repair by applying LTT welding wire was verified by a fatigue test of a large-scale plate girder specimen.

3 Fatigue test of a plate girder specimen

A fatigue test on a large-scale plate girder specimen was carried out in order to induce fatigue cracks and to reveal the fatigue strength of the specimen before repair.

3.1 Specimen

The configuration and dimensions of the specimen are shown in Figure 14. The mechanical properties of the material are given in Table 5. A plate girder specimen has two types of welded joints on its web plate, which are out-of-plane gusset joints and cross-beam connections with coped end holes. The length and thickness of all attachments are 200 mm and 12 mm, respectively. The welded joints were placed in such a way that they would be subjected to approximately the same nominal stress range. This study focused only on the out-of-plane gusset joints represented in the left side of Figure 14.

Table 5 – Mechanical properties of the material for the girder specimen

Yield strength [MPa]	Tensile strength [MPa]	Elongation [%]
583	614	35

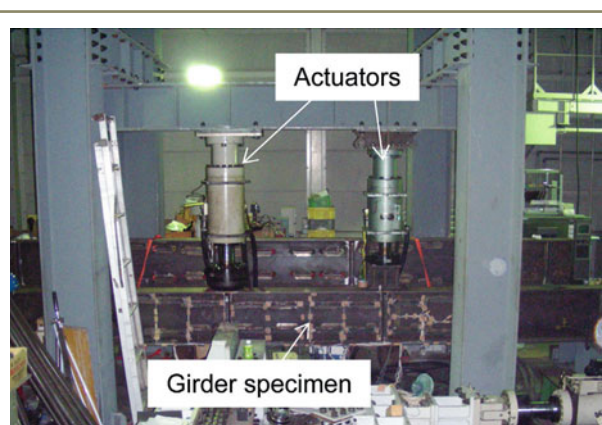


Figure 15 – Appearance of loading

3.2 Experimental procedures

Figure 15 provides a view of the experiment. The load was applied to the specimen by 4-points bending. A sinusoidal wave with the frequency of 1.0 Hz to 1.3 Hz was used in the test. Nominal stress range at the joints was about 70 MPa. Fatigue cracks were observed by Magnetic Particle testing at intervals. The loading was stopped to repair cracks after 4 million cycles.

3.3 Fatigue life before weld repair

Fatigue test results of the specimen before repair are shown in Figure 16. The fatigue life was defined as the number of cycles when the crack propagated to 10 mm in length on the web (total crack length was about 48 mm). In the graph, fatigue strength curves proposed by JSSC are also presented. The fatigue strength of this out-of-plane gusset detail scatters from JSSC-G to E class, and the lowest is located slightly below JSSC-F class.

4 Application of weld repair to the plate girder specimen

The plate girder specimen was repaired by LTT welding wire and re-tested to investigate its fatigue strength.

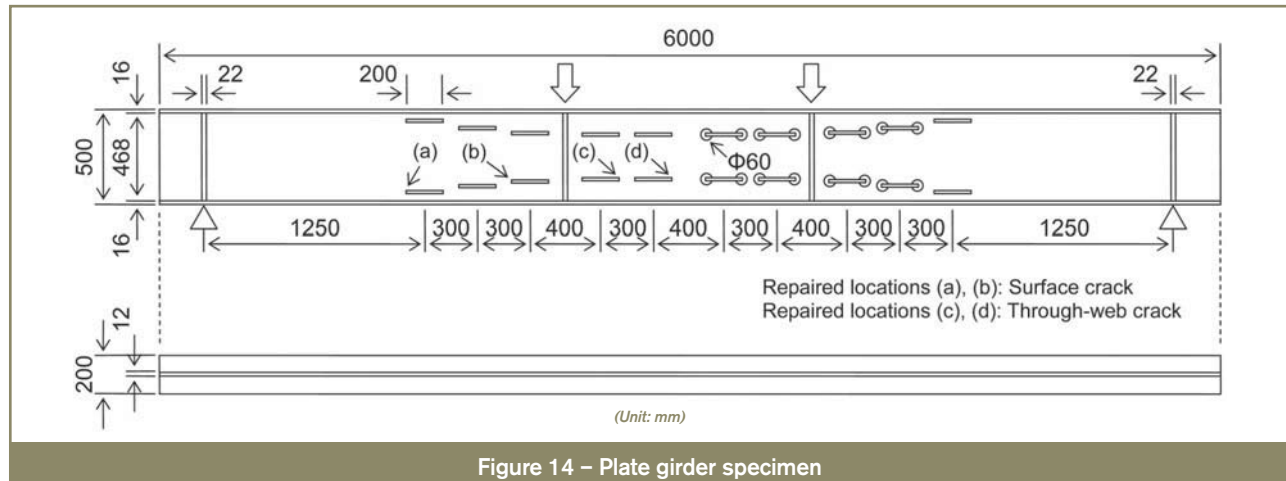


Figure 14 – Plate girder specimen

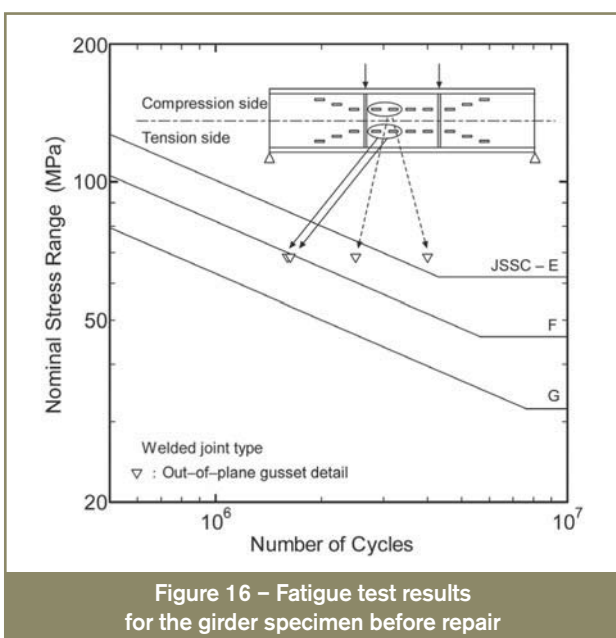


Figure 16 – Fatigue test results for the girder specimen before repair

The test was performed using the same procedures as before repair. Due to crack growth from longitudinal welds between the lower flange and the web, the test had to be ended after about 3.5 million cycles.

4.1 Weld repair procedures

As concluded in Section 2, compressive residual stresses introduced by weld repair have retardation effects on

crack initiation and propagation, leading to improvement in the fatigue strength of cracked joints. In this study, the cracks were repaired by using both LTT and conventional welding wires, based on the preliminary examination results. The preliminary test revealed that, due to welding heat cycles, multi-pass welding with LTT welding wire sometimes makes it difficult to introduce compressive residual stress around the toe of an attachment weld, and causes weld defects in its deposit. In order to overcome this difficulty, conventional welding wire was used for filling the gouged zone after the removal of cracks, and then additional welds using LTT wire were added to the welds made with conventional wire. The mechanical properties and chemical compositions of the welding material are given in Table 6.

Four locations (a) ~ (d) in Figure 14 were selected from the attachments in the tension side to clearly indicate the effect of compressive residual stresses by weld repair. Surface cracks and through-web cracks existed in (a), (b) and (c), (d), respectively. Figure 17 illustrates the schematic procedure of the weld repair. In repair types B and C, cracks are removed completely before repair, while cracks are consciously left in the web in repair types A and D. The remaining crack depth for the through-web crack was determined from the gouging depth, and for the surface crack, it was estimated from the surface length of the crack [22, 23]. Table 7 summarizes the weld repair cases. A view of the area around the weld toe before and

Table 6 – Mechanical properties and chemical compositions of the welding wire for the plate girder specimen

Welding wire	Yield strength [MPa]	Tensile strength [MPa]	Ms [°C]	Chemical composition [%]							
				C	Si	Mn	P	S	Ni	Cr	Mo
LTT	614	1 117	250	0.029	0.15	0.19	0.022	0.007	7.07	15.66	–
Conventional	540	640	–	0.07	0.42	1.12	–	–	0.73	–	0.22

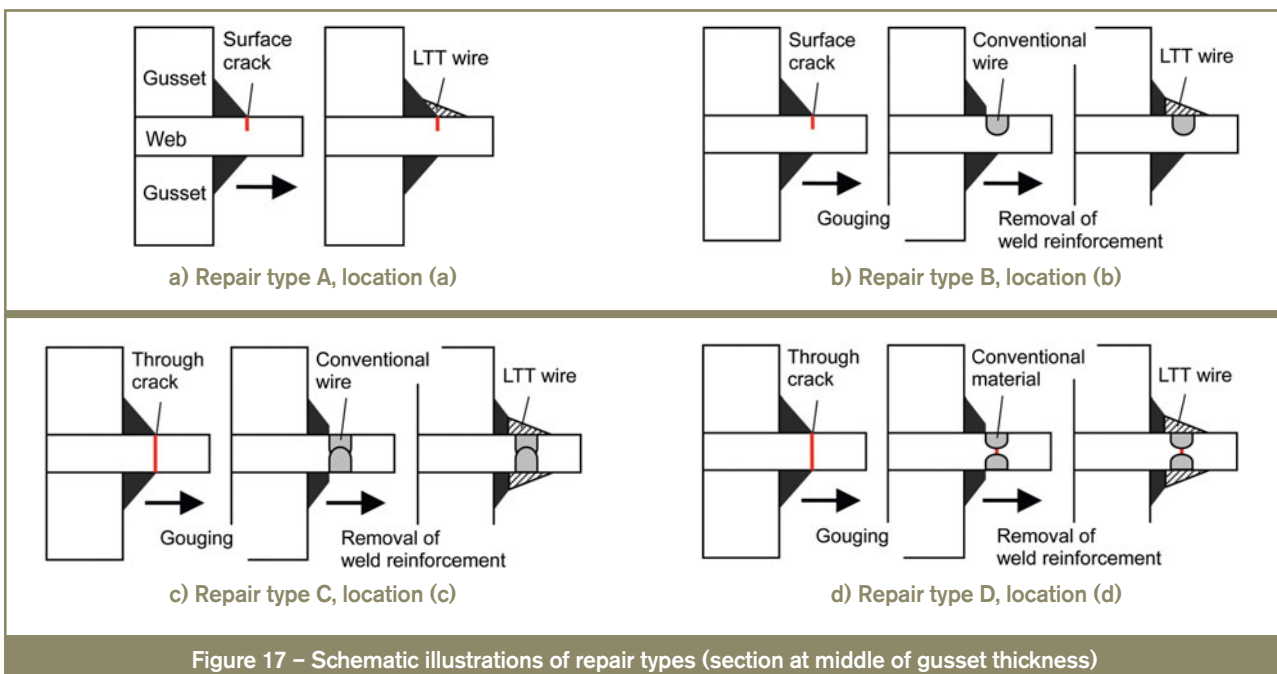


Figure 17 – Schematic illustrations of repair types (section at middle of gusset thickness)

Table 7 – Summary of weld repair cases

Repair location	a	b	c	d
Crack shape	Surface	Surface	Through	Through
Repair type	A	B	C	D
Remaining crack depth [mm]	3~5 ^{a)}	0	0	2

^{a)} Depth for surface crack was estimated from crack length on a surface.

after repair is shown in Figure 18. Table 8 provides the weld repair condition as determined according to the preliminary examination results.

4.2 Crack initiation and propagation

4.2.1 Visual observation

Figure 19 shows fatigue cracks observed during the test. The cracks were detected at two out of four repaired locations. At location (d), where the crack remained inside the web, a crack occurred from the boundary between the repaired portion and the original weld. At location (b), where the crack was completely removed, a crack originated at a weld on the opposite of the gusset plate from the repaired one, and it penetrated through the web. Another minor crack was also observed at the weld toe of the repaired portion in location (b). However, no crack was detected at locations (a) and (c).

4.2.2 Microscope observation

After the test, the repaired portions were cored and examined by optical microscopy. Images taken during the microscopy are shown in Figures 20 and 21. In location (d), crack re-initiation and a little propagation can be observed at the tip of the remaining crack, aside from the crack at the boundary between the repaired portion and the original weld. However, both cracks did not penetrate the web. At location (a), although a crack re-initiated from

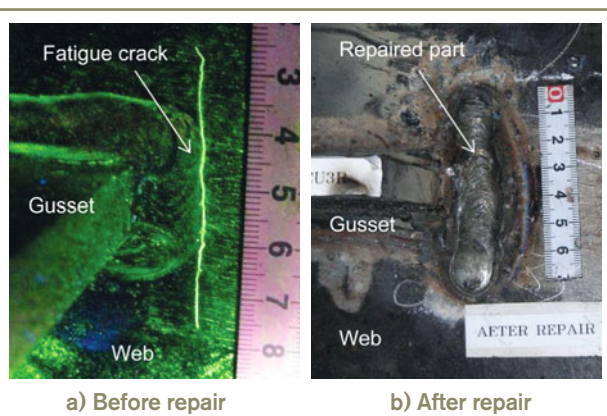


Figure 18 – Appearance of the gusset area before and after repair

Table 8 – Weld repair condition for the plate girder specimen

Current [A]	Voltage [V]	Speed [cm/min]	Heat input [J/cm]
165	36	18	19 800

the remaining crack tip, it hardly grew into the deposit of LTT welding wire. This might be because weld repair with LTT welding wire resulted in retardation or arrest of crack growth.

4.3 Fatigue life after weld repair

Figure 22 indicates the fatigue test results after repair, together with those before repair. In the graph, the results of the repaired location which did not fail during the test are represented with arrows. The fatigue strength of location (c), where no crack was re-initiated, is higher than JSSC-E class. And, at locations (a) and (d), where remaining cracks existed in the web, the fatigue strength is also satisfied with E class, although some cracks were re-initiated from the remaining crack. Therefore, it can be concluded that weld repair with LTT welding wire provides the possibility of restoring and also improving the fatigue strength of a cracked joint.

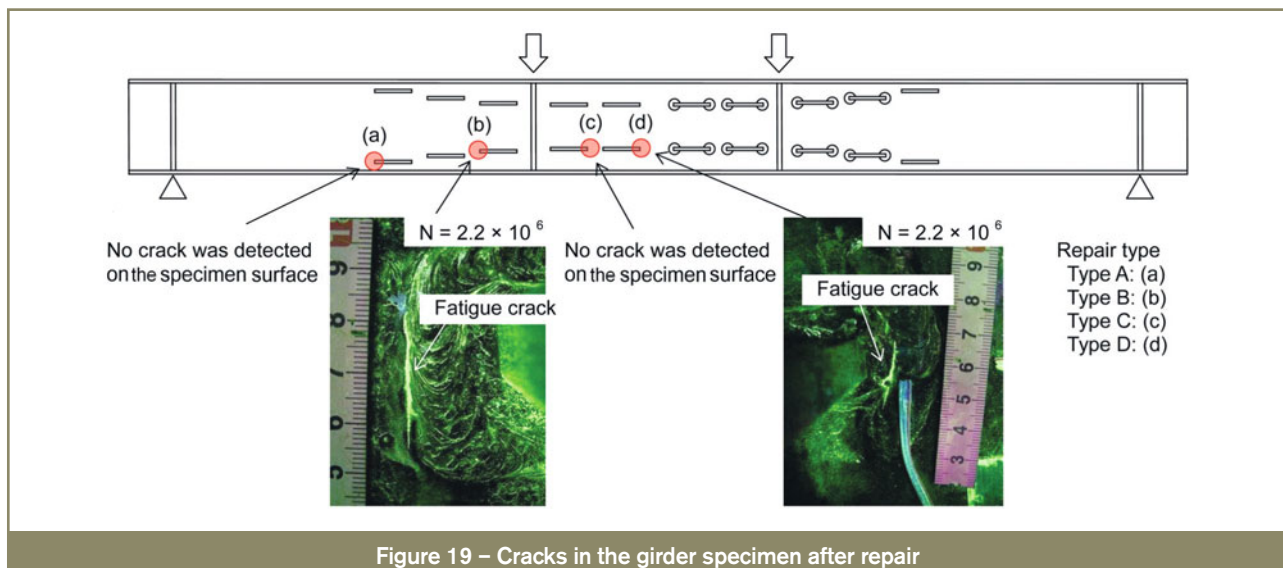


Figure 19 – Cracks in the girder specimen after repair

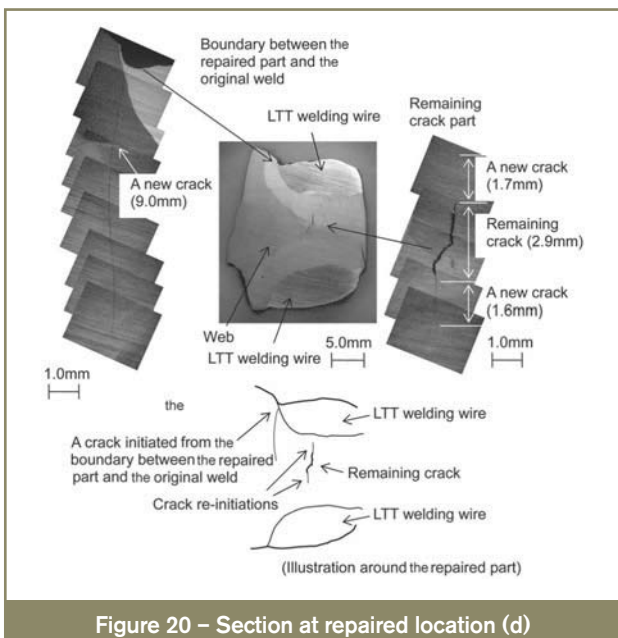


Figure 20 – Section at repaired location (d)

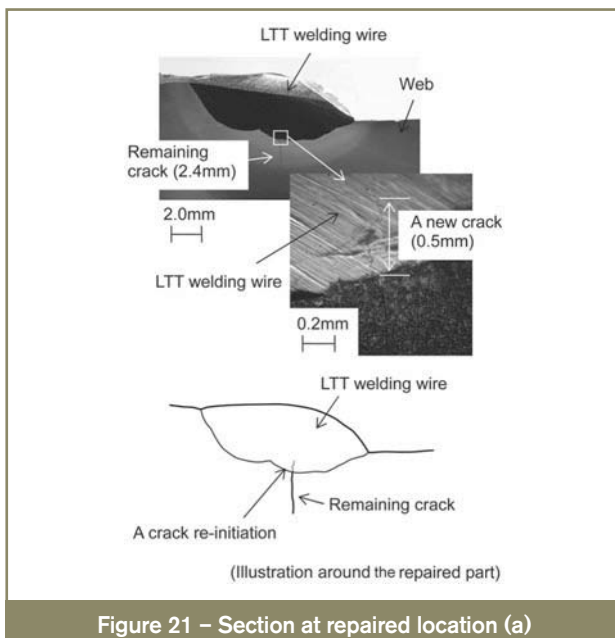


Figure 21 – Section at repaired location (a)

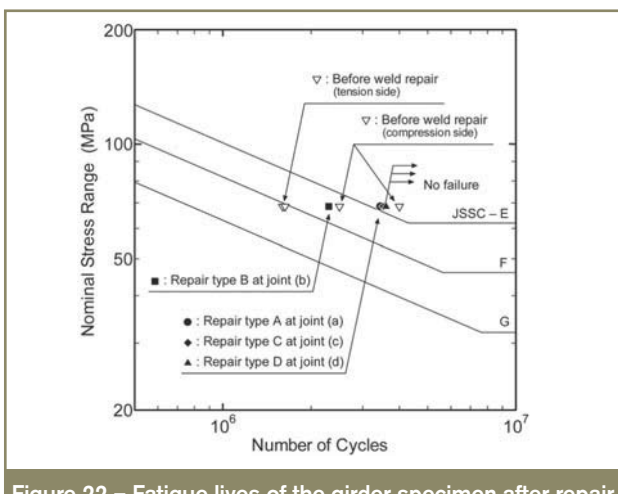


Figure 22 – Fatigue lives of the girder specimen after repair

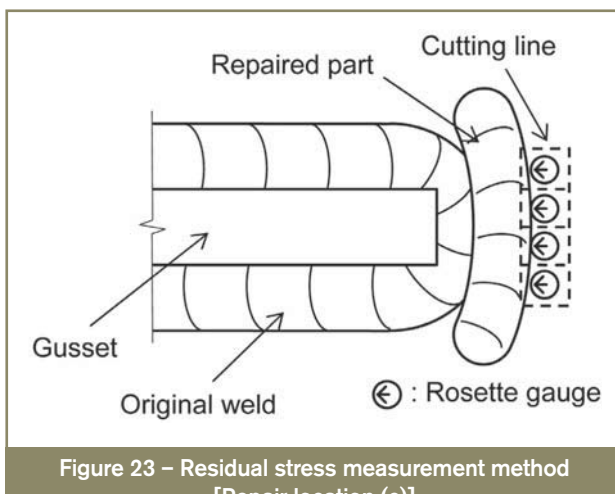


Figure 23 – Residual stress measurement method [Repair location (c)]

4.4 Residual stress measurements

Residual stress around the repaired part was measured at location (c) using the sectioning method. Figure 23 shows the locations of rosette gauges and cutting lines. Measurement results are represented in Figure 24. It is demonstrated that high compressive residual stresses are introduced around the repaired part, which can lead to the improvement of the fatigue strength of the repaired joint.

5 Summary

- In the case of a crack occurring in a compressive residual stress field, residual stress around the crack tip is re-distributed to become compression by crack propagation.
- It can be revealed that compressive residual stress introduced by weld repair with LTT welding wire has a positive effect on crack initiation and propagation behaviour.
- In a plate girder specimen, the fatigue lives of cracked joints were restored and also improved by repair with LTT welding wire.

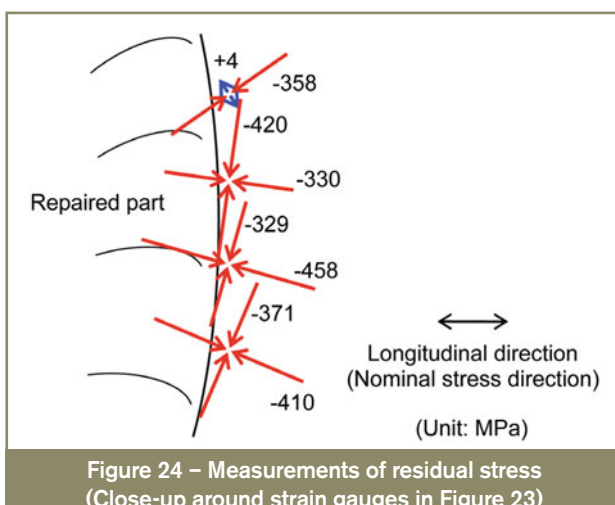


Figure 24 – Measurements of residual stress (Close-up around strain gauges in Figure 23)

- Residual stress measurements reveal that high compressive residual stresses were introduced around a repaired portion.
- It can be concluded that weld repair with LTT welding wire provides the possibility of improving the fatigue strength of a cracked joint.

Acknowledgements

The authors gratefully acknowledge the support of the Grant-in-Aid for Scientific Research (S) (18106010) in Japan.

References

- [1] Miki C.: Retrofitting engineering for fatigue damaged steel structures, IIW Doc. XIII-2284-09, 2009.
- [2] Wylde J.G.: The fatigue performance of repaired fillet welds, The Welding Institute Research Report, 1983, no. 215.
- [3] Yamada K., Sakai Y., Kondo A. and Kikuchi Y.: Weld repair of cracked beams and residual fatigue life, Proceedings of JSCE, 1986, no. 374/I-6, pp. 373s-382s.
- [4] Miki C., Takenouchi H., Mori T. and Ohkawa S.: Repair of fatigue damage in cross bracing connections in steel girder bridges, Proceedings of JSCE, 1989, no. 404/I-11, pp. 31s-39s.
- [5] Ohta A., Watanabe O., Matsuoka K., Siga C., Nishijima S., Maeda Y., Suzuki N. and Kubo T.: Fatigue strength improvement by using newly developed low transformation temperature welding material, Doc. IIW-1439, Welding in the World, 1999, vol. 43, no. 6, pp. 38-42.
- [6] Ohta A., Maeda Y., Nguyen N.T. and Suzuki N.: Fatigue strength improvement of box section beam by low transformation temperature welding wire, Doc. IIW-1481, Welding in the World, 2000, vol. 44, no. 5, pp. 26-30.
- [7] Miki C. and Anami K.: Fatigue strength improvement of welded joint by addition welding with low temperature metallurgical transformation electrode, IIW Doc. XIII-1827-00, 2000.
- [8] Ohta A., Suzuki N., Maeda Y. and Maddox S.J.: Fatigue strength improvement of lap welded joints by low transformation temperature welding wire – Superior improvement with strength of steel, Doc. IIW-1583, Welding in the World, 2003, vol. 47, no. 3/4, pp. 38-43.
- [9] Tominaga T., Ishikawa T. and Miki C.: Fatigue life improvement of existing bridge girders by low temperature transformation electrode, IIW Doc. XIII-1999-03, 2003.
- [10] Ohta A., Maeda Y. and Suzuki N.: Fatigue life extension by repairing fatigue cracks initiated around box welds with low transformation temperature welding wire, Doc. IIW-1507, Welding in the World, 2001, vol. 45, no. 5/6, pp. 3-8.
- [11] Miki C., Nishino F., Hirabayashi Y. and Takena K.: Influence of residual welding stress on fatigue crack growth rate, Proceedings of JSCE, 1983, no. 330, pp. 161-168.
- [12] Kitsunai Y., Kobayashi H., Narumoto A., Ishizuka T., Iida K. and Yoshihisa E.: Effect of residual stress on fatigue crack growth behavior of STS 42 steel weldments, Journal of JSMS, 1987, vol. 36, no. 409, pp. 1077-1083 (in Japanese).
- [13] ASTM E647-08: Standard test method for measurement of fatigue crack growth rates, 2008.
- [14] Kikukawa M., Jono M., Tanaka K. and Takatani M.: Measurement of fatigue crack propagation and crack closure at low stress intensity level by unloading elastic compliance method, Journal of JSMS, 1976, vol. 25, no. 276, pp. 899-903 (in Japanese).
- [15] Barsom J.M. and Rolfe S.T.: Fracture and fatigue control in structures, 3rd edition, ASTM International, 1999.
- [16] Barsom J.M. and McNicol R.C.: Effect of stress concentration on fatigue-crack initiation in HY-130 steel, ASTM STP 559, 1974, pp. 183-204.
- [17] Clark W.G. Jr.: Evaluation of the fatigue crack initiation properties of type 403 stainless steel in air and steam environments, ASTM STP 559, 1974, pp. 205-224.
- [18] Japanese Society of Steel Construction, Fatigue design recommendations for steel structures, 1993.
- [19] Kitsunai Y.: Effect of specimen size and configuration on fatigue crack growth behavior of mild steel butt welded joints, Journal of JSMS, 1983, vol. 32, no. 354, pp. 304-309 (in Japanese).
- [20] Murakami R. and Akizono K.: On the estimation of fatigue crack growth rate at welding residual stresses fields, Quarterly Journal of JWS, 1984, vol. 2, no. 4, pp. 144-150 (in Japanese).
- [21] Elber W.: Fatigue crack closure under cyclic tension, Engineering Fracture Mechanics, 1970, vol. 2, no. 1, pp. 37-45.
- [22] Yamada K., Makino T., Baba C. and Kikuchi Y.: Fatigue analysis based on crack growth from toe of gusset end weld, Proceedings of JSCE, 1980, no. 303, pp. 31-41 (in Japanese).
- [23] Mori T. and Miki C.: Aspect ratios of surface fatigue cracks originated in fillet welded joints, Journal of Structural Engineering, JSCE, 1995, vol. 41A, pp. 829-838 (in Japanese).

About the authors

Prof. Chitoshi MIKI (miki@cv.titech.ac.jp) and Mr Kohei TOKUNAGA (tokunaga.kab@m.titech.ac.jp), Master Course Student are both with the Department of Civil Engineering, Tokyo Institute of Technology, Tokyo, (Japan). Mr Takeshi HANJU (hanji@civil.nagoya-u.ac.jp), formerly Postdoctoral Research Assistant with the Department of Civil Engineering, Tokyo Institute of Technology is now Associate Professor with the Department of Civil Engineering, Nagoya University, Aichi (Japan).

Fatigue behaviour of welded joints with cracks, repaired by hammer peening

C. M. BRANCO¹, V. INFANTE¹ and R. BAPTISTA²

¹ICEMS/IST, Lisbon University of Technology, Lisbon, Portugal, ²ESTG/IPT, Polytechnical Institute of Setúbal, Setúbal, Portugal

Received in final form 18 February 2004

ABSTRACT Rehabilitation of a welded structure, which involves repair of cracked joints, is achieved when the local treatment for repair gives a fatigue strength in the joint equal or above the fatigue strength of the uncracked original detail. If the treatment is properly applied the rehabilitation of the detail is assured, and the nature of the weld toe improvement methods can produce a joint, after repair, with a fatigue strength and residual life greater than the initial detail. The paper presents the results obtained on a fatigue study on the rehabilitation of non-load carrying fillet welded joints loaded in bending at the main plate and with fatigue cracking at the weld toes of the attachment in the main plate and through the plate thickness. Residual stresses were measured at the surface, with X-ray diffraction. The residual stresses induced by hammer peening at the weld toe were found to be greater along the longitudinal direction of the plate than in the transverse direction. The peak residual stresses near the weld toe were found to be close to yield in compression, justifying the great benefit of hammer peening. Results of a derived gain factor, g , in fatigue life were obtained as a function of the crack depth repaired by hammer peening.

Keywords fatigue, hammer peened; improvement techniques; life prediction; weld specimens.

INTRODUCTION

The present trend is to use welded structures to the maximum of their life potential. To achieve this aim, considerable effort should be made to inspection, monitoring and repair of the damaged zones. Life extension of ageing structures is possible to achieve without putting in danger the integrity of the structures, if repair methods are introduced. Current research deals with the fatigue behaviour of welded joints in a structural steel subjected to the so-called 'local post-welding improvement techniques', and is a follow-up of research work carried out by the authors in this field.^{1,2}

The local treatment for repair should give a fatigue strength not below the fatigue strength of the original detail before it was damaged. If the treatment is properly applied, the nature of the weld toe improvement methods can produce a joint, after repair, with a fatigue strength and residual life higher than the initial detail, if this was

not subjected to an improvement treatment. The repair treatment may arrest the original fatigue cracks.

Most of the life improvement techniques, as applied to original or new welds, were established in the 1960s and early 1970s.^{3–5} A number of investigations have confirmed the benefit to be gained from improvement techniques, and large increases in the fatigue strength are usually obtained. In spite of this, some reluctance has been observed towards the introduction of improvement techniques into design recommendations, and only recently one method, toe grinding, has been allowed for in the design of offshore structures⁶ and pressure vessels.⁷

An analysis of an extensive amount of data available in the literature was made by Lieurade and co-workers.⁸ Four improvement techniques (*grinding, TIG dressing, hammer peening and shot peening*) for four types of joints (*butt, T-joints, cruciform and longitudinal joints*) were taken into account in this study.⁸ All the S-N curves were above those of as-welded assemblies. The best results were obtained with hammer peening.

The rather large increase in the fatigue strength, due to the use of improvement techniques, can be explained by

Correspondence: C. M. Branco. E-mail: cmbranco@dem.ist.utl.pt

the significant increase of a so-called initiation phase. During the initiation phase, the extension of existing 'crack-like' defects is slowed down or even stopped. The duration of this phase increases with the local fatigue life (or the decrease in the stress range).

In a review recently presented by Maddox,⁹ conclusions and recommendations were defined for hammer peening which is now part of an official IIW document of the Commission XIII.¹⁰

Damaged weld toes can be treated locally, and most frequently while the structure is in service. If the repair is successfully applied, after the treatment, a significant life extension period can be obtained. This will avoid the need for repair welding that would be the case if the detail had to be rewelded and set back into service again.

A report of significant fatigue life extensions in repaired welds by air-hammer peening is presented in Ref. [11]. In another work by the same authors¹² it is shown that air-hammer peening of the local weld toe region is a reliable technique for repairing welds with shallow surface cracks up to 3 mm long.

The more traditional fusion rewelding repair procedures are susceptible to induced metallurgical problems associated with the formation of brittle phases or another embrittling phenomenon.

There is evidence, from tests on welded steel beams, that improvement techniques, notably those relying on the introduction of compressive residual stresses, are less effective in large welded structures containing high tensile residual stresses, due to welding, than when they are used to treat small-scale specimens. That is undoubtedly

linked to the fact that the increase in fatigue life, resulting for an improvement technique—particularly one relying on compressive residual stresses—tends to decrease with increase in applied tensile mean stresses.

However, recent results obtained on real structures were very good as far as the benefit of hammer peening is concerned.¹³

Recently the authors have published data in this area, both for as-welded and defective welds.^{14–16}

The results presented in this paper cover the effect of hammer peening, mainly as a repair technique for fatigue cracks at the weld toe. Results are presented also on the impact forces, distribution of residual stresses induced by the process and S-N data for the repaired cracks.

EXPERIMENTAL DETAILS

Material, specimens and improvements processes

Table 1 gives the composition and the nominal mechanical properties of the base and weld metal used in this study—a medium strength structural steel of the 400 MPa yield class (St 52-3, DIN 17100 specification) with a weld metal in a overmatching condition. The welds were made by the covered electrode process more details of which can be found in Ref. [13]. The mechanical properties were also obtained at room temperature in tensile, compressive and LCF tests carried out in cylindrical specimens of 8–9 mm diameter and 25 mm gauge length machined from 12.5 mm thick steel plates. The results are presented in Table 2.

Table 1 Chemical compositions of base metal and weld metal

C	Si	Mn	Cr	Mo	Ni	Ti	Al	V	Cu	Co	Nb	P	S
Base metal (St 52-3 steel)													
0.131	0.413	1.44	0.063	0.024	0.034	0.009	0.029	0.043	0.018	0.013	0.005	0.011	0.005
Weld metal (E 11018-G; over matched)													
0.08	0.45	1.28	0.50	0.37	1.87							0.017	0.01

Table 2 Parameters of the monotonic and cyclic stress-strain curves [13]. St 52-3 steel

	$\sigma_{0.2}$ (MPa)	$\varepsilon_{0.2}$ (%)	E (MPa)	σ_R (MPa)	σ_f (MPa)	ε_R (%)	K'	n'	r^2
(A) Tension (monotonic) and reversed cycling ($R = -1$)									
Average	415.3	0.56	200302	571.2	356.5	14.27	—	—	—
	406.9	0.50	218254	569.4	358.3	15.04	—	—	—
Average	411.1	0.53	214273	567.3	357.4	14.65	1015.31	0.1535	0.966
(B) Compression (monotonic) and reversed cycling ($R = -1$)									
Average	0.27	205949	696.5	696.5	12.77	—	—	—	—
	0.31	203625	638.0	638.0	7.92	—	—	—	—
Average	0.29	204787	667.3	667.3	10.35	1015.31	0.1535	0.966	

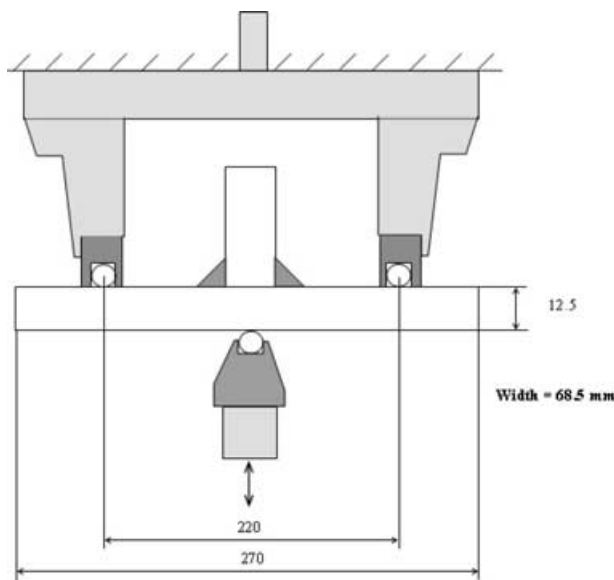


Fig. 1 Geometry of the specimens and loading arrangement. 3PB. $R = 0.1$. T-joint. St 52-3 steel.

The cyclic stress-strain curve of the material was obtained with one step level tests in cylindrical specimens and under reversed cycling ($R = -1$ and, also, $R = 0$ in tension and compression). The material exhibited mainly cyclic strain hardening behaviour. Values of the strain hardening coefficient and exponent were obtained in tension and compression.¹³ In Table 2: $\sigma_{0.2}$ and $\varepsilon_{0.2}$ are the yield stress and strain, respectively, for 0.2% offset parallel line to the elastic line, with Young's modulus, E , σ_R is σ_{UTS} , σ_f is the failure stress ($\sigma_f > \sigma_R$) ε_f is the rupture strain for σ_f . K' and n' are the cyclic strain hardening coefficient and exponent, respectively, of the Ramberg-Osgood-type curve. This was obtained with a correlation coefficient of r^2 (Table 2).

Macros of the cruciform joints of the fatigue specimens are shown in Fig. 2 as indicated. The specimen is a non-load carrying T-joint failing from the weld toe in the thickness direction. The dimensions of the specimens and details of the loading arrangement are given in Fig. 1. In the macros of Fig. 2 the boundaries of the base metal, weld metal and HAZ are clearly visible. The material has a pearlitic-ferritic-type microstructure with an average grain size of 20 μm . In the macros of Fig. 2 it is possible to detect the differences in geometry of the local geometric parameters at the weld toe, the radii, ρ and the tangent angle, θ . The toe grinding technique changes the values of ρ and θ at the weld toe as can be seen in Fig. 2.

Toe grinding was carried out with a small portable grinding fitted with a rotary barrel type tool rotating at high speed along the width of the specimen. The operation procedures were those recommended in Ref. [10].

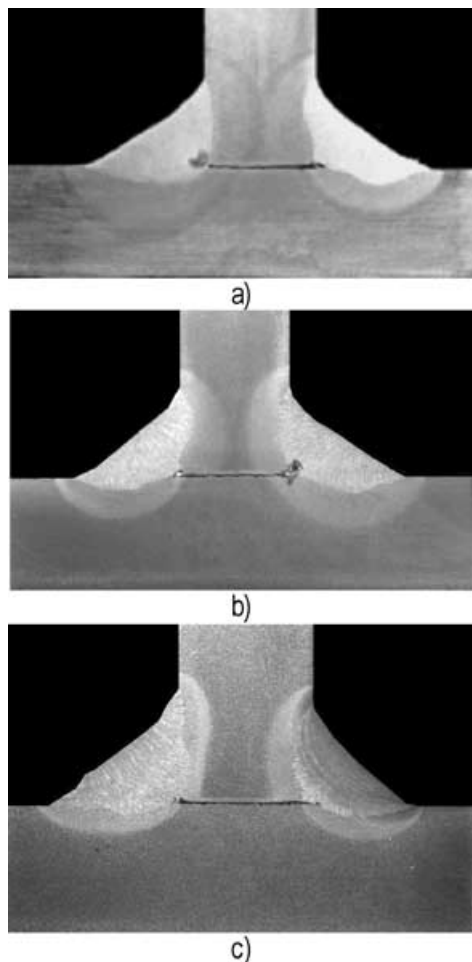


Fig. 2 Macros of the welded joints. T-joint. St 52-3 steel (a) as-welded; (b) toe ground; (c) hammer peening at weld toe.

For hammer peening, a small portable pneumatic hammer was used (Fig. 3), fitted with a special hard metal tool, instrumented with four strain gauges bonded in full bridge (Fig. 3) to measure the impact forces and stresses during the hammer peening working cycles. The tool diameter was approximately 8.5 mm, the air pressure was 3.5 bar and four passes, along the transverse direction of the specimen, were applied.¹⁰ The frequency was 3000 blows/min.

Local geometry at weld toe

Values of ρ and θ at the weld toe were obtained by optical measurement using an x - y co-ordinate table with an accuracy of 0.01 mm and 0.1 degrees, respectively. More than 100 measurements were obtained and the statistical data is given in Table 3 for the as-welded and hammer-peened specimens. A Gaussian-type correlation was obtained and the main parameters are given in Table 3 and Fig. 4a the



Fig. 3 Hammer-peening tool (high strength steel) to measure the impact forces. T-joint (Fig. 1).

Table 3 Statistical data of the measurements of radius and tangent angle at weld toe. T-joint (Fig. 1)

	Mean value	Standard deviation	Quadratic error
As-welded			
Radius	3.56 mm	2.1 mm	4.38 mm
Angle	27.33°	10.6°	112.64°
Hammer-peened			
Radius	3.05 mm	1.2 mm	1.44 mm

latter being the probability density function. The empirical fit of the probability of occurrence of the value above, is shown in Fig. 4b for the radius and for the as-welded specimens only. Analysis of the results indicates that there is a very small difference in the values of ρ between the as-welded and hammer-peened specimens. However for toe grinding ρ is greater than for as-welded and hammer peening (Fig. 2b & c). Hence the benefit of hammer peening for an increased fatigue life is due mainly to the introduction of compressive residual stresses.

Due to the morphology of the surface, in the weld toe region, after hammer peening, it was not possible to measure accurately the angle at the weld toe in the hammer-peened specimens.

Fatigue and hardness tests

The fatigue tests were carried out under constant amplitude loading in a ± 250 kN capacity servo-hydraulic fatigue test machine. The frequency was 10–15 Hz, and the stress ratio, $R = 0.1$. The bulk of the tests was carried out until complete failure of the specimen or up to a number of cycles close to 6.0×10^6 , time when the fatigue test was stopped.

In the majority of the specimens, including all the cracked ones subjected to repair, six strain gauges were bonded very close to the weld toes of the attachment. These strain gauges measured the variation of the local strain at the weld toe and along the width of the specimen, caused by the initiation and propagation of the fatigue cracks at the weld toe through the thickness direction of the longitudinal plate. The strain data were used to establish the onset of fatigue crack tip marking and to define the crack geometry to be repaired, afterwards, by

hammer peening. The strain gauge data are presented in Ref. [13].

Misalignment was checked in some specimens, using strain gauges, and it was found to be negligible.

Vickers data with 1 kg was obtained along the longitudinal directions of the plate, close to the upper and lower surfaces. The variation of hardness along the thickness of the specimen at the weld toe and in the crack propagation direction was also obtained. The main objective of these tests was to compare the hardness distributions for the as-welded and hammer-peened specimens.

RESULTS AND DISCUSSION

Analysis of the hammer-peening process

The variation of the hammer peening impact forces and stresses in the tool, as measured by the strain gauges, is depicted in Fig. 5. The duration of the treatment (working cycles) is indicated in Fig. 5. The mean values quoted in Fig. 5 are the static values that produce the same area under the dynamic stress or load cycle imposed by the tool in the material.

In the fast cycle (approximately 3 s duration) the mean force is significantly larger than in the slow cycle (approximately 35 s duration). The latter cycle follows the procedures recommended in Ref. [10] giving an impact speed between 50 and 100 mm/min in the direction of the length of the weldment (width of the specimen). With these results (Fig. 5) it is expected that the residual stresses in fast cycles will be higher than in the recommended slower impact cycles. Work is in progress to assess this behaviour.

The fatigue tests were only carried out with specimens treated with 'fast' cycle (Fig. 5a).

Hardness data

In the hammer-peened joints, an increase in hardness was obtained, and the hardness profile, through the plate thickness, shows peak values close to 260 HV near the surface at the weld toe zone (Fig. 6). Figure 6 also shows that the depth of the zone affected by the hammer peening is about 2.5 mm, i.e. the material has hardened up to this depth, and this could be the limit of the residual stress field created by hammer peening. This result also indicates that the treatment could be effective if the crack is inside this hardened zone, where the hardness increases

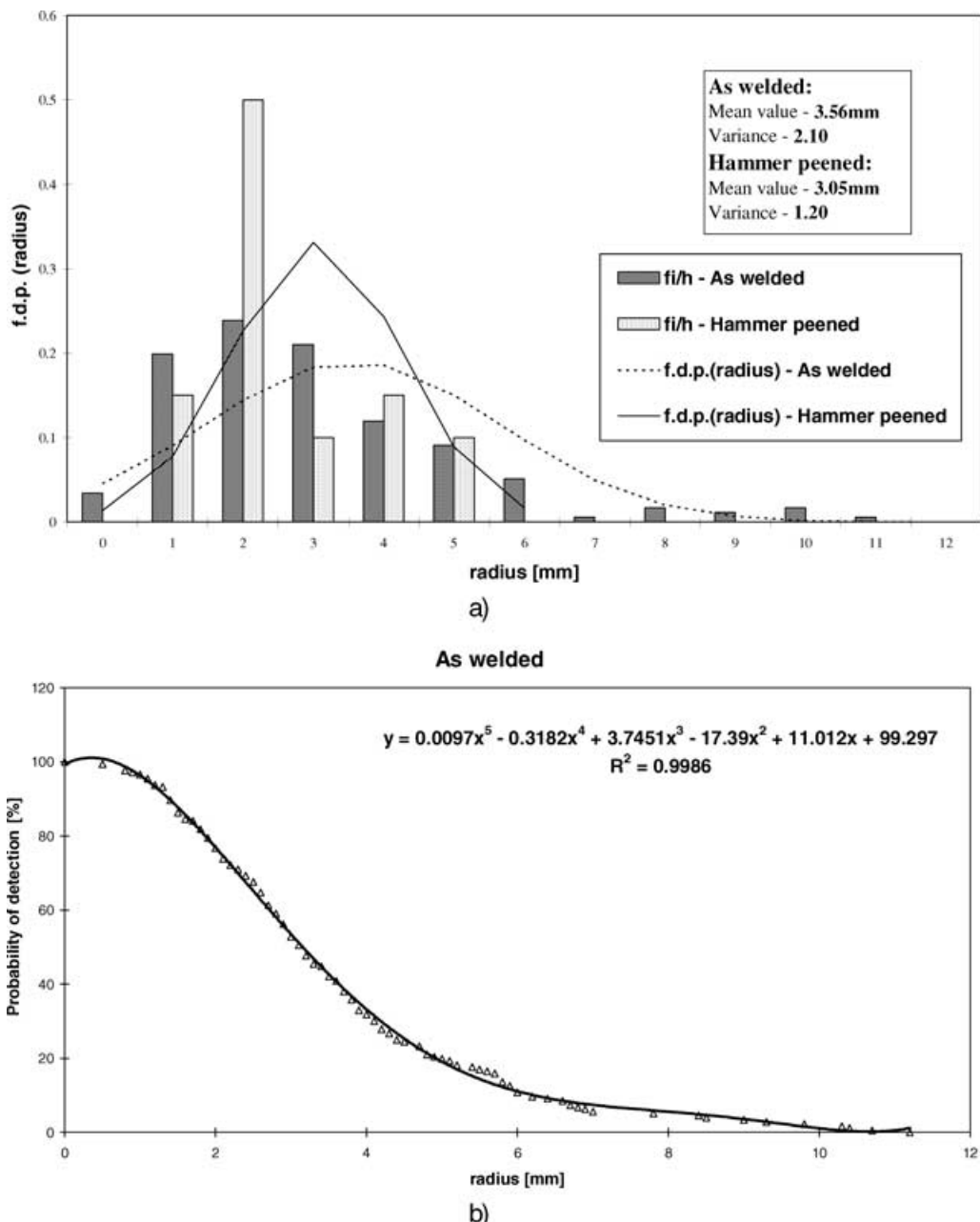


Fig. 4 Statistical data of the local geometry at the weld toe. T-joint (Fig. 1). St 52-3 steel (a) P.D.F. for the radius ρ (as-welded and hammer-peened joints); (b) probability of occurrence of the value above for the radius ρ . As-welded joints.

from near the value 190 HV of the base metal up to near 260 HV at the surface at the weld toe in the WM/HAZ hammer-peened zone.

Fatigue data in the welded joints

Two typical plots of the variation of strain in the weld toe region are shown in Figs 7a and b. These can be used to detect crack initiation life, N_i , and also to define a crack marking death, at the associated number of cycles, N_{bm} ,

or the number of cycles of crack propagation, N_{bh} , before hammer peening was carried out N_{bh} .

The crack initiation life, N_i was defined for the first variation in strain in the strain gauge(s) due to the nucleation of the crack near the strain gauge closest to the crack. (strain gauge 5 in Fig. 7a and strain gauge 2 in Fig. 7b). The depth of the repaired cracks was defined as indicated in Fig. 7.

Specimens failed by crack propagation from the weld toe and through the plate thickness.

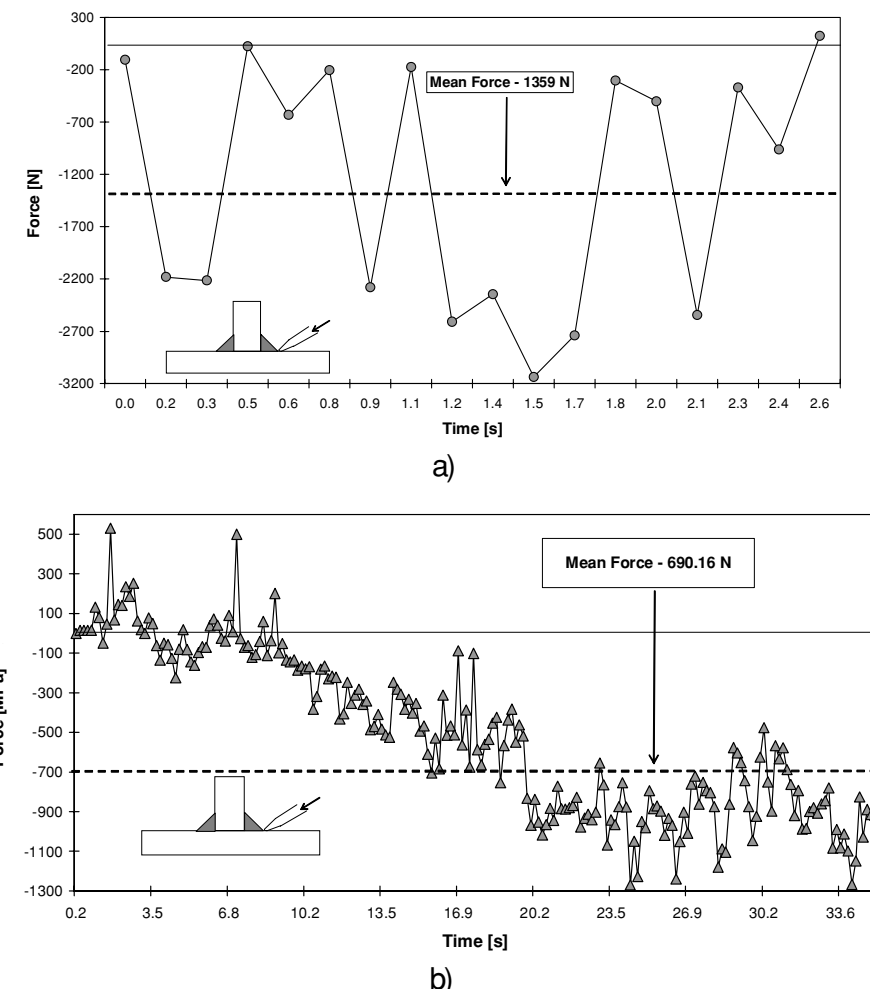


Fig. 5 Variation of impact forces and stresses measured in the hammer-peening tool (Fig. 3) during the treatment at weld toe (one pass). (a) Fast hammer-peening cycle; (b) slow hammer-peening cycles (recommended in Ref. [10]).

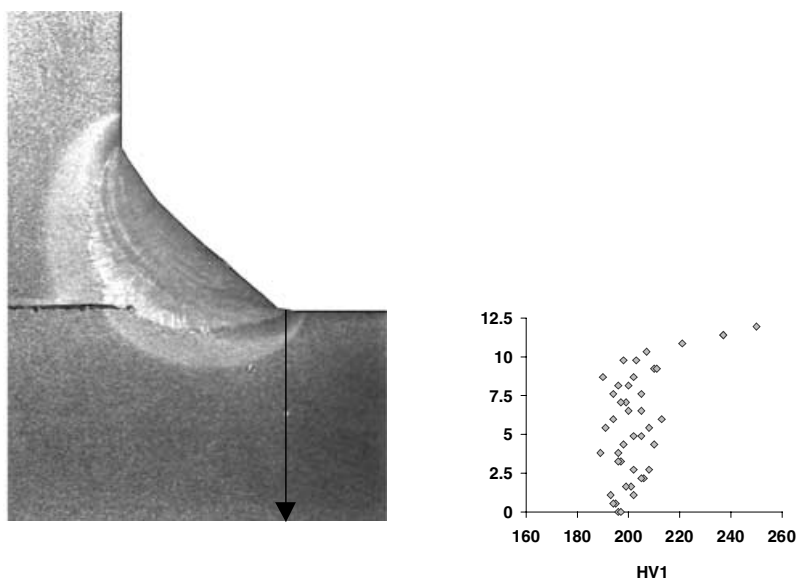


Fig. 6 Hardness plot along the plate thickness y_i in the weld toe line for the hammer-peened joints. HV1. T-joints. St 52-3 steel.

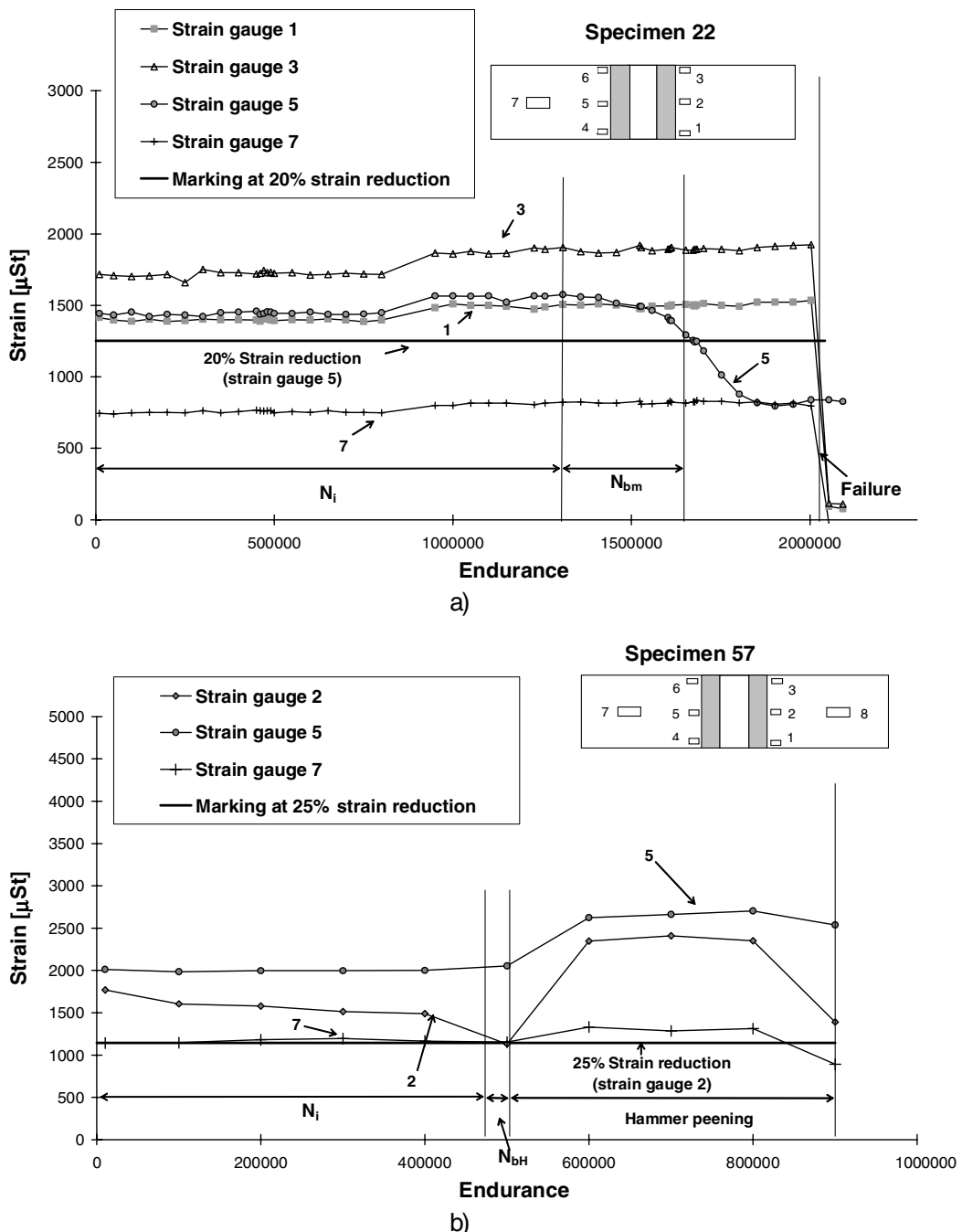


Fig. 7 Variation of strain, at weld toe region, with the number of cycles to detect crack initiation and define number of cycles to detect crack initiation and define number of cycles of marking. N_{bm} . T-joints (Fig. 1). $R = 0.1$. St 52-3 steel (a) as-welded with marking of a crack depth $a_H = 1.67$ mm. $\Delta\sigma = 325$ MPa (20% of strain reduction); (b) specimen repaired by hammer peening of a crack of $a_H = 1.27$ mm (25% reduction of strain) $\Delta\sigma = 325$ MPa.

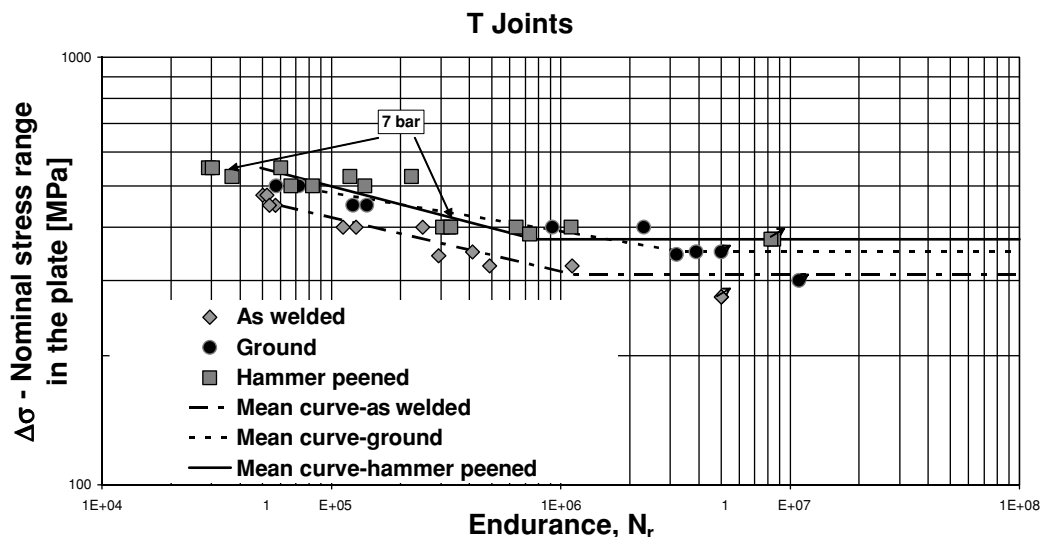
An improvement in fatigue behaviour was obtained in the treated joints. Thus, for fatigue lives above 10^6 cycles, hammer peening provides higher fatigue strength since higher fatigue limit stresses were obtained (≈ 350 MPa). Progressively higher fatigue crack initiation periods were obtained in the toe ground and

hammer-peened joints, as reflected by the higher values of m in the equation of the S-N curve (Table 4 and Fig. 8).

The results (Fig. 8) show that the fatigue strength of this detail is very high. Comparisons can be made with available fatigue design S-N codes.^{17,18}

Table 4 Values of K_o and m for the non-repaired specimens. S-N curves. $N_r = \frac{K_0}{(\Delta\sigma)^m}$ T-joint. 3 PB. $R = 0.1$ (Fig. 1)

Ref. ($R = 0.1$)	M	K_o	r^2	Gain in fatigue strength (2×10^6 cycles)	Gain in fatigue strength (3×10^6 cycles)	Gain in fatigue life ($\Delta\sigma = 350$ MPa)
As-welded	8.263	4.99×10^{26}	0.9469	1	1	1
Toe grinding	11.068	4.93×10^{34}	0.9380	$(367.4/294.0) = 1.25$	$(350.0/294.0) = 1.19$	$(3.4 \times 10^6/4.7 \times 10^5) = 7.22$
Hammer peening	6.751	1.85×10^{23}	0.7866	$(325.6/294.0) = 1.11$	$(375.0/294.0) = 1.27$	$(1.2 \times 10^6/4.7 \times 10^5) = 2.60$

**Fig. 8** S-N data and best fit of data for the as-welded, toe ground and hammer-peening joints. T-joint (Fig. 1). Unrepaired specimens. $R = 0.1$. 3PB. St 52-3 steel.**Table 5** S-N data for the repaired joints by hammer-peening T-joint (Fig. 1)

Ref.	$\Delta\sigma$ (MPa)	N_i (cycles)	N_r (cycles)	Condition
22	325	1 357 537	2 024 529	As-welded only with fatigue marking
23	325	260 000	489 201	As-welded only with fatigue marking
24	325	65 100	1 398 259	As-welded initially and repaired by hammer peening
26	400	75 000	156 255	As-welded initially and repaired by hammer peening
27	400	10 000	230 613	As-welded initially and repaired by hammer peening
28	400	100 000	379 581	As-welded initially and repaired by hammer peening
29	300	2 080 000	3 401 893	As-welded initially and repaired by hammer peening
53	400	100 000	543 810	As-welded initially and repaired by hammer peening
		261254*	—	As-welded initially and repaired by hammer peening
54	325	360 000	514 619	As-welded initially and repaired by hammer peening
57	325	470 000	3 506 191	As-welded initially and repaired by hammer peening
		263809*	—	As-welded initially and repaired by hammer peening
57	400	—	900 266	As-welded initially and repaired by hammer peening
38	500	10 000	111 939	Hammer-peened initially and repaired by hammer peening
46	500	85 000	144 252	Hammer-peened initially and repaired by hammer peening
47	500	30 000	93 809	Hammer-peened initially and repaired by hammer peening

Note: $\Delta\sigma$ is the nominal stress range in bending in the weld toe area. It was only possible to obtain N_{iaH} values after hammer peening in a few specimens (Table 5).

* N_{iaH} —Number of cycles of crack initiation after hammer peening.

Fatigue endurance was defined as the number of cycles, N_r , to initiate and propagate fatigue cracks up to final failure.

Results of fatigue life in the repaired joints

The S-N data is given in Table 5 and these results are plotted in Figs 9 and 10 for comparison with the appropriate S-N curves for the unrepaired joints shown in Fig. 8. It is seen that, for the initial untreated welded joints (Fig. 8), an increase in fatigue life was obtained after repair by hammer peening (Fig. 9) because all the data points (Table 5) of the

repaired joints are above the S-N curve of the unrepaired as-welded joints. Also, the results of the repaired joints are very close to the S-N curve of the specimens which were subjected initially to the hammer-peening treatment (Fig. 10). Therefore repair of fatigue cracks by hammer peening gives an improved life in comparison with the unrepaired joints and only a negligible variation of fatigue life was obtained as against the fatigue life results obtained in the joints subjected to hammer peening initially (with no fatigue cracks). Then repair by hammer peening of existing fatigue cracks gives a very similar improvement in fatigue life as if the treatment was applied initially.

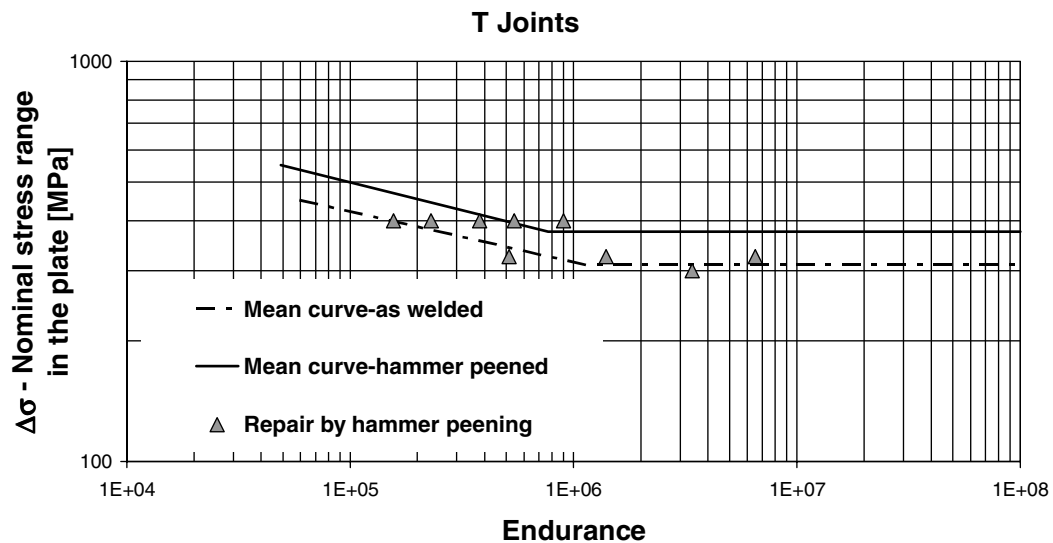


Fig. 9 S-N results for the as-welded specimens with fatigue cracks repaired with hammer peening. T-joints (Fig. 1). $R = 0.1$. 3PB. St. 52-3 steel.

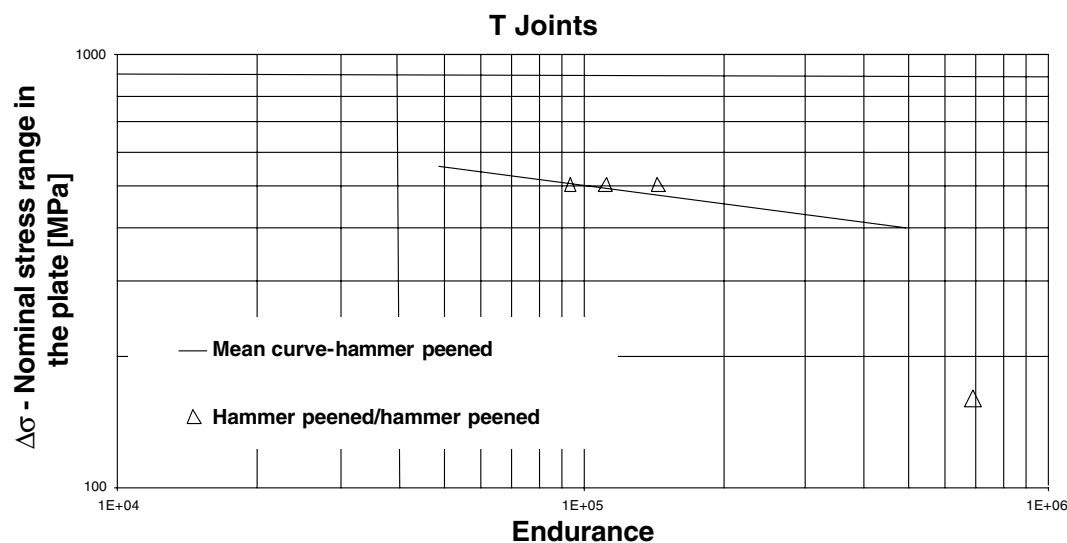


Fig. 10 S-N results for hammer-peened specimens with fatigue cracks repaired by hammer peening. T-joints (Fig. 1). $R = 0.1$. 3PB. St 52-3 steel.

Table 6 Fatigue life data for as-welded specimens with cracks treated (repaired) by hammer peening. $R = 0.1$. T-joint (Fig. 1)

Specimen	$\Delta\sigma$ (MPa)	$\Delta\sigma$ (as-welded) (MPa)	a_H (mm)	c_H (mm)	N_{bH} (cycles)	N_i (cycles)	N_{paH}^{**}, N_{aH}^*
24	325	307	2.41	5.36	202306	65100	1130853*
26	400	400	3.18	18.29	42321	75000	38934**
27	400	382	2.50	7.72	88458	10000	132155*
28	400	360	4.0	9.21	109237	100000	170344**
29	300	276	3.3	5.81	427107	2080000	1194786**
53	400	344	1.44	11.96	38746	100000	405064*
54	325	347	6.1	26.84	132775	360000	21914**
57	325	275	1.27	3.69	—	470000	—
57	400	324	1.27	3.69	—	—	394075*

N_{paH}^{**} , Calculated values of N_{paH} ; $N_{iaH} = 261254$ cycles.

For the repaired joints (Fig. 9) a correlation was not fitted to the results since crack depth is another variable, but comparisons can be made on a basis of constant stress or for a range of fatigue lives.

From data in Fig. 9 it is apparent that a crack may not change significantly the compressive residual stress field of hammer peening. For initial hammer-peened joints (Table 5) a second hammer-peening treatment applied for repair of an existing crack does not provide any significant improvement in fatigue life as shown in Fig. 10. This is due to the fact that the beneficial effect of hammer peening is mainly a consequence of the initial residual stress field left in compression, due to hammer peening, as will be analysed later.

For the conditions in Fig. 10 the material attains a shake down state in the initial treatment by hammer peening, and any additional impact stresses induced by a second set of hammer peening will not change significantly the residual stress field.

Detailed work is in progress in this area using an elastic-plastic 3D FE model to compute the residual stresses caused by hammer-peening operations.¹⁹

Gain factors g_N and g_s to quantify the beneficial effects of hammer peening in repair could be defined as:

$$g = \frac{N_r}{N_e}. \quad (1)$$

For g_N , N_r is the fatigue life of the repaired joint and N_e is the expected fatigue life of the joint if it was not repaired. The g factor depends on the crack depth, a_H of the repaired crack and also on the applied stress range. No correlation was obtained with the stress range but a correlation was obtained with the crack depth. This is valid since for these specimens stress range variation in the fatigue specimens was small (Table 5).

In Eq. (1a) N_r and N_e are given by the equations

$$N_r = N_i + N_{bH} + N_{aH}, \quad (2)$$

where N_i is the crack initiation life before the first crack for repair starts (Figs 7a & b); N_{bH} is the fatigue life in crack propagation (Figs 7a & b) and Table 6 before repair by hammer peening was carried out in a crack with dimensions a_H ; and c_H and N_{aH} is the fatigue life after repair which will include crack initiation and crack propagation periods (Fig. 7a & b). Both N_{bH} and N_{aH} were obtained experimentally:

$$N_{aH} = N_{iaH} + N_{paH}. \quad (3)$$

N_{iaH} was obtained experimentally and N_{paH} can also be calculated.¹³

Finally, N_e will be given by the equation:

$$N_e = N_i + N_{bH} + N'_{aH}, \quad (4)$$

where N'_{aH} is the fatigue life (in crack propagation) that would be obtained in the specimen if repair by hammer peening was not introduced.

N'_{aH} is therefore the number of cycles to propagate an initial crack from the size (a_H ; c_H) to the size for the failure criterion ($a_H = B/2$) where B is the specimen plate thickness. This failure criterion is acceptable as seen in the macros of fracture surfaces in Fig. 11a and b, since the applied nominal stress range has not varied very significantly in the specimens (Table 5).

Calculated values of N_{paH} were obtained from integration of the Paris law of the material with values of constant C and exponent m obtained in crack propagation tests carried out on the same material²⁰ $C = 1.36 \times 10^{-11}$ [mm/cycle]; $m = 3.34$. The appropriate LEFM K solution was taken from B57910.²¹

For the specimens in Table 5 the results obtained for the terms in Eqs (2)–(4) are presented in Tables 6 and 7 and the values of the gain factor g_N (Table 7) are plotted in Fig. 12 against crack depth of the repaired crack.

More appropriate values of C and m should have been used to predict the N_{paH} values in the hammer-peened material (Fig. 11b). However, it is known in the

literature^{8,9} that the values of C and m do not vary significantly with the hardness and strength in carbon steels. Therefore crack propagation behaviour in the hammer-peened zone is expected to have values very similar to the metal leading also to similar values of N_{paH} for both regions. Thus, the increase in fatigue life in hammer-peened joints is due to increased crack initiation life induced by the compressive residual stresses in the critical areas. A discussion on residual stress values is presented in the section 'Residual stress management'.

For the initial as-welded joints the gain factor g_N increases for small repaired crack depths and one order of

magnitude in fatigue life $g \approx 10$ could be obtained for crack depths in the region 1–1.5 mm. For crack depths above 3 mm, the increase in fatigue life is very small (Fig. 12) (g_N between 1 and 2.5) and for crack depths above 5 mm, the value of g_N is very close to 1 (no benefit). Therefore, repair by hammer peening is effective if the crack tip region is still within the depth of the region where hardness has increased due to the hammer-peening treatment (Fig. 6). The scatter obtained in the results of Fig. 12 should be mainly attributed to the values of stress range, $\Delta\sigma$, in the specimens which were not constant (Tables 6 & 7) although with a small variation.

For the initial hammer-peened specimens, and as expected from above and from the S-N curves in Fig. 10, the gain factor is very small (Fig. 12 & Table 7). In the majority of specimens the number of cycles after repair by hammer peening, N_{aH} , was greater than N_{bH} . This is due to the greater crack initiation phase after hammer peening ($N_{iaH} > N_{paH}$ in Eq. (3)). Work is in progress to predict the crack initiation phases using LCF data obtained in the base metal (Table 2) applied to local stress-strain models.²² Also for the specimens subjected to the second hammer peening for repair (Fig. 10) prediction of N_{aH} should be made taking into account the strain hardening and increase in hardness induced by the initial hammer peening applied after welding.

The gain factor for strength, g_S was calculated for the fatigue endurance, N_r of the repaired specimens. The values of g_S are in Table 7 and the plot g_S against crack depth a_H , as in Fig. 12, is in Fig. 13. In Eq. (1b) for g_S , $\Delta\sigma$ is the applied stress range in the fatigue tests of the repaired specimens and $\Delta\sigma_{aw}$ is the fatigue strength for the as-welded specimen and for the same value of N_r , whose values are in Table 7. The results for g_S show some scatter due to the difference in N_r values from specimen to specimen. However g_S is always greater than 1, and increases

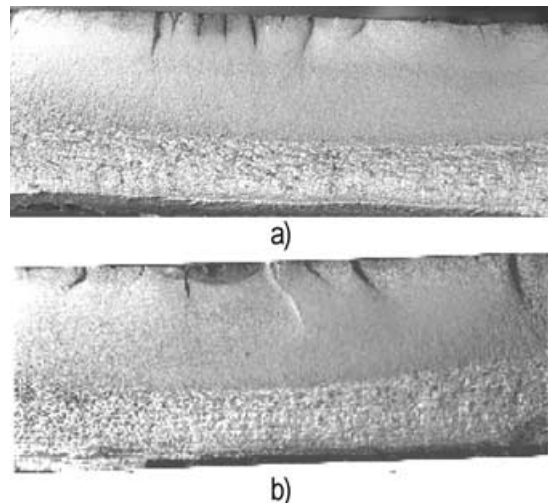


Fig. 11 Macros of fracture surfaces of fatigue specimens. T-joints (Fig. 1). 3PB. $R = 0.1$ St 52-3 steel. (a) As-welded only with fatigue marking at 40% strain reduction. $a_H = 3.86$ mm. $\Delta\sigma = 325$ MPa. $N_T = 489201$ cycles. (b) Repaired by hammer peening of a crack depth of 1.27 mm. Fatigue marking of 25% strain reduction. $\Delta\sigma = 325$ MPa. $N_T = 900266$ cycles.

Table 7 Continuation of Table 6 and also Hammer-peening specimens repaired by hammer peening. $R = 0.1$. T-joint (Fig. 1)

Specimen	$\Delta\sigma$ (as-welded) [Mpa]	a_H (mm)	N_{paH}^{**}, N_{aH}^*	N_e	N_r	g_N	g_S
24	307	—	344398**	344399	1398259	4.06	1.06
26	400	—	124523*	125004	156255	1.25	1.00
27	382	—	126741**	126710	230613	1.82	1.05
28	360	—	230795*	208561	379581	1.82	1.11
29	276	—	2603875*	2074325	3401893	1.64	1.09
53	344	—	147153**	415122	543810	1.31	1.16
54	347	—	493360*	139086	514619	3.70	0.94
57	275	—	594434**	6255953	3506181	1.04	1.18
57	324	—	—	82211	900206	10.95	1.23
38	417	2.37	36107	86107	111939	1.30	1.20
46	404	3.98	19330	137383	144252	1.05	1.24
47	426	2.87	33507	80870	93809	1.16	1.17

$N_{iaH} = 263809$ cycles.

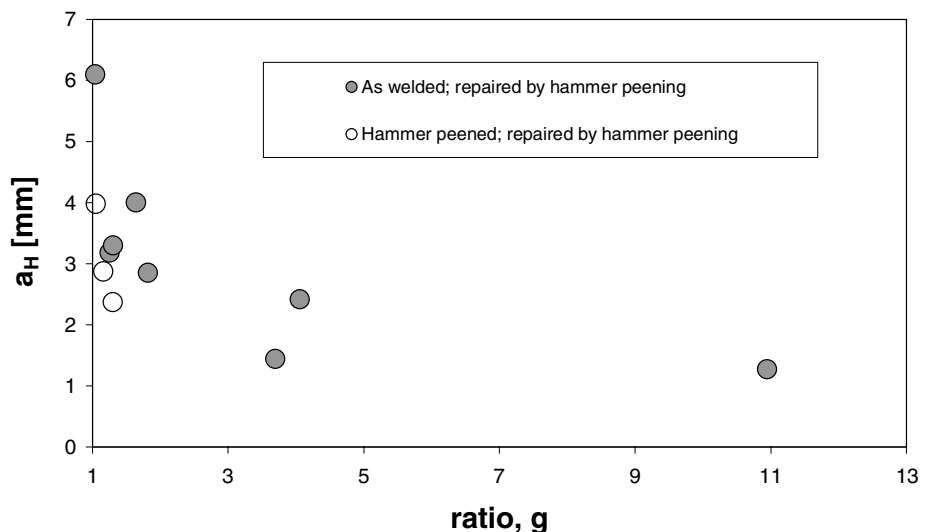


Fig. 12 Gain factor, g_N , in fatigue life, against depth of fatigue crack repaired by hammer peening. T-joints (Fig. 1). $R = 0.1$. 3PB. St 52-3 steel.

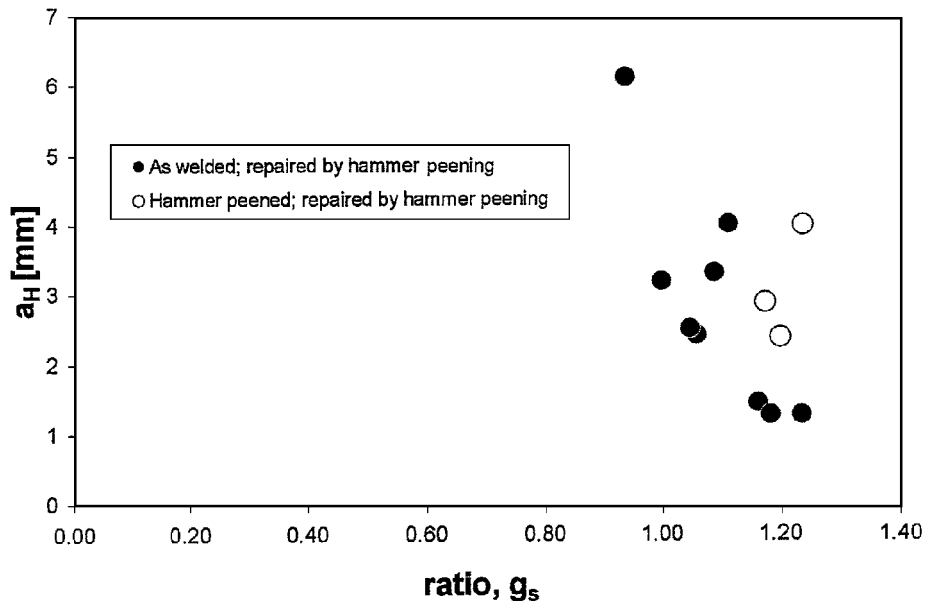


Fig. 13 Gain factor, g_s is strength against depth of fatigue crack repaired by hammer peening and for the N_r values. T-joints (Fig. 1). $R = 0.1$. 3PB. St 52-3 steel.

when the depth of the repaired crack decreases (Fig. 13). This result indicates that the fatigue strength of the repaired joints is above the as-welded joint (Figs 13 & 9). Hence, with repair by hammer peening there is gain in fatigue life and fatigue strength from very tiny cracks up to cracks with a depth close to half of the thickness of the specimens.

Scatter in the results of gain factors can be reduced by testing treated specimens with variable crack depths, and fixed (few) stress ranges, to obtain g_N , or with fixed (few) crack depths and variable stress ranges, to obtain g_s data.

Residual stress measurements

Values of the residual stresses were obtained in some selected specimens by X-ray diffraction at the weld toe and at 1–3 and 5 mm from the weld toe in the longitudinal x -direction. The residual stresses were obtained for different types of specimens, as-welded and hammer-peened after a fatigue test. The objectives of these tests were to quantify the residual stresses introduced by the hammer-peening process. The residual stresses decrease as the x -distance increases (Table 8(a) & 8(b)).

Table 8a Values of the longitudinal residual stress, σ_x (MPa) at the surface along the longitudinal direction, x from the weld toe. X-ray diffraction (for orientation see axes in Fig. 1)

	Weld toe $x = 0$	$x = 1$ mm	$x = 2$ mm	$x = 3$ mm	$x = 5$ mm
As-welded not tested	–	–	–18	–	14
Hammer-peened	–334	–298	–258	–185	–7

Table 8b Values of the transverse residual stress, σ_z (MPa) at the surface along the longitudinal direction, x from the weld toe. X-ray diffraction. (for orientation see axes in Fig. 1)

	Weld toe $x = 0$	$x = 1$ mm	$x = 2$ mm	$x = 3$ mm	$x = 5$ mm
As-welded before fatigue testing	22	–	–	–	11
Hammer-peened	–439	–288	–213	–172	–22

The results (Table 8(a) & 8(b)) have shown that the residual stresses in the x -direction are usually significantly higher than in the transverse z -direction. This effect is predicted in the theory of welding. Both in the x - and z -directions, the residual stresses in the hammer-peening condition are above those of the as-welded condition. The maximum value of residual stresses is compressive, and occurs in the location at the weld toe and in the transverse z -direction.

Because the residual stress is of yield magnitude in compression its effect is beneficial for the fatigue behaviour of the joint, thus explaining the large increase in fatigue strength obtained for the hammer-peened joints. The results also show that the effect of hammer peening, in terms of residual stresses, is localized near the weld toe where the treatment is applied since, at the zone 5 mm away from the weld toe $x = 5$ mm, the residual stresses are negligible (Table 8(a)). The residual stresses decrease as the longitudinal distance from the weld toe increases (Table 8(a) & 8(b)).

The residual stresses in the as-welded tested specimens are low, at least 5 mm away from the weld toe. Some relaxation effect of stresses may occur after the fatigue tests.

CONCLUSIONS

For non-load carrying T-joints loaded in 3PB in the main plate, gain factors, g , were obtained to assess the fatigue lives of repaired fatigue cracks at the weld toe, using the hammer-peening process. A correlation was found between g and the crack depth, a_H , of the repaired crack.

The results of hardness distributions at the weld toe have shown that the depth in the thickness direction of the zone affected by hammer peening is about 2.5 mm, the limit of the compressive residual stress fields induced by hammer peening.

For the as-welded joints with fatigue cracks of known size obtained by marking, and repaired by hammer peening, the fatigue lives were found to be significantly above the fatigue lives of the initial as-welded specimens only.

Beneficial effects of repair were found to be greater (high values of gain factors, g) in small repaired fatigue cracks with depths below 2.5 mm.

For specimens initially subjected to hammer peening, treatment repair of the fatigue cracks by hammer peening did not produce any significant increase in fatigue life. However the fatigue data obtained in the repaired specimens fitted rather well with the S-N curve for the as-welded hammer-peened specimens without fatigue cracks. Hence the benefits of hammer peening, in terms of increase in fatigue life, are identical whether there is or is not a fatigue crack at the weld toe.

In the hammer-peened specimens, values close to the yield stress in compression were obtained at the weld toe region using the X-ray diffraction technique, which is the main reason for the great increase in fatigue life when hammer peening is applied.

Acknowledgements

This project was financed by FCT, in Portugal, under the PRAXIS XXI program (Contract 3.1/CEG, 2705/95). The specimens were kindly supplied by The Welding Institute (TWI), Cambridge, U.K. The authors express their gratitude for the support and useful discussions with Dr S.J. Maddox, of TWI.

REFERENCES

- 1 Branco, C. M. and Dickerson, T. Final Report of ECSC/EEC project Weld Improvement Methods for Low Cycle Fatigue Applications, Contract Nr. 7210 – MC/931, CEMUL/IST, July 94 (in cooperation with TWI, UK, under contract ECSC 7210 – MC/801).

- 2 Branco, C. M. and Gomes, E. C. (1995) Development of fatigue design curves for weld improved joints. In: *Proceedings of the International Conference on Fatigue Design 95, FD95, Helsinki, Finland*, Vol. III, pp. 9–21.
- 3 Maddox, S. J. (1991) *Fatigue Strength of Welded Structures*, Abington Publishing, Cambridge, UK.
- 4 Branco, C. M., Fernandes, A. A. and Castro, P. T. (1999) *Fatigue of Welded Structures (in Portuguese)*, Cap. 11, Ed. Calouste Gulbenkian Foundation, Lisbon.
- 5 Booth, G. S. (1999) (8 edn) *Improving the Fatigue Performance of Welded Joints*, The Welding Institute, Cambridge, UK.
- 6 Offshore Installations; Guidance on Design, Construction and Certification, UK Department of Energy, HMSO, Fourth Edition, 1990.
- 7 *British Standard Specifications for Unfired Fusion Welded Pressure Vessels*, BS5500, 1990, British Standards Institution, London, UK.
- 8 Huther, I., Lieurade, H. P., Sonissi, R., Nussbaumer, A., Chabrolin, B. and Janosh, J. J. (1996) Analysis of results on improved welded joints. *Weld. World* **37**, 242–266.
- 9 Maddox, S. J. (1998) The application of fatigue life improvement techniques to steel welds. In: *IIW Commission XIII Workshop on Improvement Methods, International Institute of Welding, Proceedings of the 51st Annual Assembly, Hamburg, Germany*.
- 10 Haagensen, P. J. and Maddox, S. J. (2001) Specifications for Weld Toe Improvement by Burr Grinding, TIG Dressing and Hammer Peening for Transverse Welds. IIW Document, Commission XIII, Working Group 2, WG2, International Institute of Welding.
- 11 Fisher, J. W. and Dexter, R. J. (1994) Weld improvement for fatigue life extension. In: *Proceedings of the International Conference on Fatigue*, Toronto, Canada, 9–10 May 1994, AWS, pp. 82–87.
- 12 Fisher, J. W. and Dexter, R. J. (1994) Field experience with repair of fatigue cracks. In: *Proceedings of International Conference on Fatigue*, Toronto, Canada, 9–10 May 1994, AWS, pp. 82–87.
- 13 Infante, V. (2002) An Analysis of the Improvement of the Fatigue Behaviour of Welded Joints (in Portuguese), *PbD Thesis*, IST, Lisbon University of Technology, Portugal.
- 14 Infante, V. and Branco, C. M. (2000) A comparative study on the fatigue behaviour of repaired joints by hammer peening. Doc. XIII 1836-2000, 53rd IIW Meeting, Florence, Italy, International Institute of Welding, Commission XIII.
- 15 Infante, V. and Branco, C. M. (2000) A study on the fatigue behaviour of damaged welded joints repaired by hammer peening. In: *Proceedings of ECF13, 13th European Conference on Fracture*, (Edited by San Sebastian). ESIS.
- 16 Infante, V., Branco, C. M. and Baptista, R. An analysis of the effect of hammer peening on the repair of fatigue cracked welded joints. In: *Proceedings of ECF14, 14th European Conference on Fracture, Cracow, Poland, September 2002*, ESIS, Vol. II, pp. 13–21.
- 17 Eurocode 3: Design of Steel Structures, Part 1, General Rules for Buildings, Commission of the European Communities, 1990.
- 18 Fatigue design of welded joints and components. International Institute of Welding, IIW (Edited by A. Hobbacher). Abington Publishing, Cambridge, UK, 1996.
- 19 Baptista, R. (2002) A Study of the Hammer Peening Parameters on the Fatigue Behaviour of Welded Joints, *MSc Thesis*, IST, Technical University of Lisbon.
- 20 Infante, V. and Gomes, E. C. (1999) Fatigue performance of TIG and plasma welds in thin sections. *Int. J. Fatigue* **22**, 589–602.
- 21 British Standards Institution. (2000) Guidance on methods for the acceptance of flaws in structures. Annex J, PD6493, BS7910, UK.
- 22 Glinka, G. (1988) Relations between the strain energy density distribution and elastic-plastic stress-strain fields near cracks and notches and fatigue life calculations. ASTM, STP 942, pp. 1022–1047.

PII: 0102-1123(96)00029-1

Fatigue damage repair: a comparison of some possible methods

C.S. Shin, C.M. Wang and P.S. Song^t

Department of Mechanical Engineering, National Taiwan University, No. 1, Sec. 4,
Roosevelt Road, Taipei, 10617 Taiwan, ROC

^tDepartment of General Courses, Chung Cheng Institute of Technology, Twhsi,
Taoyuan, Taiwan, ROC

(Received for publication 15 March 1996)

When a fatigue crack is discovered in an engineering component, some expeditious temporary repair may be needed before more thorough treatment is available. Conventional repair methods, such as grinding removal of the crack and stop drilling, are often employed. In this work, the method of drilling crack-flank holes near to but not at the crack tip has been studied. It was found that retardation still occurred. Moreover, if the holes were drilled a small distance ahead of the tip, the crack was likely to grow into the hole, achieving a considerable amount of life extension. The effects of inducing artificial crack closure by infiltrating epoxy resin, alumina powder and a mixture of both have also been investigated. These were compared with the effect of overload-induced retardation. In all the methods studied, different degrees of crack growth retardation have been achieved, and they have the potential to be developed into practical fatigue crack repair methods. Copyright © 1996 Elsevier Science Limited

(Keywords: fatigue repair; hole drilling; artificial infiltration; crack closure)

It is well known that fatigue fracture accounts for a great number of mechanical failures. When a fatigue crack is discovered in a critical component during routine maintenance, replacement of the component may not be feasible, as there may not be stocks, or the available down-time is too limited. Some expeditious temporary fixing may then be needed to allow the component to operate safely until more elaborate repair or replacement can be arranged.

Different methods for repairing fatigue damage have been studied, and some of these are being employed in practical application. Early work found that by removing the surface layer of a smooth specimen repeatedly from time to time, the specimen fatigue life can be extended indefinitely¹⁻⁴. Intermittent heat treatment had been employed in the hope of reversing early cyclic damages⁵⁻⁹. Despite the varying degrees of success reported in some of these works, the difficulty of treating full-scale components and the lack of consistent performance rendered these early attempts futile for practical engineering applications. Above all, these attempts were based on the infinite life design concept, which will invariably break down when pre-existing flaws occur.

A number of more practical methods have been employed for cracked components. One simple repair technique is to grind away the fatigue crack altogether if it is shallow¹⁰. If this will significantly weaken the structure, a weld overlay or welding of replacement

parts may be required after grinding. When welding is involved, one has to take precautions to avoid the problems commonly associated with the welding process, such as residual stresses, stress corrosion cracking, and hydrogen embrittlement¹¹.

One may also drill a stop hole to remove the crack tip singularity¹²⁻¹⁴. In this case, the crack has to be re-initiated before growth can continue. The stop hole may further be cold expanded to introduce favourable residual stress to delay crack re-initiation and subsequent growth^{13,14}. Residual stresses that reduce fatigue crack growth rates may also be introduced by pressing steel balls or rollers to plastically deform the material in the vicinity of the crack tip region¹⁴⁻¹⁷. In grinding or stop drilling, one must take care to remove the crack tip completely. *In-situ* drilling is difficult to control precisely, and often the fatigue crack tip is not easily located. If the hole is drilled a little bit behind, thereby missing the crack tip, the crack may behave as if it is a short crack growing out of a notch. Such notch cracks can have anomalously high growth rates¹⁸, making the outcome of the repair unpredictable. An alternative method is to drill a pair of holes on the crack flank. The stress intensity factor for the resulting configuration is lower than before, and crack retardation has been observed¹⁹.

In the case when a crack is too long for grinding and the crack tip is not easily accessible for drilling, other crack repair methods must be sought. Stop drill-

ing is also impracticable for surface cracks or corner cracks emanating from holes because these crack fronts are non-uniform through the thickness. Adhesive patching with composite materials across a crack has been used in the aircraft industry to retard the growth of a fatigue crack. However, patching has been applied mainly to thin-walled components, and its effect on thick components under large applied loading may be limited.

FATIGUE CRACK REPAIR BY INFILTRATION

It is well known that a tensile overload can cause fatigue crack growth retardation (e.g. ref. 20). This beneficial effect has been made use of as a by-product in the proof testing of pressure vessels to increase their fatigue life²¹. The deliberate use of tensile overload to prolong fatigue life may risk causing a momentary stretch growth or even catastrophic fracture. It would be very useful if we could induce the mechanisms that cause overload retardation by some means other than applying a tensile overload directly. The mechanisms underlying overload retardation may be varied²²⁻²⁸, yet premature crack closure stands out to be one of the most significant mechanisms²⁹⁻³¹. In a recent study of the overload effect in AISI 304 stainless steel, plasticity-induced crack closure has been identified to be the major mechanism for crack growth retardation³¹. Residual plastic deformation leaves extra material behind on the crack flanks, causing premature crack closure and reduction in the effective crack-driving force.

It seems that foreign materials may be introduced into the crack flanks to achieve a similar purpose. Vecchio *et al.*³² had tried to introduce a spurious asperity such as needle tip into the wake of the crack tip. They found that by so doing the crack closure load increased from an original 5–10% to ~50% and even ~70% of the loading range. According to Elber's modified Paris law²⁸, such a great reduction in crack opening duration predicts a large reduction in crack growth rate. In reality, it was observed that growth rates had reduced only slightly, to ~75–88% of the original rate³². This discrepancy probably occurred because the asperity behind the crack tip triggered the closure instrumentation but did not really cause much closure at the crack tip, where fatigue damage occurred. In a preliminary attempt the present author has shown that careful infiltration of epoxy resin into a fatigue crack can bring the growth rate down to ~4–10% of the original value in some compact tension specimens³³. This order of reduction is similar to that caused by a 100% overload³³. In the current work, the infiltration and hole-drilling crack repair methods have been applied to 3 m long 165 mm diameter seamless piping. Their effects on the fatigue crack growth behaviour were studied. The same repair techniques have also been applied to small three-point bending specimens machined from the pipe. This is to check how well small specimens reflect the effect of crack repair on full-scale components. It is hoped that the results may provide some guidelines on the development of practical *in-situ* repair methods for fatigue-cracked mechanical components.

EXPERIMENTAL PROCEDURES

Pipe experiments

A four-point bending fixture that can accommodate up to 170 mm diameter piping was constructed³⁴. The inner and outer spans of the bending fixture are 1 m and 2.52 m respectively. At each of the four gripping points, free longitudinal motion and rotation of the pipe were allowed through appropriate roller and bearing arrangements. Three metre long seamless AISI 304 stainless steel pipes, with outer diameter 165 mm and thickness 11 mm, were tested. A Shimadzu 500 t servo-hydraulic machine was used for the pipe experiments. Fatigue testing was carried out under a constant stress intensity range (ΔK) of 45 MPa m^{0.5} using a sinusoidal waveform. The load ratio (minimum load/maximum load) was fixed at 0.1. Owing to the large load-line displacements involved, the testing frequency achieved by the machine was only about 0.5 Hz. A through-thickness starter notch subtending a half-crack angle of 40° was saw-cut in the mid-section of the pipe. Details of the experimental set-up and stress intensity calibration have been documented in ref. 34.

Owing to a limited budget and the high equipment rental and specimen costs, a series of different repair methods had to be performed on the same pipe. To avoid complication in data interpretation, a minimum of 3 mm of stable growth (constant growth rate) was allowed before a new repair was carried out. The following sequence of repairs had been performed:

1. A first set of holes was drilled on both sides of the crack, as shown in *Figure 1*. The hole diameter d was 4.5 mm, and the distance L of the hole centres from the crack tip was 5 mm.
2. A second set of holes was then drilled. This time $d = 2.7$ mm and $L = 2$ mm.

During the drilling operations, the average strains near the crack tip were closely monitored by strain gauges stuck just clear of the crack tip. This was to make sure that, in the entire drilling process, no unwanted plastic deformation had been introduced that

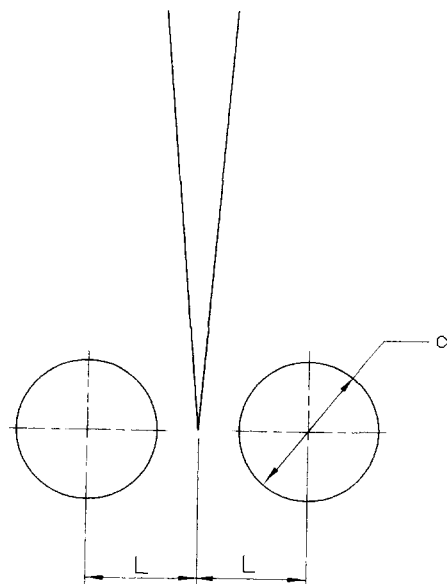


Figure 1 Relative positions between the drilled holes and the crack

might complicate the results. *Table 1* shows the maximum strains measured, which are small and well within the elastic limit. It is therefore reasoned that the effect of the associated residual stress on the growing crack is probably insignificant.

3. Infiltrations of epoxy resin. A partial vacuum was created in the interior of the pipe by a vacuum cleaner with sealing plastic tape at suitable places. The crack was held open by applying 90% of the maximum loading to facilitate infiltration.
4. Infiltration of alumina powder in the form of an aqueous suspension. Four infiltrations were attempted. The average diameters of the powder were 380 nm, 585 nm, 690 nm and 1100 nm respectively.

To serve as a control, a single tensile overload ($K_{\text{overload}} = 88.7 \text{ MPa m}^{\frac{1}{2}}$) was applied in a second pipe specimen cycled under the same constant baseline ΔK of $45 \text{ MPa m}^{\frac{1}{2}}$. This corresponded to an overload ratio $[(K_{\text{overload}} - K_{\min})/\Delta K]$ of 1.86.

Throughout the tests, data on the crack length a and the number of cycles N were recorded automatically by a reversing d.c. potential drop system hooked up to an IBM PC. This method has been shown to have sufficient accuracy in a previous work³⁴. Periodic manual measurement of the crack length confirmed the accuracy of the acquired data.

Three-point bending specimen tests

Three-point bending (3P) specimens of length 145 mm and width 30 mm were machined from the same pipe after the crack repair experiment. The longitudinal axes of the 3P specimens run parallel to the long axis of the original pipe so that fatigue crack growth in the pipe and the 3P specimens occurred in parallel planes. In order to obtain flat specimens from the curved pipe section, the specimen thickness had to be reduced from 11 mm to 9 mm. Fatigue tests were carried out by an MTS 810 closed-loop servohydraulic machine. A constant baseline ΔK of $25 \text{ MPa m}^{\frac{1}{2}}$ was employed in all tests to give a similar value of growth rate as in the pipe specimen. The stress intensity calibration given in ASTM E399³⁵ was employed to compute the crack driving force. The applied stress intensity range was smaller, as the remaining ligament of the 3P specimen was much smaller than that of the pipe specimen, giving rise to considerable differences in crack closure response and growth rate under the same ΔK .

A sinusoidal waveform with a frequency of 10 Hz was used. Crack length was monitored using the reversing d.c. potential drop method mentioned in the last section. As in the pipe experiment, the above series of hole drilling, infiltration as well as the overload tests were carried out on 3P specimens. In this case,

Table 1 Crack tip strain recorded during hole drilling on pipe specimen

Hole diameter	After drilling the first hole	After drilling the second hole
4.5 mm	-32 $\mu\epsilon$	-47 $\mu\epsilon$
2.7 mm	-66 $\mu\epsilon$	-84 $\mu\epsilon$

each repair was performed on a different specimen. The hole-drilling experiment was repeated five times. Hole diameters were all 2.7 mm, and the distance between the hole centre and the crack plane was 2 mm. As in the pipe specimen, the average crack tip strains were monitored during each drilling operation. The maximum crack tip strain recorded among the five specimens was $-293 \mu\epsilon$. This is larger than those from the pipe specimen, but is still well within the elastic limit of the material.

Infiltration of the 3P specimens was first carried out in vacuum, making use of capillary action. Details of the process have been reported in a previous paper³⁴. During infiltration, the crack was pulled open using 90% of the maximum cyclic load, as in the case of the pipe specimen. After encountering failure in infiltrating alumina powder, a number of other methods were tried³⁶. It was found that using pressurized nitrogen as propellant to drive the infiltrant into a crack gave a higher and more consistent success rate. As a result, a later series of tests employed the new method to infiltrate alumina-reinforced epoxy resin into the 3P specimen cracks.

Crack closure measurement

In each of the above tests, crack opening load was measured by the compliance method aided by an offset procedure similar to that proposed by Kikukawa *et al.*³⁷. The relevant displacement for compliance information was measured with a strain gauge straddling the crack just behind the crack tip. Crack tip strain gauges were normally fixed with the specimen removed from the testing machine. A low-pass filter with a cut-off frequency of 1 Hz was used to reduce electrical noise. As a result, the testing frequency was reduced to 0.05 Hz during closure measurement to avoid distortion of the signals. The degree of crack closure, U , was defined as the fraction of the load range for which the crack is open:

$$U = \frac{K_{\max} - K_{\text{op}}}{K_{\max} - K_{\min}} = \frac{\Delta K_{\text{eff}}}{\Delta K} \quad (1)$$

where K_{op} is the stress intensity at which the crack started to become fully open and ΔK_{eff} is the effective range of stress intensity available for growing a crack.

RESULTS AND DISCUSSION

Baseline fatigue crack propagation data

In general, fatigue crack growth rate and ΔK may be related through Paris' law:

$$\frac{da}{dN} = C(\Delta K)^m \quad (2)$$

Elber²⁸ suggested taking premature crack closure into account. In this case, the crack growth rate may be correlated through ΔK_{eff} :

$$\frac{da}{dN} = C_c(\Delta K_{\text{eff}})^{m_c} \quad (3)$$

where ΔK_{eff} is as defined in Equation (1).

In the current work, constant-loading-amplitude crack growth tests were carried out at a load ratio of 0.1 in 3P specimens, with crack closure closely monitored. It was found that in the small 3P specimens,

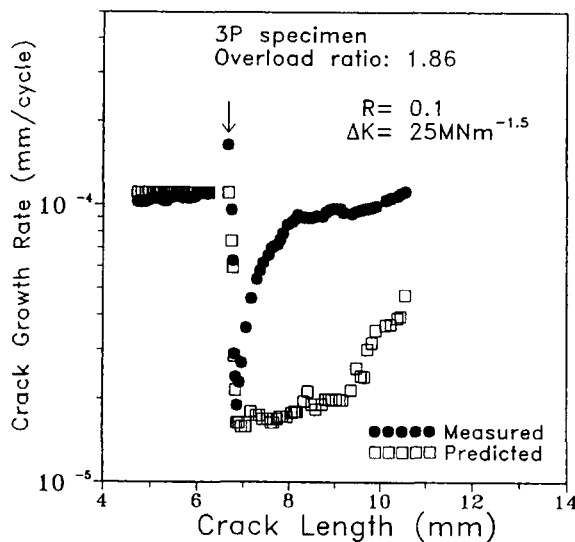


Figure 2 Crack growth rate versus crack length behaviour of the 3P specimen suffering a tensile overload. Arrow shows the crack tip position during overload

fatigue cracks stayed open throughout the whole loading cycle, and so the coefficients and exponents in Equations (2) and (3) are virtually the same. Thus $C = C_c = 5.39 \times 10^{-10}$ and $m = m_c = 3.8$; da/dN is in mm cycle^{-1} and ΔK_{eff} is in $\text{MPa m}^{\frac{3}{2}}$. Available growth rate data span a ΔK_{eff} range from 20 to 60 $\text{MPa m}^{\frac{3}{2}}$. It is reasoned that in larger specimens where sufficient elastic enclave exists to bring about premature crack closure, C and m will be different from that reported above. On the other hand, as Equation (3) has taken closure into account, C_c and m_c should still remain the same. Hence in later crack growth rate prediction only Equation (3) will be used.

Retardation caused by single overload

The black circles in Figures 2 and 3 show the effect of a single tensile overload on the crack growth rate in the 3P and pipe specimens respectively. The general

trends of behaviour are similar in the two specimens. The overload ratio as defined above was 1.86 in both cases. On applying the overload, the pipe crack growth rate increased immediately from $2 \times 10^{-4} \text{ mm cycle}^{-1}$ to $4.74 \times 10^{-4} \text{ mm cycle}^{-1}$, while that in the 3P specimen increased from $1.05 \times 10^{-4} \text{ mm cycle}^{-1}$ to $1.64 \times 10^{-4} \text{ mm cycle}^{-1}$. The application of the overload stretched open the crack, giving rise to the observed instantaneous acceleration. Since the pre-overload crack in the 3P specimen was already nearly fully open, the effect of further stretching by the overload was limited, and so the instantaneous acceleration in the 3P specimen was not as pronounced as that in the pipe specimen. In both cases, deceleration to the minimum growth rates occurred relatively more steeply than the subsequent acceleration back to normal conditions. The minimum growth rate reached in the pipe specimen was $9.28 \times 10^{-5} \text{ mm cycle}^{-1}$, occurring at 12.9 mm from the point of overload. In the 3P specimen, the minimum growth rate was $1.9 \times 10^{-5} \text{ mm cycle}^{-1}$, occurring at 0.6 mm from the point of overload.

The overall crack lengths affected by the overload transient were ~ 4 mm in the 3P specimen and ~ 27 mm in the pipe specimen. Life extensions in terms of number of cycles were 17 000 and 95 000 for the 3P and pipe specimens respectively.

Figures 4 and 5 show the development of crack closure in the 3P and pipe specimens respectively. The crack in the 3P specimen was nearly fully open before the overload. Following the overload, crack closure decreased abruptly to 0.6. It then increased gradually. In the pipe specimen, the crack closure value U stayed more or less constant around 0.76 before the overload. On applying the overload, the crack became fully open ($U = 1$) immediately. Thereafter, U decreased abruptly at first and then more gradually until a minimum of 0.46 was reached. Afterward it rose gradually. In both the 3P and pipe specimens, the positions of minimum crack growth rate corresponded well to those of the minimum U value. Over the crack length under test, crack closure did not regain the pre-overload U values.

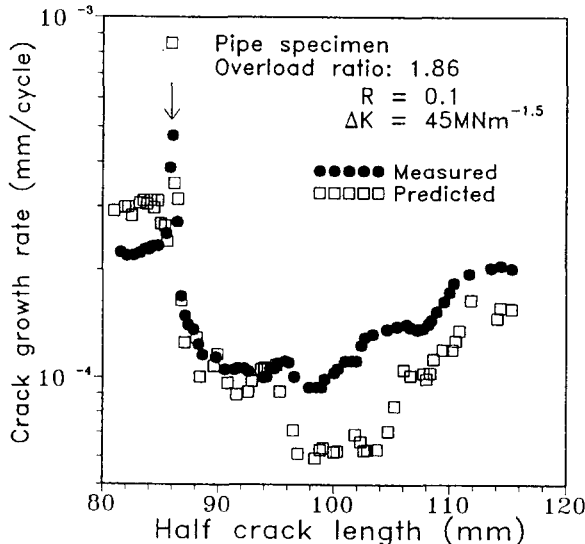


Figure 3 Crack growth rate versus crack length behaviour of the pipe specimen suffering a tensile overload. Arrow shows the crack tip position during overload

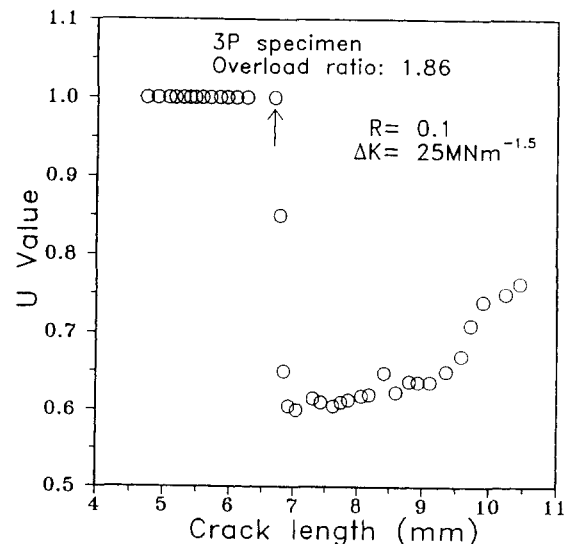


Figure 4 Crack closure versus crack length behaviour of the 3P specimen suffering a tensile overload. Arrow shows the crack tip position during overload

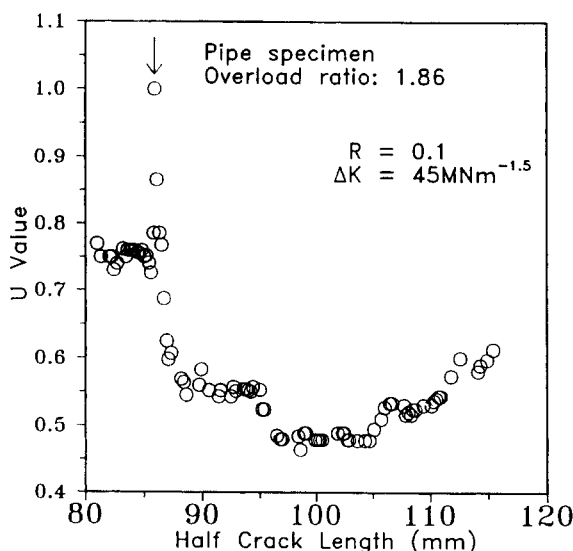


Figure 5 Crack closure versus crack length behaviour of the pipe specimen suffering a tensile overload. Arrow shows the crack tip position during overload

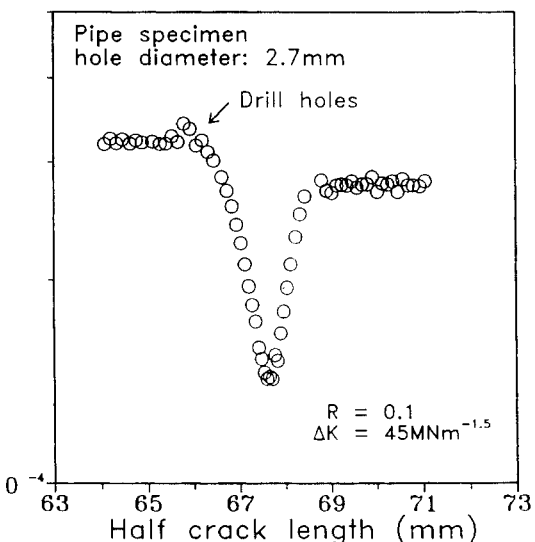


Figure 6 Effect of drilling holes near the crack tip on the crack growth behaviour in pipe specimen. Arrow shows the crack tip position during hole drilling

The quantitative differences in the amount of retardation achieved and the overload-affected zone sizes are presumably due to the difference in size between the two kinds of specimen. This size effect will give considerable difference in the overall elastic-plastic response, which affects the crack opening displacement, the crack closure development, and hence the crack growth rate. In the pipe specimen, which has a large remaining ligament, the ligament was nominally elastic with a localized overload plastic zone. This favoured the development of a greater amount of crack closure, and resulted in more growth retardation. In the 3P specimen, the remaining ligament was small. The crack opening displacement under the same ΔK was therefore larger. This gave rise to a higher growth rate as well as a less pronounced overload retardation effect. The occurrence of this *size effect* suggests that using small specimens to evaluate the overload retardation effect on full-scale components is likely to seriously underestimate the beneficial effect.

The open squares in Figures 2 and 3 are predictions based on the measured crack closure values and Elber's correction of Paris law (Equation (3)). The predicted crack growth rates agree well with observed rates from the beginning up to the point of minimum growth rates. Thereafter, Equation (3) tends to underestimate moderately in the pipe specimen and heavily in the 3P specimen. The cause of these underestimations is due to the phenomenon of 'discontinuous closure' identified in a previous paper³¹. Discontinuous closure arose when the exceptionally large humps of residual plastic wake some distance behind the crack tip, created by the overload, came into contact and triggered the closure instrumentation while the crack tip region still stayed open. Thus closure instrumentation will record an U value smaller than what is actually seen by the crack tip. As a result, the effective crack driving force, ΔK_{eff} , as well as the crack propagation rate, are underestimated. The difference in the degrees of underestimation is probably due to the difference in elastic constraints in the two specimens, as discussed before.

Retardation caused by crack-flank holes

Drilling the first set of 4.5 mm diameter crack-flank holes did not cause any observable change in crack growth rate in the pipe specimen. It was reasoned that the holes, being 5 mm from the crack plane, were too far away to exert enough influence on the crack. As a result, a second set of holes was drilled only 2 mm from the crack plane. The diameter must necessarily be reduced in order not to drill away part of the crack. Figure 6 shows the development in growth rate for this case. The hole centres were in line with the instantaneous crack tip on drilling. The crack growth rate gradually decreased from 3.2×10^{-4} mm cycle⁻¹ to 1.41×10^{-4} mm cycle⁻¹ after a crack growth increment of 1.2 mm. Thereafter, growth rate increased gradually back to normal. The overall affected crack length was 2.5 mm.

The corresponding effect on the 3P specimen (3PH1) is shown in Figure 7. Before drilling holes, the crack

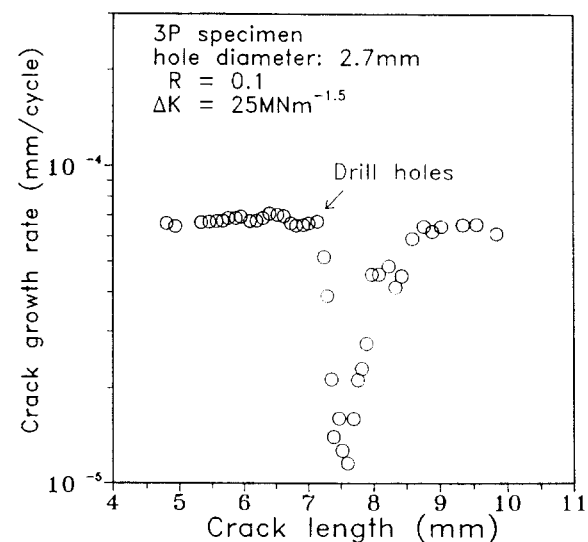


Figure 7 Effect of drilling holes near the crack tip on the crack growth behaviour in 3P specimen. Arrow shows the crack tip position during hole drilling

growth rate was 6.5×10^{-5} mm cycle $^{-1}$. This gradually decreased to a minimum rate of 1.16×10^{-5} mm cycle $^{-1}$ after a crack growth increment of 0.5 mm. The total crack length affected was 1.5 mm. Qualitatively, the same behaviour was observed in both pipe and 3P specimens. The amount of life extension was ~ 5000 cycles in the pipe specimen and $\sim 40\,000$ cycles in the 3P specimen. This difference may be attributable to the difference in the changes in stress intensity factor, as the same hole size was used in the large pipe and small 3P specimens. However, as the stress intensity for the current configuration of a crack approaching two holes is available only for an infinite plate, further numerical analysis is needed to clarify the above postulation. In contrast to the overload experiments, although the amounts of life extension were again different, the affected crack length increments were similar and of the same order of magnitude as the hole diameter in both the pipe and 3P specimens. This suggests that extents of the effect of a pair of holes are similar in large and small specimens. The current result indicates that if we use standard laboratory specimens to evaluate the beneficial effect of hole drilling on full-scale components, care should be taken against possible overestimation of the amount of life extension.

To study the sensitivity of this repair method to the accuracy of hole alignment and location, some further experiments with hole drilling have been carried out in 3P specimens. In a second and third specimen (3PH2 and 3PH3), *in-situ* drilling under unfavourable conditions was simulated. The hole centres were located by a centre punch, and a hand drill was used. The resulting hole locations were not precise, but were as close to the desired position as the hand tool allowed. It was later revealed that the centre axes of the holes were not perfectly perpendicular to the surface of the specimens. On testing, the crack on the front surface of 3PH2 grew into one of the holes, and stopped growing. However, it was later discovered that the crack on the back surface had not grown into a hole. Growth of this crack probably continued on the back surface and through the thickness, leading to a sudden re-emergence of the crack on the front surface 2.9 mm ahead of the hole position. As load shedding to maintain a constant ΔK was based on the front surface crack length, the crack might have seen a driving force larger than intended ($25 \text{ MPa m}^{1/2}$) for some length of time. As it re-emerged on the front face, the calculated ΔK was $32 \text{ MPa m}^{1/2}$. Despite the occurrence of a larger ΔK , a life extension of 25 000 cycles was obtained.

In 3PH3, crack branching was observed on the front surface, and one minor branch grew into a hole. No branching or growing into hole occurred on the back (Figure 8). A life extension of 11 000 cycles over an affected crack length of 1.4 mm was obtained.

From the above three tests, it seems that the amount of life extension generated is sensitive to the correct positioning and accurate alignment of the holes. Moreover, as the hole centres were in line with the crack tip, it was not easy for a crack to grow into a hole. Even if that happened, it might probably have occurred over a small part of the thickness, and could not lead to long life extension.

Instead of keeping in line with the instantaneous crack tip, holes were drilled 1 mm (3PH4) and 4 mm

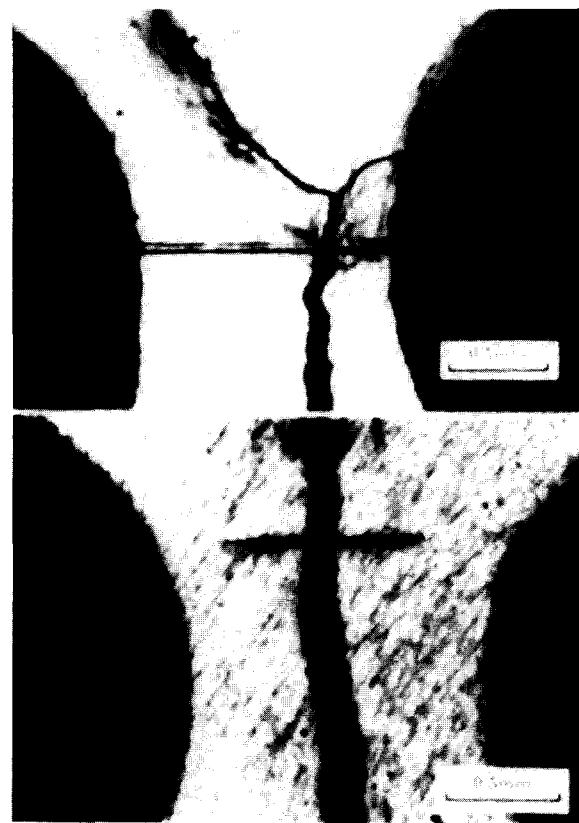


Figure 8 Crack branching on the front surface of 3PH3, with one branch growing into a hole. No branching occurred on the back surface

(3PH5) ahead of the crack tip in the 3P specimens. Three phenomena are worth noting in these cases. First, the crack started to decelerate once the holes were drilled. As a result, a longer retardation-affected crack length could be achieved. Second, on growing near the hole, crack branching sometimes occurred, with each hole attracting one branch of the crack. A larger amount of retardation in growth rate than for the unbranched crack was then obtained. Third, the attraction of the crack might sometimes be great enough to deflect it and make it grow into the holes. Crack branching and deflection by itself can reduce the crack tip stress intensity by a considerable amount²⁶. If the crack grows into a hole, the crack tip singularity is removed altogether (Figure 9). The third effect is

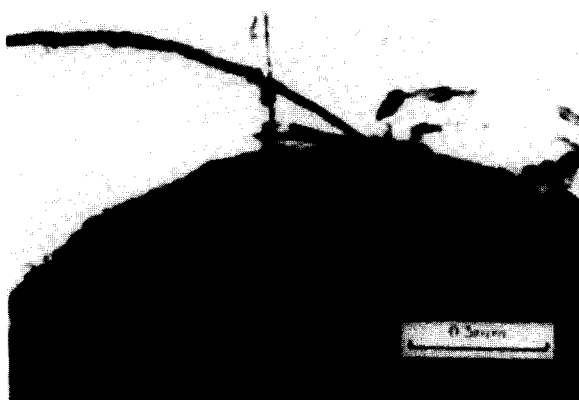


Figure 9 Crack deflection and growth into a hole on the front surface of 3PH4

the most beneficial, as it caused a very favourable extension of the total fatigue life. In 3PH4, although a crack on only one surface was observed to grow into a hole, such behaviour might have occurred over a considerable portion through the thickness, resulting in a life extension of 126 000 cycles. In 3PH5, cracks on both the front and back surfaces grew into the same hole. The resulting life extension was 112 000 cycles. Thus the life extension in terms of the number of cycles in 3PH4 and 3PH5 amounted to seven to eight times that achieved by the above-mentioned 1.86 times overload.

Good precision is difficult to procure in *in-situ* drilling. Simulated drilling showed that the hole centres might not be well aligned, and that the holes might not be perpendicular to the specimen plane. As a result, the hole on one surface may be slightly ahead of the crack tip, although it was intended to be in line with the tip. If this happened, a crack on that surface might grow into the hole while one on the other surface did not. The life extension achieved would then be less than achieved by those growing into the hole completely but still comparable with or larger than those that grew clear of the holes. In all cases, the 3P specimens repaired by the hole-drilling method derived much better extension in fatigue life than from the corresponding 1.86 times overload.

From this series of crack-flank hole experiments, it may be concluded that the best technique to employ is to drill holes close enough to the crack plane while slightly ahead of the current crack tip. A favourable amount of life extension can be obtained, as the crack tends to be attracted and grows into one of the holes. In this way, stringent requirements on drilling precision to remove the crack tip completely are not required, yet the same effect can be attained. Even if the crack misses the holes, a considerable amount of retardation will still be generated due to a reduction of crack driving force. The drawback of this type of method is that it cannot be conveniently applied to surface cracks or to fluid-tight vessels.

Retardation caused by infiltration of epoxy resin

The black circles in Figures 10 and 11 show the effect of epoxy resin infiltration on fatigue crack growth rate in the pipe and 3P specimens respectively. Immediate retardation was attained, and the crack growth rate gradually returned to normal.

The pre-infiltration crack growth rate was $2.8 \times 10^{-4} \text{ mm cycle}^{-1}$ in the pipe specimen. This dropped immediately to $5 \times 10^{-5} \text{ mm cycle}^{-1}$, and then gradually increased back to the normal rate. The affected crack length was 3.6 mm, and the resulting life extension was 12 600 cycles. In the 3P specimen, the growth rate dropped from $1.05 \times 10^{-4} \text{ mm cycle}^{-1}$ to $3.69 \times 10^{-5} \text{ mm cycle}^{-1}$ immediately on infiltration. It took a crack growth increment of 3.2 mm to regain the original growth rate. The resulting life extension obtained was 15 400 cycles.

The development of crack closure behaviour (Figures 12 and 13) closely matched the development of growth rate transients. A large decrease in U value was recorded. In the pipe specimen, U dropped from 0.7 to 0.21. In the 3P specimen, U dropped from 1 to 0.36. These amounts of decrease were larger than that caused by the 1.86 times overload. The minimum

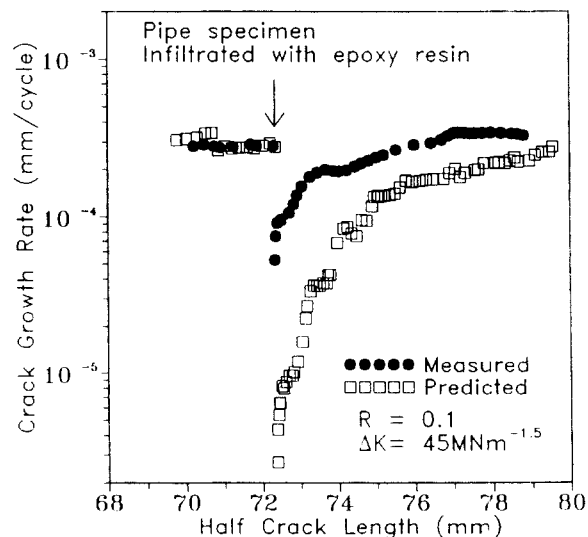


Figure 10 Effect of suction infiltration with epoxy resin on crack growth behaviour in the pipe specimen. Arrow shows the crack tip position during infiltration

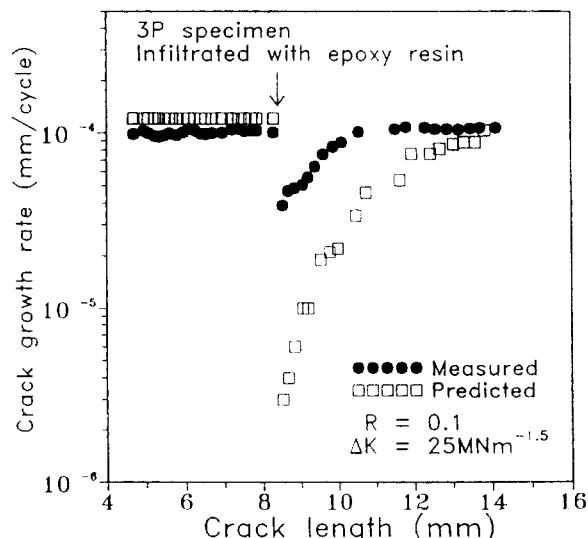


Figure 11 Effect of vacuum infiltration with epoxy resin on crack growth behaviour in the 3P specimen. Arrow shows the crack tip position during infiltration

growth rates resulting from infiltration were also lower than that due to the overload. These phenomena may be understood in the following terms. Large decreases in U value and growth rate occurred because the cracks were pulled open at 90% of maximum load so that the crack flanks were fully filled with epoxy resin. The thickness and extent of resin filled were much larger than that in the overload case. However, as the overloaded crack grew, continual release of residual plastic wake material occurred. This helped to maintain a low level of crack opening for a considerable crack growth increment. In the infiltrated cases, no such continual supply of extra wedging material took place. Thus retardation could not be sustained for as large a crack growth increment as that in the overload case for the infiltrated pipe specimen. As a result the overall life extension achieved was much less. In the 3P specimen, continual release of extra plastic wake was offset by the increasing crack opening due to the small

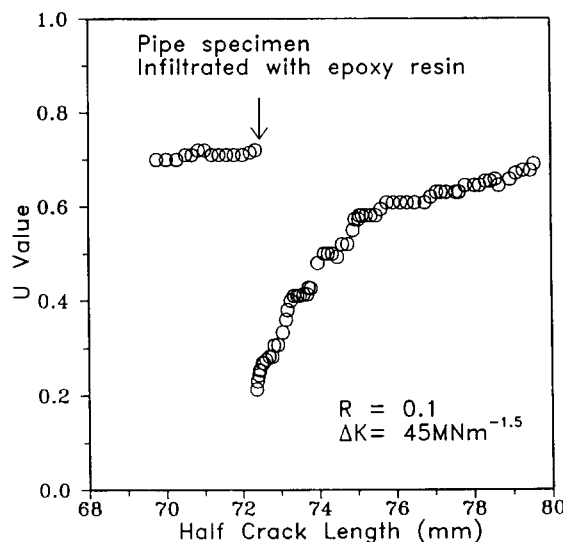


Figure 12 Effect of suction infiltration with epoxy resin on crack closure behaviour in the pipe specimen. Arrow shows the crack tip position during infiltration

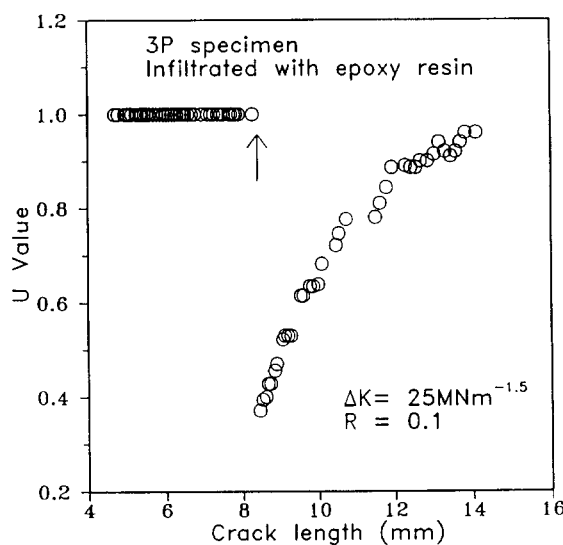


Figure 13 Effect of vacuum infiltration with epoxy resin on crack closure behaviour in the 3P specimen. Arrow shows the crack tip position during infiltration

remaining ligament size. The overload retardation effect was therefore not extensive, and the amount of life extension was comparable to the infiltrated case.

The open squares in Figures 10 and 11 represent the prediction based on measured crack closure and Equation (3). Serious underestimation occurs throughout the whole crack growth transient. On fracturing the 3P specimen after test, a trace of the infiltrated epoxy resin could be found on the fracture surface. However, judging from the position of the epoxy resin, it was evident that the resin had probably not gone all the way into the instantaneous crack tip region. We have therefore had a similar situation as that of Vecchio *et al.*'s needle tip³², as mentioned above, and Equation (3) will obviously give serious underestimation of growth rate. It is reasoned that a much more favourable life extension should be obtained if we have more efficient methods to ensure that the resin reaches the crack tip region.

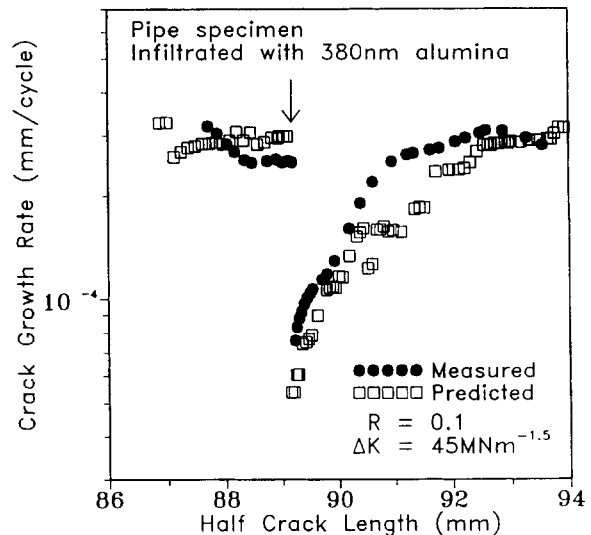


Figure 14 Effect of suction infiltration with 380 nm alumina powder on crack growth behaviour in the pipe specimen. Arrow shows the crack tip position during infiltration

Retardation caused by infiltration of alumina powder

Infiltration of aqueous alumina suspension into the 3P specimen was carried out using the same technique as that for epoxy resin. No observable change in crack growth rate was noted. Some success was obtained with the pipe specimen. The black circles in Figures 14–17 show respectively the effect of infiltration of 380 nm, 585 nm, 690 nm and 1100 nm diameter alumina powder on crack growth rate in the pipe specimen. No retardation is observed in Figures 15 and 17, while immediate retardation occurred in Figures 14 and 16. The best retardation effect was achieved with the 380 nm diameter powder. The growth rate immediately dropped from 2.6×10^{-4} mm cycle⁻¹ to 7.6×10^{-5} mm cycle⁻¹. The affected crack length was 2.5 mm and the extension in life was 7000 cycles. The next best retardation was achieved with the 690 nm diameter powder. In this case, the growth rate immediately dropped from 2.9×10^{-4} mm cycle⁻¹ to

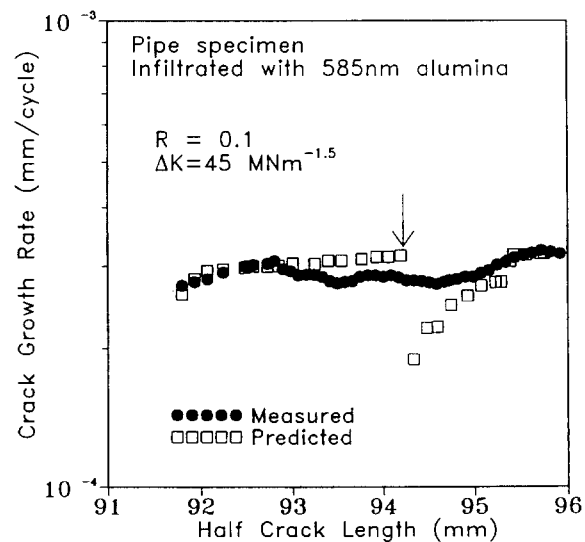


Figure 15 Effect of suction infiltration with 585 nm alumina powder on crack growth behaviour in the pipe specimen. Arrow shows the crack tip position during infiltration

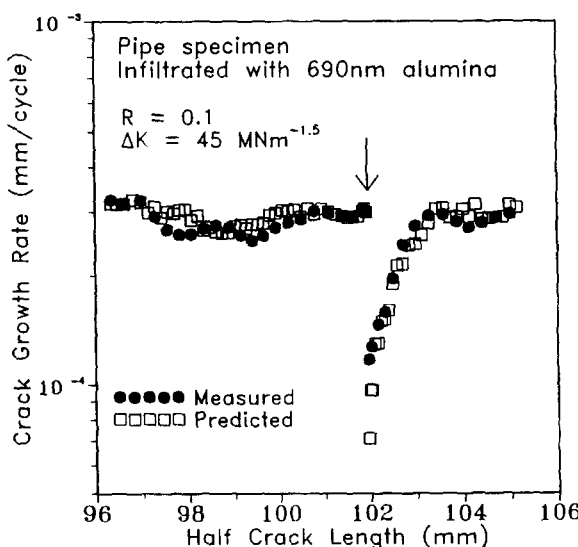


Figure 16 Effect of suction infiltration with 690 nm alumina powder on crack growth behaviour in the pipe specimen. Arrow shows the crack tip position during infiltration

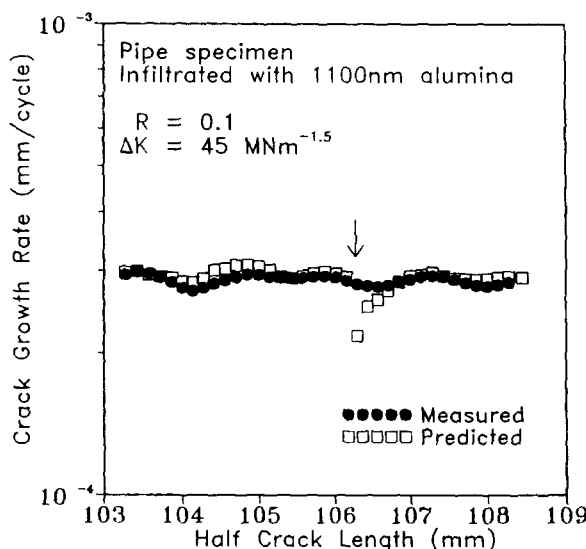


Figure 17 Effect of suction infiltration with 1100 nm alumina powder on crack growth behaviour in the pipe specimen. Arrow shows the crack tip position during infiltration

1.16×10^{-4} mm cycle $^{-1}$. The affected crack length was 1.4 mm and the extension in life was 2900 cycles. The development in crack closure matched that of the growth rate (*Figures 18 and 20*). In the remaining two cases (*Figures 19 and 21*), although no retardation was observed, there was a marked drop in *U* value for the 585 nm diameter powder. A slight but distinct drop in *U* value also occurred for the 1100 nm powder. The open squares in *Figures 14–17* show the crack growth rate calculated using Equation (3) and the recorded *U* values. Unlike the overload and epoxy resin infiltrated cases, the predicted growth rate agrees very well with the measured. No serious underestimation exists, implying that the phenomenon of discontinuous closure has probably not occurred.

The absence of retardation in some of the cases was probably caused by the failure of alumina powder to get into the crack. The crack tip opening displacement in the pipe specimen was estimated to be at least

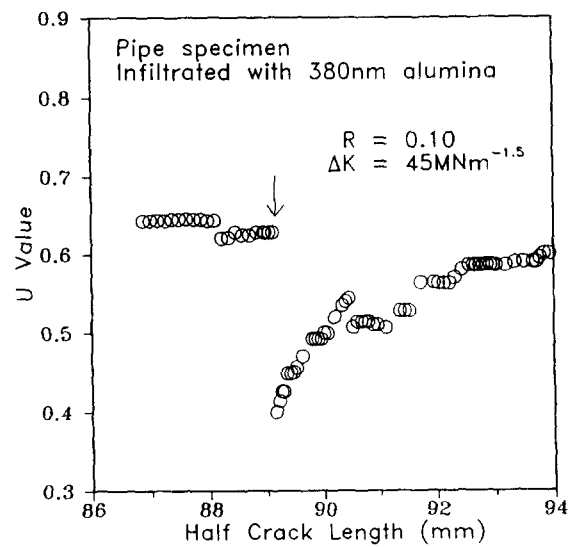


Figure 18 Effect of suction infiltration with 380 nm alumina powder on crack closure behaviour in the pipe specimen. Arrow shows the crack tip position during infiltration

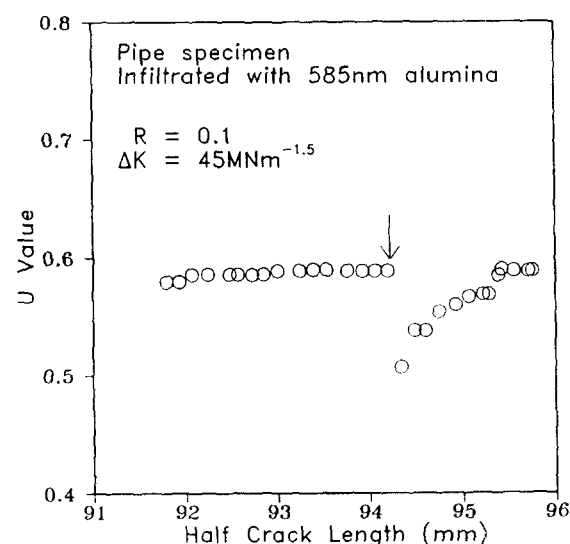


Figure 19 Effect of suction infiltration with 585 nm alumina powder on crack closure behaviour in the pipe specimen. Arrow shows the crack tip position during infiltration

7400 nm. Hence failure of infiltration was not caused by large particle size. It is probably due to the inefficiency of the aqueous carrier and the infiltration method. In the pipe specimen, infiltrant was to some extent drawn into the crack by a partial vacuum. In the 3P specimens, although infiltration was done in a better vacuum, capillary action alone operated. This explains why a limited success was obtained in the pipe specimen but a total failure occurred in the 3P specimens. A more efficient carrier and infiltration method are needed.

Previous work using epoxy resins of different hardness³³ suggested that a harder infiltrant might be more effective in bringing about retardation. In the current case, the harder alumina is apparently less effective than the softer epoxy resin. Besides the possible difference in the infiltration efficiency of these two materials, the small particle size of alumina powder may also be responsible. Assuming a successful infiltration, epoxy

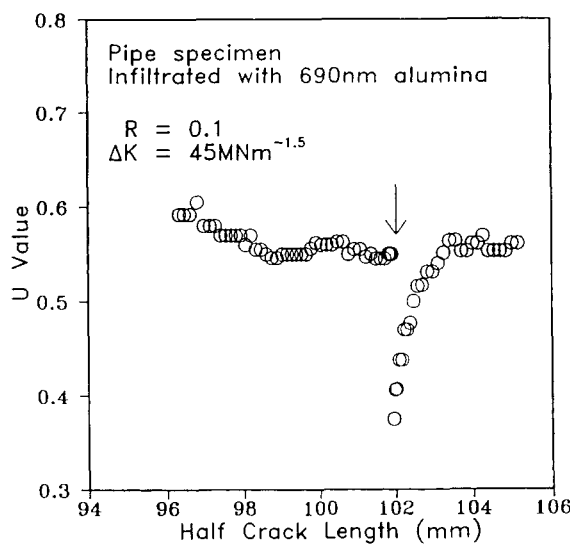


Figure 20 Effect of suction infiltration with 690 nm alumina powder on crack closure behaviour in the pipe specimen. Arrow shows the crack tip position during infiltration

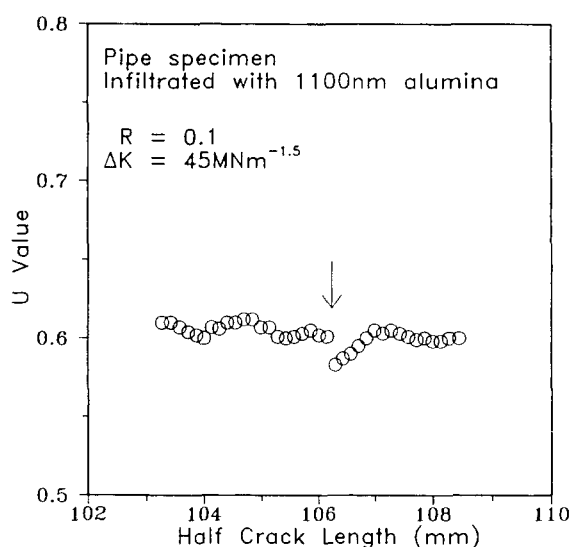


Figure 21 Effect of suction infiltration with 1100 nm alumina powder on crack closure behaviour in the pipe specimen. Arrow shows the crack tip position during infiltration

resin can take up fully the space between the crack flanks, while only a single or a few layers of alumina powder can probably be built up on the fracture surface. The additional amount of crack closure brought about by alumina will be much less than that caused by epoxy resin, noting that the crack tip opening displacement is much larger than the alumina particle size. This is also the likely reason for no serious underestimation in the predicted growth rates in Figures 14–17. One improvement may be to employ powder with a wide range of sizes so that the largest allowable particles can get into the crack and induce the maximum amount of closure. The other possible way is to mix alumina powder with epoxy resin so that an alumina-reinforced epoxy resin composite is infiltrated. Preliminary results of the latter options are reported next.

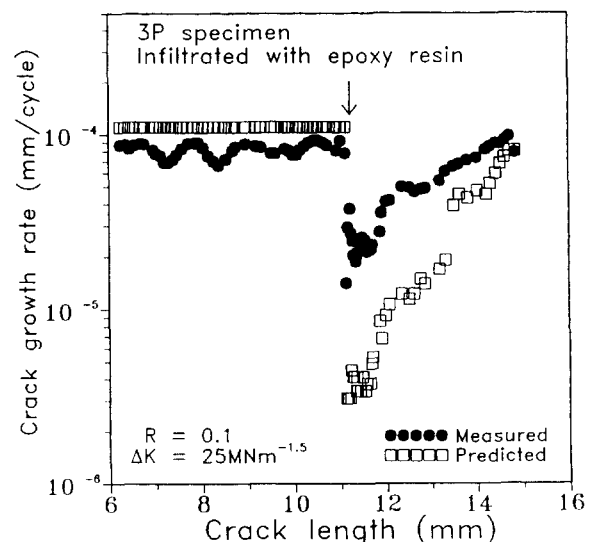


Figure 22 Effect of pressure infiltration with epoxy resin on crack growth behaviour in the 3P specimen. Arrow shows the crack tip position during infiltration

Retardation caused by infiltration of epoxy resin reinforced by alumina powder

Following the failure in infiltrating aqueous alumina suspension, a new technique using pressurized nitrogen to force infiltrant into a crack was developed³⁶. Epoxy resin was infiltrated into a 3P specimen again using this new technique. For comparison purposes, epoxy resin mixed with 0.2 µm and 0.5 µm mean diameter alumina powder (weight ratio = 1 : 1) was also used. The black circles and open squares in Figures 22–24 show respectively the measured and predicted growth rates for these three cases. The growth transients and the deviation between the measured and predicted responses exhibit qualitatively the same trends as that discussed above for the 3P specimen infiltrated with epoxy resin (i.e. Figure 11). The affected crack lengths in the four cases were similar. Being more efficient in transporting material into a crack, the pressure infil-

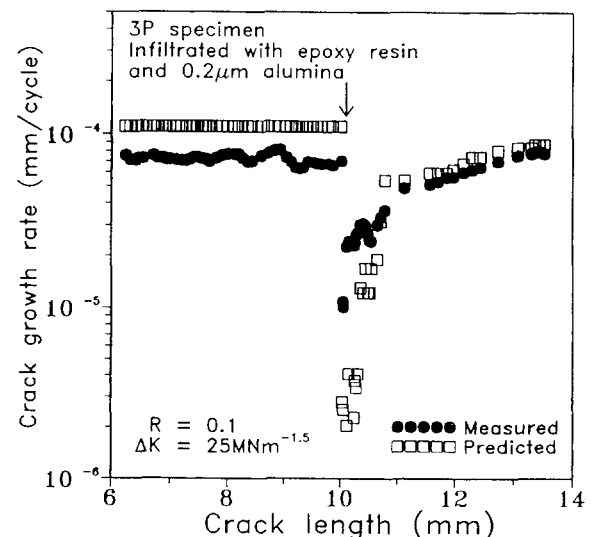


Figure 23 Effect of pressure infiltration with epoxy resin plus 0.2 µm alumina on crack growth behaviour in the 3P specimen. Arrow shows the crack tip position during infiltration

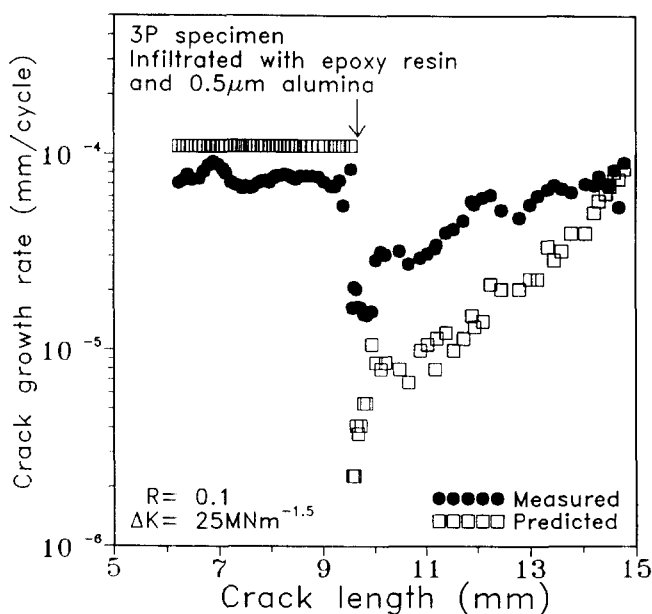


Figure 24 Effect of pressure infiltration with epoxy resin plus $0.5 \mu\text{m}$ alumina on crack growth behaviour in the 3P specimen. Arrow shows the crack tip position during infiltration

tration method brought about lower minimum growth rates and longer life extensions (see Table 2).

Comparison between the current three cases showed that reinforcing epoxy resin with different-sized alumina powder did not cause significant differences in retardation and life extension. Subsequent examination of the fracture surfaces suggested that the differences in growth response and life extension were probably associated with how well the resin filled up the crack to the crack tip. Reinforcement with a wider range of particle size and particle mechanical properties is needed to clarify whether a harder infiltrant will give a better repair.

The five methods employed above all induced retardation in growth rate and hence extension in fatigue life to different amounts. The most straightforward parameter to quantify the beneficial effect of a repair method is the amount of life extension, expressed in number of cycles. The severity of retardation (minimum growth rate/baseline growth rate) and the

overall affected crack growth increment also reflect the effectiveness of a repair method. Though not as direct as life extension, the latter two parameters tend to shed some light on the direction towards which a particular method should be improved. Tables 2 and 3 document these three parameters for each of the tests in the 3P and pipe specimens respectively. Overload retardation is the most convenient method to apply in general. It may be applied to most configurations. Its retardation effect is fairly certain, and repeated applications can easily be achieved. However, the major drawback that probably precludes its use on practical components is that it carries the risk of causing stretch-tearing growth or even catastrophic fracture. This risk is difficult to avoid, as in most engineering applications the exact fracture toughness of the material concerned is often not known. On the other hand, hole drilling and infiltration do not carry the above risk.

Of the five methods investigated, hole drilling gave the longest life extension, and by drilling ahead of a crack the requirement of strictly removing the crack tip is not necessary, yet a very favourable effect can still be obtained. In the case where hole drilling is not appropriate, infiltration is a potential candidate. Currently the infiltration technique needs to be improved before it can have practical value. It is reasoned that, to be successful, we must be able to infiltrate foreign materials well into the crack tip region in a reproducible manner. Moreover, the thickness of the infiltrated materials should be large enough to cause a sufficient amount of crack closure so that the crack growth rate can be decreased to a very low level. If this cannot be achieved, repeated applications should be attempted.

The above comparison between pipe and 3P specimens showed that the beneficial effect of overload on pipe specimen cannot be accurately predicted from small 3P specimens. Further numerical analysis on stress intensity factor will clarify whether we can predict from small specimens the effect of hole drilling on full-scale components. Although the effect of infiltration repair depends very much on whether infiltration has taken place, current results show that the responses of the pipe and 3P specimens are similar. This suggests that the more economical tests on standard specimens

Table 2 Summary of the effectiveness of various repair methods on 3P specimens

Method	Severity of retardation ^a	Affected crack growth increment (mm)	Life extension (no. of cycles)
1.86 times overload	0.18	3.9	17 000
Crack-flank holes (3PH1)	0.18	1.5	40 000
Hand tool (3PH2)	Stopped ^b	—	25 000
Hand tool (3PH3)	0.17	1.4	11 000
1 mm ahead of tip (3PH4)	Stopped	—	126 000
4 mm ahead of tip (3PH5)	Stopped	—	112 000
Aqueous alumina infiltrant	1	—	—
Vacuum-infiltrated epoxy resin	0.35	3.2	15 400
Pressure-infiltrated epoxy resin	0.17	3.1	36 000
Epoxy resin + 0.2 μm alumina	0.27	3.2	31 000
Epoxy resin + 0.5 μm alumina	0.16	4.2	60 000

^aSeverity of retardation = Minimum growth rate/baseline growth rate.

^bCrack grew into a hole and stopped on the front surface only.

Table 3 Summary of the effectiveness of various repair methods on pipe specimen

Method	Severity of retardation ^a	Affected crack growth increment (mm)	Life extension (no. of cycles)
1.86 times overload	0.46	27	95 000
4.5 mm crack-flank holes	—	—	—
2.7 mm crack-flank holes	0.44	2.5	5 000
Epoxy resin infiltrant	0.18	3.6	12 600
380 nm alumina infiltrant	0.29	2.5	7 000
585 nm alumina infiltrant	—	—	—
690 nm alumina infiltrant	0.4	1.4	2 900
1100 nm alumina infiltrant	—	—	—

^aSeverity of retardation = Minimum growth rate/baseline growth rate.

may be used to investigate the possible extension in life under infiltration repairs.

CONCLUSIONS

The effects on crack growth caused by hole drilling near the crack tip and artificial induction of crack closure by tensile overload, infiltration with epoxy resin, alumina powder and a mixture of both have been studied in 165 mm diameter pipe and three-point bending specimens. Except for a poor infiltration technique to transport aqueous alumina suspension into 3P specimens, all five methods achieved crack growth retardation and successfully extended the fatigue life, to different extents. The introduction of an overload may risk fracturing the cracked structure, and so is not a good candidate for fatigue crack repair technique. Crack-flank hole drilling and infiltration are relatively safe. In this preliminary work, hole drilling was more effective than infiltration in extending the fatigue life. The best retardation effect was obtained by drilling very near to the crack plane while slightly ahead of the crack tip. More efficient infiltration techniques are needed for this method to be of practical value.

ACKNOWLEDGEMENTS

The authors gratefully acknowledge the financial support provided by the National Science Council under the projects NSC-83-0401-E-002-087 and NSC-84-2212-E-002-024.

REFERENCES

- Thompson, N., Wadsworth, N.J. and Louat, N. *Phil. Mag.* 1956, **1**, 113
- Christensen, R.H. In 'Metal Fatigue' (Eds. G. Sines and J.L. Waisman) McGraw-Hill, New York, 1959, pp. 376-412
- Bentele, M. and Lowthian, C.S. *Aircraft Eng.* 1952, **24** (276), 32
- Raymond, M.H. and Coffin, L.F. *J. Basic Eng.* 1963, **85** (4), 548
- Sinclair, G.M. and Dolan, T.J. In 'Proc. First US National Congress of Applied Mechanics', ASME, New York, 1952, p. 647
- Sandor, B.I. In 'Achievement of High Fatigue Resistance in Metals and Alloys', ASTM STP 467, American Society for Testing and Materials, Philadelphia, 1970, pp. 254-275
- Wright, M.A. and Greenough, A.P. *J. Inst. Met.* 1964-65, **93**, 309
- Ivanova, V.S., Antikain, P.A. and Sabitova, N.S. *Metallovedenie i Termicheskaya Obrabotka Metallov* 1965, No. 1, Jan., 7
- Cousland, S.McK. and Sargent, K.R. *J. Inst. Met.* 1963-1964, **92**, cited in ref. 10
- Popp, H.G., Wilber, L.G. and Erdeman, V.J. In 'Metal Fatigue Damage—Mechanism, Detection, Avoidance and Repair' (Ed. S. Manson), ASTM STP 495, American Society for Testing and Materials, Philadelphia, 1971, p. 228
- Linnert, G.E. 'Welding Metallurgy', Vol. 2, American Welding Society, New York, 1967
- Broek, D. 'Elementary Engineering Fracture Mechanics', 4th edn. 1986, Martinus Nijhoff Publishers, The Hague
- de Rijk, P. Nat. Aerospace Inst. Amsterdam Report TR 70021, 1970, cited in Ref. 12
- van Leeuwen, H.P. *et al.* Nat. Aerospace Inst. Amsterdam Report TR 70029, 1970, cited in ref. 12
- Eggwirtz, S. Swedish Aerospace Inst. FFA Report TN-HE-1270, 1969, cited in ref. 12
- Blazewicz, W. Results reported in Schijve, J. *Eng. Fract. Mech.* 1979, **11**, 182
- Landy, M.A., Armen, H. Jr. and Eindoff, H.L. In 'Fatigue in Mechanically Fastened Composite and Metallic Joints', ASTM STP 927, American Society for Testing and Materials, Philadelphia, 1986, pp. 190-220
- Shin, C.S. and Smith, R.A. *Eng. Fract. Mech.* 1988, **29** (3), 301
- Miyagawa, H. and Nisitani, H. *Bull. Jpn. Soc. Mech. Eng.* 1985, **28** (244), 2219
- von Euw, E.J.F., Hertzberg, R.W. and Roberts, R. In 'Stress Analysis and Growth of Cracks, Proc. 1971 National Symposium on Fracture Mechanics', Part I, ASTM STP 513, American Society for Testing and Materials, Philadelphia, 1972, pp. 230-259
- Novotny, I.G. *Proc. Inst. Mech. Eng.* 1986, **C268/86**, 249
- Christensen, R.H. 'Metal Fatigue', McGraw-Hill, New York, 1959
- Schijve, J. and Brock, D. *Aircraft Eng.* 1962, **34**, 314
- Jones, R.E. *Eng. Fract. Mech.* 1973, **5**, 585
- Suresh, S. *Scr. Metall.* 1982, **16**, 995
- Suresh, S. *Eng. Fract. Mech.* 1983, **18** (3), 577
- Elber, W. *Eng. Fract. Mech.* 1970, **2**, 37
- Elber, W. In 'Damage Tolerance in Aircraft Structures', ASTM STP 486, American Society for Testing and Materials, Philadelphia, 1971, pp. 230-242
- Shin, C.S. and Fleck, N.A. *Fatigue Fract. Eng. Mater. Struct.* 1987, **9** (5), 379
- Fleck, N.A. In 'Basic Questions in Fatigue', Vol. 1 (Eds. J.T. Fong and R.J. Fields) ASTM STP 924, American Society for Testing and Materials, Philadelphia, 1988, pp. 157-183
- Shin, C.S. and Hsu, S.H. *Int. J. Fatigue* 1993, **15** (3), 181
- Vecchio, R.S., Crompton, J.S. and Hertzberg, R.W. *Int. J. Fract.* 1986, **31**, R29
- Shin, C.S. and Hsu, S.H. *Eng. Fract. Mech.* 1992, **43** (4), 677
- Shin, C.S., Tseng, R.P. and Jao, W.T. *Int. J. Pressure Vessels Piping* 1994, **57**, 169
- 'Standard Test Method for Plane-Strain Fracture Toughness of Metallic Materials', ASTM E399-90, American Society for Testing and Materials, Philadelphia, 1990
- Song, P.S., Wang, C.M. and Shin, C.S. In 'Proc. 1994 Far East Conference on NDT (FENDT '94) and ROCSNT Ninth Annual Conference', Taipei, ROC, Nov. 1994, pp. 221-228
- Kikukawa, M., Jono, M. and Tanaka, K. In 'Proc. ICM2', Boston, 1976, pp. 254-277

FATIGUE IMPROVEMENT OF WELD REPAIRED CRANE RUNWAY GIRDER BY ULTRASONIC IMPACT TREATMENT

T. Tominaga^aK. Matsuoka^aY. Sato^bT. Suzuki^c

^a Steel Structure Development Center, Nippon Steel Corporation

^b Kimitsu works, Nippon Steel Corporation

^c Material Characterization Research Laboratory, Nippon Steel Corporation
(Japan)

ABSTRACT

The fatigue improvement method using ultrasonic impact treatment was examined. This method was applied to in-plane-gusset detail and out-of-plane gusset detail of existing crane runway girders. Comparison with other fatigue improvement methods was based on fatigue tests performed on small-scale welded specimens, and UIT gave the best result. Also, applicability to mild steel and the influence of repair welds was examined through girder fatigue tests. Fatigue improvement was obtained for 400 MPa class mild steel, even after repair welding.

IIW-Thesaurus keywords: Combined processes; Fatigue improvement; Low carbon steels; Maintenance; Post weld operations; Repair; Steels; Ultrasonic processing; Unalloyed steels.

1 INTRODUCTION

Crane runway girders (hereafter CRG) are the structures that support rails for cranes. They resemble bridge structures and, as with bridges, fatigue is a design criterion. Moreover, in the absence of a deck structure, working stresses in CRGs are usually larger than in bridges. Actually many fatigue cracks have been found in these structures [1]. Also the CRG structures built before the early 1970s have flange gusset details which though not used now, give poor fatigue performance. The same detail has been the source of fatigue problems in Shinkansen railway bridge structures [2].

Weld toe grinding treatment has already been applied to many of these structures, but they are now approaching

the end of the estimated fatigue life of these. To extend the fatigue life further, some kind of additional treatment was needed. Therefore, various fatigue improvement methods were compared and their effects were evaluated. As a result ultrasonic impact treatment (UIT) was selected.

With regard to the application of UIT to flange gussets, out-of-plane gussets and vertical stiffeners, the following issues are examined.

- (a) Comparison with other fatigue improvement methods on performance or ease of operation.
 - (b) Applicability of UIT to mild steels.
 - (c) Possible influence of repair welds.
 - (d) Quality control of UIT.
- (b) was considered because, for fatigue improvement methods based on the introduction of compression residual stress are known to be more effective when applied to high strength materials. Low Temperature

Doc. IIW-1860-07 (ex-doc. XIII-2170r1-07) recommended for publication by Commission XIII "Fatigue behaviour of welded components and structures".

Transformation welding material (hereafter LTT) is also more effective for high strength steels [3]. Also, many of Fisher's investigations of UIT were conducted using specimens made from HPS70 (ASTM 709), which are 600 MPa class steels [4]. However, existing old CRG structures are mostly built from 400 MPa class mild steels.

It is also known that the toughness of ferrite-pearlite steels can be reduced as a result of large compressive strain [5]. Only 1-2 mm in depth is affected by UIT, and so no such decrease of toughness is expected. Even so, this effect was also examined.

For subject (c), the problem envisaged was the large residual stress induced from repair welds. Many existing CRGs are already repaired by welding. Repair welds are conducted under conditions of high restraint, so high residual stresses are usually induced in a large area of the structure. The concern was that large tensile residual stress would reduce the beneficial effect of the compressive stress induced by UIT.

With regard to (d), a standard quality control method for UIT is already provided by Applied Ultrasonics, the company providing the UIT equipment. However, this does not include any means of controlling the residual stress level. So, from that point of view, additional quality control parameters were examined.

The resulting study included fatigue tests on welded joint specimens and large-scale components, Charpy impact tests, residual stress measurements and treatment tests to develop the application of UIT to CRGs.

2 EVALUATION OF FATIGUE PERFORMANCE BY SMALL SCALE WELDED JOINT SPECIMENS

2.1 Test parameters

Specimens consisting of plates with in-plane attachments welded to their edges (Figure 1) were used to

represent flange gusset type joints in CRGs. The weld toe condition (as-welded, toe ground or UIT) and the presence or not of a repair weld were the parameters investigated, as summarized in Table 1. The specimen geometry and details of the repair welds are shown in Figure 1. The flange gusset fillet weld size was 6 mm. Flange gussets are usually attached with full-penetration welds. However, to examine the effect of weld defects, no special care was taken to achieve these in the present specimens with the result that slight lack of penetration defects remained at the weld roots. The specimens were made from SS400 steel with L-55 weld filler material with the properties shown in Table 2.

Details of the repair welds are also shown in Figure 1. These simulated the repair of fatigue cracking from the toe of the weld around the end of the gusset, as indicated in Figure 2 a). In practice, the end of the gusset is cut away before repair, Figure 2 b), to allow sufficient access for the welding. As a result, the gusset length is reduced by around 50 mm and the repair weld does not coincide with the gusset fillet weld, Figure 2 c) and d). To simulate this, the repair welds in the present specimens were located 30 mm from the gusset ends, as indicated in Figure 1. The repair welds were made into 45 degree grooves ground into the plate to leave a 6 mm root gap. A backing plate was used and the weld was made with an interpass temperature of 50-200 °C. After the repair welding, the backing plate was gas-

Table 1 – Specimen details

No	Toe condition	Repair weld	Test stress (MPa)
1	as-welded	No	100
2			150
3		Yes	100
4			150
5	ground	No	100
6			150
7		No	100
8			150
9	UIT	Yes	100
10			150

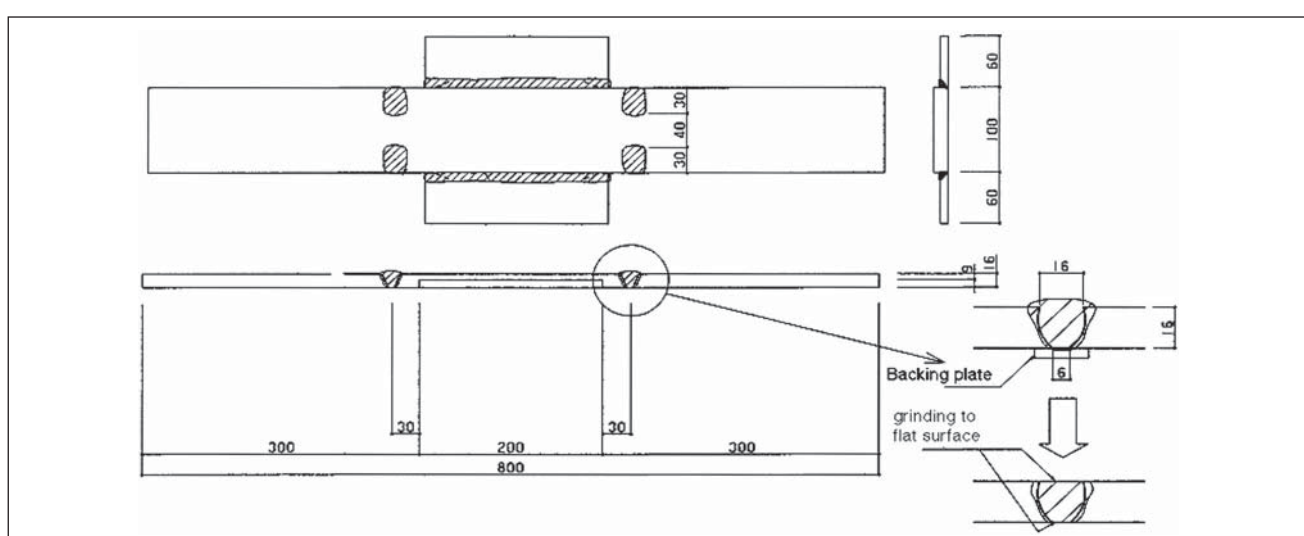


Figure 1 – Geometry of joint specimen

Table 2 – Mechanical properties of materials

Spec.	Thickness (mm)	YS (MPa)	UTS (MPa)	Elongation (%)	Note
SS400	16	286	433	34	main plate
SS400	9	311	449	31	gusset
L-55	φ 4	486	567	30	weld material

cut and the weld cap and root were ground flush with the adjacent plate surfaces.

With regard to the two weld toe improvement techniques used, both of which were applied to as-welded toes, grinding was performed with a 5 mm diameter burr grinder while UIT was carried out using a 27 kHz Esonix tool with 3 mm pins. The treatments were applied to the weld toes at the ends of the gusset and for 30 mm along the fillet weld length; the gusset side of the weld toe was not treated.

2.2 Fatigue test results

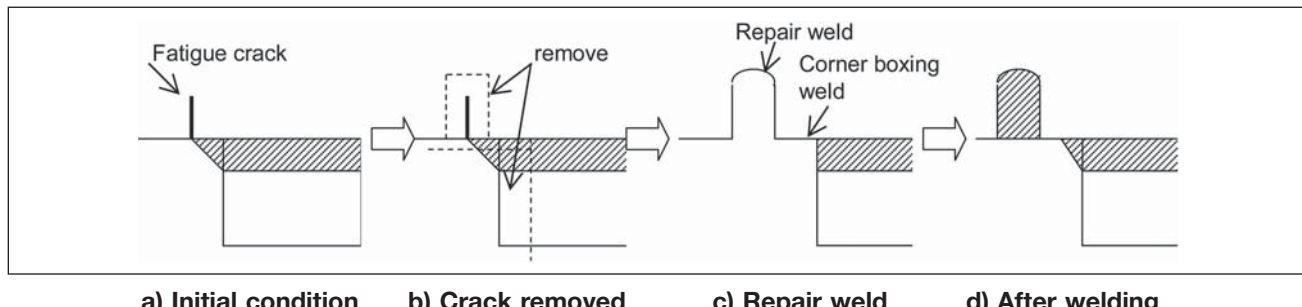
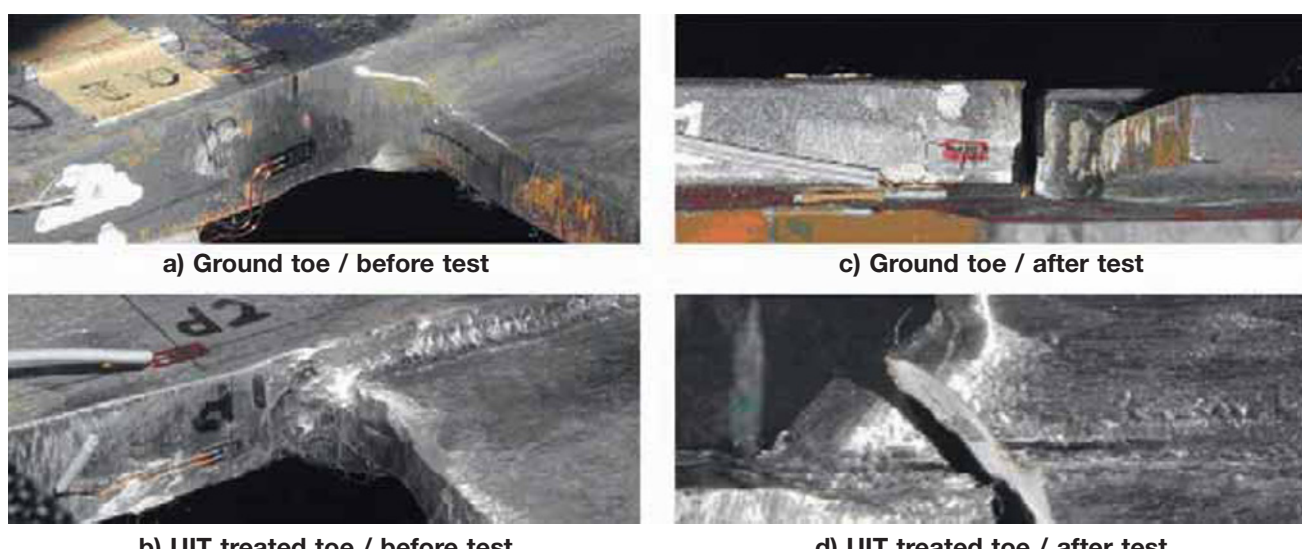
Fatigue tests were conducted at stress ranges of 100 MPa and 150 MPa, both at $R = 0.1$. These stresses were based on field measurements made on Nippon Steel CRGs, from which the maximum stress ever measured in a girder flange was 108 MPa.

Examples of weld toes before and after testing are shown in Figure 3. Both the ground and UIT treated surfaces were very smooth.

The fatigue test results are shown in Figure 4. Compared with grinding, UIT produced the best improvement in fatigue life. Furthermore, the benefit of UIT was not reduced as a result of the presence of repair welds. However, their presence has reduced the fatigue lives of the as-welded specimens. Examples of fatigue cracks produced in the ground and UIT treated types of specimen are shown in Figure 3. The UIT specimens failed from the weld root while the others failed from the weld toe. Thus, UIT provided effective improvement in the fatigue performance of the weld toe.

2.3 Residual stress and toe profiles

The effect of UIT was investigated further on the basis of examination of the weld toe profile and the residual

**Figure 2 – Weld repair procedure****Figure 3 – Welded details**

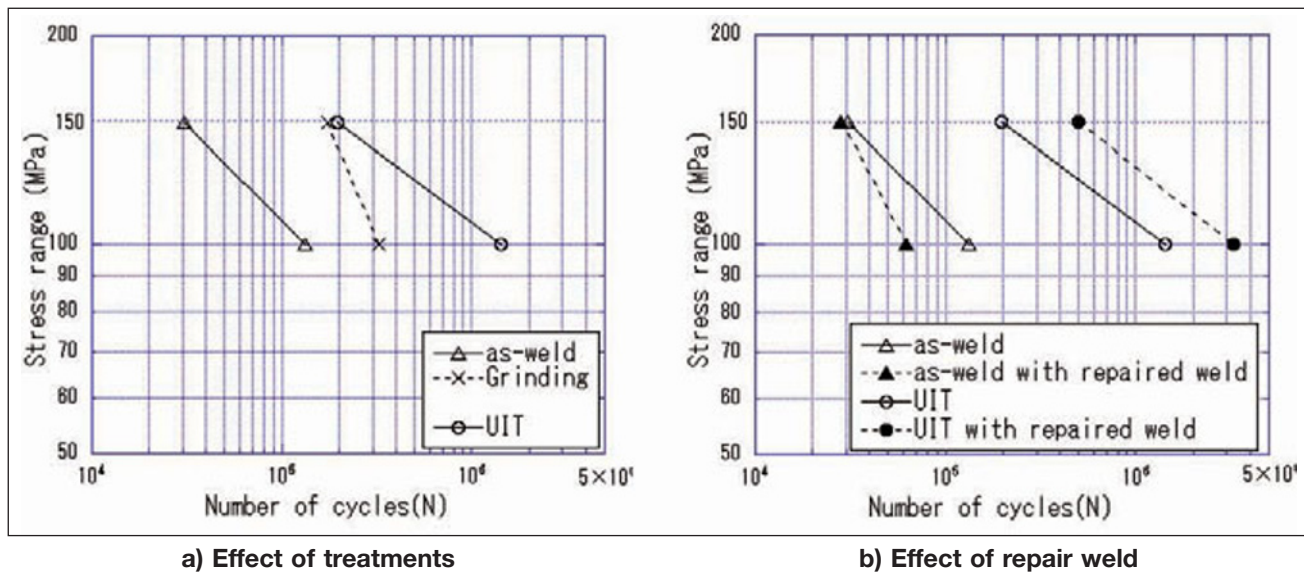


Figure 4 – Fatigue test results

stress in the specimen. The weld profiles were replicated using silicon rubber and used to measure the weld toe radius and flank angle along both sides of the weld bead. Corresponding stress concentration factors were calculated by Atokawa's method for considering a cruciform joint [6]. This was multiplied by 1.5 to allow for the additional stress concentrating effect of the flange gusset to give the final estimate of K_t . After the fatigue testing, residual stresses were measured in the tested specimens near weld toes that did not experience any fatigue cracking. Strain gauges were attached 5 mm from the weld toe. The cutting method was used to measure residual stress, the cutting position being as shown in Figure 5, and residual stresses deduced from the strain changes when the material containing the gauge was cut out (see Figure 5). The gauge position 5 mm from weld toe is too far to measure the resi-

dual stress at the toe, but it is considered suitable for measuring the residual stress from the repair weld.

Details of the toe profiles and average value of K_t are shown in Figure 6. K_t for UIT treated toes is about 75 % of that for the as-welded.

The results of the residual stress measurements are shown in Table 3. These show that the repair weld has introduced tensile residual stress in the as-welded specimens. However, the fact that the residual stress was compressive after UIT in specimens with

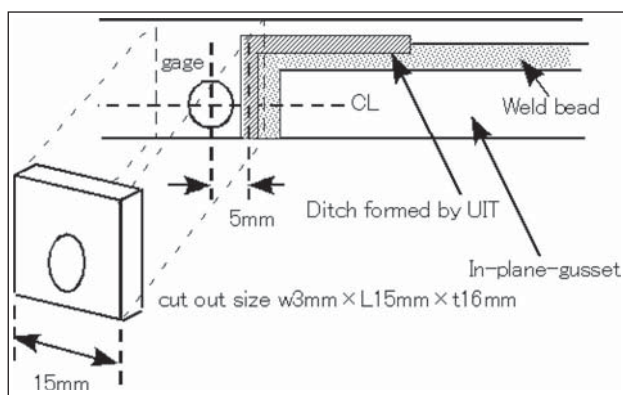


Figure 5 – Geometry of cutting method

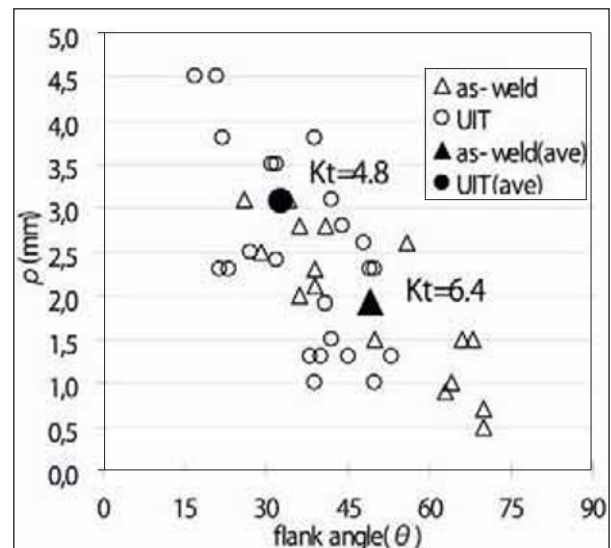


Figure 6 – Toe profiles and stress concentration factor

Table 3 – Results of residual stress measurements

No	Toe condition	Repair weld	Test stress (MPa)	Residual stress (MPa)
1	as-welded	No	100	-21
3		Yes	100	121
9	UIT	No	100	-65
11		Yes	100	-63

or without repairs indicates that this tensile stress was then changed to a compressive residual stress by UIT. Compressive residual stress was measured in the as-welded specimen without UIT. This might be due to stress re-distribution from fatigue test loading.

Thus, these results confirm that UIT is beneficial in terms of reduced stress concentration and the introduction of compressive residual stress. They also verify that residual stress improvement by UIT is not affected by the presence of a repair weld.

3 LARGE SCALE FATIGUE TESTS

3.1 Test parameters

Large scale fatigue tests were conducted on two specimens with the geometry shown in Figure 7. This was a welded plate girder structure with in-plane gussets, out-of-plane gussets and vertical stiffeners. To examine the effect of steel strength [subject (b)], it was fabricated from 400 MPa class mild steel. To examine the effects of UIT [subject (a)] and repair welds [(subject (c)], tests were conducted according to the procedure shown in Table 4.

Specimen No. 1 was the case of UIT without a repair weld, so the UIT treatment was conducted before the initial loading started. (Toes were not ground, before UIT.) Specimen No. 2 was the case of a toe ground beam in which, after initiating a fatigue crack, the crack

was repaired by welding. Then, UIT treatment was conducted after weld repair, giving a UIT with repair weld case. (Repair welded toes were not ground, before UIT.) In this way, for each specimen, both the effect of UIT (N1 and N2) and the effect of repair welding on the benefit of UIT (N1 and N = Ne2 - N2) could be examined.

The toe grinding and UIT conditions were the same as those used to treat the small-scale welded joint specimens. For the UIT treatment time, 32 weld toes in out-of-plane gussets on one side of a web could be treated in about 26 minutes, including the time taken for the operator to change position. Therefore about 50 seconds of treatment time was needed for each weld detail including the position changing. The treatment was done in the flat position. Examples of weld toes at the end of gussets after UIT are shown in Figure 8.

3.2 Test procedure

The applied fatigue test load was 50-460 kN, which produced a stress of 15-154 MPa in the flange at the centre of the bending section. The highest stress for in-plane flange gussets detail was 15-154 MPa, with 12-125 MPa for out-of-plane gussets. These stresses are very high compared with the allowable stress for 400 MPa class steel.

Small, 1 mm gauge length, strain gauges were attached near each weld detail, 5 mm from the weld toe. By

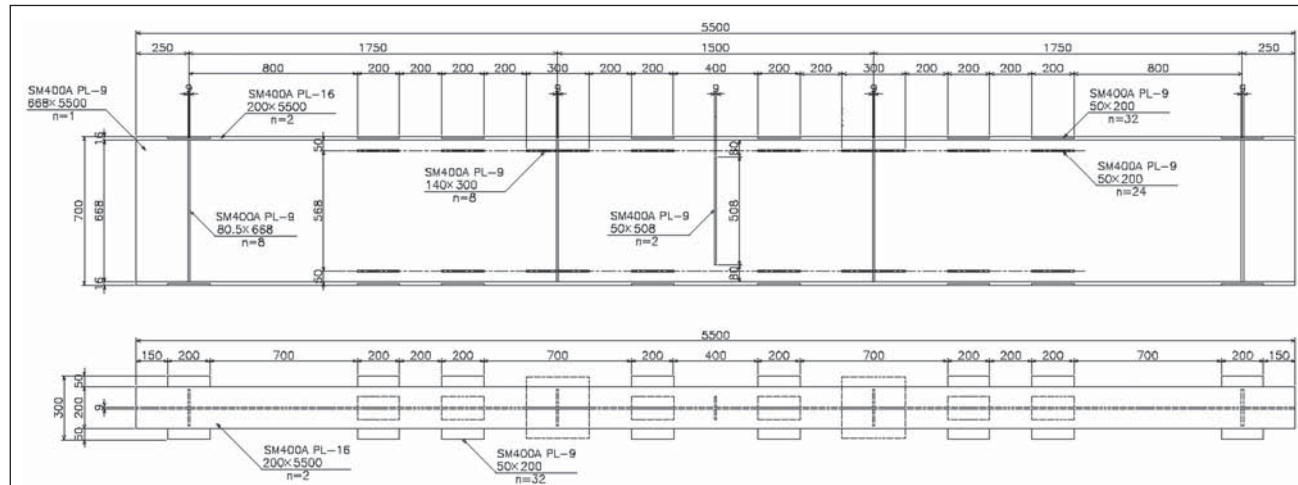


Figure 7 – Geometry of large scale specimen

Table 4 – Test procedure for each specimen

Condition	No. 1	No. 2	Loading cycles
Initial	UIT	grinder	0
Repairing method	crack removal and bolted splice	repair weld and UIT	N1, N2
Finished condition	Ne1, Ne2		
N1	: Number of cycles, when crack initiated in No. 1 specimen (for each crack).		
Ne1	: Total loading cycles of No-1 specimen.		
N2	: Number of cycles, when crack initiated in No. 2 specimen (for each crack).		
Ne2	: Total loading cycles of No-2 specimen.		



a) Weld toe at end of in-plane gusset

b) Weld toe at end of out-of-plane gusset
(boxing weld)

Figure 8 – UIT treated details on flanges

placing them very close to the toe, the local stress change due to applied load was measured. Among the attached strain gauges, 24 highly stressed details were monitored continuously during the fatigue testing. If a local stress change was observed, the loading was stopped immediately and the weld toe checked by magnetic particle testing (MT) for evidence of fatigue cracking. At the same time, a static loading test was conducted.

When the crack length reached 10 mm, the fatigue endurance was recorded as N_f cycles. When the length of cracks at flange gusset details exceeded 10 mm, they were removed by grinding, or gas cutting. The cracks at out-of-plane gussets were stopped by drilling holes at their tips (stop-hole). In the case of specimen No.1, when many cracks had initiated and the remaining cross-section became too small, the parts where cracks had been removed were stiffened by bolting additional plates over them. For specimen No. 2, after removing cracks by grinding or gas cutting, repair welding was conducted. The repair welds were made using 4 mm S-16 electrodes (YP: 460 MPa, UTS: 540 MPa), and ceramic soft backing. To improve the root fatigue performance, the weld size at the end of the flange gusset was increased by making the repair weld in two passes (see section 3.4). The resulting repair welds around the ends of the gussets were not

ground but simply treated with UIT to prevent fatigue cracking from weld toe.

The aim of this procedure was to achieve as many fatigue loading cycles as possible, so that many fatigue cracks could be observed.

3.3 Strain changes due to the first applied loading

Longitudinal gusset details in the as-welded condition usually contain very high tensile residual stress, sometimes greater than yield, due to welding. However, re-distribution of such stresses can take place during the first applied loading. If a fatigue improvement method that controls the residual stress is applied, this re-distribution at the first cycle should be affected by the improvement method. So, useful information is often obtained from the stress measurement data obtained during the first loading cycle.

Typical stress-strain curves at the first cycle for both details are shown in Figure 9. UIT treated and untreated cases are shown for both flange gusset (hereafter FG) and out-of-plane gusset (hereafter WG). The comparison is also done for both the tension and compression sides of the beam. For the normal weld on the tension side, large plastic strains were induced and

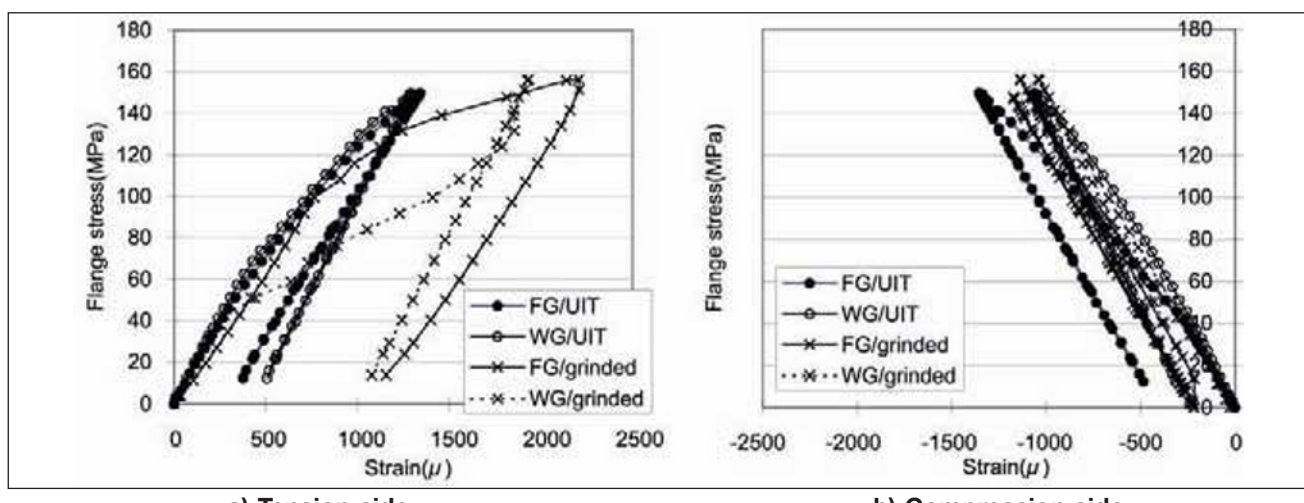


Figure 9 – Stress-strain relation during first loading cycle

tensile residual strains were left. This is consistent with the presence of high tensile residual stress, such that the subsequent application of additional tensile stress from loading produces extensive plasticity. In contrast, large plasticity did not take place in the UIT treated details and the residual strains were smaller. This is because before applying the loading the material was in compression, from the compressive residual stress induced by applying UIT. Also, for the compression side, the residual strains are slightly larger for the UIT treated details, due to the residual stress induced by UIT. In this way, tensile residual stresses provide residual strain for the tension side and compressive residual stresses provide residual strain for the compression side. Thus, from the first time loading residual strain, the stress condition at welded toes can be estimated roughly. Relations of residual strain and applied nominal stress for all the welded toes in the specimens are shown in Figure 10. One graph is for the flange gussets and other is for the out-of-plane gussets. UIT treated cases have smaller residual strain on the tension side, but larger in the compression side. Residual strains for untreated cases are larger for out-of-plane gussets than flange gussets. A possible explanation for this is that the stress concentration factor for the out-

of-plane gusset is higher than that of flange gussets. But the slopes of the stress-load curves in Figure 9 are almost the same for out-of-plane gussets and flange gussets.

Residual strains obtained from first loading of details containing repair welds are also shown in Figure 10. All these cases refer to UIT treated welds. However, comparing the data for normal UIT and repair weld UIT, no significant difference can be found. Tensile residual stress might be induced by the repair weld in a comparatively large area, but the stress condition formed by UIT at each detail is not affected by the original residual stress condition, before UIT treatment.

3.4 Repair welds

Repaired welded details are shown in Figure 11. For the flange gussets, Figure 11 b), it proved to be very difficult to produce good welds due to welding position limitations. As noted previously, to increase the root fatigue resistance, the weld size at the end of the gusset was made larger than that of the original welds (6 mm).

Repair welding changes the residual stress in a relatively large area surrounding the repair. This is evi-

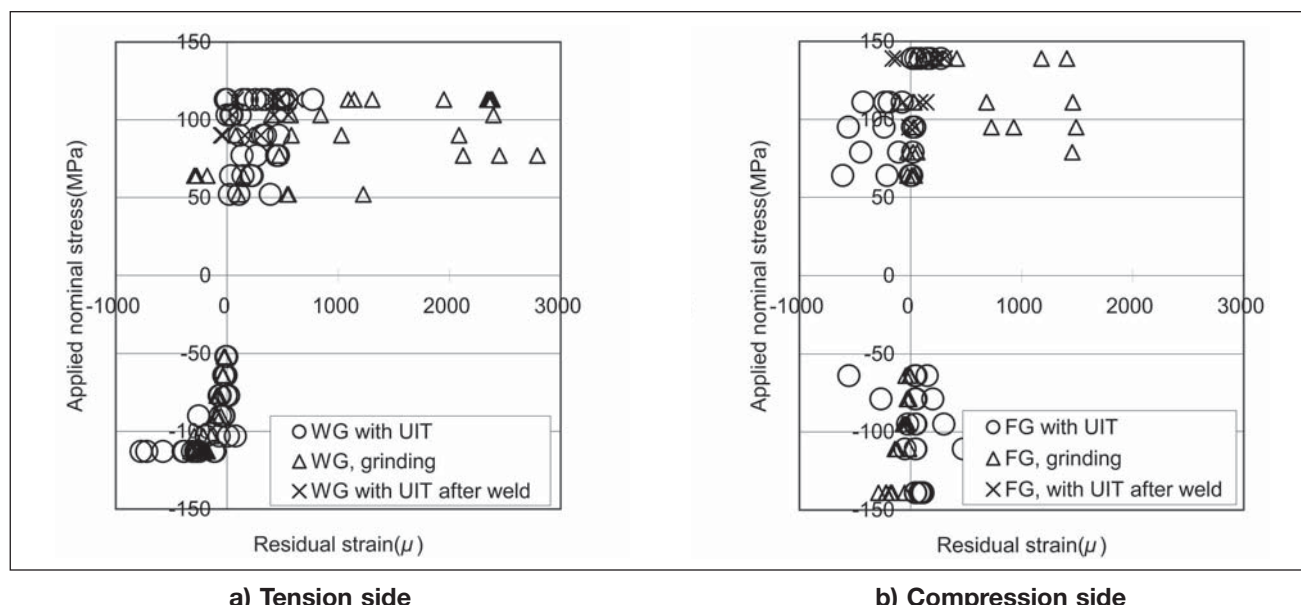


Figure 10 – Residual strain-applied stress relation



a) Flange gusset



b) Out-of-plane gusset

Figure 11 – Repaired welded details

dent from Figure 12 which shows the change of strain following repair welding close to location B3. It will be seen that the strain change was over 600 micro strain at the flange edge on the opposite side to the repaired flange. This is an increase in tensile residual stress of about 120 MPa, assuming all the strain is elastic. The strain change has dropped to 200 micro strain at B2, 200 mm from the repair weld, but is still 100 micro strain (20 MPa) 400 mm away. Also, for the upper flange, the compressive stress increased.

A total of nine repairs were carried out but re-application of UIT for relevant adjacent details that had been

UIT treated previously was not carried out. But from the obtained data, if the repaired welding is conducted and there is UIT treated (treated before the repair welding) detail within 300-400 mm, re-treatment is favourable to recover residual stress condition.

3.5 Fatigue performance

Typical fatigue cracks are shown in Figure 13 and the fatigue test results are plotted in Figure 14, together with relevant design S-N curves from the Japanese

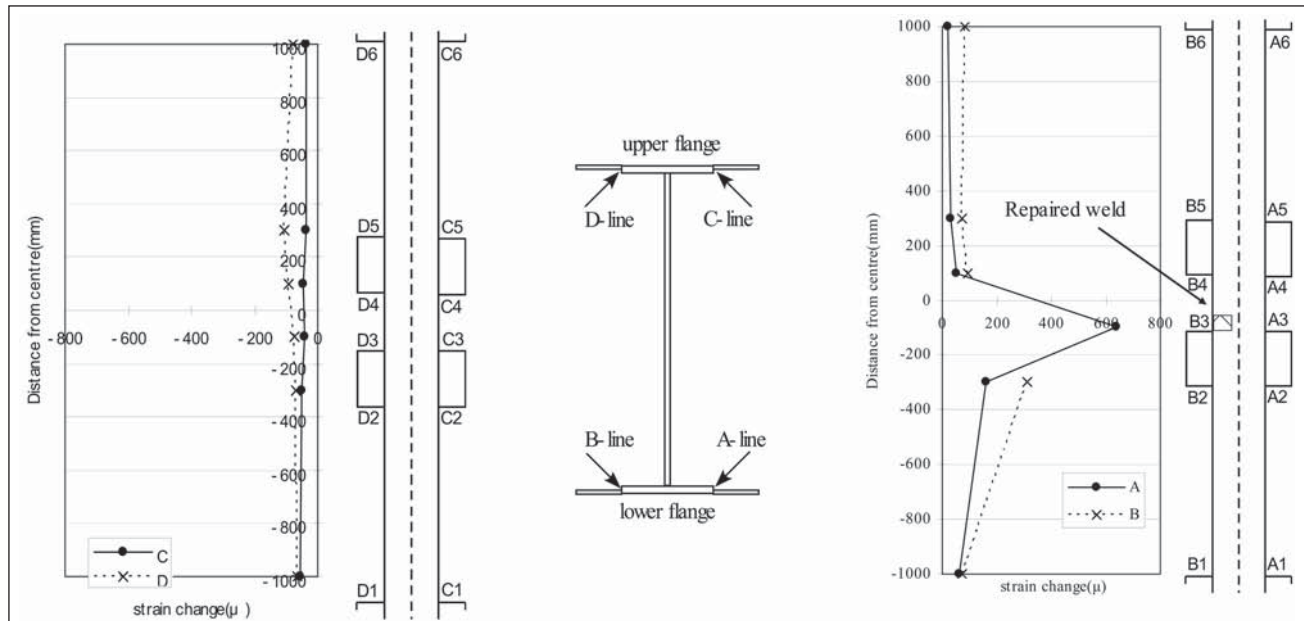


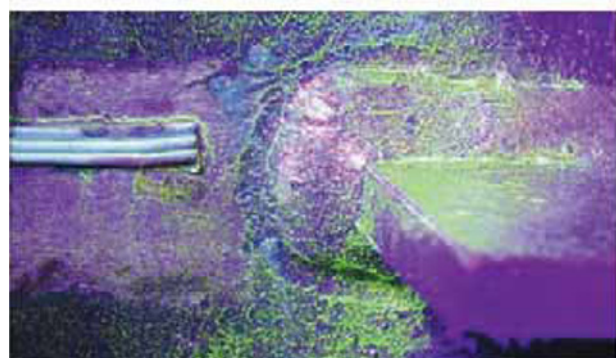
Figure 12 – Strain distribution change due to repaired weld



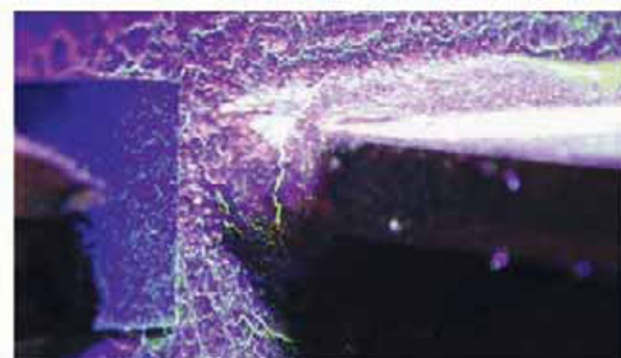
a) Flange gusset / ground



c) Flange gusset / UIT



b) Out-of-plane gusset / ground



d) Out-of-plane gusset/ UIT

Figure 13 – Typical fatigue cracks

JSSC fatigue design code. Specimen No. 1, which started with weld toes treated by UIT, was tested for 2.01 million cycles. Specimen No. 2, which started with ground weld toes, continued for 1.36 million cycles, at which time a fatigue crack initiated at the fillet weld between the flange and web end, the test had to be terminated. (This detail was UIT treated in specimen No. 1 and there was no evidence of fatigue cracking). In Figure 14, "No crack" means there was no evidence of cracking from the detail at the end of the fatigue test. Symbols with the arrow are results without fatigue cracks. Fatigue classes are classified by JSSC (Japan Society of Steel Construction) standards.

For the ground welds, toe cracks initiated at a very early stage of loading. However, all the fatigue cracks in UIT treated details initiated at the weld root. In the case of the flange gussets, for a stress range of 139 MPa the first crack initiated at about 110 000 cycles for the ground toe compared with about 390 000 cycles, 3.5 times longer, in the UIT treated detail. In fact, there was a significant decrease of strain in the toe ground

case after about 70 000 cycles. This may have been due to crack initiation, in which case the margin between crack initiation in toe ground and UIT details increases to more than 5. At lower applied stress ranges the difference is larger, corresponding to a factor of about 8.8 at a stress of 111 MPa. Similar effects were observed in the out-of-plane gussets. At a stress range of 113 MPa, the first crack in a toe ground detail was observed at 260 000 cycles, compared with 1.36 million cycles for the UIT case, about 5.2 times higher. The flange gusset detail is classified as JSSC Class H. Referring to Figure 14, toe grinding increased the performance by one class to G. However, UIT improved it by three classes, to E. For the out-of-plane gusset, only G-E class performance was obtained by grinding, whereas again UIT improved the performance by three classes, to D. For some details treated by grinding, there was no improvement. Many of the grooves formed by grinding were more than 1 mm depth. Thus, these comparatively short lives were attributed to over-grinding.

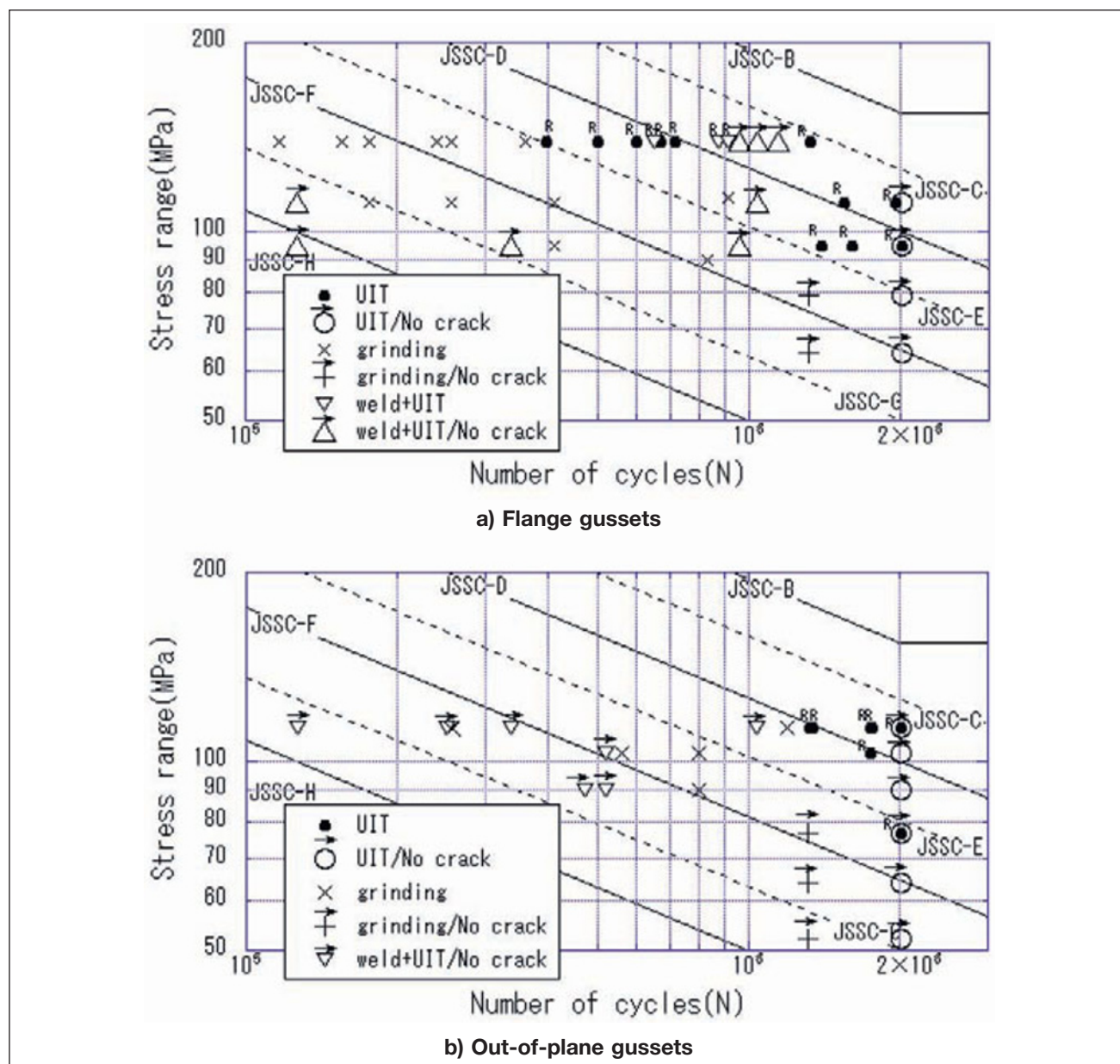


Figure 14 – S-N relations

No fatigue cracks initiated from the edges of UIT treated weld repaired gussets. However, some cracks initiated from the repair weld. As the repair welding conditions were very poor, cracks initiated from weld defects within the weld metal. However, even in that case, about 650 000 cycles were achieved. This is longer than the lowest life of 390 000 cycles achieved by UIT treatment of normal welds, a result that is believed to reflect the extra benefit obtained by increasing the weld size when making the repair welds.

Similarly no fatigue cracks initiated from UIT treated repaired out-of-plane gusset details. The maximum fatigue life obtained from these details was 1.03 million cycles, which is very close to the life of 1.32 million cycles obtained from the UIT treated normal weld, without a repair. If it had not been necessary to terminate the test due to fatigue cracking from the flange to web fillet, clearly a greater improvement may have been obtained.

4 TREATMENT TESTS

4.1 Ease of operation

To compare the 'ease of operation' of UIT to other improvement methods [subject (a)], basic treatment tests were conducted. Acceleration of the tool and noise were measured. Figure 15 shows the configurations of the basic treatment test and the measuring equipment. The UIT tool was set on the support frame and the treatment was applied onto steel plates under constant load. An acceleration meter was set on the tool and a microphone was located 2 m from the tool.

Measurements were also made during hammer peening (HP) and the results compared. For the hammer peening, a compressed air powered ACJ-16 (product of NITTO KOHKI Co.) gun was used. The tip of the tool was modified to a shape suitable for peening. The force needed to keep the tool in contact with the plate during treatment was 3.5 kgf for UIT, and 20 kgf for HP.

The measured acceleration and noise are given in Table 5. Both the noise and acceleration were smaller in the case of UIT, especially the latter.

As UIT is powered by an ultrasonic generator, the density of impulses is very large. Consequently, uniform

Table 5 – Acceleration and noise

Tool	Acceleration rms (m/s^2)	Max acceleration (m/s^2)	Noise (dB)
UIT	16 ~ 18	90	69 ~ 74
HP	562 ~ 631	1 200	83 ~ 87

deformation of the steel surface can be produced. An example of a uniform and smooth treated surface is shown in Figure 16.

4.2 Residual stress

To find the parameter for controlling residual stress [subject (d)], a further basic treatment test was conducted, again using the configuration shown in Figure 15. The test plate was placed on slider, and moved back and forth manually. Both operating parameters and the plate treated were varied and measurements made on surface geometry and residual stress produced.

The parameters varied were pin type, power, treatment speed, number of treatment passes, treatment time, applied force, welding, and steel strength. The test plate size was 300 mm length and 100 mm width. Both 9 mm and 28 mm thickness plates were used. Geometry measurements were made using a contact roughness meter having 1 micron accuracy. Residual stresses were measured by X-ray diffraction (RIKEN 20 kV/10 mA). A 2 mm collimator was used because no significant difference was found between the results for 1 mm and 2 mm collimators.

One of the sets of results is shown in Figure 17. A close relation is found between the width of the groove

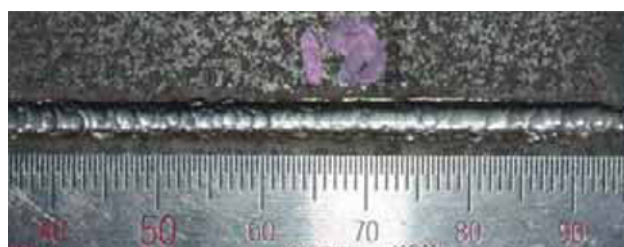


Figure 16 – Surface deformation produced by UIT

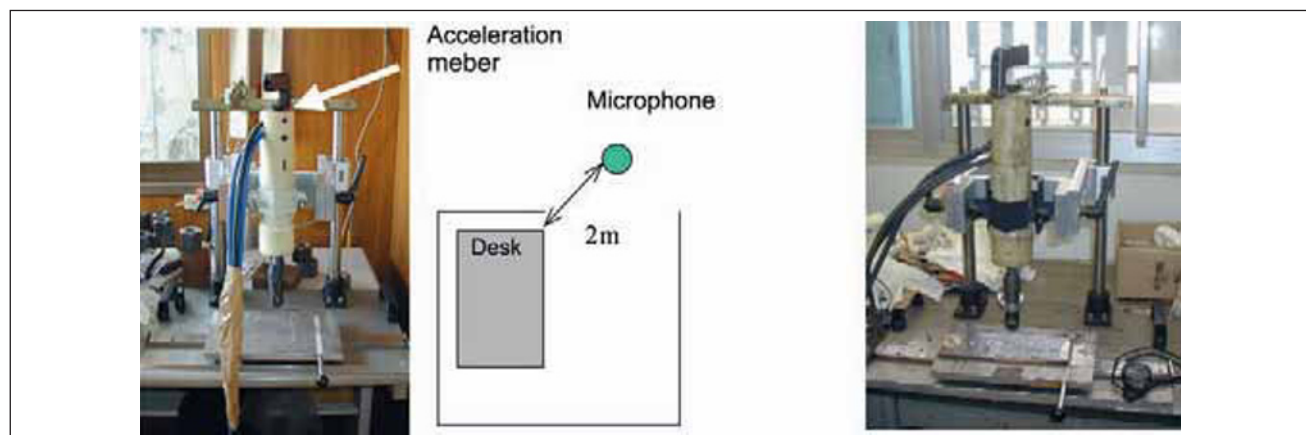


Figure 15 – Configuration of treatment and measurements

produced by deformation of the surface metal and the magnitude of the induced compressive residual stress acting transverse to the groove direction. So the size of the groove formed is selected as an important quality control parameter, leading to the requirement of a groove width of 4 mm.

4.3 Field efficiency test

Test treatment was conducted on existing structures to examine the practicability of applying UIT in the field as compared with grinding. Using the full scale girder model shown in Figure 18, test treatment was conducted by UIT and grinding in the flat, horizontal, and overhead positions. After using in one position, the equipment set was dismantled, carried to a new location, and then set up again. The treatment length for each operating position was 2 m. Scaffolding was required in order to apply treatment in the horizontal and overhead positions. The grinder was air driven

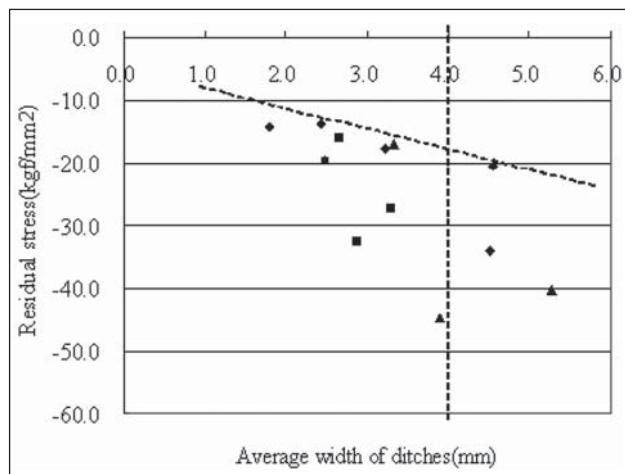


Figure 17 – Relation between residual stress and UIT groove width



and was applied using a high strength tool with a cone shaped tip. The time consumed carrying out each treatment was measured to examine the relative efficiency in field conditions of the two treatment methods.

The test results are shown in Table 6. The average treatment speed of UIT was about 4 times faster than that of grinding. The physical burden from UIT treatment is much smaller than that from a grinder with the result that the treatment time rate can be higher. The estimated treatment length in one day, calculated from the treatment time rate, is shown in Table 7. This shows that the treatment efficiency of UIT can be 4.4 to 6.6 times greater than that of grinding.

Table 6 – Measured treatment time

	UIT 27 kHz	Grinder
Average treatment speed [cm/min]	43.0	11.0
Equipment transfer time [min]	10.0-10.8	0.5-0.9
Break time/ treatment time [min]	0/10	8.0/45.2

Table 7 – Treatment efficiency

UIT		Grinder	
Treatment time rate	Treatment length of toes of welds	Treatment time rate	Treatment length of toes of welds
35 %	6 540 cm/day	30 %	1 410 cm/day
50 %	9 340 cm/day	-	-

5 TOUGHNESS OF WELDED JOINTS

UIT causes plastic deformation of the metal surface and hence the introduction of compressive residual stress. It has been suggested that the depth of plastic deformation up to 1.5-2.5 mm, and the depth of the residual compressive stress field extend up to 15 mm



Figure 18 – Condition of field treatment test

[7]. This residual stress decreasing effect has not yet been verified. However, if such a large-scale effect really exists, it should be confirmed that there is no degradation in the fracture toughness of the material as a result of UIT treatment, especially for ferrite-pearlite steel [subject (b)]. Therefore, a simple examination was conducted involving the use of Charpy impact tests to detect evidence of possible reduced toughness following the application of UIT.

In particular, the influence on toughness of the following parameters was investigated.

- a) With or without UIT.
- b) With or without welding.
- c) Direction C and L; (L is rolling direction of the plate, C is the transverse).

Three tests were performed for each parameter leading to 24 Charpy tests, all conducted at 0 degrees C.

The geometries of the specimens are shown in Figure 19. They were made from 16 mm thick SN490

steel plate with the chemical composition and mechanical properties, from the mill sheet data, shown in Table 8. For the welded sample, in order to produce a re-heated zone (heat-affected zone of both beads) with poor toughness, 2 weld beads are laid side by side. The weld material was YM-26 and the heat input was 2.5 kJ/mm. UIT was applied along the centre of the plate in the L-direction using 27 kHz tool with 3 mm diameter pins at a treatment density of 3 sec/cm. For the welded specimen, the treatment was applied between the two weld beads. The Charpy specimen notches were placed just under the groove produced by UIT. The Charpy specimens were standard 10 mm size, with a 2 mm deep notch.

The Charpy test results obtained are presented in Table 9. It will be seen that the UIT has not influenced the toughness of the steel in either the L or C direction. The toughness of the welded specimens was lower but again not influenced by the application of UIT.

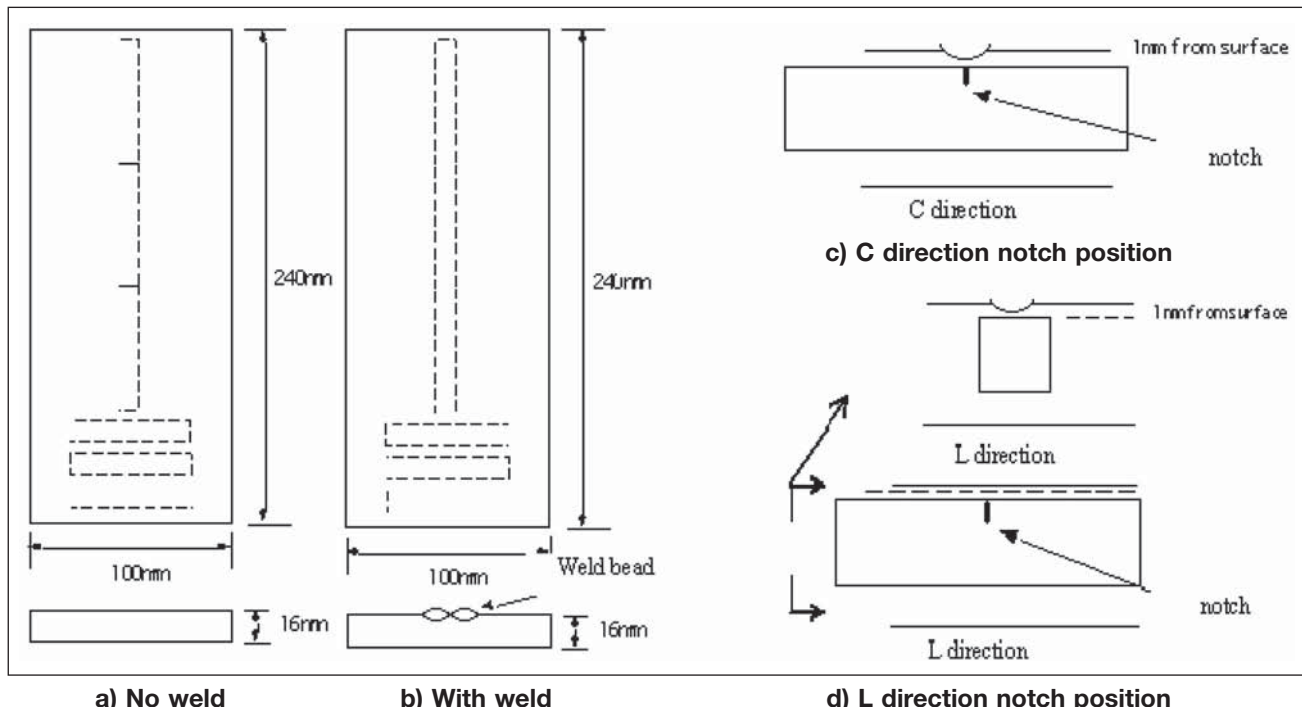


Figure 19 – Geometry of specimens

Table 8 – Chemical compositions

C	Si	Mn	P	S	Ni	Mo	Cr	CEQ	YS (MPa)	TS (MPa)	EL (%)
0.16	0.35	1.44	0.025	0.005	0.02	0.01	0.03	0.42	352	543	25

(※ unit: weight%)

Table 9 – Charpy results

Condition		C-direction		L-direction	
		Charpy (J)	Ave.	Charpy (J)	Ave.
No welding	UIT	209.1, 224.7, 231.3	221.7	213.6, 189.9, 223.2	208.9
	no UIT	216.2, 227.2, 222.8	222.1	175.3, 214.6, 217.2	202.4
Welding	UIT	109.2, 104.4, 108.7	107.4	111.6, 108.2, 104.4	108.1
	no UIT	108.7, 116.4, 116.9	114.0	97.3, 113.5, 109.2	106.7

6 CONCLUSIONS

In this study, the conditions needed for the application of UIT to existing welded 400 MPa class mild steel structures and its effect in terms of improved fatigue resistance were examined on the basis of fatigue tests on small-scale welded joints and large scale welded structures, together with Charpy impact tests. The following conclusions may be drawn.

- a) UIT improved the fatigue performance of flange gusset details, both original welds and repair welds, by an amount equivalent to a 3-class increase in the JSSC fatigue design rules (life increase of approximately 8). Toe grinding was less effective, around one-class increase.
- b) The benefit of UIT was not reduced in the presence of an adjacent weld repair.
- c) UIT was also more efficient than grinding in the treatment of weld toes at the ends of both in-plane and out-of-plane gussets. UIT was also more favourable than hammer peening with regard to ease of operation, including noise level.
- d) There was no evidence that the plastic deformation due to UIT reduced the fracture toughness of the steel.
- e) The most effective measure of quality control for weld toe UIT treatment was the size of the groove produced.



Figure 20 – UIT treatment work

As a result of the study described in this paper, Nippon Steel started to apply UIT to CRGs. Figure 20 shows the treatment being carried out on one CRG. The result of such treatment of existing steel structures will be more healthy, safe and economical operation of facilities.

ACKNOWLEDGEMENTS

We appreciate the support and good advice from Dr. Statnikov of Applied Ultrasonics on UIT treatment.

We also appreciate the kind and practical advice from Prof. Wohlfahrt of T.U. Braunschweig and his colleagues on the X-ray residual stress measurement technique.

REFERENCES

- [1] Tenjousoukoubari Konnwakai: Report of crane girders fatigue damages, JSSC, 1976, Vol. 12, No. 128, pp. 9-22.
- [2] Miki C., Sugimoto I., Kaji H., Megishi H., Ito Y.: A Study on fatigue strength improvement of flange gusset in existing steel railway bridges, Journal of structural mechanics and earthquake engineering, 1998.1, No. 584/I-42, pp. 67-77.
- [3] Tominaga T., Miki C., Takahashi K., Kasuya T., Morikage Y.: Fatigue improvement method for existing bridge by low temperature transformation welding materials, Journal of structural mechanics and earthquake engineering, 2004.4, No. 759/I-67, pp. 355-367.
- [4] Takamori H, Fisher J.W.: Tests of large girders treated to enhance fatigue strength, Transportation research record 1696, paper no. 5B0093, 1999.
- [5] Sasaki E., Arakawa T., Miki C., Ichikaw A.: Required fracture toughness of steel to prevent brittle fracture during earthquakes in steel bridge piers, Journal of structural mechanics and earthquake engineering, 2003.4, No. 731/I-63, pp. 93-102.
- [6] Ushirokawa O., Nakayama E.: Stress concentration factor at welded joints, Ishikawajimaharima Gihou, 1983, Vol. 23, No. 4.
- [7] Statnikov E.Sh.: Application of operational ultrasonic impact treatment (UIT) technology in production of welded joints, IIW Doc. XIII-1667-97, 1997.



Fatigue Life Prediction of Repaired Welded Structures

J. T. P. Castro, J. L. F. Freire

Mechanical Engineering Department, Catholic University of Rio de Janeiro, Rio de Janeiro 22453-900, Brazil

&

R. D. Vieira

Mechanical Engineering Department, CEFET-RJ and StrainLab Stress Analysis, Rio de Janeiro 22461-900, Brazil

ABSTRACT

This paper discusses the fatigue life prediction of welded structures which had cracked in service and were repaired by welding reinforcing plates over the cracked sections. The maximum working stress histories under actual loading conditions were measured and the fatigue lives of the welded repairs were predicted using international design codes. These damage evaluations were compared with the actual numbers of cycles to failure obtained in industrial operation.

1 INTRODUCTION

This paper discusses the fatigue life prediction of three repaired welded steel traveling cranes which are used for ingot manipulation in a steel slab rolling mill. Each crane is composed of two parallel all-welded bridges which have box girder shapes and support a traveling trolley. The two bridges have 30 m spans and are connected at their end sides by head girders which are supported on wheels and rails. All 12 end sides of the three traveling cranes developed fatigue cracks in the transition regions which connect the bridges to the head girders, after six years of normal operation, and were repaired by welding reinforcing plates directly over the cracked regions (Fig. 1).

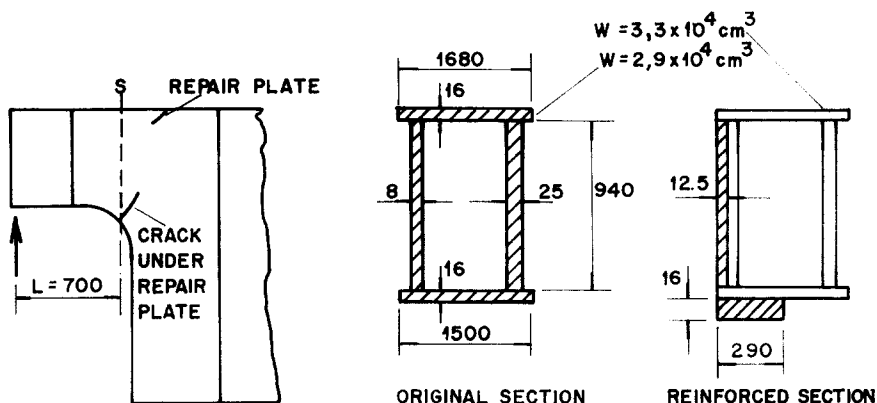


Fig. 1. The reinforcing plates and the cross-sections before and after repairing.

To predict the fatigue life of these welded repairs, working stresses were measured under normal operation and fatigue damage was calculated using several welded structures design codes (IIW,¹ ECCS,² AWS,³ BSI,⁴ AISC,⁵ NBR⁶). The following sections report the stress measurement results, the fatigue damage calculations, and the evaluation of the reliability of these calculations using data from failures which occurred under normal operation.

2 STRESS ANALYSIS

Two elementary models were used to estimate the nominal stress in the structure critical sections. The first model considered the structure as a simple supported beam. The second model used a finite element commercial package. The transition region connecting the bridge to the head girder was modeled by 2D six-node elements. This simple model showed that the stress concentration at the critical sites was larger than 2·0.

The two models were used to indicate the levels of stresses which should be measured in a static experimental stress analysis. Combined with the cracks which appeared in the original cranes, these two models have also shown the best locations for the strain gages in the critical region of the repaired structure.

One of the repaired cranes was instrumented using welded uniaxial (U) strain gages, bonded triaxial rosettes (R) and also reflective photoelastic coatings, as shown in Fig. 2.

The experimental stress measurements were made in two steps. In the first, a quasi-static incremental loading was applied to the crane by lifting ingots of known weights and slowly moving the traveling trolley from one

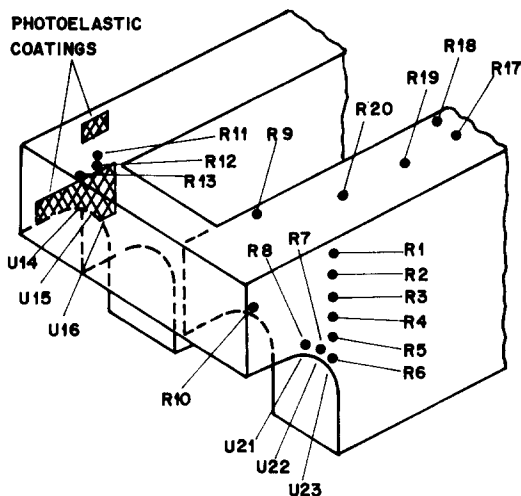


Fig. 2. Location of the uniaxial strain gages (U), rosettes (R) and photoelastic coatings.

bridge end to the other. It was concluded that the maximum static stress was 3.7 times the nominal stress calculated using the simple-supported beam theory and it occurred in the reinforcing repair plate at the same location where cracks have initiated in the non-reinforced structure. This position coincides with the location of the strain gage U23 shown in Fig. 2.

The second experimental step involved the dynamic strain measurements of the most loaded strain gages while the traveling crane was operated in its actual production service. The measured dynamic signals were recorded in a FM tape recorder and correlated with each kind of service executed by the traveling crane. A typical loading history is presented in Fig. 3. This strain history represents the actual variations of the stress ranges ($\Delta\sigma$) which occur in the most loaded point of the structure. It already includes the stress concentration due to the structure geometry (transition region), but does not take into account the geometric imperfections due to the welding details. These imperfections, together with other strength reduction factors, are conveniently considered by the design codes.

3 THE FATIGUE DAMAGE EVALUATION

Fatigue damage was evaluated using five design codes,¹⁻⁵ a S-N Wohler Gerber procedure⁷ and the Brazilian NBR 8400⁶ standard for hoisting structures. The principal difference among these damage evaluation procedures is that the first five consider that fatigue damage is only dependent

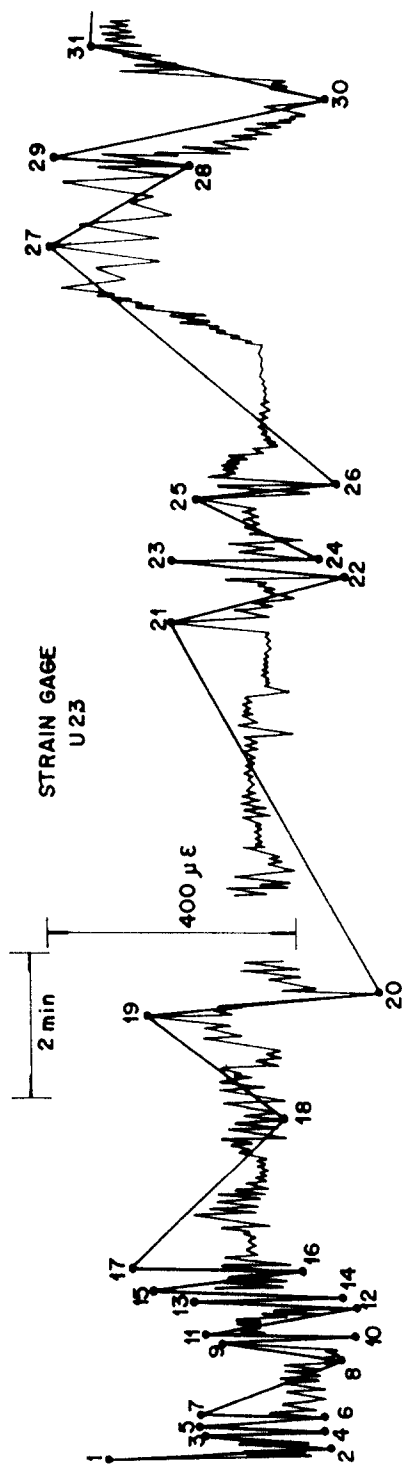


Fig. 3. Typical strain-loading history.

on the stress range. The last two procedures also include the mean stresses as variables which influence the fatigue damage.

For complex loading histories such as the one presented in Fig. 3, all design codes and methods are unanimous in proposing the use of the Palmgren-Miner linear cumulative damage rule.⁷

Cycle counting was carried out by applying the rain-flow^{8,9} counting procedure to the typical loading history presented in Fig. 3. To avoid the inclusion of small load excursions that do not cause fatigue damage, the load history was filtered by using the race-track⁸ method with an amplitude high-pass filter fixed in $\Delta\sigma = 38 \text{ MPa}$.

This value is the fatigue limit of the IIW class 50 welding detail. This means that any value of $\Delta\sigma$ smaller than 38 MPa will not cause any fatigue damage on welded joints of this class (or higher class). Use of this limit assumes that no crack has already been developed. In Fig. 3, the filtered history is presented by a gross continuous trace with numbers identifying each peak that was considered for the rain-flow counting procedure.

Table 1 resumes the fatigue damage evaluation which was determined using the IIW design methodology. The procedures carried out for the

TABLE 1
Lives N_i Corresponding to Each Measured Stress Range (in 10^4 Cycles) for the IIW Welding Detail Classes 50 to 100

$\Delta\sigma_i$ (MPa)	No. $n_i/2$ of half-cycles	Life N_i for the welding classes:						
		50	56	63	71	80	90	100
38	6	523						
39	2	478						
41	2	401						
43	6	339	504					
45	2	290	430					
48	2	321	343	518				
50	2	200	298	449				
53	2	163	243	366				
68	2	68	101	153	233	353		
69	1	65	96	145	221	336	506	
84	1	33	48	73	111	169	254	368
88	1	28	41	62	94	143	216	313
103	1	16	24	36	54	83	124	180
Damage caused by the event ($\times 10^{-6}$)		12.5	7.69	4.53	2.56	1.68	0.93	0.57
No. of similar events allowed ($\times 10^5$)		0.80	1.30	2.18	3.90	5.96	10.7	17.4

other methodology²⁻⁷ are quite similar and only their final results will be reported in Table 2.

Table 1 presents the lives N_i corresponding to each measured stress range $\Delta\sigma_i$ and to each welding class detail strength of the IIW design methodology. Its first column lists the measured stress ranges and the second lists the number of half-cycles each stress range acted in the piece, as counted by the rain-flow method in the filtered history of Fig. 3.

Columns 3-9 list the fatigue lives (considering a 97.3% reliability) the structure would have if it was loaded only by the corresponding $\Delta\sigma_i$, for each class of welding detail proposed by the IIW. The blank spaces mean that the stress range does not cause any damage to the structure, because it is below the fatigue limit of that particular welding detail.

The penultimate line of Table 1 lists the fatigue damage that each measured event would cause in welding details from class 50 to class 100. These damage values were obtained by the application of the Miner's rule, i.e. $\sum n_i/N_i = 1$.

Finally, the last line presents the total lives expected for each welding detail class, in number of 'typical loading history' events.

For example, the damage that the Fig. 3 loading history would cause in a class 50 details is 12.5×10^{-6} . Therefore, fatigue failure of a IIW class 50 detail would be expected before 80 000 'typical load history' events in only 2.7% of the cases (the IIW fatigue strength curves are specified for a 97.3% reliability).

To close the fatigue analysis, it is necessary to classify the welded repair in one of the IIW classes. Inspection of the weld fillets in the field revealed

TABLE 2

Comparison Between the Various Prediction Methods. Predicted Fatigue Life in 10^3 'Typical Load Events' (about 110 000 'typical load events' per year)

Method	Original structure		Repaired structure	
	Joint class	Predicted life	Joint class	Predicted life
IIW	80 or 100	342 or 800	63 or 71	218 or 390
ECCS	80 or 90	252 or 361	64 or 72	187 or 268
AWS	B	356	D or C	60 or 227
BS5400	E or D	257 or 376	F or F	161 or 237
AISC	B-3	500 or 2000	E-3	100 or 500
Gerber				150
NBR			Group 6, K-3	200

many imperfections such as cold spots, overlaps and undercuts. Moreover, the (unremoved) original plate worked as a backing bar. Therefore, it was decided to classify the joint as belonging to a low class, the 71 or the 63. For those classes, the repairs' expected fatigue lives were, respectively, 390 000 and 218 000 'typical loading history' events. As each crane repeats this loading history 110 000 times per year, the 97·3% expected life of the welded repairs would range from two to four years.

The validity of the above predictions depends on the success achieved on the determination of the strain-loading history for the critical point as well as on the actual strength of the welding details.

A possible source of information to support the above analysis is to apply the loading history of Fig. 3 to the original structures which had all their critical points cracked after six years of operation. Figure 2 shows that the repaired critical section had its inertia increased by approximately 15%. Considering that the operational conditions of the traveling crane did not change throughout the years, the typical loading history, presented in Fig. 3, could be increased by a factor of 1·15 and be used to calculate the fatigue damage of the original structures. A new race-track-rain-flow calculation was carried out for this modified loading history and compared to the original structure weld class detail. In this case, the class detail was upgraded because all the original weldings were carried out under good fabrication and inspection conditions. Life predictions for the original structures resulted in 342 000 and 800 000 events, respectively, for the 80 and 100 weld class details, which means three to seven years of service operation. These predictions are compatible with the actual service lifes which did not exceed six years.

The fatigue lives calculated for the original and the repaired crane structures using the IIW design procedure are presented in Table 2 together with the predictions calculated using other design procedures. It can be seen that life predictions indicate fatigue failures for the repaired cranes from approximately one to three years in most cases. Care should be taken when comparing the lives predicted in Table 2, since the reliabilities embedded in the different methods are not equal.

A final verification of the fatigue damage evaluations presented in Table 2 for the repaired structures uses a recent information that one of the 12 repairs has cracked after one year in service. This first to fail welded repair specimen has a 5·61% median rank.⁷ Considering a normal failure distribution and a standard deviation of 15%,¹⁰ the mean life expected for the 12 repairs is 144 000 events. The 2·7% failure life (which considers a 97·3% reliability) is calculated to be equal to 93 000 events. It

can be seen that those numbers are compatible with the fatigue lives predicted in Table 2 for the repaired structures.

4 CONCLUSIONS

The transition regions between the bridge and the head girders of three traveling cranes presented cracks after six years of normal operation. These critical sections were repaired by welding reinforcing plates over the original cracked plates. The present paper showed that it is possible to predict the expected life of the repaired structures by determining the working stresses in the critical regions using experimental methods, and by comparing the race-track filtered and rain-flow counted load history with the fatigue strengths for weld details presented by several design codes or methodologies.

It was concluded that all methodologies indicated that the expected repair lives would range from one to three years. This period of time is smaller than the lives achieved by the original structures. Although the reinforcement plates reduced the working stresses by 15%, the procedure used to weld the repairs lowered the strength of the weld details in larger proportions.

The methodologies used in the life predictions had their accuracy satisfactorily evaluated by their application to the field data generated by the previously fatigue damaged structures. The first crack which appeared in the repaired structure after one year of normal operation also confirmed the accuracy of those predictions.

ACKNOWLEDGMENTS

The Secretaria de Ciéncia e Tecnologia of the Brazilian Government and StrainLab Stress Analysis Ltd, of Rio de Janeiro, Brazil partially financed this work. Eng. Alvaro Pio from Cia. Siderúrgica Tubarão kindly provided the field support for the measurements.

REFERENCES

1. IIW 693-81: Design recommendations for cyclic loaded steel structures. *Welding in the World*, 7/8 (1982).
2. ECCS, *Fatigue Design Rules*, European Convention of Constructional Steel-work, Nov. 1983.

3. AWS D1.1, Structural welding code, 1981.
4. BS 5400, Steel concrete and composite bridges code, 1980.
5. AISC, Specification for the design, fabrication and erection of structural steel for buildings, 1978.
6. NBR 8400, Cálculo de Equipamentos para Levantamento e Movimentação de Cargas. Associação Brasileira de Normas Técnicas, Rio de Janeiro, 1984.
7. Shigley, J. E. & Mischke, C. R., *Mechanical Engineering Design* (5th edn). McGraw Hill, New York, 1989.
8. Rice, R. C., *SAE Fatigue Design Handbook*. Society of Automobilistic Engineers, Warrendale, PA, 1988.
9. Dowling, N. E., Fatigue life prediction for complex load versus time histories. *J. Eng. Mater. & Technol.*, **105** (1983) 206–14.
10. Mischke, C. R., Prediction of stochastic endurance strength. *J. Vibration, Acoustics, Stress and Reliability in Design*, **109** (1987) 113–22.



Contents lists available at ScienceDirect

Engineering Failure Analysis

journal homepage: www.elsevier.com/locate/efa



Fracture and fatigue crack growth analyses on a weld-repaired railway rail



Hyun-Kyu Jun ^a, Jung-Won Seo ^a, Il-Sik Jeon ^b, Sang-Hwan Lee ^c, Yoon-Suk Chang ^{c,*}

^a Korea Railroad Research Institute, Uiwang, Gyeonggi-do 437-755, Republic of Korea

^b Korea Railroad Corporation, Cheongju, Chungcheongbuk-do 363-951, Republic of Korea

^c Dept. of Nuclear Engineering, Kyung Hee Univ., Yongin, Kyonggi-do 446-701, Republic of Korea

ARTICLE INFO

Article history:

Received 9 July 2015

Received in revised form 12 October 2015

Accepted 4 November 2015

Available online 5 November 2015

Keywords:

Failure analysis

Fatigue crack growth

Residual stress

Rolling contact fatigue

Welding technology

ABSTRACT

Although repair by arc welding is a well-known method for damaged rail surface recovery due to its ease of application, the method is vulnerable to the creation of cracks. In this study, a series of failure analyses and crack growth analyses were carried out on a fractured weld-repaired rail to determine the cause of the rail failure and the effect of residual stress on the crack growth rate. For this purpose, the residual stress profiles of rails under various conditions were obtained by both sectioning the physical rail and simulating the weld-repair process of the rail using the finite element method. Subsequently, the fatigue crack growth in the weld-repaired rail was simulated by assuming that a semi-elliptical crack was initiated at the boundary between the weld pool and heat-affected zone. From these analyses, it was found that weld defects, such as porosity, lamella line cracks, and quick transitions in material hardness and microstructure, especially at the boundaries, could be the causes of the crack initiation. The crack growth rate was strongly influenced by the magnitude of the residual stress, while it was significantly increased in the presence of high tensile residual stress at the rail head due to the weld repair. Therefore, reducing the tensile stress magnitude and increasing the compressive stress magnitude in the rail head is crucial to solving this problem in railway rail weld repair.

© 2015 Elsevier Ltd. All rights reserved.

1. Introduction

A rail head surface is continuously exposed to repetitive wheel rail contact fatigue [1], wheel burns due to slips [2], and flying ballast imprinting during the railway operating service, all of which cause damage to the head surface of the rail. The damaged rail head surface should be repaired immediately to secure good riding comfort and to prevent the failure of the rail by implementing a proper repair method. When the surface damage is light, it can be corrected by the simple grinding of the entire damaged area. Grinding of the damaged area [3] is a well-known rail surface maintenance method in the railway industry that is used because of its ease of immediate application over a large area. However, this method requires a long grinding area to minimize the impact from vertical winding, even though it offers the elimination of point defects. In the case of a high-speed rail, sometimes the length of the grinding area needs to be 2000 times the damage depth in both directions of the rail. When the surface damage is moderate and it is too difficult to repair by using only grinding, the damaged region needs to be removed and built up with a new material. An overlay weld-repair method has been frequently used as a build-up method in conventional railway networks in many countries [4–7]. When the damage is severe, it is necessary to cut out the entire damaged section and replace it with a new section [8–13]. Each repair method has advantages and disadvantages, so it is difficult to determine a single method that

* Corresponding author.

E-mail address: yschang@khu.ac.kr (Y.-S. Chang).

is best in all cases. In this context, the railway operator needs to carefully choose the proper repair method by considering various factors such as the risk of poor quality of repair, cost and time, and required the availability of the rail network.

The method of repairing the surface has many advantages because of its ease of implementation and its freedom from the risks associated with restructuring existing rail constructions. Because the method only requires cutting out a small portion of the rail, even in a worst-case scenario, the rail can still maintain its strength. However, although this method has significant potential, it has not been extensively utilized in high-speed railways for safety reasons because it is vulnerable to the creation of cracks. These cracks are difficult to detect because the weld boundary reflects the echo signal of ultra sound, preventing it from penetrating the boundary. Many studies [14–19] have shown that a welded rail is more vulnerable to defects than a parent rail. It is extremely important to fully understand the method of surface repair by welding for the application to high-speed rails, because inclusions, porosity, lack of fusion, and high residual stresses, are possible causes of crack initiation. However, few studies on this topic have been [5–10] published.

The objectives of this study are to find the causes of failure in a weld-repaired rail and to calculate the growth speed on a crack created at the weld boundary to assist in the development of a cost-effective and enhanced-durability weld-repair method. For this purpose, a series of failure analyses were performed on cracked weld-repaired rails. The residual stresses along the depth of the weld were obtained by both sectioning the physical rails and simulating the weld-repair process of the rail using finite element (FE) analysis. Finally, the crack growths were calculated based on fracture mechanics analyses by assuming that a crack is initiated at the boundary between the weld pool and the heat-affected zone (HAZ).

2. Failure analyses of a cracked weld-repaired rail

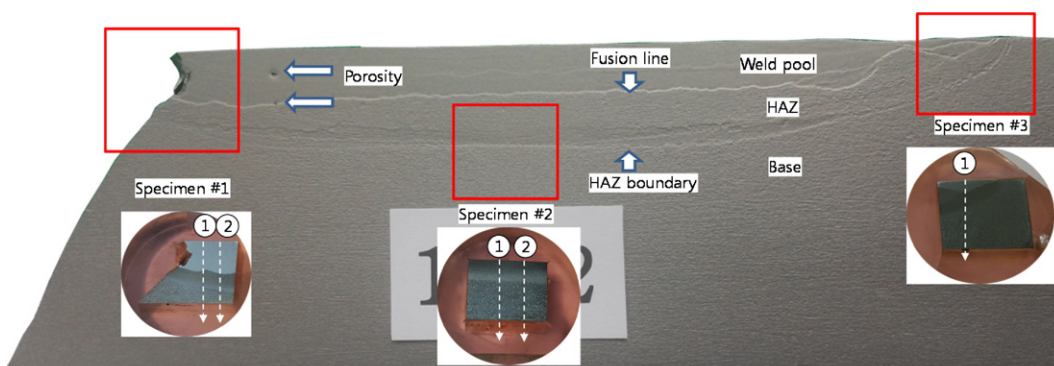
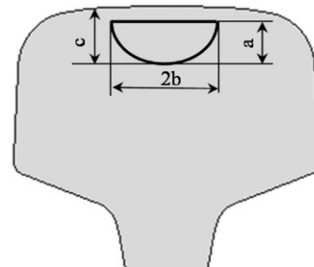
A series of failure analyses on a cracked weld-repaired rail were carried out to determine the cause of weld failure and to further study crack growth. The analyses consist of a macroscopic visual inspection of the failure surface, a chemical content analysis, a material microhardness analysis, and a microstructure analysis on the weld.

2.1. Macroscopic visual inspection

Macroscopic visual inspection on the failure surface of the weld-repaired rail was performed to determine the cause of crack initiation. Fig. 1(a) shows the vertical cross-section of the rail. A dark and smooth fractured surface at the rail head, which is thought to be formed by fatigue crack propagation, can be clearly observed, and is clearly distinguished by the rough gray surface formed by the cleavage fracture. The physical crack was idealized as a semi-elliptical shape, which is 57 mm wide ($2b$) and 28 mm deep (a). The crack area ($A = \pi \times a \times 2b / 2$) was 1254 mm^2 corresponding to approximately 41% of the total rail



(a) Cross-section of a crack and its idealized shape



(b) Longitudinal cross-section

Fig. 1. Fracture morphology of the fractured weld-repaired rail.

head area (3092 mm^2) of UIC 60 rail. From the shape and surface roughness of the crack, it is thought to be initiated at the border between the fusion zone, which is defined as the weld pool, and the base. Subsequently, it propagated to the top and bottom directions of the rail. Fig. 1(b) shows the longitudinal cross-section of the rail. The depth of the weld repair is measured to be approximately 7 mm from the rail top surface. The inclination angle of the crack is measured to be approximately 20° against the vertical axis of the rail, which shows that the crack growth is influenced by the shear stress that is induced when a train passes over the crack. A fusion line between the weld pool and the HAZ can be clearly observed, and it is also clearly distinguished by the color difference of the specimens that were cut out of the sectioned rail and etched to microscopically inspect the material. The boundary between the HAZ and the base of the material can also be clearly observed. Small and fine-size porosities were observed in the weld pool and the fusion zone.

2.2. Chemical analysis

Chemical analyses were carried out on the weld along its depth, for which specimen #3, shown in Fig. 1(b), was used. The rail material analyzed was UIC60 Gr.260 rail steel, which is often used for high-speed rail networks, and the filler material was MF-1-GF-300, manufactured by TRANSLARAIL. Table 1 presents the chemical compositions of the parent rail and filler materials. The carbon, phosphorus, and sulfur contents of the filler material are very low compared with those of the rail material. In contrast, the content of manganese is high. Fig. 2 shows a total of 8 points for the chemical analysis along the depth of weld. The point denoted by (a) is the point in the middle of the weld pool, 0.6 mm from the surface. Point (b) is at the fusion line between the weld pool and the HAZ, 2.8 mm from the surface. Point (c) is at the HAZ and is 3.8 mm from the surface, while point (d) is also at the HAZ and is 5.0 mm from the surface. Point (e) is at the boundary between the HAZ and the base material and is 6.6 mm from the surface. Point (f) is in the middle of the base material and is 7.6 mm from the surface.

Inductively coupled plasma (ICP) by PerkinElmer and scanning electron microscopy (SEM) with energy dispersive X-ray spectroscopy (EDS) were utilized to conduct the analyses. The weld pool denoted as (a) was analyzed with the ICP (which has a higher resolution for the study of the chemical composition) instead of the HAZ, and the base materials denoted as (b)–(f) were analyzed using SEM to study the variation of the chemical compositions along the depth of the weld. Fig. 3 depicts the spectrum of the chemical compositions at point (b), and Table 2 shows the variation of the chemical compositions obtained along the depth of the weld. The carbon content in the weld pool is slightly increased from 0.11 wt.% to 0.24 wt.%, which is thought to be caused by the mixtures of filler and rail materials. In addition, the carbon content increases to 1.00–1.50 wt.% in the HAZ and base material. A variation of the silicon content is not found in the weld pool but it increases in other areas from 0.40 wt.% to 0.60–0.80 wt.%. A variation of the manganese content is not found but slightly increases in other areas from 1.50 wt.% to 1.80–2.10 wt.%.

2.3. Vickers microhardness of the weld

The material microhardness of the weld-repaired rail along the depth of the weld was investigated. Three specimens were prepared by cutting in three different weld locations, as shown in Fig. 1(b). A $50 \times$ Vickers microhardness tester was used to obtain more accurate measurement results. The specimens were measured along the depth of the weld from the rail surface to the rail bottom every 0.2 mm. The hardness of the filler material is 320 Hv, and that of the UIC60 Gr.260 rail steel is 310 Hv. Fig. 4 shows the measured hardness values along the depth of the weld. The hardness values measured near the surface of the rail are slightly higher than those of the parent filler material, and they gradually increase with the depth of the weld pool until the fusion zone to a peak value over 400 Hv. However, the hardness values rapidly decrease after the fusion zone until they reach the boundary between the HAZ and the base material. The lowest hardness value is approximately 210 Hv, and it gradually increases to the hardness level of the parent rail material.

2.4. Microstructural characteristics of the weld

The microstructure of the weld-repaired rail along the depth of the weld was also investigated on the three specimens, as shown in Fig. 1(b), but only the result from specimen #3 is shown in this paper due to the limited space. The specimens were polished and etched with 2% Nital for 150 s after finishing the Vickers hardness testing to easily measure the depth from the surface by counting the number of marks for the hardness test. The HAZ and base materials were well etched, as shown in the shaded area, while the weld pool remained in the white area. Fig. 2(a) shows the microstructure of the weld pool, where it is 0.6 mm from the rail surface of specimen #3. Although, it is not clearly distinguished because of its white color, we can see the dendrite in the microstructure, which mostly consists of a ferrite area and a light cementite stem. Because the carbon content of the weld pool is low compared with that of the rail material, most of the area is thought to consist of ferrite material. The diamond-shaped mark at the center is a mark indicating the Vickers hardness test. Many fine pores were found in the entire area of the

Table 1

Chemical compositions of the rail and filler material.

	[Unit: wt.%]										
	C	Si	Mn	P	S	Cr	Ni	Al	N	Mo	H
Rail	0.65–0.82	0.13–0.60	0.65–1.25	~0.030	0.008–0.030			~0.004	0.010		~2.5 ppm
Filler	0.11	0.40	1.50	0.005	0.002	0.30	2.8	1.40	0.5		

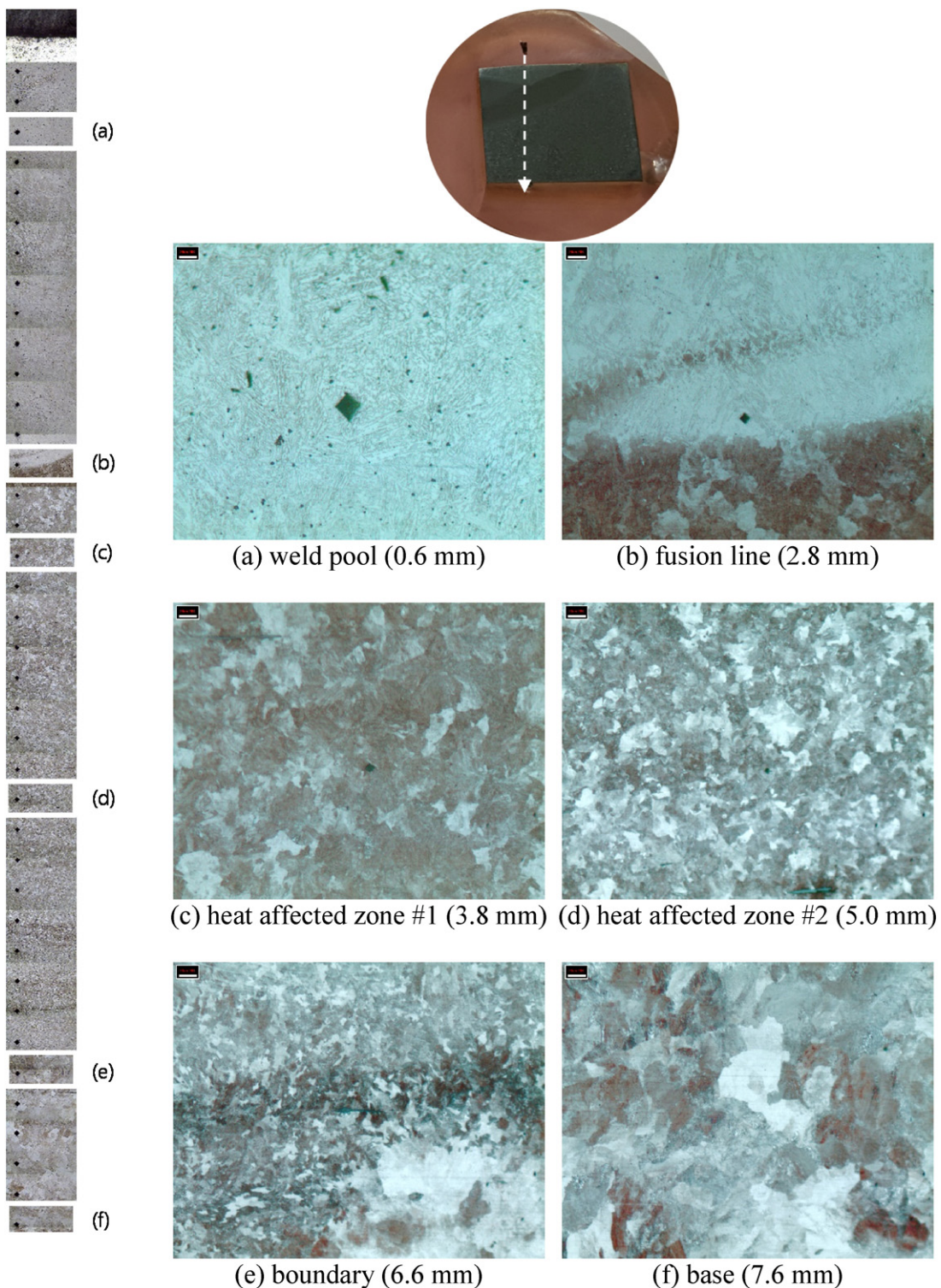


Fig. 2. Schematic of the chemical composition analysis location and the microstructure of the material.

weld pool. Fig. 2(b) shows the microstructure of the fusion zone, where the microstructure is 2.8 mm from the rail surface. The boundary between the weld pool and the HAZ is clearly distinguished by the difference in color and grain size. The color transforms into a mixture of black and white due to the increment of the carbon content and because the grain size of the HAZ is much

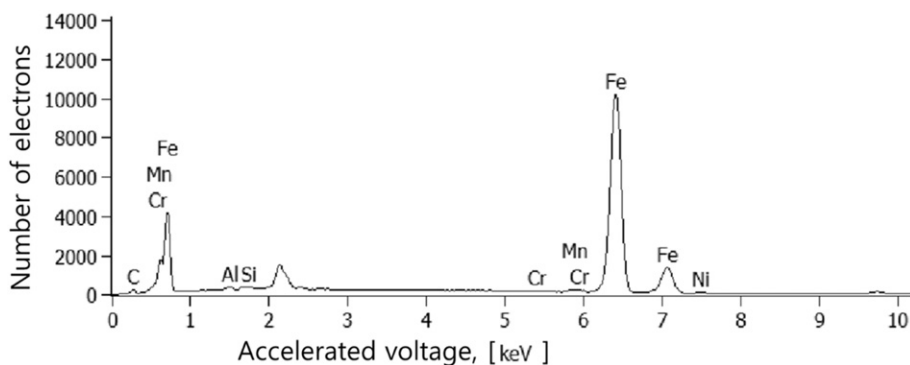


Fig. 3. Spectrum of the chemical compositions at point (b).

larger than that of the weld pool. Fig. 2(c) and (d) shows the microstructure of the boundary between the HAZ and the base material, which are 3.8 mm and 5.0 mm from the rail surface, respectively. The grain sizes are small compared with those of the base material, and the microstructure shows a mixture of ferrite and cementite. Fig. 2(e) shows the microstructure of the boundary between the HAZ and the base. The grain sizes are clearly distinguished bordering the boundary. Fig. 2(f) shows the microstructure of the base material, where it is 7.6 mm from the surface of the rail. It consists of large grains made up of ferrite and pearlite, and the grain sizes are much larger than those of HAZ. The diamond shape of the Vickers hardness test mark is not found, and the mark is thought to have been worn out during polishing.

2.5. Discussion

To understand the cause of rail failure in the weld-repaired rail, systematic analyses of the weld were performed. From the visual inspection, the crack is found to be initiated at the boundary between the weld pool and the HAZ, and the boundary is thought to be vulnerable compared with other areas such as the weld pool, the HAZ, and the base material. Repeated fatigue stresses in the normal and shear directions are thought to accelerate the crack growth from the beach-marked fracture surface of the rail and the inclination of the crack angle. The crack can be idealized as a semi-elliptical shape for the crack growth analysis. From the chemical composition analysis, it is found that the variation of the carbon content at the weld pool is low, but that it changes quickly bordering the fusion zone, which is thought to derive from measurement error due to the low resolution of SEM-EDS. The difference in the chemical composition between the filler material and the weld pool is thought to be minimal, and the mixture of the filler and the rail material seems to not be a concern. From the hardness test on the weld, it is found that the hardness of the fusion zone between the weld pool and the HAZ changes considerably, and the hardness value of the HAZ is very low compared with that of the parent rail material, which can negatively affect the rail strength. From the microstructure analysis of the weld, it is found that the materials between the weld pool and the HAZ differ significantly and that the grain sizes also differ, while many fine pores and small lamella-type cracks are found as shown in Fig. 5. The weld-repair environment of the rail in the field is not as conducive as one that is indoors, and various welding defects can therefore be produced. These welding defects are thought to be triggers of crack initiation, and the crack growths along the boundary are found in other specimens. Therefore, maintaining a good quality of welding is crucial, especially in harsh environments of the field.

3. Residual stress analysis of the weld-repaired rail

When a train passes over a cracked rail, the crack undergoes dynamic global bending and experiences local contact stresses in addition to static residual and thermal stresses. Among these, the residual and contact stress components are known to have a significant effect on fatigue crack initiation and propagation due to their higher stress magnitude than other forms of stress. The global bending stress, local contact stress, and thermal stress can be calculated from previous research [20]. However, because

Table 2

Variations of the chemical composition along the depth of rail from the surface.

Description	[Unit: wt.%]							Method
	C	Si	Mn	Cr	Ni	Al	Fe	
(a) Weld pool (0.6 mm)	0.24	0.38	1.54	0.31	2.07	1.2	94.26	ICP-OES
(b) Fusion line (2.8 mm)	1.00	0.70	1.80	0.10	0.80	0.30	95.30	SEM-EDS
(c) HAZ (3.4 mm)	1.50		1.90				95.60	
(d) HAZ (5.0 mm)	1.30		2.00				96.70	
(e) Boundary (6.6 mm)	1.30		1.90				96.80	
(f) Base (7.6 mm)	1.20	0.60	1.90				96.30	

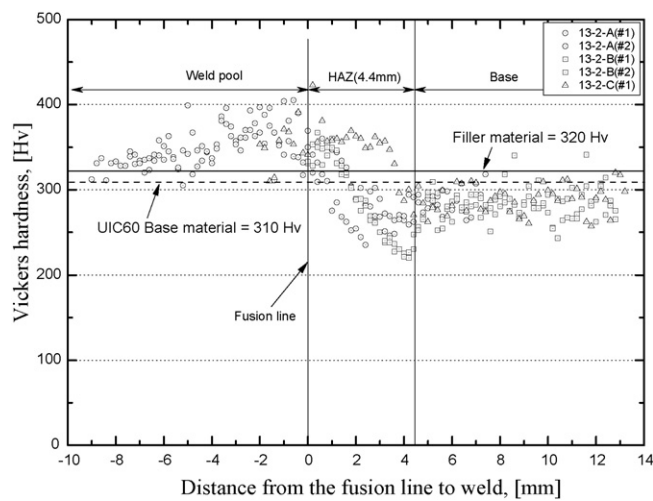


Fig. 4. Hardness variation along the depth of the weld.

the residual stress in the rail changes considerably depending on the rail operating condition, the distribution and magnitude first need to be quantified to calculate the crack growth in the weld-repaired rail.

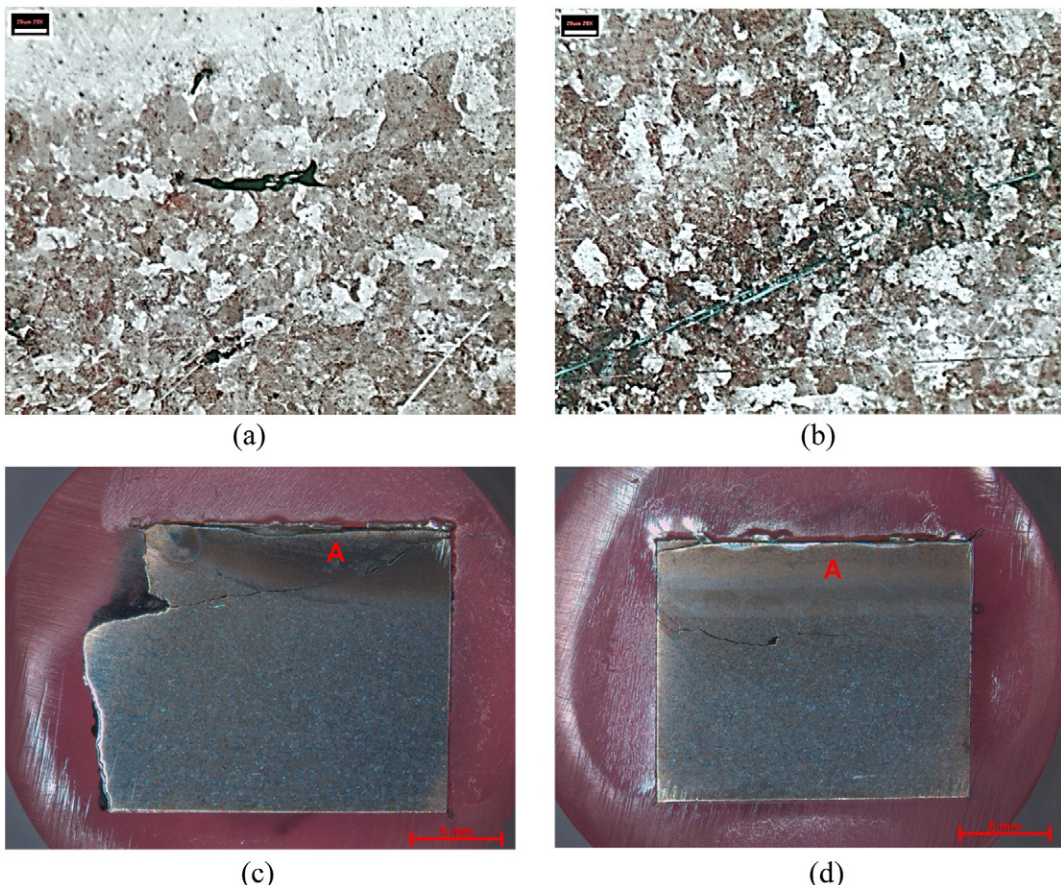


Fig. 5. Welding defect found in the fusion line in a lamellar crack shape (a, b) and an example of crack growth along the boundary in the other fractured rail (c, d).

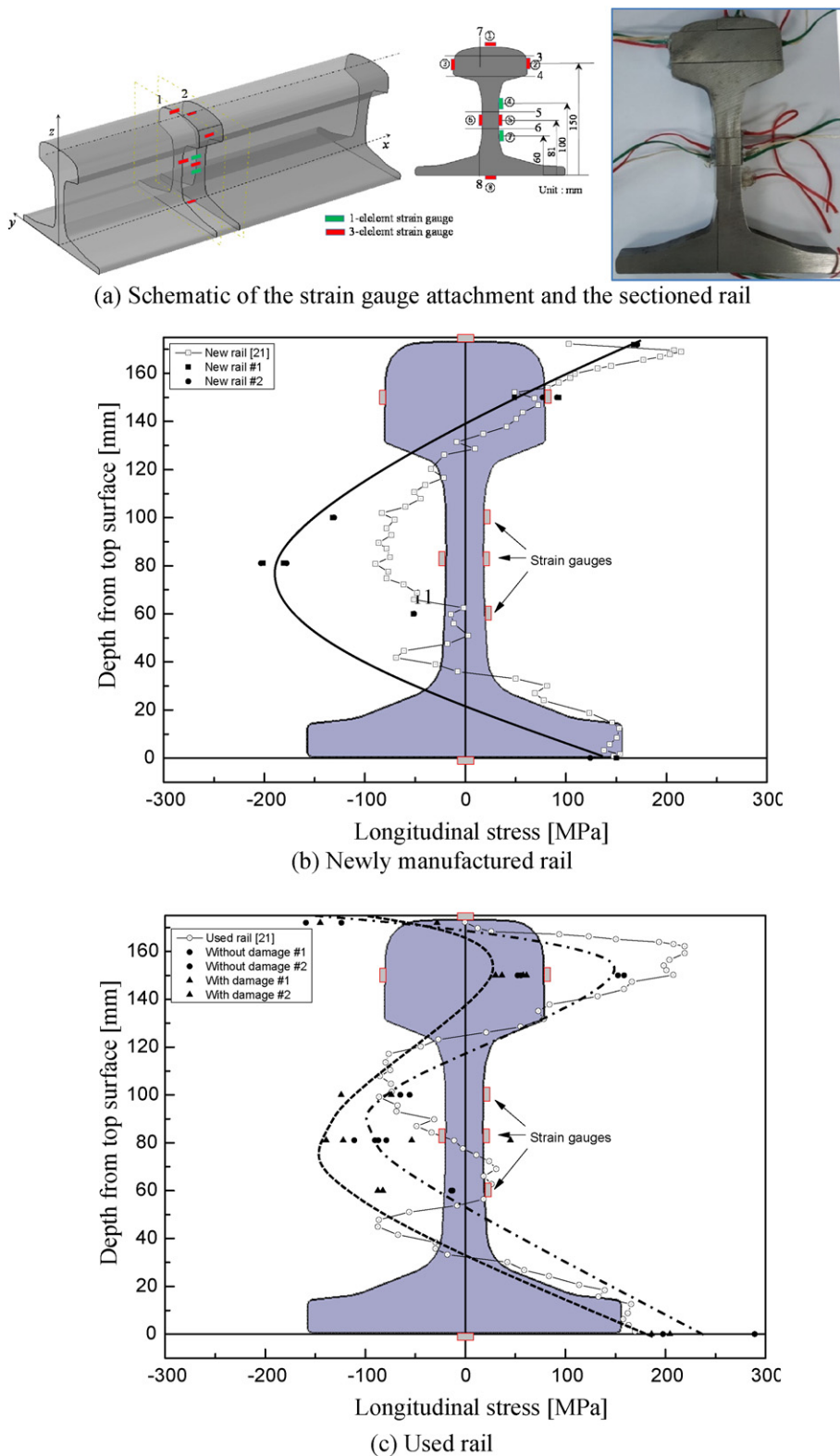


Fig. 6. Residual stress measurement and distribution of the UIC60 rails [21].

3.1. Residual stress measurement

The residual stresses, in the non-weld repaired new and used rails as well as the weld-repaired rail were measured through their partial sectioning. Fig. 6(a) shows the schematic of the residual stress measurement by applying the strain gauges in the rail head, web, and bottom. The residual strains were measured at two points on the rail head surface, at two points on each side of the rail head, at three points on one side of the web and one point on the other side of the web, and two points on the bottom of the rail. Both sides of the rail, apart from approximately 10 mm from the center of the strain gauge, were cut into sections with a mechanical band saw to achieve fully relieved residual stress on every strain gauge. Enough coolant was applied to avoid a temperature increment during the sectioning. Fig. 6(b) and (c) shows a comparison of the residual stress in the longitudinal direction of the rail with that from a previous study [21]. For the new rails, very high tensile stresses are observed in the rail head compared with those of the previous study, and they become compressive stresses in the web of the rail and tensile stresses in the base of the rail. For the rails used, very high compressive residual stresses, with a magnitude of approximately 150 MPa, compared with those of the previous study are observed, but they soon become tensile stresses and show a similar trend to the case of the new rail. For the weld-repaired rails, that were cut from the rail network after several years of service following the repair, high (150 MPa) and low (30 MPa) compressive residual stresses are observed.

3.2. Residual stress analysis of weld-repaired rail

A FE simulation in accordance with the weld-repair process was performed to determine the residual stress distribution of the rail. The commercial software ABAQUS was utilized to perform the elastic–plastic FE analysis by using 8-node linear heat transfer and reduced integration elements (element types DC3D8 and C3D8R in the ABAQUS element library) through sensitivity analyses. To calculate the residual stresses according to welding processes, the isotropic strain hardening law and the incremental plasticity option were employed. The details of the FE model are shown in Fig. 7, and relevant information can be found in a previously published paper [10]. A moving point heat, which is defined as a step by step heat input process for the arc welding simulation, was applied in this study at three different defect depths of 2, 5 and 10 mm; to build up a 2 mm deep defect, it was necessary to model one welding layer that consists of 6 welding passes. Two welding layers that consist of 12 welding passes were needed to build up a 5-mm deep defect. Finally, to build up a 10-mm depth of defect, three welding layers that consist of 18 welding passes were needed. Because each welding pass consists of 20 analysis steps, 123 steps of analysis related to the pre-heating and post-cooling were required for one-layered welding, and 363 steps of analysis were necessary to build up a three-layered weld. All of the analyses required a considerably long simulation time and extensive computation resources.

Fig. 8 shows the temperature distributions along the depth from the fusion line to the rail bottom during the welding process. The temperatures were obtained at points along the depth in the middle of the weld. The temperature distributions consist of peaks and valleys according to the degree of closeness of the welder to the point. Fig. 8(a) shows the temperature distribution of a weld repair with a 2-mm depth. As the welder approaches the point, the temperature increases rapidly and reaches a peak value of 931 °C, before dropping rapidly to 749 °C at the end of the welding pass as the welder moves further away from the point. Therefore, if we calculate the phase transformation of the weld based on only the temperature, which is higher than the eutectoid temperature (723 °C), a phase transformation is expected to occur from the 3rd passage to the 5th passage and to continue for approximately 20 s at each pass. The phase transformation is thought to be induced at approximately 7-mm depth from the fusion line. Fig. 8(b) shows the temperature distribution of a weld repair of with a 5-mm depth, in which we can see the two ridges consisting of peaks and valleys. The first ridge indicates the weld repair of the 1st layer, and the second indicates the weld repair of the 2nd layer. The peak of the second ridge is very low compared with the peak of the first ridge when we weld the second layer because the distance from the fusion line is greater than that of the first layer. Because the phase transformation at the second layer is induced at a depth of only approximately 3.5 mm, it seems that the weld repair of the first layer is more dominant than the weld repair of the second layer. Fig. 8(c) shows the temperature distribution of a weld repair with a 10-mm depth. We can see the three ridges consisting of peaks and valleys. The peaks of the second and third ridges gradually decrease. The phase transformation at the third layer is not expected to be induced because the peak

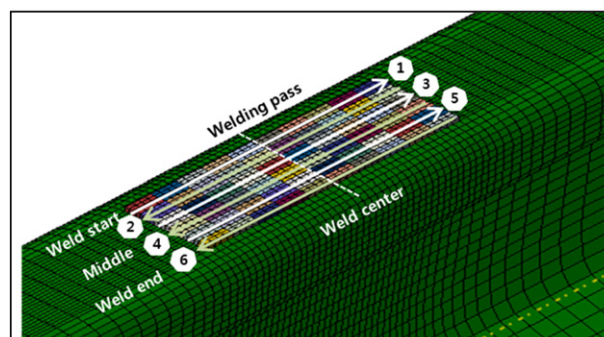


Fig. 7. FE welding passes by moving the point heat on the slot and cutting head weld repair [10].

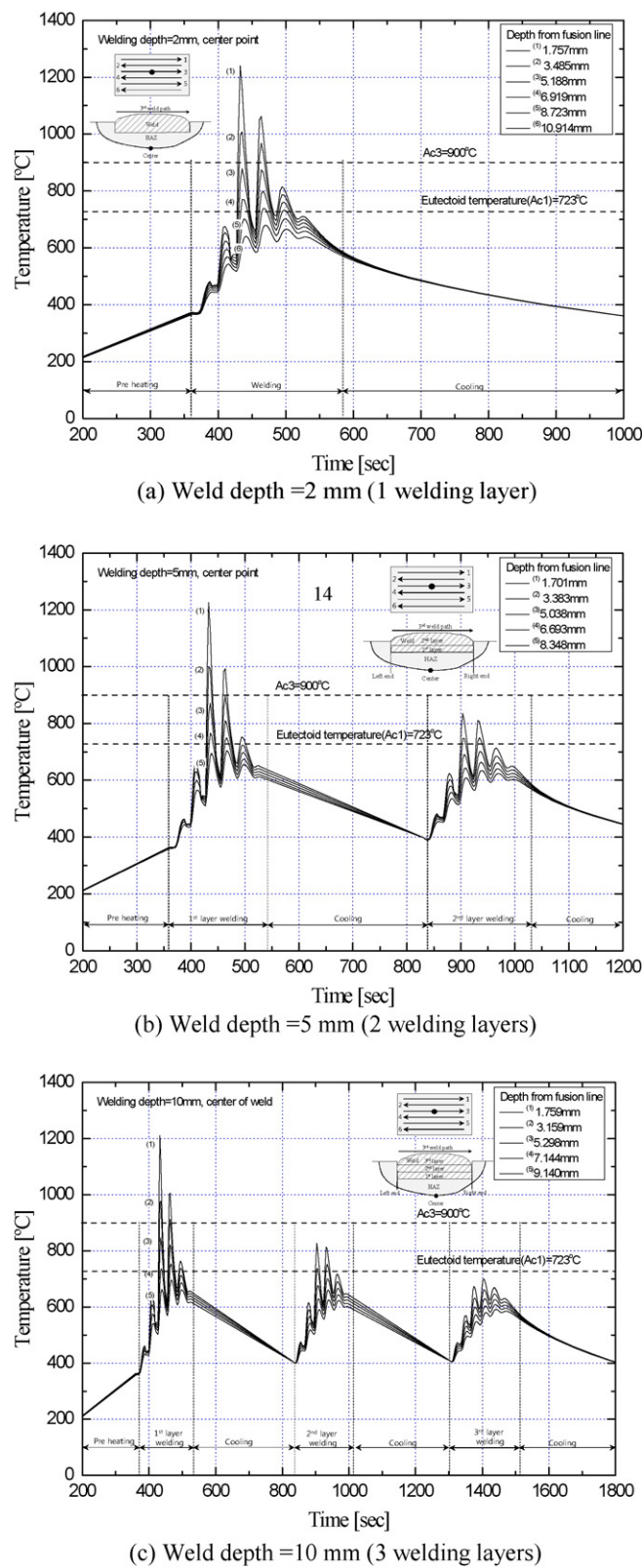


Fig. 8. Temperature distributions during the weld repair along the depth of the rail.

temperature is lower than the eutectoid temperature. Therefore, we can deduce that the weld-repair process for building up the 1st layer determines the depth of the heat-affected zone where the phase transformation occurs.

Fig. 9 presents the residual stress distributions obtained from FE analyses. In the case of the longitudinal stress distribution of the weld-repaired rail, in which high tensile stresses are observed at the surface of the rail head, they gradually become compressive stresses in the web and are finally neutralized at the bottom of the rail. The magnitude of the residual stress is much higher than that of the measured stress, as shown in Fig. 6(c). In the case of the vertical stress distribution along the depth of the rail, compressive stresses are observed at the rail head, and the magnitude increases with depth and is fully neutralized at the bottom of the rail. In the case of the shear stress distribution along the depth of the rail, the magnitudes are very low compared with those of the longitudinal and vertical stresses.

3.3. Discussion

The magnitude and distribution of the residual stress in a rail were obtained by both measuring the physical rail and performing an FE analysis on a computer model of the rail. The tensile residual stress was obtained by measuring the head of a new rail. In contrast, the compressive residual stress was obtained from a used rail that was cut from the servicing railway line. The transition from tensile to compressive stress is thought to be due to the high compressive contact stress between the wheel and rail when a railway service changes the residual stress in the rail head, as shown in Fig. 10. Meanwhile, a very high tensile residual stress was obtained from the simulation of the weld repair process by FE analysis. With this method, the local shrinkage of the weld pool at the rail head brings a very high tensile stress in the rail head compared with the other section rail welding methods such as the flash-butt weld, gas pressure weld, and thermite weld methods. Fig. 11 shows a comparison of the residual stress distributions of the weld-repaired rail and the flash-butt welded rail [15]. In the flash-butt welding method, the entire section of the rail is melted, and subsequently, shrinkage occurs across the entire section in different amounts; a high compressive residual stress is thus induced at the rail head. Generally, the compressive stress at the rail head prevents a crack growth by closing the crack face; the flash-butt weld method is thus thought to be better for preventing crack growth. Therefore, it is necessary to relieve the high tensile stress at the head of the weld-repaired rail for practical use in the rail industry.

4. Fatigue crack growth in the weld-repaired rail

4.1. Analysis model

In this section, a crack growth in a weld-repaired rail under fatigue loading is predicted. Semi-elliptical shaped cracks of three different depths (2, 5 and 10 mm) were modeled to be initiated at the boundary between the weld pool and the HAZ. Repeated fatigue loading was applied to the crack while a series of trains passed over the crack. The total stress was then determined based

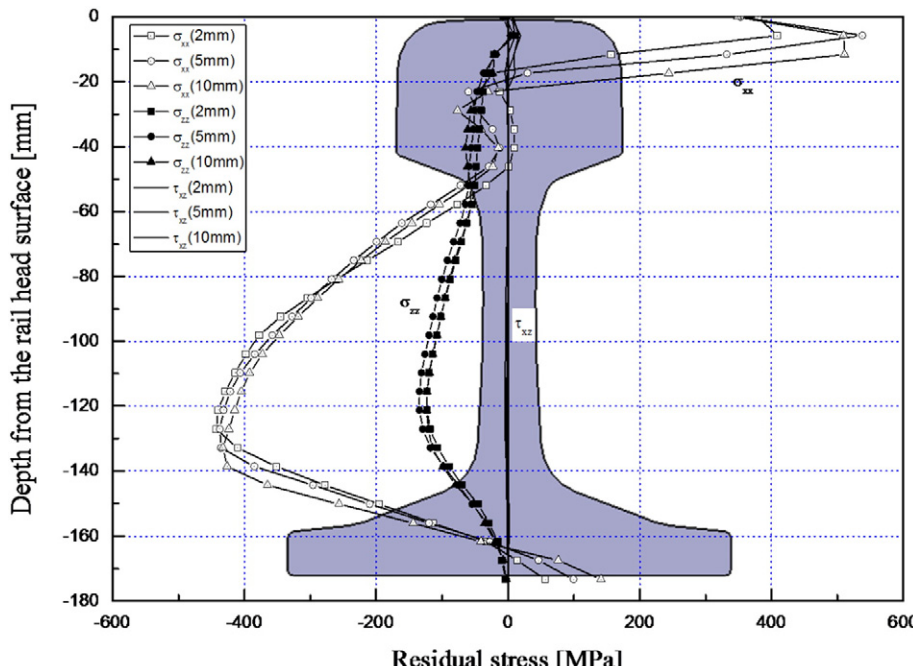


Fig. 9. Residual stress profiles along the depth of the rail.

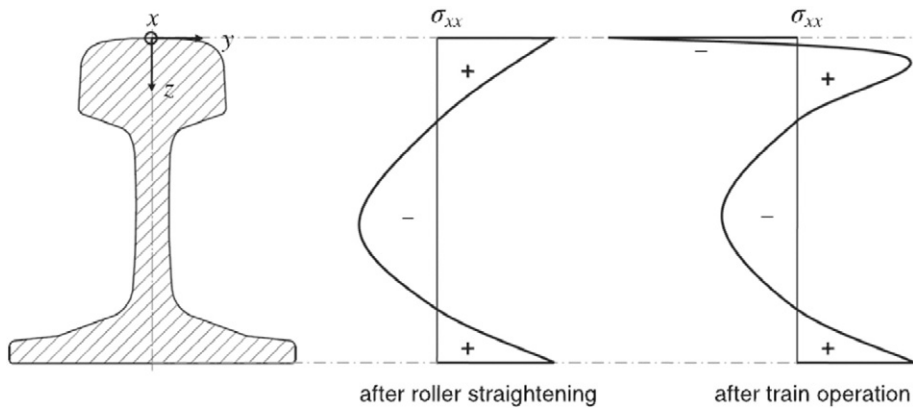


Fig. 10. Residual stress profiles of the rail in the center-line after roller straightening and after train operation [22,23].

on the global bending (σ_B), contact (σ_c), thermal (σ_T), and residual (σ_r) stresses as shown in Fig. 12. The contact and bending stresses varied with the distance between the wheel position and the crack location, while the thermal and residual stresses were sustained regardless of the distance. Particularly, the contact stress along the rail was calculated from the Hertz contact theory [24], and the bending stress was calculated by the application of the elastic beam theory by Zimmermann [25]. The thermal stress was calculated from the temperature difference between the stress-free neutral temperature T_n and the railway operating temperature T_o as $\sigma_T = 1.14 \times 10^{-5} E (T_n - T_o)$, and the weld residual stress was used as the aforementioned analyzed and measured data. Each stress component at the crack tip was superposed as below.

$$\sigma_{\text{total}} = \sigma_B + \sigma_c + \sigma_T + \sigma_r. \quad (1)$$

Fig. 13 depicts the schematics of the weld-repaired crack, modeled as an embedded semi-elliptical shape, which was assumed to be initiated at the boundary between the weld pool and the HAZ. The crack was modeled with an inclined angle θ to the vertical axis of the rail and having a crack mouth length $2b$ and a crack depth a . The depth from the rail surface to the crack mouth is denoted by d . The crack is assumed to have grown along the crack plane, and the crack aspect ratio a/b is assumed to be

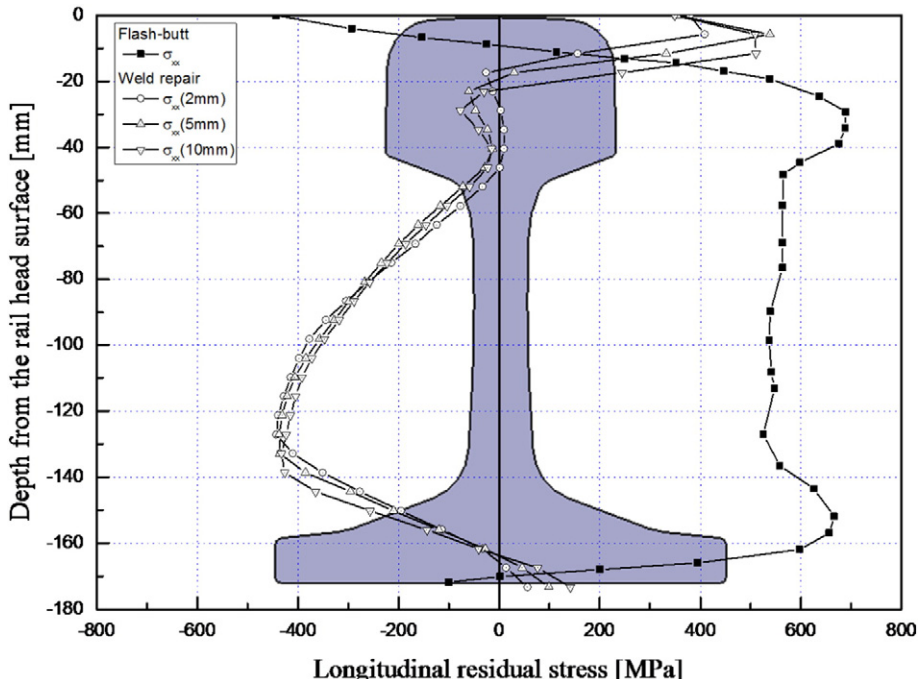


Fig. 11. Comparison of longitudinal residual stress distributions between the weld-repaired rail and the flash-butt welded rail [15] along the depth of the rail.

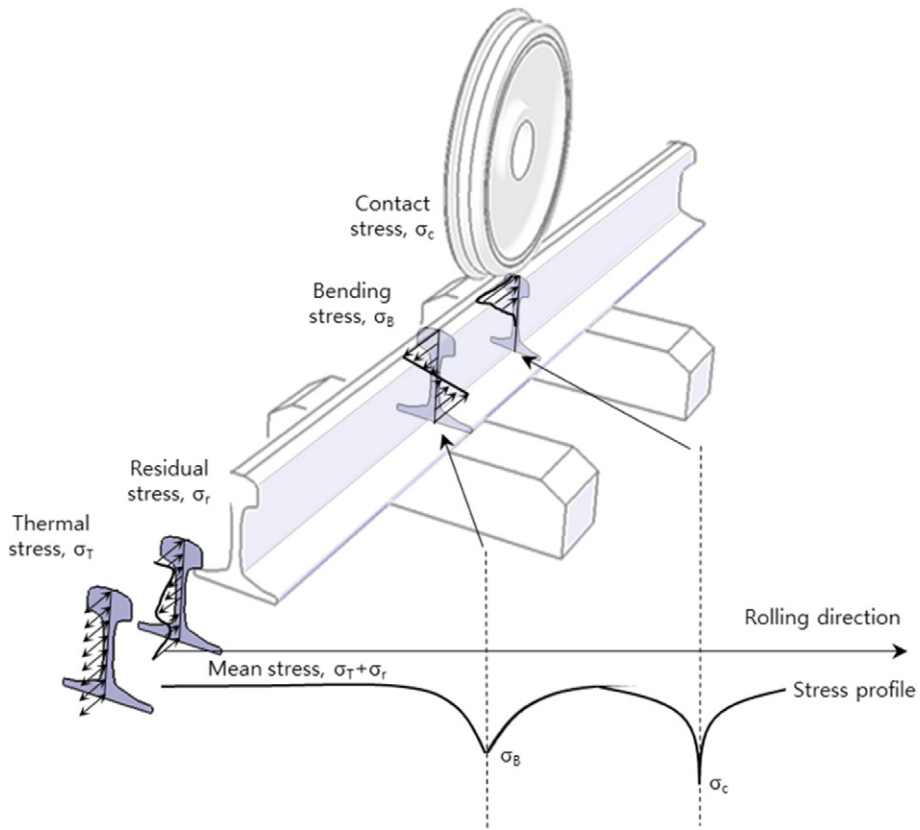


Fig. 12. Schematics of loading in a rail during a wheel rolling over a crack [3].

maintained during growth. The contact-induced loading and the thermal and residual stresses were applied to the crack face. The resulting stress intensity factor (SIF) for a semi-elliptical crack, as suggested by Jeong [26], was implemented as follows:

$$K = 1.12 M \sigma \frac{\sqrt{\pi a}}{E(k)} \quad (2)$$

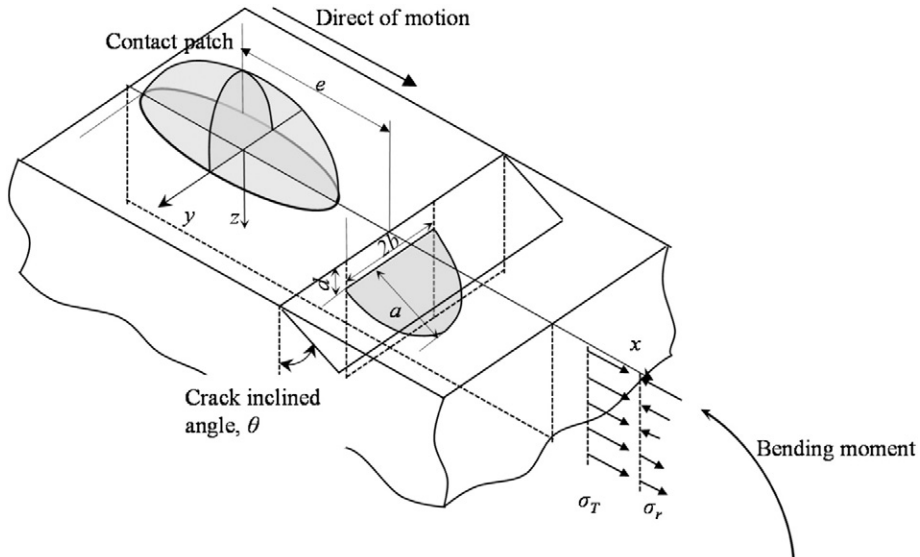


Fig. 13. Schematic of the weld-repaired crack model.

where M is an empirical factor to account for the finite cross-section of the rail head and $E(k)$ is the elliptic integral of the second kind:

$$E(k) = \int_0^{\frac{\pi}{2}} \sqrt{1-k^2 \sin^2 \theta} d\theta$$

$$k = \sqrt{1-(a/b)^2}.$$

The stress intensity factors were converted into crack growth rates using the following crack growth curve [26] for rail-wheel contact on a pearlite rail.

$$\frac{da}{dN} = 1.74 \times 10^{-13} \frac{\Delta K^4}{(1-R)^{1.63}} [m/cycle] \quad (3)$$

where da/dN is the crack growth per cycle, ΔK is the stress intensity factor range, and R is the superposed stress ratio.

4.2. Parametric study

Crack growth analyses were conducted under complex loading in which a series of trains passed over a cracked rail several thousand times. Particularly, a high-speed railway operating condition was incorporated, and two types of simulation were performed. The first simulation is for a crack located in the head of the non-repaired rail, in which the used and weld-repaired statuses of the residual conditions are applied, as shown in Fig. 6(c). The other simulation is for the crack located in the head of the weld-repaired rail, in which the residual stress obtained by FE analysis is applied, as shown in Fig. 9. While the crack growth rate curves of the base and weld materials might differ, in this study, we ignored the difference because the identification itself is another considerable issue. The same crack growth rate curve was used for both simulations so that further investigation is necessary for a more accurate prediction of crack growth.

Table 3 shows a list of input variables for the simulation. A train set with a 920-mm diameter railway wheel, which is the conventional high-speed railway wheel size, was used for the simulation, and a UIC60 rail with a 300-mm crown radius was used. The axle load was 17 tons; the initial crack size was assumed to be the crack depth, $a = 0.5$ mm; and the crack length was $2b = 2.0$ mm. Therefore, the crack aspect ratio a/b was set as 0.5 and was maintained during the entire simulation process. As described previously, the depth from the rail surface to the crack was assumed to be constant at 5 mm in the first parametric study and to vary between 2, 5 and 10 mm in the second study.

To study the effect of the residual stress on the crack growth rate, parametric crack growth studies with the four different residual stress profiles shown in Figs. 6(c) and 11 were performed. The crack location of 5 mm was used in all cases to ensure the same contact stress conditions. Fig. 14 shows the calculated crack growth curves of the four different states of residual stress. The differences in the crack growth rate are significant. The high compressive residual stress in the rail head of the flash-butt weld denoted as (1) shows the longest crack growth life, and the low compressive residual stress of the weld-repaired rail (4) shows a comparatively short crack growth life. In contrast, the weld-repaired rail with a higher compressive stress at the rail surface (3) shows a longer crack growth life than that of case (4), so it is found that the compressive stress at the rail head is beneficial to delay the crack growth in the rail.

Fig. 15 shows the predicted crack growth curve on a weld-repaired rail with different repair depths of 2, 5 and 10 mm using the residual stresses obtained by the FE analysis shown in Fig. 9. The differences in the crack growth speed among the repair depths are large. The 2-mm deep crack denoted as (1) has the longest life until the crack reaches unstable crack growth, and this is thought to be because the tensile residual stress of the 2-mm deep weld-repair case is the smallest. The 10-mm deep crack has the second longest life, and this is thought to be because although the magnitude of the tensile stresses of the 5-mm and 10-mm deep weld-repair cases are almost the same; the contact stress of the 10-mm depth is low, so the crack growth of the 10-mm deep crack of the rail is slower than that of the 5-mm deep crack.

Table 3

List of the input values for the simulation.

Wheel radius, R_w [mm]	Rail radius, R_R [mm]	Wheel load, P [ton]	Elastic modulus, E [MPa]	Poisson ratio, ν	Peak contact pressure, p_0 [MPa]	Contact patch radius
460	300	8.5	207,000	0.3	1174	7.21 5.68
Crack shape	Initial crack depth, a [mm]	Initial crack length, $2b$ [mm]	Crack aspect ratio a/b	Crack location, d [mm]	Surface friction coef., u_{cf}	
Semi-elliptical	0.5	2.0	3.0	2, 5, 10	0.45	

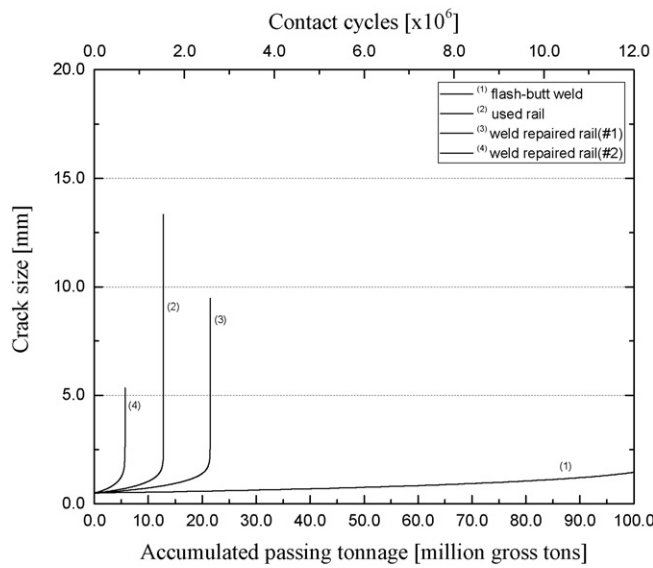


Fig. 14. Fatigue crack growth with the residual stress of a used rail.

4.3. Discussion

The longitudinal residual stress in a rail head plays an important role in the growth of cracks because the direction of the crack growth is perpendicular to the direction of the force applied. Tensile residual stress opens the crack when a train set passes over the crack and accelerates the crack growth. In contrast, compressive residual stress closes the crack and decelerates the crack growth. Therefore, it is very important to change the tensile stress to compressive stress at the rail head to reduce the unanticipated initiation and propagation of the crack. The transition from tensile to compressive stress due to contact stress is beneficial to prevent the crack from growing, especially on the rail surface. Although the 2-mm deep weld repair shows the longest life due to the comparatively low tensile stress magnitude, the 10-mm deep weld repair is recommended, considering the good quality of welding.

5. Conclusions

In this study, failure analyses on a fractured weld-repaired rail were performed, and the residual stresses at various stages of the rail were obtained. The fatigue crack growth in the weld-repaired railway rail was also simulated by assuming a semi-elliptical

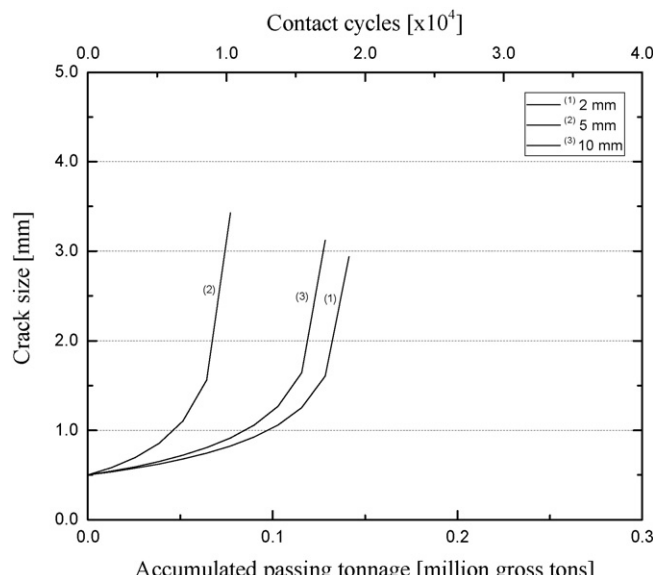


Fig. 15. Fatigue crack growth with the residual stress of the weld-repaired rail.

crack to be initiated at the boundary between the weld and heat-affected zones. Based on these successive analyses, the following key findings were observed.

1. Many pores, and lamella cracks, a rapid drop of material hardness, a transition in the chemical composition and microstructure of the material, and a high longitudinal tensile residual stress were found in the fractured rail. This observation is consistent with that of crack growth in other weld-repaired rails, and these are the causes of weld-repaired rail failure.
2. The longitudinal residual stresses in the heads of the new and weld-repaired rail were highly tensile, but changed into compressive stress with a magnitude of approximately 150 MPa soon after train operation because of the high compressive contact stress.
3. The residual stress distribution generated in the head of the rail greatly influenced the crack growth speed. Moreover, among the three weld-repair conditions, the crack growth at the deepest depth of 10 mm from the surface led to a longer life of the crack until unstable crack growth occurred. These trends are consistent with previous observations relating to the crack initiation life of weld-repaired rails.

Acknowledgments

This study was supported by a grant from the R&D Program of the Korea Railroad Research Institute, Republic of Korea (PK1502d-2).

References

- [1] S.L. Grassie, Traction, curving and surface damage of rails, part 2: rail damage, *Proc. Inst. Mech. Eng. F Rail Rapid Transit* 229 (3) (2015) 330–339.
- [2] S. Pal, W.J.T. Daniel, C.H.G. Valente, A. Wilson, A. Atrens, Surface damage on new AS60 rail caused by wheel slip, *Eng. Fail. Anal.* 22 (2012) 152–165.
- [3] E. Magel, M. Roney, J. Kalousek, P. Sroba, The blending of theory and practice in modern rail grinding, *Fatigue Fract. Eng. Mater. Struct.* 26 (2003) 921–929.
- [4] BS EN 15594, Railway applications—track—restoration of rails by electric arc welding, British Standard, 2009.
- [5] A. Allie, H. Aglan, M. Fateh, Microstructure-fracture behavior relationships of slot-welded rail steel, *Miner. Met. Mater. Soc. ASM Int.* 42A (2011) 2706–2715.
- [6] D. Workman, R. Kral, Flash butt wedge repair of weld head defects, *Proceedings of the ASME/ASCE/IEEE 2011 Joint Rail Conference* 2011, pp. 1–7.
- [7] Z. Zheng, H. Qi, H. Zhang, D. Ren, Laser repairing of damaged steel rail with filler wire, *Proceedings of Measuring Technology and Mechatronics Automation* 2014, pp. 383–386.
- [8] H.A. Aglan, S. Ahmed, K.R. Prayakarao, M. Fatch, Effect of preheating temperature on the mechanical and fracture properties of welded pearlitic rail steels, *J. Eng.* 5 (2013) 837–843.
- [9] D. Bajic, G.V. Kuzmenko, I. Samardzic, Welding of rails with new technology of arc welding, *Metalurgija* 52 (2013) 399–402.
- [10] S.H. Lee, S.H. Kim, Y.S. Chang, H.K. Jun, Fatigue life assessment of railway subjected to welding residual and contact stresses, *J. Mech. Sci. Technol.* 28 (2014) 4483–4491.
- [11] AWS D15.2/D15.2 M, Recommended practices for the welding of rails and related rail components for use by rail vehicles, American Welding Society, 2013.
- [12] Y. Chen, F.V. Lawrence, C.P.L. Barkan, J.A. Dantzig, Heat transfer modelling of rail thermite welding, *Proc. Inst. Mech. Eng. F Rail Rapid Transit* 220 (2006) 207–217.
- [13] Y. Chen, F.V. Lawrence, C.P.L. Barkan, J.A. Dantzig, Weld defect formation in rail thermite welds, *Proc. Inst. Mech. Eng. F Rail Rapid Transit* 220 (2006) 373–384.
- [14] Z. Cai, M. Nawafune, N. Ma, Y. Qu, B. Cao, H. Murakawa, Residual stresses in flash butt welded rail, *Trans. JWRI* 40 (1) (2011) 79–87.
- [15] B.L. Josefson, J.W. Ringsberg, Assessment of uncertainties in life prediction of fatigue crack initiation and propagation in welded rails, *Int. J. Fatigue* 31 (2009) 1413–1421.
- [16] H. Desimone, S. Beretta, Mechanisms of mixed-mode fatigue crack propagation at rail butt-welds, *Int. J. Fatigue* 28 (2006) 635–642.
- [17] A. Allie, H.A. Aglan, M. Fateh, Mechanical and fracture analysis of welded pearlitic rail steels, *J. Mech. Mater. Struct.* 5 (2) (2010) 263–276.
- [18] Y. Terashita, M. Tatsumi, Analysis of damaged rail weld, *Q. Rep. RTRI* 44 (2) (2003) 59–64.
- [19] A. Skyttebol, A. Josefson, J.W. Ringsberg, Fatigue crack growth in a welded rail under the influence of residual stresses, *Eng. Fract. Mech.* 72 (2005) 271–285.
- [20] V.A. Profillidis, *Railway engineering*, Ashgate Publishing Company, 2000 89–104.
- [21] P.J. Webster, X. Wang, G. Mills, G.A. Webster, Residual stress changes in railway rails, *Physica B* 180&181 (1992) 1029–1031.
- [22] M. Steenbergen, R. Dollevoet, On the mechanism of squat formation on train rails – part II: growth, *Int. J. Fatigue* 47 (2013) 373–381.
- [23] S.L. Srimani, J. Basu, An investigation for control of residual stress in roller-straightened rails, *J. Strain Anal.* 38 (3) (2003) 261–268.
- [24] Engineering Science Data Unit, *Contact phenomenon III: calculation of individual stress components in concentrated elastic contacts under combined normal and tangential loading*, HIS 85007 (1994).
- [25] V.A. Profillidis, *Railway engineering*, Ashgate Publishing, 2000 68–74.
- [26] D.Y. Jeong, Correlations between rail defect growth data and engineering analyses, part 1: laboratory tests. UIC/WEC Joint Research Project on Rail Defect Management, 2003 12–15.

FATIGUE IMPROVEMENT OF WELDED ELEMENTS AND STRUCTURES BY ULTRASONIC PEENING

Yuri Kudryavtsev

Structural Integrity Technologies Inc.
Markham, Ontario, Canada

Jacob Kleiman

Structural Integrity Technologies Inc.
Markham, Ontario, Canada

ABSTRACT

The ultrasonic impact treatment (UIT) is relatively new and promising process for fatigue life improvement of welded elements and structures. In most industrial applications this process is known as ultrasonic peening (UP). The beneficial effect of UP is achieved mainly by relieving of tensile residual stresses and introducing of compressive residual stresses into surface layers of a material. The secondary factors in fatigue improvement by UP are decreasing of stress concentration in weld toe zones and enhancement of mechanical properties of the surface layers of the material. Fatigue testing of welded specimens showed that UP is the most efficient improvement treatment as compared with traditional techniques such as grinding, TIG-dressing, heat treatment, hammer peening and application of LTT electrodes. The developed computerized complex for UP was successfully applied for increasing the fatigue life and corrosion resistance of welded elements, elimination of distortions caused by welding and other technological processes, residual stress relieving, increasing of the hardness of the surface of materials. The UP could be effectively applied for fatigue life improvement during manufacturing, rehabilitation and repair of welded elements and structures. The areas/industries where the UP process was applied successfully include: Shipbuilding, Railway and Highway Bridges, Construction Equipment, Mining, Automotive, Aerospace. The results of fatigue testing of welded elements in as-welded condition and after application of UP are considered in this paper. It is shown that UP is the most effective and economic technique for increasing of fatigue strength of welded elements in materials of different strength. These results also show a strong tendency of increasing of fatigue strength of welded elements after application of UP with the increase in mechanical properties of the material used.

INTRODUCTION

The ultrasonic impact treatment (UIT) is one of the most efficient techniques for fatigue life improvement of welded elements and structures [1-7]. In most industrial applications this process is also known as ultrasonic peening (UP) [8-12]. The beneficial effect of UIT/UP is achieved mainly by relieving of harmful tensile residual stresses and introducing of compressive residual stresses into surface layers of materials, decreasing of stress concentration in weld toe zones and enhancement of mechanical properties of surface layers of the material. The fatigue testing of welded specimens showed that the UP is the most efficient improvement treatment when compared with such traditional techniques as grinding, TIG-dressing, heat treatment, hammer peening, shot peening and application of LTT electrodes [1, 13, 14].



Fig.1a. Basic ultrasonic peening system for fatigue life improvement of welded elements and structures [6]

The developed system for UP treatment (total weight - 11 kg) includes an ultrasonic transducer, a generator and a laptop (optional item) with software for optimum application of UP - maximum possible increase in fatigue life of parts and welded elements with minimum cost, labor and power consumption. In general, the basic UP system shown in Figure 1a could be used for treatment of weld toe or welds and larger surface areas if necessary.

Also the special ultrasonic system was designed to perform underwater UP at the depth of up to 30 meters [26]. Figure 1b shows the process of underwater UP of welded samples in preparation for their subsequent fatigue testing.



Fig.1b. The process of underwater ultrasonic peening by using of the specially designed tool

The most recent design of the UP equipment is based on "Power on Demand" concept. Using this concept, the power and other operating parameters of the UP equipment are adjusted to produce the necessary changes in residual stresses, stress concentration and mechanical properties of the surface layers of materials to attain the maximum possible increase in fatigue life of welded elements and structures. From other side, this approach prevent the possibility to overwork the treated surface and decrease the efficiency op UP.

The effects of different improvement treatments, including the UP treatment, on the fatigue life of welded elements depend on the mechanical properties of used material, the type of welded

joints, the parameters of cyclic loading and other factors. For effective application of UP, depending on the above-mentioned factors, a software package for Optimum Application of UP was developed that is based on original predictive model. In the optimum application, a maximum possible increase in fatigue life of welded elements with minimum time/labor/cost is thought [15].

The developed technology and computerized complex for UP were successfully applied for increasing of the fatigue life of welded elements, elimination of distortions caused by welding and other technological processes, relieving of residual stress, increasing of the hardness of the surface of materials and surface nanocrystallization. The areas/industries where the UP was applied successfully include: Railway and Highway Bridges, Construction equipment, Shipbuilding, Mining, Automotive and Aerospace to name a few.

PRINCIPLES, TECHNOLOGY, EQUIPMENT FOR UP *Freely Movable Strikers*

The UIT/UP equipment is based on known technical solutions from the 40's of last century of using working heads with freely movable strikers for hammer peening. At that time and later on, a number of different tools based on using freely movable strikers were developed for impact treatment of materials and welded elements by using pneumatic [16, 17] and ultrasonic [18-24] equipment. A more effective impact treatment is provided when the strikers are not connected to the tip of the actuator but could move freely between the actuator and the treated material. Figure 2 shows a standard set of easy replaceable working heads with freely movable strikers for different applications of UP.



Fig.2. A set of interchangeable working heads for UIT/UP [7]

Ultrasonic Impact and Effects of Ultrasound

The UP technique is based on the combined effect of high frequency impacts of the special strikers and ultrasonic oscillations in treated material. Some specific features of the ultrasonic impact treatment of metals are described in [16]

where it is shown that the operational frequency of the transducer and the frequency of the intermediate element-striker are not the same.

During the ultrasonic treatment, the striker oscillates in the small gap between the end of the ultrasonic transducer and the treated specimen, impacting the treated area [18-21]. This kind of high frequency movements/impacts in combination with high frequency oscillations induced in the treated material is typically called the ultrasonic impact.

There are a number of effects of ultrasound on metals that are typically considered: acoustic softening, acoustic hardening, acoustic heating, etc. In the first of these (acoustic softening that is also known as acoustic-plasticity effect), the acoustic irradiation reduces the stress necessary for plastic deformation. In general, the effect of ultrasound on the mechanical behavior could be compared with the effect of heating on a material. The difference is that acoustic softening takes place immediately when a metal is subjected to ultrasonic irradiation. Also, relatively low-amplitude ultrasonic waves leave no residual effects on the physical properties of metals after acoustic irradiation is stopped [25].

Technology and Equipment for Ultrasonic Peening

The ultrasonic transducer oscillates at a high frequency, with 20-30 kHz being typical. The ultrasonic transducer may be based on either piezoelectric or magnetostrictive technology. Whichever technology is used, the output end of the transducer will oscillate, typically with amplitude of 20 – 40 μm . During the oscillations, the transducer tip will impact the striker(s) at different stages in the oscillation cycle. The striker(s) will, in turn, impact the treated surface. The impact results in plastic deformation of the surface layers of the material. These impacts, repeated hundreds to thousands of times per second, in combination with high frequency oscillations induced in the treated material result in a number of beneficial effects of UP.

The UP is an effective way for relieving of harmful tensile residual stresses and introducing of beneficial compressive residual stresses in surface layers of parts and welded elements. The mechanism of residual stress redistribution is connected mainly with two factors. At a high-frequency impact loading, oscillations with a complex frequency mode spectrum propagate in a treated element. The nature of this spectrum depends on the frequency of ultrasonic transducer, mass, quantity and form of strikers and also on the geometry of the treated element. These oscillations lead to lowering of residual welding stresses. The second and the more important factor, at least for fatigue improvement, is surface plastic deformation that leads to introduction of the beneficial compressive residual stresses.

In the fatigue improvement, the beneficial effect is achieved mainly by introducing of the compressive residual stresses into

surface layers of metals and alloys, decrease in stress concentration in weld toe zones and the enhancement of the mechanical properties of the surface layer of the material. The schematic view of the cross section of material/part improved by UP is shown in Figure 3 with the attained distribution of the stresses after the UP. The description of the UP benefits is presented in Table 1.

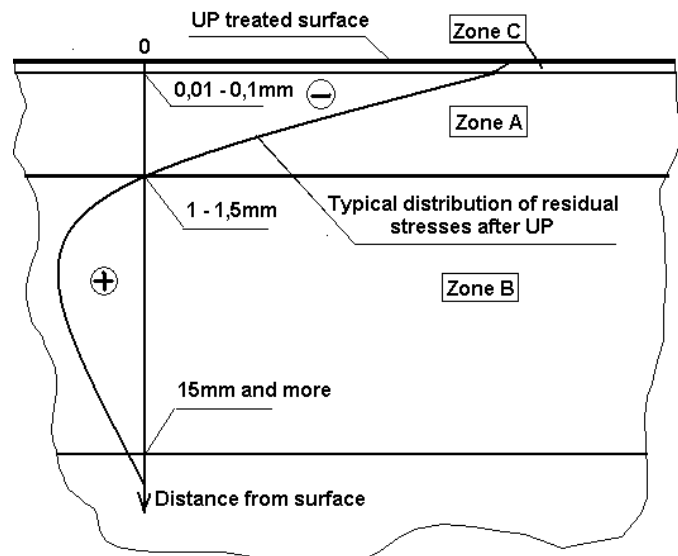


Fig.3. Schematic view of the cross section of material/part improved by Ultrasonic Peening [9]

Table 1. Zones of Material/Part Improved by Ultrasonic Peening [9] (see Figure 3 for illustration of the zones)

Zone	Description of zone	Distance from surface,	Improved characteristics
A	Zone of plastic deformation and compressive residual stresses	1 – 1.5 mm	Fatigue, corrosion, wear, distortion
B	Zone of relaxation of welding residual stresses	15 mm and more	Distortion, crack propagation
C	Zone of nanocrystallization (produced at certain conditions)	0.01 – 0.1 mm	Corrosion, wear, fatigue at elevated temperature

The most important, from the fatigue improvement point of view, is the zone A where the beneficial compressive residual stresses are induced by UP due to the plastic deformation of the surface layers of material [4]. The zone of nanocrystallization C could be produced by UP at certain conditions [27]. This

zone is characterized by a small depth of only 10-100 micrometers and does not contribute significantly to the fatigue increase of welded elements by UP. In case of surface nanocrystallization the fatigue cracks initiate under this thin layer.

Figure 4 illustrates the concept of the fatigue life improvement of welded elements by UP. In case of welded elements, it is enough to treat only the weld toe zone – the zone of transition from base metal to the weld, for a significant increase of fatigue life. The width of the zone of UP treatment is typically 2-5 mm.

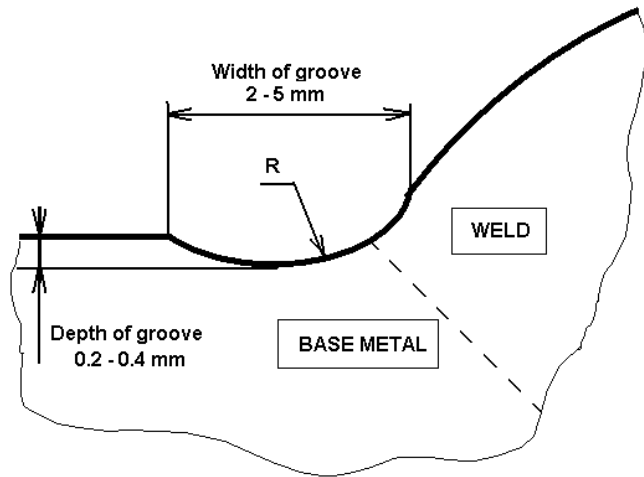


Fig.4. Profile of weld toe improved by Ultrasonic Peening [9]

A so-called groove, shown in Figures 4 and 5, characterized by certain geometrical parameters is produced by UP. This groove is a result of a surface plastic deformation of material during UP [2, 4].



Fig.5. The view of the butt welds in as-welded condition (left side sample) and after application of UP (right side sample) [7]

APPLICATION OF UP FOR FATIGUE IMPROVEMENT

The UP could be effectively applied for fatigue life improvement during manufacturing, rehabilitation and repair of welded elements and structures. Examples of all three applications will be described below.

Manufacturing and Rehabilitation

Three series of large-scale welded samples, designed as shown in Figure 6, were subjected to fatigue testing to evaluate the effectiveness of UP application to the existing welded structures: 1 – in as welded condition, 2 – UP was applied before fatigue testing, 3 – UP was applied after fatigue loading with the number of cycles corresponding to 50% of the expected fatigue life of samples in as-welded condition [9]. Material properties: yield strength – 360 MPa, ultimate strength – 420 MPa. The samples were tested at stress ratio R=0. Test frequency – 5 Hz.

All considered in this paper welded specimens were UP treated with the following standard parameters: speed of treatment – 0.4 meter/minute, level of amplitude of oscillation - 4, working head – one row, four pins, diameter of pin - 3mm.

The results of fatigue testing of the large-scale welded samples imitating the transverse non-load-carrying attachments (Fig. 6) with UP applied to specimens in as-welded condition and also after 50% of expected fatigue life are presented in Figure 7.

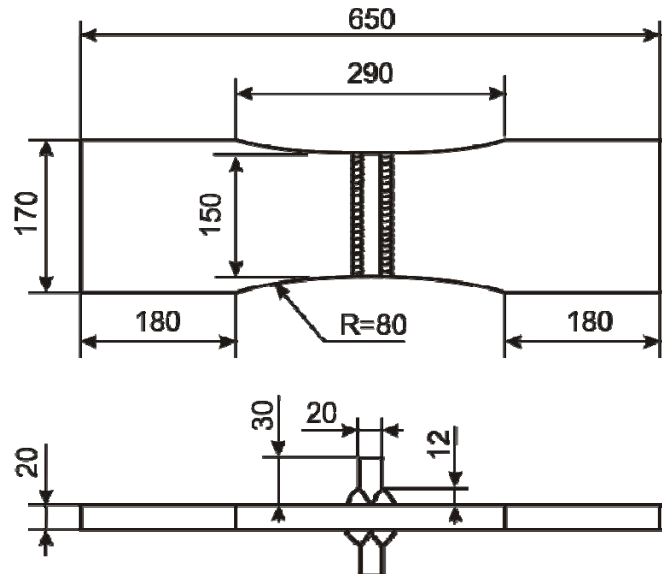


Fig.6. The general view of welded sample for fatigue testing

The UP caused a significant increase in fatigue strength of the considered welded element for both series of UP treated samples. The increase in limit stress range at $N=2 \cdot 10^6$ cycles of welded samples is 49% (from 119 MPa to 177 MPa) for UP treated samples before fatigue loading and is 66% (from 119 MPa to 197 MPa) for UP treated samples after fatigue loading.

with the number of cycles corresponding to 50% of the expected fatigue life of the samples in as-welded condition. A slightly higher increase of fatigue life of UP treated welded elements for fatigue curve #3 could be explained by a more beneficial redistribution of residual stresses by UP after cyclic loading than in as-welded condition and/or by "healing" of fatigue damaged material by recrystallization [27] during UP in comparison with the fatigue curve #2.

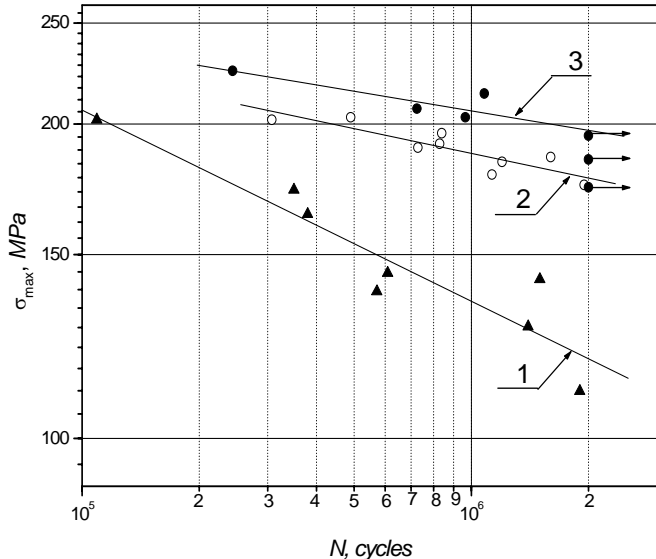


Fig.7. Fatigue curves of welded elements (transverse non-load-carrying attachment): 1 – in as welded condition, 2 – UP was applied before fatigue testing, 3 – UP was applied after fatigue loading with the number of cycles corresponding to 50% of expected fatigue life of samples in as-welded condition

Weld Repair

In this paper the rehabilitation is considered as a prevention of possible initiation of fatigue cracks in existing welded elements and structures that are in service. The UP could also be effectively used during the weld repair of fatigue cracks [7, 10].

Figure 8 shows the drawing of a large-scale welded specimen containing non-load carrying longitudinal attachments designed for fatigue testing [7]. Material properties: yield strength – 360 MPa, ultimate strength – 420 MPa. Such specimens were tested in as-welded condition and after weld repair with and without application of UP.

The testing conditions were zero-to-tension stress cycles ($R=0$) with different level of maximum stresses. Test frequency - 5 Hz.

The fatigue testing was stopped and the number of cycles was recorded when the length of fatigue crack on surface reached 20 mm. Then, the fatigue crack was repaired by gouging and welding and the fatigue test was continued. After repair, a

number of samples were subjected to UP. The weld toe of the "new" weld was UP treated. The results of fatigue testing of welded specimens in as-welded condition and after weld repair of fatigue cracks are presented in Figure 9.

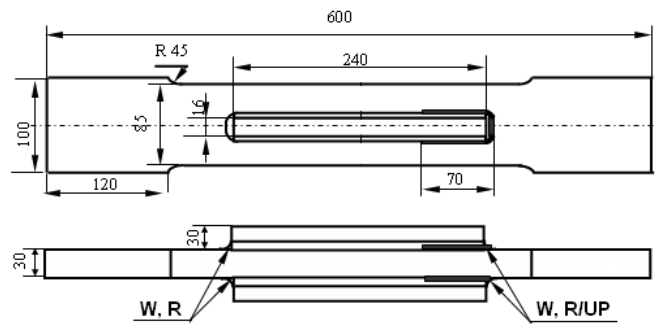


Fig.8. Drawings of welded specimens for fatigue testing at different conditions: W – as-welded condition; R - repair by gouging and welding; R/UP – repair by gouging, welding and UP

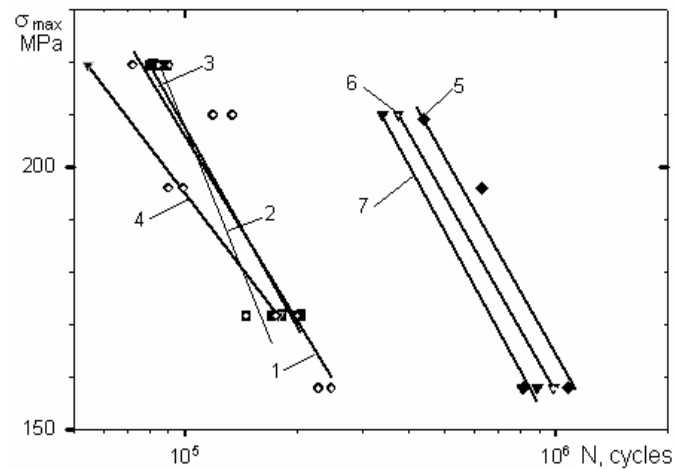


Fig.9. Results of fatigue testing of welded elements:
1 - as-welded condition, 2, 3 and 4 – after first, second and third weld repair, 5, 6 and 7 - after first, second and third weld repair with application of UP

The fatigue testing of large scale specimens showed that the repair of fatigue cracks by welding is restoring the fatigue strength of welded elements to the initial as-welded condition. Second and third repair of fatigue cracks also practically restored the fatigue life of repaired welded elements to initial as-welded condition.

The application of UP after weld repair increased the fatigue life of welded elements by 3-4 times. Practically the same significant fatigue improvement of repaired welded elements by UP is observed also after second and third repair of fatigue cracks in welded elements.

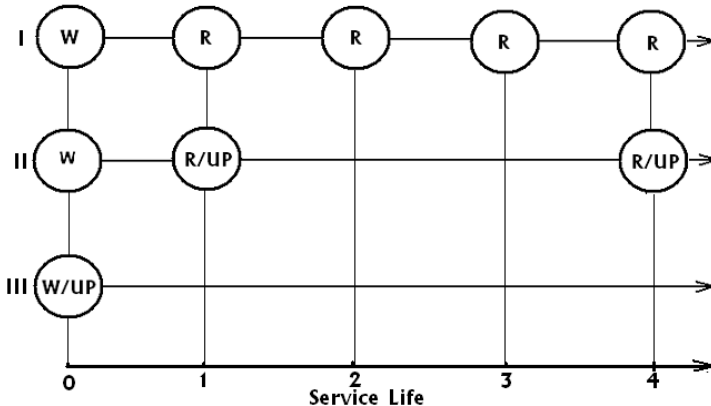


Fig.10. Diagram showing the endurance of welded elements:
 Line I - fatigue crack is repaired by gouging and welding,
 Line II - fatigue crack is repaired by gouging, welding and UP,
 Line III – UP is applied before/during the first phase of service
 life, W – as-welded condition, R - repair by gouging and
 welding, R/UP – repair by gouging, welding and UP,
 W/UP- welding and UP

A comparison of the efficiency of weld repair of fatigue cracks with and without application of UP is presented in Figure 10. This diagram illustrates the fatigue behavior of the same welded elements in cases when UP is not applied (I), when UP is applied after weld repair (II) and UP is applied before/during the first phase of service life (III). Here, 1 unit of service life corresponds to ~ 240,000 cycles of loading at the stress range 158 MPa and to ~ 75,000 at the stress range 220 MPa. Every circle, marked R or R/UP, in Fig.10 starting from the number 1 on service life axis indicates a fatigue fracture and a repair of the welded element. As can be seen from Fig.10, the benefit from application of UP for weld repair and rehabilitation of welded elements is obvious.

ULTRASONIC PEENING OF HSS WELDED ELEMENTS

700 MPa yield strength steel

Four series of large-scale welded samples were subjected to fatigue testing to evaluate the effectiveness of UIT/UP application for fatigue life improvement of welded elements made from 350 MPa and 700 MPa yield strength steels [13]. The fatigue specimens were designed as 80 mm wide by 8 mm thick steel plates with longitudinal non-load carrying fillet welded attachments, as shown in Figure 11.

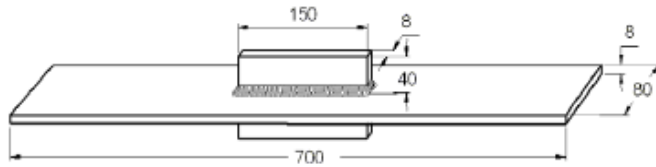


Fig.11. Welded specimen for fatigue testing of 350 and 700 MPa yield strength steel welded elements [13]

All testing has been conducted under constant amplitude axial tension in servo-hydraulic fatigue testing machines. The applied stress ratio has been $R=0.1$, with test frequencies varying from 2 to 6 Hz depending on load levels. Failure is defined to have taken place upon complete separation of the specimen. The results of fatigue testing are presented in Figure 12.

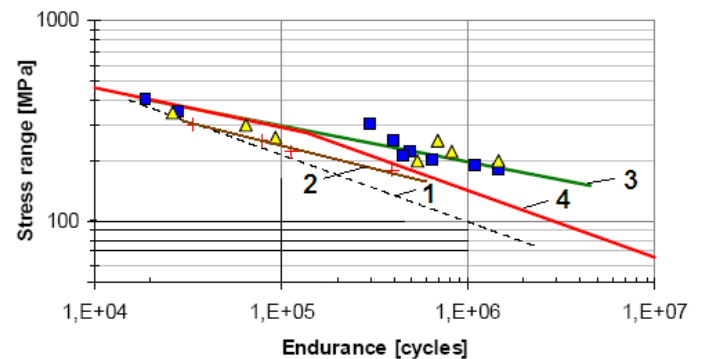


Fig.12. Fatigue test results for 350 and 700 MPa yield strength steel welded specimens [13]: 1- in as-welded condition, 350 MPa and 700 MPa yield strength steels, 2 - after UIT, 350 MPa yield strength steel, 3- after UIT/UP, 700 MPa yield strength steel, 4- FAT 112 design curve

As can be seen from Figure 12, the UIT/UP provided significant increase in fatigue performance of considered welded element for 700 MPa yield strength steel. The increase in limit stress range at 2 millions cycles of loading was 81% for welded samples treated by UIT/UP in comparison with as-welded condition, while TIG-dressing provided a 36% increase in limit stress range of welded element (see Table 2).

TABLE 2. INCREASE IN LIMIT STRESS RANGE OF WELDED ELEMENT AT 2 MILLIONS CYCLES OF LOADING [13]

S-N curve	Slope m	FAT value [MPa]	Improvement at FAT value [%]
As-welded S355 and S700	-3 (fixed)	71.3	-
UIT/UP S700	-5 (fixed)	129.4	81
Robotized TIG-dressing S700	-3 (fixed)	97.0	36.0

960 MPa yield strength steel

Four series of large-scale welded samples were subjected also to fatigue testing to evaluate the effectiveness of UIT/UP application for fatigue life improvement of welded elements made from 960 MPa yield strength steel [14]. The fatigue specimens were designed as 50 mm wide by 6 mm thick steel

plates with longitudinal non-load carrying fillet welded attachments, as shown in Figure 13.

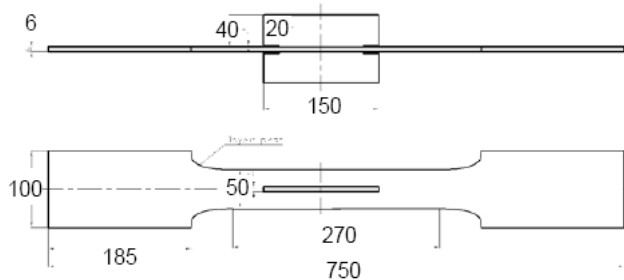


Fig.13. Specimen geometry for fatigue testing of 960 MPa yield strength steel welded elements [14]

The testing has been conducted under constant amplitude using $R = -1$. All of the as-welded specimens failed at the weld toe at the end of the longitudinal stiffeners. For the improved by UIT/UP welds, tested using constant amplitude loading, a variety of other failure modes were observed. The results of fatigue testing are presented in Figure 14.

As can be seen from Figure 14, the UIT/UP treatment with an instrument based on piezoelectric transducer provided the highest increase in fatigue performance of considered welded element for 960 MPa yield strength steel in comparison with the efficiency of application of magnetostrictive transducer and LTT electrodes.

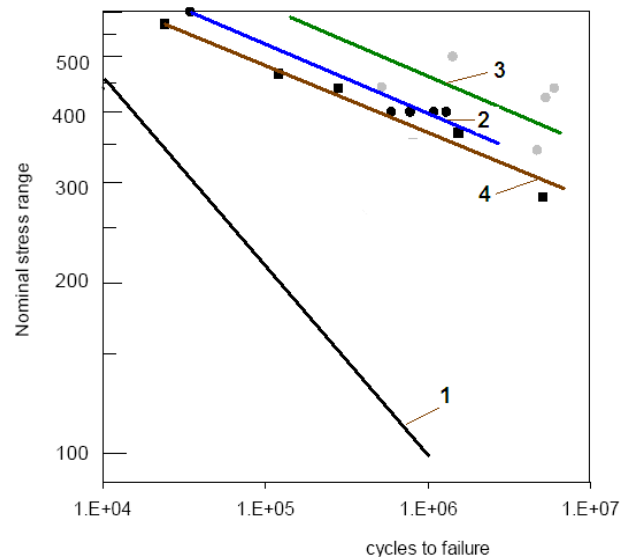


Fig.14. Fatigue test results for 960 MPa yield strength steel welded specimens [14]: 1- in as-welded condition (results of approximation of fatigue data received earlier), 2 and 3 - after UIT/UP based on using magnetostrictive and piezoelectric transducers respectively, 4- after application of LTT electrodes

INDUSTRIAL APPLICATIONS OF UP

As was demonstrated, the UP could be effectively applied for fatigue life improvement during manufacturing, rehabilitation and repair of welded elements and structures. The UP technology and equipment were successfully applied in different industrial projects for rehabilitation and weld repair of parts and welded elements. The areas/industries where the UP was applied successfully include: Railway and Highway Bridges, Construction Equipment, Shipbuilding, Mining, Automotive and Aerospace.

An example of application of UP for repair and rehabilitation of welded elements subjected to fatigue loading in mining industry is shown in Figure 15. Around 300 meters of welds, critical from fatigue point of view, were UP treated to provide improved fatigue performance of two large grinding mills located near Labrador City, NL, Canada..



Fig.15. Application of UP for rehabilitation of welded elements of a large grinding mill

The second example is based on the fatigue data and the solution described in [10]. The UP was also applied during the rehabilitation of welded elements of a highway bridge over the Ohio River in the USA. The bridge was constructed about 30 years ago. The welded details of the bridge did not have macroscopic fatigue cracks. The motivation for application of the UP for fatigue life improvement of this bridge was the fatigue cracking in welded elements and failure of one of the spans of another bridge of approximately the same age and design. More than two thousand and five hundred welded details of the bridge structure that were considered to be fatigue critical were UP treated.

CONCLUSIONS

1. Ultrasonic Impact Treatment (UIT/UP) is a relative new and promising technique for fatigue life improvement of welded elements and structures in materials of different strength including HSS with the yield strength of 700-1000 MPa. The results of fatigue testing show a strong tendency of increasing of fatigue strength of welded elements after application of UP with the increase in mechanical properties of the material used. It allows using to a greater degree the advantages of the HSS in welded elements, subjected to fatigue loading.
2. The fatigue testing of welded specimens also showed that the UP is the most efficient improvement treatment as compared with post weld techniques such as TIG-dressing and application of LTT electrodes.
3. The developed computerized complex for UP was successfully used in different applications for increasing of the fatigue life of welded elements, elimination of distortions caused by welding and other technological processes, relieving of residual stress, increasing of the hardness of material surfaces and surface nanocrystallization. The areas/industries where the UP was applied successfully include: Railway and Highway Bridges, Mining, Construction Equipment, Shipbuilding, Automotive and Aerospace.

REFERENCES

1. V. Trufyakov, P. Mikheev and Y. Kudryavtsev. Fatigue Strength of Welded Structures. Residual Stresses and Improvement Treatments. *Harwood Academic Publishers GmbH, London. 1995. 100 p.*
2. Y. Kudryavtsev, V. Korshun and A. Kuzmenko. Improvement of Fatigue Life of Welded Joints by Ultrasonic Impact Treatment. *Paton Welding Journal. 1989. No. 7. p. 24-28.*
3. V. Trufyakov, P. Mikheev, Y. Kudryavtsev and D. Reznik. Ultrasonic Impact Peening Treatment of Welds and Its Effect on Fatigue Resistance in Air and Seawater. *Proceedings of the Offshore Technology Conference. OTC 7280. 1993. p. 183-193.*
4. Y. Kudryavtsev, P. Mikheev and V. Korshun. Influence of Plastic Deformation and Residual Stresses Created by Ultrasonic Impact Treatment on Fatigue Strength of Welded Joints. *Paton Welding Journal. 1995. No. 12. p. 3-7*
5. V. Trufiakov, P. Mikheev, Y. Kudryavtsev and E. Statnikov. Ultrasonic Impact Treatment of Welded Joints. *International Institute of Welding. IIW Document XIII-1609-95. 1995.*
6. Y. Kudryavtsev and J. Kleiman. Fatigue Improvement of Welded Elements and Structures by Ultrasonic Impact Treatment (UIT/UP). *International Institute of Welding. IIW Document XIII-2276-09. 2009.*
7. Y. Kudryavtsev and J. Kleiman. Increasing Fatigue Strength of Welded Elements and Structures by Ultrasonic Impact Treatment. *International Institute of Welding. IIW Document XIII-2318-10. 2010.*
8. Patent of USA # 6467321. 2002. Device for Ultrasonic Peening of Metals.
9. Y. Kudryavtsev, J. Kleiman, L. Lobanov et al. Fatigue Life Improvement of Welded Elements by Ultrasonic Peening. *International Institute of Welding. IIW Document XIII-2010-04. 2004. 20 p.*
10. Y. Kudryavtsev, J. Kleiman, A. Lugovskoy et al. Rehabilitation and Repair of Welded Elements and Structures by Ultrasonic Peening. *International Institute of Welding. IIW Document XIII-2076-05. 2005. 13 p*
11. Y. Kudryavtsev, J. Kleiman, A. Lugovskoy et al. Fatigue Life Improvement of Tubular Welded Joints by Ultrasonic Peening. *International Institute of Welding. IIW Document XIII-2117-06. 2006. 24 p.*
12. Y. Kudryavtsev, J. Kleiman and Y. Iwamura. Fatigue Improvement of HSS Welded Elements by Ultrasonic Peening. *Proceedings of the International Conference on High Strength Steels for Hydropower Plants, July 20-22, 2009. Takasaki, Japan.*
13. P. Haagensen. Progress Report on IIW WG2 Round Robin Fatigue Testing Program on 700 MPa and 350 MPa YS Steels. *International Institute of Welding. IIW Document XIII-2081-05. 2005.*
14. G. Marquis and T. Björk. Variable Amplitude Fatigue Strength of Improved HSS Welds. *International Institute of Welding. IIW Document XIII-2224-08. 2008.*
15. Y. Kudryavtsev. Residual Stress. *Springer Handbook on Experimental Solid Mechanics. Springer – SEM. 2008. P. 371-387.*
16. Patent of USA No. 2,356,314. 1944. Scaling Tool. Reo D. Grey and James R. Denison.
17. Patent of USA No. 3,349,461. 1967. Descaling Tool. Joseph F. Niedzwiecki.
18. Krilov N. A., Polishchuk A. M. Using of ultrasonic apparatus for metal structure stabilization. *Physical background of industrial using of ultrasound. Part 1. LDNTP. Leningrad.-P. 70-79. 1970.* (in Russian)
19. Patent of USA No. 3,609,851. 1971. Metal Working Apparatus and Process. Robert C. McMaster and Charles C. Libby.
20. Patent of USA No. 3,595,325. 1971. Intermediary Impact Device. Charles C. Libby and William J. White.
21. C. Feng and K. Graff. Impact of a Spherical Tool against a Sonic Transmission Line. *The Journal of the Acoustical Society of America. Volume 52, Number 1 (Part 2), 1972. pp. 254-259.*
22. I. Polozky, A. Nedoseka, G. Prokopenko et al. Relieving of welding residual stresses by ultrasonic treatment. *The Paton Welding Journal. 1974. № 5.- p. 74-75. (in Russian)*
23. Author's Certificate (USSR) # 472782. 1975. Ultrasonic head for strain hardening and relaxation treatment. E.

Statnikov, L. Zhuravlev, A. Alexeyev, Yu. Bobylev, E. Shevtsov, V. Sokolenko and V. Kulikov. (in Russian)

24. Author's Certificate (USSR) # 601143. 1978. Ultrasonic multiple-strikers device. G. Prokopenko and V. Krivko. (in Russian)

25. B. Langenecker. Effects of Ultrasound on Deformation Characteristics of Metals. *IEEE Transactions on Sonics and Ultrasonics*. Vol. SU-13, No. 1, March 1966, pp. 1-8.

26. Yuri Kudryavtsev, Jacob Kleiman and Alexander Lugovskoy. Underwater Ultrasonic Peening of Welede Elements and Structures. Proceedings of the 4th International Conference on INTEGRITY, RELIABILITY & FAILURE (IRF2013), Funchal, Portugal, 23-27 June, 2013.

27. N.R. Tao, Z.B. Wang, W.P. Tong et al. An investigation of surface nanocrystallization mechanism in Fe induced by surface mechanical attrition treatment. *Acta Materialia*, 50, 2002, 4603-4616.



Refill Friction Stir Spot Weld Repair of a Fatigue Crack

Prepared by:

Sean Long Fox

Undergraduate, Metallurgical Engineering

Faculty Advisors:

Dr. Michael West

REU Site Director, Department of Materials and Metallurgical Engineering

Dr. Bahrat Jasthi

Research Associate, SDSMT Advanced Materials Processing Center

Dr. Alfred Boysen

Professor, Department of Humanities

Program Information:

National Science Foundation

Grant #: 0852057

Research Experience for Undergraduates

Summer 2010

South Dakota School of Mines and Technology

501 E Saint Joseph Street

Rapid City, SD 57701

TABLE OF CONTENTS

Abstract.....	3
Introduction.....	4
Broader Impact.....	5
Procedure.....	6
Materials Prep.....	6
Pre-cracking and Fatigue Crack Growth.....	7
Fatigue Test.....	8
Optimization of Parameters.....	8
Surfacing and Penetration.....	11
Stitch Welding.....	12
Cold Spray.....	12
Results.....	15
Discussion/Conclusion.....	16
Future Work.....	16
References.....	17

ABSTRACT

The main objective of this project is to repair a fatigue crack using Refill Friction Stir Spot Weld Technology. This involved developing a procedure to stitch, or overlap, single spot weld to repair fatigue cracks. A pre-cracking procedure was also developed to provide simulated fatigue cracks on which repairs could be made. First, the welding parameters were optimized for 2024 Al T3 with a thickness of .125 inches. 2024 powder is then deposited using Cold Spray Deposition to fill the pre-crack. The welds were then overlapped and repairs were made. The repairs were found to have defects and the defects are characterized to show how they reduced fatigue life. Good repairs are also characterized and show improvement in fatigue life over cracked samples. Improved repair methods are discussed to allow for better repairs in the future.

INTRODUCTION

Fatigue life is a very important factor in many applications. For instance, a plane wing will undergo fatigue cycles as the wing flutters during flight. Over time this cyclic fatigue will cause fatigue cracks. With every cycle, the fatigue crack grows larger. Many times these fatigue cracks act as an indicator that the part in question must be replaced. These replacements are costly and require constant manufacturing. Recently, a new friction stir process was developed called Refill Friction Spot Welding. With this new idea, Harms and Wende of Germany has developed a small RFSW machine. The RFSW process differs from traditional friction spot welding. The friction stir refill process uses a pin and sleeve (shoulder) that move independently from each other. While both pin and sleeve are rotating, the sleeve is plunged into the material to be welded. At the same time, the pin retracts upward; drawing plasticized material up as well. Once the sleeve has reached its full depth, both sleeve and pin return to their original position. As the pin moves down, it re-introduces the plasticized material back into the weld. This method of friction stir spot welding has been shown to be superior to the fixed pin of friction spot welding. Using the RFSW process, a procedure for repairing existing fatigue cracks could be developed. Repairing a part can be much more cost effective when compared with simply replacing the part. It is with this goal in mind that a procedure for RFSW fatigue crack repair will be developed.

In order to repair a fatigue crack, it must first be created in a sample that can be analyzed. 2024 Aluminum in a T3 state will be used as the material to be tested. A thickness of 0.125 inches will be used as it is a common size for many Al skin applications. This thickness is also near the limit of the RFSW machine's welding depth. A sample configuration was selected as per ASTM E647 for a notched sample. The specimen is a dog bone configuration. The samples are then machined under high tolerances and a pre-crack is introduced into the test cross section. The pre-crack acts as a stress concentrator and helps to grow the fatigue crack. The crack will be

grown under cyclic loading condition in a MTS 810 tensile testing machine. Once a fatigue crack is present, the pre-crack volume loss must then be filled to allow for proper surfacing during RFSW repair. For this a Cold Spray Process will be used to introduce 2024 Al powder into the pre-crack. Then, stitch welds will be used to repair the fatigue crack that remains in the sample. A stitch weld is simply overlapping welds to form a continuous repair. Once repaired, the sample will then undergo addition fatigue test to show the resulting fatigue life. This is then compared to the fatigue life of parent metal samples and to that of unrepairs samples. The un-repaired samples simply have the unrepairs fatigue crack present. Ultimately this will show whether the procedure outlined in this project will give an improved fatigue life for this material.

BROADER IMPACT

In order for a part to develop a fatigue crack the part simply must undergo cyclic stress at a level below the materials flow stress. The crack will generally form near a stress concentrator. Sharp ninety degree angles, or areas of weakness, make good stress concentrators. Once the crack is started it will spread to a point when the part may fail in a catastrophic manner. Replacement parts are costly and they rely on their supply. One good example of how fatigue cracks can be harmful would be the United States Military's aging equipment. For instance, the F-15 eagle is an aircraft that has been around since the early 1970's. As this aircraft flies through the air, the tips of the wings flutter up and down. This causes fatigue cracks to form in the wing. A replacement wing is a costly option, but what if it could be effectively repaired? Time, money, and resources could be saved with an effective repair procedure. Solution such as this are needed to caring aging equipment into the future without having to maintain the associated infrastructure. This means that a piece of machinery could still be used even without parts being actively manufactured. The military example is not where the possibilities end. The private sector could also benefit much from an effective fatigue crack repair process.

PROCEDURE

Materials Preparation

The materials that were used in this project were 2024 Aluminum in the T3 state. The 2024 Aluminum plate was 0.125 inches thick. Originally, this material was a single plate. This plate was then sheered to a dimension with approximated 0.125 inches excess in each dimension. It should be noted that the length (12in) of the specimen is the original direction of rolling. The raw sheered plates where then squared to within .1 inches of their final dimensions. This was done using a manual milling machine, with great care taken to achieve high tolerances. Instead of the traditional 0.02 inches tolerances, 0.01 inches was selected. Precisely machined samples are needed to ensure good results. ASTM E466 was the standard referred to while finalizing the sample configuration. The rectangular plates then needed some final milling to introduce the reduced section. This milling was performed using a CNC milling machine. The radius of the reduced section was 0.5 inches. The final pass in the CNC was a high tolerance and surfacing pass. This means that only 0.005 inches were removed on the last pass in order to maintain the high tolerance. The samples were stacked 8 high or 1 inch thick for the CNC milling process. Figure 1 illustrates the final specimen and the location of the pre-crack, while Figure 2 shows the Solidworks model used to develop the tool paths for final CNC milling.

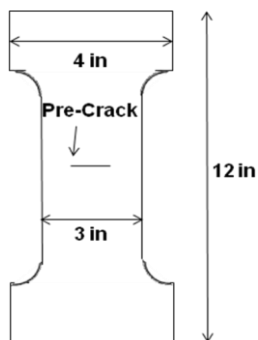


Figure1: Sample Configuration

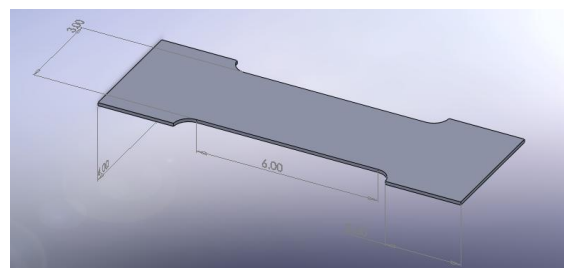


Figure 2: Solidworks Coupon Model

Pre-Cracking and Fatigue Crack Growth

The pre-crack growth procedure was setup using a Dremel power tool. The tool had a 1/8 inch thick disk made of silicon carbide. The procedure was to cut a .80 inch deep and .75 inch long slot out of the fatigue coupon to initiate a fatigue crack growth.

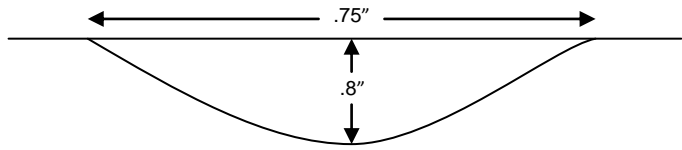


Figure 3: Pre-Crack Dimension (front)

Figure 3 shows the diagram and shows the dimensions of the pre-crack.

This was the first step in artificially creating a fatigue crack. After the pre-crack was initiated the coupon was then loaded into a tensile test machine. The coupons were run in cyclic fatigue to broaden the width and depth of the fatigue crack. The range for the load of the cyclic fatigue was from .675 kips to 6.75 kips. The 6.75 kips is thirty percent of the flow stress of the material. The range of the load needed to be low to ensure a plastic region did not form around the crack. The test were performed at 20 Hz and reached approximately 50,000 cycles. Figure 4 shows a close look on a finished fatigue crack. It can be seen that the pre-crack dominates the visual; however there are microscopic cracks on each side of the pre-crack. The total width of the crack was approximately .78 inches to .65 inches. A closer look at this macroscopically indicates that indeed a crack was propagated in the pre-crack. In Figure 5, it shows the crack at a 50x resolution.



Figure 4: Fatigue Crack Width

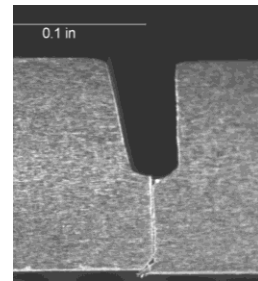


Figure 5: Fatigue Crack Macro (side)

Fatigue Test

The cyclic fatigues of the samples are broken up into three categories. The categories consist of parent, un-repaired and repaired samples. Each category will have 4 load levels applied to them. These are expressed as percentage of flow stress. The load levels include 20% at .45 kips to 4.5 kips, 30% at .675 to 6.75 kips, 40% at .9 kips to 9.0 kips and 50% at 1.125 kips to 11.25 kips. Making the total flow stress for the coupon to be 22.5 kips. These are the cyclic fatigues lower and upper limits and will proceed until failure of the material is reached. In Figure 6, an unrepaired sample that was run until failure is shown.

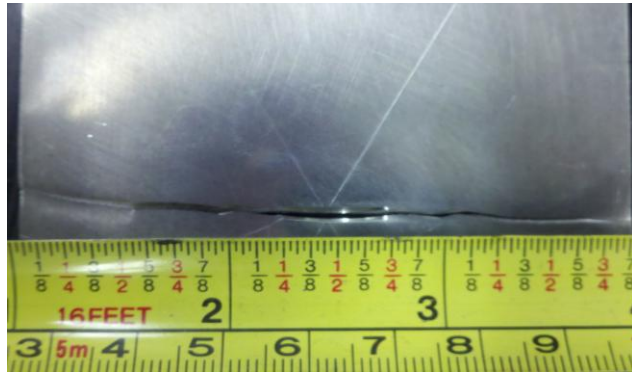


Figure 6: Failure of an Un-Repaired Sample

Optimization of Parameters

For the welding part of the project, optimized parameters are needed. Previous work was done using this exact procedure of optimization, however, the state of RFSW machine was unsteady at that time. A parameter matrix was developed and can be seen below in Figure 7. In order to show the best combination of weld time and rotational speed, each must be varied to show the overall affect on weld defects. By increasing these variables an increase in the mixing and heat input may be seen. In order to see the best combination, 1400 to 1600 rpm was tested, with the total weld time varying from 6 to 10 seconds. It should be noted that the total weld time includes

the plunge time and the retraction time. In this experiment the plunge time is equal to the retraction time. The clamping pressure is constant at 3.5 bar. Clamping pressure is applied through a standard pneumatic c-gun which forms the frame of the RFSW. The clamp, or gun, is actuated at the beginning of the welding cycle and lifts the material up to the clamping ring, which contains the sleeve and pin. Additional clamping is applied to the front and the back of the plate in the form of secured blocks. This prevents the coupon from rotating during the welding process. After the welds were made for the parameter matrix, the samples were polished down to a one micron diamond polish and then etched with Kellar's.

The parameter matrix in Figure 7 shows the results of the parameter development process. The sections marked no weld are the result of the machine retaining most of the material that was plasticized. This resulted in a large hole in the aluminum plate. This most certainly indicates unacceptable parameters. Early in the parameter investigation, parameters were explored below the range shown in the chart with a particularly bad result, current limits were triggered. This means that the force required to rotate the tools required an amount of current outside the operational range of the RFSW machine. The parameters expressed on the chart are the lowest within the operation range of the machine. This tells us that with bad welds at higher variable levels and force limits on the low end of the matrix, an optimized parameter should be within the matrix. Another consideration in the welding procedure is the surfacing. An addition welding step was added at the end of the welding process in order to give the best surfacing possible. This was kept constant as a 1 mm plunge, 1 sec total weld time, and 1400 rpm plunge. As a result, the material along the surface is returned to the 2024 aluminum plate and a nearly flush surface is achieved. This surfacing step will be discussed in further detail.

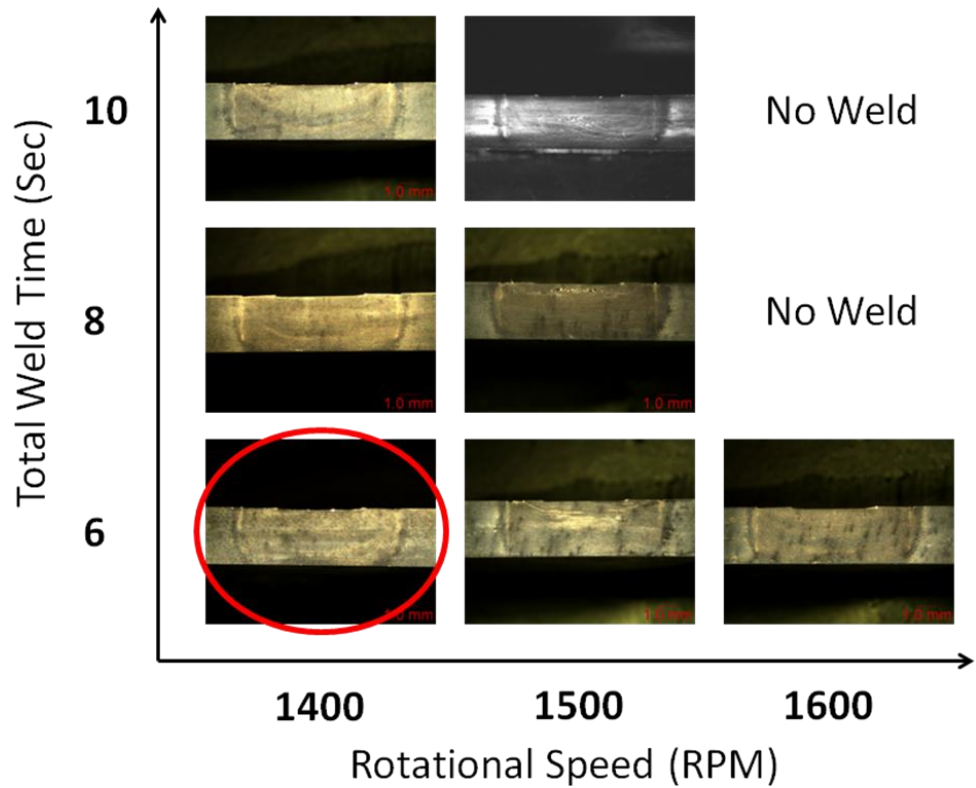


Figure 7: Developmental Matrix

Within the matrix, observations were made to show the best set of parameters. The criterion of a good weld involves observation of the formation of defects. In the 1500 rpm set of samples, a lack of mixing near the surface can be seen. In 1500 rpm sample, the six and eight second welds show voiding near the surface as a result of the lack of mixing. These features can very easily initiate fatigue cracks and thus are seen as un-acceptable welds. Another consideration is the mixing along the walls of the weld. A thin light colored line can be seen in all welds along the left and right sides of each weld. This feature is caused by the sleeve plunging into the plate. The 1400 rpm, 6 second sample shows the best mixing in the walls of the weld. Using these observations, it was decided that the 1400 rpm, 6 second weld, is the most optimized

parameter. Once again it is important to keep in mind that at variable levels below this yield no welds due to machine limits.

Surfacing and Penetration

Beyond the variation of RPM and Time, there are two other major factors in showing a good weld from a fatigue standpoint: penetration and surfacing. When it comes to penetration, this machine is at its limit with 3.175 mm (0.125 inch) thick material. Luckily the area under the pin is stirred and a full depth plunge is not necessary. As a result, the plunge depth for all welds is 2.8 mm. As seen in the parameter matrix, all welds were stirred all the way to the bottom surface. This is important because the fatigue crack to be repaired extends through entire thickness of the plate. The other major factor left to discuss is surfacing. Right angles and indentations along the surface may be initiation sites for fatigue cracks, so the surface must be as flush as possible. This is accomplished by ensuring that there has been no volume loss from the fatigue cracking process, and by having a proper home position for the pin and sleeve. The volume loss is addressed by filling the pre-crack using a cold spray process. This process will be discussed in greater detail later. The home position is set by having the proper pin, sleeve, and clamping ring alignment. When the part is clamped, it is pressed upwards against the downward facing clamping ring. Within the clamping ring is the sleeve and pin. The bottom surface of these three components must be aligned when the tool is first installed into the machine. Further adjustments can be made after twenty conditioning welds using identical material. These conditioning welds fill the tool with aluminum, and prevent additional volume loss. Once the surface is as flush as possible the tool is ready to make repairs.

Stitch Welding

A single weld will not repair the entire fatigue crack. In order to stir the entire length of the crack, single spot welds must be overlapped into what is referred to as a stitch weld. In the previous year's study it was found that tensile strength varies with varying overlaps. Using digital image correlation to illustrate stress distribution around each configuration of stitch weld and the hardness across each configuration, an optimized stitch weld was found. It was shown that overlapping 4 welds by 0.216 inches, centered about the center of the fatigue crack, would give the best properties. This study was a comparison of configurations with identical weld conditions so this study is used for this project as well.

Cold Spray

Cold spray deposition will be used to fill the pre-crack that was created to grow the fatigue cracks. It is critical to make up for the volume loss, or else risk creating a fatigue initiation point along the surface. The cold spray process involves injecting a particle into a stream of gas and impacting the particle onto a substrate. The idea is that the particle needs enough energy to plasticize and bond with the surfacing. Energy is transferred from the gas to the particle as it accelerates within a nozzle. Generally the nozzle will involve converging and diverging chambers. The gas is also heated to allow for higher velocities. A cold spray deposition trial can be seen in Figure 8.

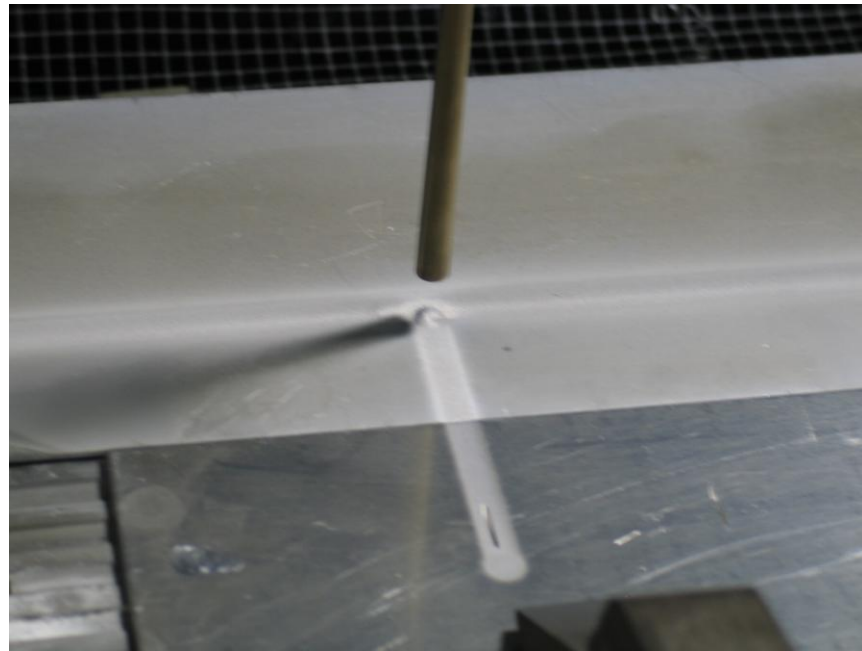


Figure 8: Cold Spray Deposition Trial with 2024 Al Powder (400 mesh)

Abdulaziz Alhulaifi is currently preparing a dissertation on the subject. With Abdulaziz's work we have a better understanding of the process. The critical velocity can be calculated using Equation 1. This equation is the result of the energy balance. Note that the melting point for the material, 2024 Al in this case, is reduced by 30%. This is because only 70% of the melting temperature is needed for plasticization. The C_p and T_m come from Al 2024 known properties. The T_i is the temperature of the gas. The gas is generally heat between 250°C and 450°C. The gas can be varied, but compressed air between 80psi and 140psi has been the gas of choice up to this point. Using this equation the critical velocity for the 2024 Al powder was found to be 590 m/s. Additionally, the size of the sprayed particle is crucial for achieving a deposit. The 2024 Al powder begins as 140 mesh, which means 105 microns is the largest size particle.

$$V_{critical} = \sqrt{C_p (0.7T_m - T_i)}$$

Equation 1: Critical Velocity

After attempting to spray the 105 micron size material, it was found that no particles were sticking to the substrate. The variables were explored in depth with no positive result. In order to overcome this, the powder was sieved to reduce the size of particle sprayed. 44 micron and 37 micron particles were sieved. The pressure of the compressed air was varied from 80 psi to 140 psi and the temperature of the gas from 250°C to 450°C with only minimal deposition. The pressure is limited by the range that the lab air compressor can operate in. The deposition occurred with the 37 micron particle at max pressure and temperature. Loss was very large as few particles actually deposited. The possibility of strain hardened particles was explored. First, a polished sample was examined for geometry. This can be seen in Figure 9 below. Clearly the Al powder particles are small spheres, most likely from being atomized. Meaning it is less likely that they are strain hardened. Second, a micro hardness test was needed. A sample was prepared in an epoxy mount. This sample was then tested for Vicker's hardness. After 20 points were tested it was found that the average hardness was about 125 on the Vicker's scale. This is within 10 of the known 2024 Al hardness value, thus it was confirmed that no strain hardening occurred. After consulting Abdulaziz, he calculated that the system was not reaching the critical velocity and adjustments would be needed.

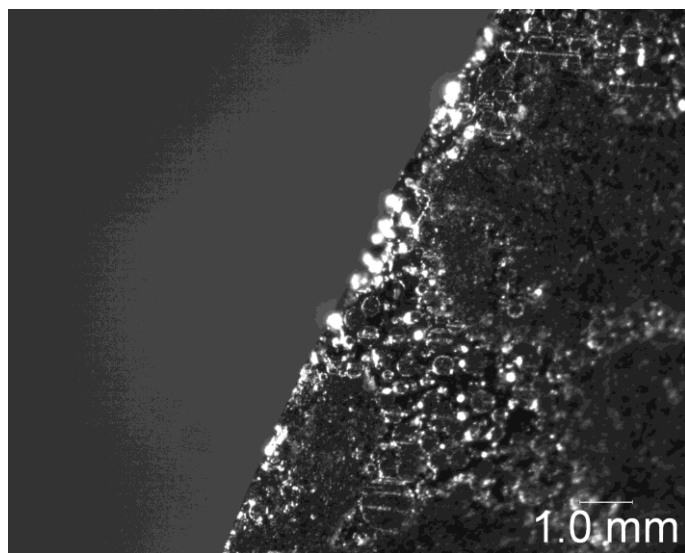


Figure 9: 2024 Al Powder in Bakelite at 2.5x

RESULTS

The cold spray process has not yet yielded a deposition. As a result, the final repairs have not yet been made. The fatigue testing of the parent material has been complete and can be seen in Figure 10. These values form the basis of a comparison with repaired and unrepaired samples.

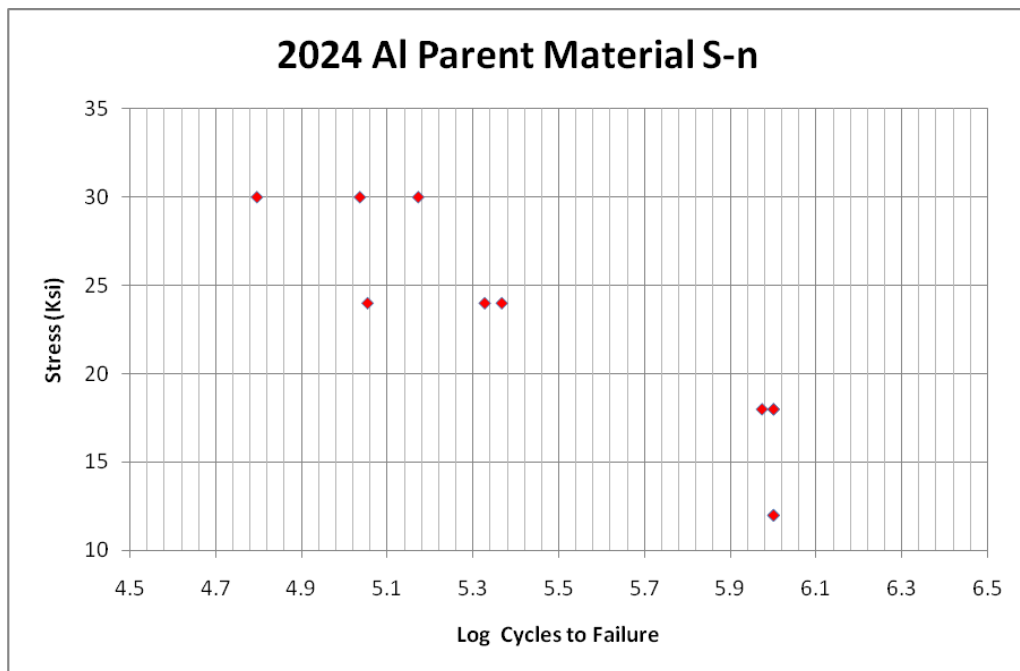


Figure 10: 2024 Al Parent Metal Fatigue Results

CONCLUSION/DISCUSSION

Future Work

Cold spray deposition and final repairs have yet to be completed. The cold spray deposition will require further investigation. In order to achieve this deposition, one of two methods will be used. One method involves depositing pure aluminum into the pre-crack. This method would involve a tertiary study on the effect of the pure aluminum addition on the properties of the resulting RFSW. If found the improve properties (tensile and fatigue), or if the properties remain unchanged, the method will be used for final repair. The second method for 2024 Al cold spray deposition involves further investigation into depositing the 2024 Al powder. Using the data from the previous attempts to deposit this material, we know that we must achieve a higher velocity. This may be achieved by one of several ways. First, the cold spray nozzle could be extended. This will give the particles more time to accelerate to the critical velocity. Another way this may be accomplished is simply by changing the distance from the end of the nozzle to the substrate from 13mm to 20mm. This may have a similar effect to the longer nozzle solution. Lastly, the gas used in the cold spray deposition process could be changed. Regardless of the gas chosen, the high pressure tanks that are delivered can provide much higher pressure than 140 psi. This may allow us to achieve double the pressure previously used. The gas may also be varied. Helium, and possibly nitrogen, may be used to propel the aluminum particles as well. The density of the helium gas may allow for higher impact velocities. The nitrogen gas will behave in a similar manner to the compressed air, but serve as a higher pressure source. Once the cold spray deposition process is finalized, final repair and testing can begin.

REFERENCES

Russel, SG. 2001. Static, Fatigue and Crack Growth Behavior of FSW 7075 T-6 and 2024 T-3 Aluminum Alloys. TMS Friction Stir Welding and Processing, Vol. 1, Pg 93

Oberembt, Clark. 2008 Effects of Process and Parameters on Joint Properties of Refill Friction Stir Spot Welded Magnesium-Aluminum Alloy. SDSMT Thesis.

Alhulaifi, Abdulaziz. 2009. Cold Spray Modeling for Spraying Nano Particle Powders. SDSMT Research Proposal.

Uematsu and Tokaji. 2008. Effect of Re-filling Probe Hole on Tensile Failure and Fatigue Behaviour of Friction stir Spot Welded Joints in Al–Mg–Si Alloy. International Journal of Fatigue, Vol. 10-11, Pg 1956-1966.

Uemetsu, 2009. Comparison of Fatigue and Tensile Behaviour Between Resistance Spot Welds and Friction Spot Welds. Science and Technology of Welding and Joining. Vol 14, Pg 62.

Referenced ASTM Standards:

ASTM E647- Measuring Fatigue Cracks

ASTM E466- Fatigue Test Practices

ASTM E468- Reporting Fatigue Test Results

Offshore fatigue crack repair by grinding and wet welding

J. E. RODRÍGUEZ-SÁNCHEZ¹, A. RODRÍGUEZ-CASTELLANOS²,
F. PÉREZ-GUERRERO³, M. F. CARBAJAL-ROMERO⁴ and S. LIU⁵

¹Instituto Mexicano del Petróleo, Coordinación de Aguas Profundas, Eje Central Lázaro Cárdenas Norte 152, 07730 México Distrito Federal, Mexico,

²Instituto Mexicano del Petróleo, Dirección de Ingeniería, Eje Central Lázaro Cárdenas Norte 152, 07730 México Distrito Federal, Mexico, ³Instituto Mexicano del Petróleo, Coordinación de Aguas Profundas, Eje Central Lázaro Cárdenas Norte 152, 07730 México Distrito Federal, Mexico, ⁴Instituto Politécnico Nacional, Sección de Estudios de Posgrado, Avenida de las Granjas 682, 02350 México Distrito Federal, Mexico, ⁵Colorado School of Mines, Metallurgical & Materials Engineering, Hill Hall 254 Golden, Colorado 80401, USA

Received in final form 25 Oct 2010

ABSTRACT A fatigue crack repair option based on crack removal by grinding and subsequent filling of the resultant groove by wet welding is presented. Author's experimental and fracture mechanics analysis experience on fatigue crack removal by grinding has demonstrated that a fatigue life extension factor of 2 to 3 is feasible for crack removal done before crack penetration has reached 30% of the plate thickness. However, it has also been demonstrated when groove is left empty, that fatigue life extension after crack removal is mainly due to the stage of fatigue initiation because crack propagation after removal has a higher rate than in as-welded condition. To overcome this situation, this work proposes for an underwater application like in the offshore industry, that filling the grinded groove by means of wet welding would produce a crack repair with a longer fatigue life than the empty groove case.

Keywords crack repair; fatigue life; grind; groove; notch; offshore repair; wet weld.

NOMENCLATURE

a	= crack depth
C	= material constant
da/dN	= crack growth rate
m	= material constant
Y	= modification factor (Y factor)
ΔK	= stress intensity range $K_{\max} - K_{\min}$
$\Delta\sigma$	= surface stress range of uncracked welded joint at the crack site

INTRODUCTION

Fatigue cracks in offshore structures are frequently found during inspection campaigns, and their effect on the structural integrity can become quite relevant depending on the redundancy of the structure. For the case of jacket structures it is widely known that hot spot stress locations at main tubular welded joints are prone to fatigue cracking, fortunately jackets are quite redundant structures that can safely continue operating with some cracked joints considering that they are regularly inspected to monitor crack growth depth and length. This practice of en-grossing NDT inspection plans to sustain integrity when fatigue cracks are found is mainly due to the fact that

underwater fatigue crack repairs are not an easy task to perform, otherwise a repair would partially reinstate the as-welded condition and general visual inspection would be enough to sustain integrity after a fatigue crack repair is performed.

Present practice for fatigue crack repair of jackets tubular joints basically relies on mechanical clamps rather than on crack removal. However, clamping solutions require considerable economical resources for the fabrication and installation of the clamps and frequent stress monitoring of the studs during the operating life of the jacket. Therefore, the fatigue crack repair option presented in this paper is a feasible option to reduce the economical resources required for fatigue crack repair of offshore jackets.

Correspondence: José Efraín Rodríguez-Sánchez. E-mail: ersanche@imp.mx

This paper gathers author's experience obtained experimentally and in the field on fatigue crack repairs and on wet welding procedures. It has to be stated that at this stage of wet welding technology, it is only applicable up to 100 m of water depth, thus what is presented here has the same limitations. The repair procedure presented combines crack removal by grinding and subsequent filling of the groove by means of wet welding trying to reinstate the as-welded condition. The grinding experience assures that the crack is adequately removed and the wet welding experience provides a procedure that leads to maximize the weld quality of the repair. Additionally, because the grinding tool is available as it was used for the crack removal, the tool can also be used to improve the weld toe profile to reduce the stress concentrations and extend the fatigue initiation life. It is known that after crack removal by grinding when the groove is left empty, the fatigue life extension is due to the fatigue initiation stage because crack propagation stage has a higher rate than in as-welded condition.¹ Therefore, for a crack removal to reduce the fatigue propagation to a similar rate of the as-welded condition it has been considered the application of wet welding. Thus, the repair procedure presented has been conceived as follows:

To remove the crack and reinstate as-welded conditions

- 1** Fatigue crack removal by grinding
- 2** Groove filling with wet weld to reduce the fatigue crack propagation rate due to the stress riser effect of the groove

To extend fatigue initiation life

- 3** Wet weld toe profiling
- 4** Induce surface compressive stresses

FATIGUE CRACK REMOVAL BY GRINDING

Grinding of fatigue cracks has been used mainly in underwater offshore applications to remove the crack tip and stop crack propagation. For the case of welded tubular joints and welded plates, the profile of the groove along the crack length produced by grinding is highly relevant on the fatigue life of the repaired component. For the case of crack re-initiation after crack removal by grinding, the profile of the groove prescribes the location of crack initiation along the groove. Analytical and experimental work on crack repair geometry has been done where the concept of short repair is introduced and its usefulness demonstrated for the case of removal of fatigue cracks by grinding in underwater conditions.² Crack initiates at the location of highest stress, which for the as grinded condition occurs at the bottom of the groove or at both ends of the groove where the groove reaches the plate surface. Occurrence of one or the other case would depend on the groove geometry; the second case is known as short repair. The main advantage of a short repair is that after a crack removal is performed and if crack re-initiation occurs, this would always be at the groove ends located at the top of the plate, reinstating the original plate thickness for crack propagation and also facilitating the inspection of the repair because plate surface inspection is easier than inspection in a narrow groove.² Crack re-initiation for repairs that do not comply with the short repair conditions will always take place on the bottom of the groove. From Fig. 1, groove ends and bottom of the groove locations for a surface crack short repair are illustrated.

It is worth pointing out that if a repair profile is left empty this is, not filling the groove with wet weld, a short repair

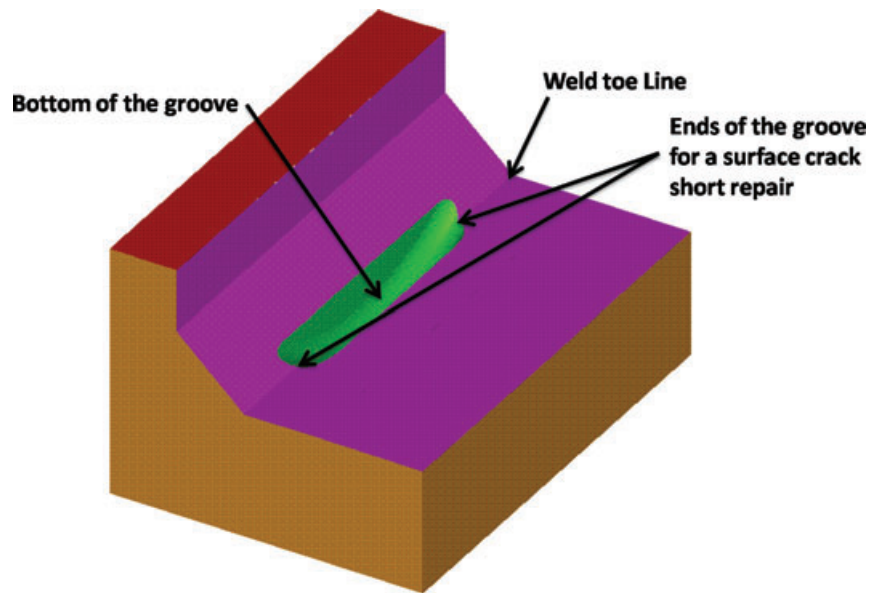


Fig. 1 Locations of groove ends and bottom of the groove for a surface crack short repair on a *t*-butt welded connection.

profile is only effective for the removal of surface cracks. For the case of edge cracks after crack removal is performed and leaving the groove empty, crack re-initiation will always take place on the bottom of the repair.² Thus, the wet weld groove filling benefit is to erase the repair profile shape that defines if crack re-initiation starts on the surface of the plate or on the bottom of the repair making feasible to perform the repair procedure proposed in this work for surface and edge cracks.

For the case of fatigue crack repairs by grinding and subsequently filled with wet weld, it has been considered that the use of short repairs is not recommended because the profile requirement is stringent and no benefits are expected due to the profile geometry because the groove stress distribution effect is erased by the wet weld filling that tends to reinstate the as-welded condition. Additionally, it is expected that the use of longer grooves facilitates the application of wet welds.

Grooves are generally machined by divers using rotating burrs and quality control of the groove profile geometry becomes difficult due to the amount of force required to penetrate into the metal, thus burrs skip sideways before a deep groove track is obtained resulting in poor groove profile geometry. The use of wet weld to fill the groove can help to overcome the difficult task of assuring the quality of the groove profile because the groove profile effect is erased by filling the groove.

GROOVE FILLING WITH WET WELD

Wet welding has been used by offshore oil operators in the Gulf of Mexico for the repair of offshore structures damaged by hurricanes, boat impacts, dropped objects from the decks, etc. It is well known that fatigue cracks typically initiate at the weld toe and propagate though the thickness of the structural component. As mentioned earlier, crack removal is an option to extend the fatigue life for crack depths up to 30% of plate thickness. However underwater inspection of a narrow groove is difficult, thus, risk of incomplete crack removal by grinding is feasible, which would lead to increased fatigue crack propagation rate instead of extending the fatigue life. Therefore, an effective option to assure that crack propagation is halted, even if the crack is not totally removed, is by fusing the crack tip when melting the bottom of the groove during wet weld deposition. Although a total removal of the crack is intended by design, if a crack tip is left unintentionally its size is minimum due to the inspection equipment accuracy and can be fused while wet weld is deposited.

Once a fatigue crack has been detected a decision has to be made whether it is only grinded out leaving an empty groove or in addition to grinding out the crack, filling the groove with wet weld. The first case is preferably applica-

ble to surface cracks repaired with short repairs, limited to a crack depth removal up to 30% of plate thickness. The second case is preferably recommended for edge crack repairs because crack re-initiation will always take place on the bottom of the groove making underwater inspection even more complicated. However, it is worth pointing out that the uncertainty of total crack removal for both cases remains an issue due to inspection equipment accuracy. Thus, groove filling with wet weld is always recommended if resources are available to increase the reliability of the repair.

POROSITY OF WET WELDS

Porosity is one of the main disadvantages of wet welding, it was reported in 1986 that porosity in welds deposited with commercial electrodes increased from 1% at 5 m water depth to approximately 8% at 60 m water depth, see data represented by D4301, D4313 and D4327 in Fig. 2 where nomenclature refers to commercial electrodes.³

By 2002, research efforts led to reduced porosity in wet welds, from approximately 0.8% at 21 m water depth to 1.6% at 60 m water depth. These welds were produced using rutile electrodes with low titanium and low boron additions (see also Fig. 2).⁴ From the same figure, by 2007, enhanced rutile grade electrodes with ultra low carbon in the steel rod produced wet welds with less than 1% porosity at 50 m water depth.^{5,6} These electrodes were water proofed with varnish to protect the electrode flux coating from water absorption from the surroundings. Advances in porosity mitigation made wet welding a truly underwater structural repair option. Shielded metal arc welding (SMAW) process with direct current electrode positive (DCEP) has been the preferred process for wet welding with rutile grade electrodes. Wet welds made with direct current electrode negative (DCEN) polarity and rutile electrodes exhibit deeper penetration and more porosity than the DCEP wet welds.⁷

POROSITY AND FATIGUE

Matlock *et al.* reported results from fatigue tests performed on three types of welds fabricated with commercial rutile E6013 electrodes.^{8,9} The types of multiple-pass welds in these works were: surface weld, hyperbaric or habitat weld and underwater wet weld.

Surface welds are typically considered pore-free and their data were used to define the base line for comparison. The hyperbaric dry welds contained low porosity, in the range of 3%. The wet welds contained considerably higher porosity with approximately 12% porosity. Porosity was measured on the fracture surfaces of tested specimens.

Crack growth rate (da/dN) values of the surface weld are lower than the wrought carbon steel, but higher than the

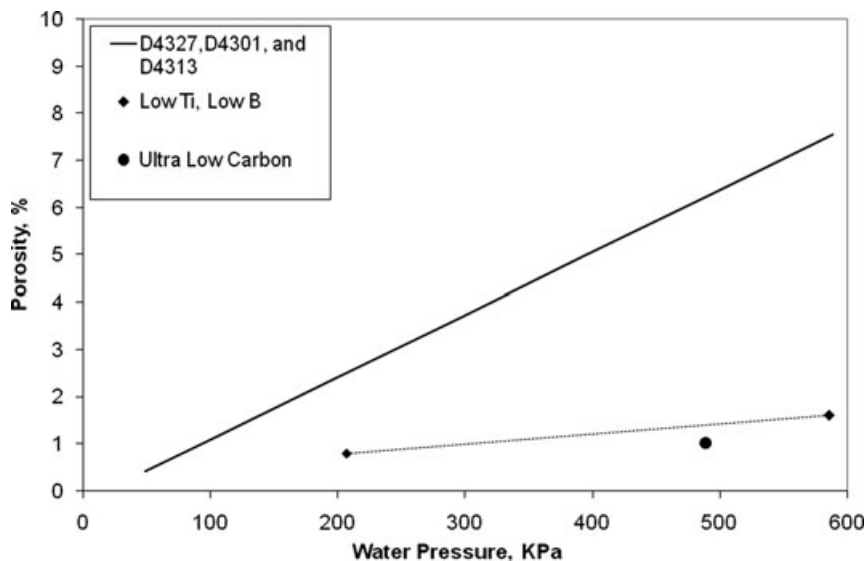


Fig. 2 Effect of pressure on weld porosity of commercial,³ low Ti – low B⁴ and ultra low carbon electrodes.^{5,6}

habitat weld. At low stresses the wet weld reported smaller $d\alpha/dN$ values than the surface and the habitat welds. However at high stresses the wet weld presented higher $d\alpha/dN$ values. These results imply that at low stresses porosity was beneficial in retarding the fatigue crack propagation. Pores acted like pinning sites at the crack front, arresting the crack growth for finite number of stress cycles.^{8,9} However, it is important to mention that the porosity values achieved in wet welds made at 50 m water depth were at the order of 1%, which is considerably less than the 12% reported in this fatigue study.^{5,6}

MECHANICAL PROPERTIES

Another problem that has limited the application of wet welding is related to poor mechanical properties of the weld metal. The main reason behind the reduced mechanical properties is associated with the loss of alloying elements such as carbon, manganese and silicon. On the other hand, oxygen content in the weld metal increases with water depth until a saturation value is reached. It is well known that the above mentioned alloying elements have strong affinity for oxygen at the arc fusion welding temperatures. Carbon forms carbon monoxide gas (CO) that contributes to porosity formation while silicon and manganese form non-metallic inclusions in the weld metal.^{5,6,10} Parts of the CO bubbles and oxide inclusions escape from the weld pool and the remaining gas bubbles and second phase particles are trapped in the weld metal. Only if the alloying elements are distributed in solid solution in the steel matrix of the weld, they contribute to the mechanical properties of the weld metal. Pores and

non-metallic inclusions are detrimental to the mechanical properties.

From Fig. 3 a tensile strength of 490 MPa has been reported for wet welds made with experimental E6013 rutile grade electrodes with alloying additions at 50 m water depth (see F1–50 and F64–50).^{5,6} For wet welds made with similar electrodes, but with ultra-low carbon steel core rods, a tensile strength of 393 MPa was observed (see F65–50). As expected, the 100 m water depth welds showed lower tensile strengths, 372 and 345 MPa for the F64–100 and F65–100 electrodes, respectively. Porosity was shown to reduce in Fig. 2 with the ultra low carbon content steel rods; however, strength was also reduced for the same reason. Other cause of strength decrease is the increase of water depth and an increasing loss of alloying elements and increasing volume fractions of non-metallic inclusions. Strength reduction due to water depth can be overcome by replenishing the alloying elements in the flux coating of the electrode.

Fig. 4 shows a wet weld bead made with ultra-low carbon electrode on a plate. The weld exhibited good weld bead morphology with very well-defined ripples, which are evidence of constant feeding and good arc stability. Note also the absence of typical spatter present in wet welds.

Among commercial electrodes for dry applications, the E6013 rutile grade electrodes can be modified to produce acceptable wet welds with less than 2% porosity.

LOCATION OF FATIGUE CRACKS

Fatigue cracks in offshore jackets are more frequently found in tubular welded joints close to the splash zone

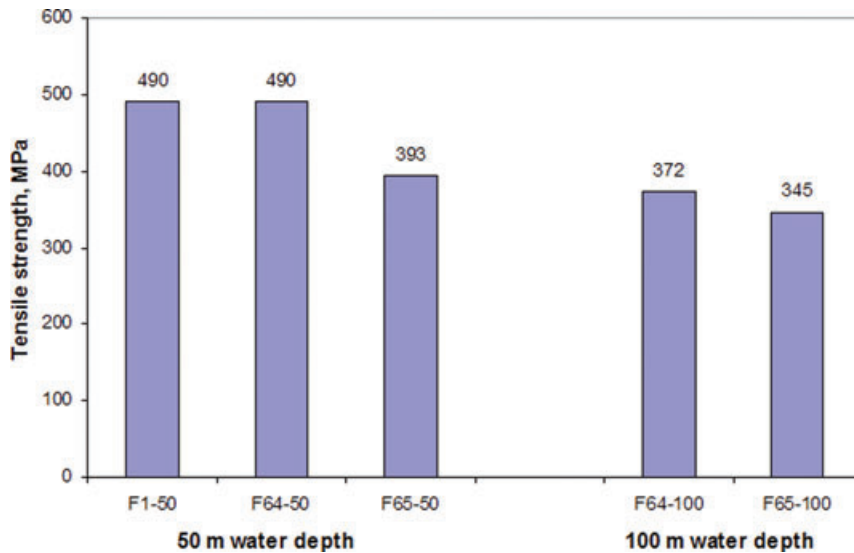


Fig. 3 Tensile strength of wet welds made at 50 and 100 m water depth using rutile base electrodes with alloying additions.



Fig. 4 Weld bead of rutile grade electrode with ultra-low carbon content in the steel rod deposited at 50 m water depth.^{5,6}

of the jacket. Other locations of high incidence of fatigue cracks are the welds that join top submerged horizontal framings that provide lateral support to well conductor pipes to the jacket in drilling platforms. In offshore floating structures, fatigue cracks can develop in the welded joints of the plate framing that provide stiffness to the caissons or hulls. A beneficial factor in both cases is the relative low water depth where these fatigue cracked joints are located which favour high quality wet welding applications.

WET WELD STRESS-STRAIN PROPERTIES

Wet weld stress-strain properties were obtained experimentally from ASTM tensile tests performed in a research project to produce wet weld electrodes^{5,6}; this study demonstrated that porosity is randomly distributed in the weld, thus a mean value of the stress-strain properties of the wet welds made with F1 rutile electrodes previously presented was used. Fig. 5 shows the mean wet weld stress-strain curve and a stress curve of ASTM A-36 structural steel; it can be observed that wet weld ultimate resistance is close to the experimentally obtained from an A-36 structural steel. A-36 steel is mainly used for tubular members of offshore jacket structures in the Gulf of Mexico, for the case of tubular joints they are usually fabricated with high strength steel; in this paper A-36

was considered because steel for tubular joints can vary depending on stress level and location of the fabrication yard; it has to be noted that location of crack initiation is not dependent on steel type or yield strength.

Young's modulus (E) is determined from the linear range of the stress-strain curves in Fig. 5. In Fig. 6, linear equations were fitted and E is obtained from the first derivative of these equations. Thus, $E_{\text{wetweld}} = 199 \text{ GPa}$ and $E_{\text{A-36}} = 228 \text{ GPa}$.

ESTIMATED FATIGUE LIFE EXTENSION BY CRACK REMOVAL AND GROOVE FILLING WITH WET WELD

Extensive analysis and experimental tests have been performed on fatigue life extension for the case of crack removal by grinding.^{1,2,11} Thus, a similar process based on fracture mechanics was proposed to analyze the effects of groove filling by means of wet weld deposition after fatigue crack removal. Fatigue life extension is estimated by comparison of the number of cycles needed to initiate and propagate a crack from as grinded condition as compared with groove wet weld filled condition. It is worth mentioning that crack initiation cannot be determined from fracture mechanics calculations, thus only crack propagation can be analyzed using fracture mechanics.

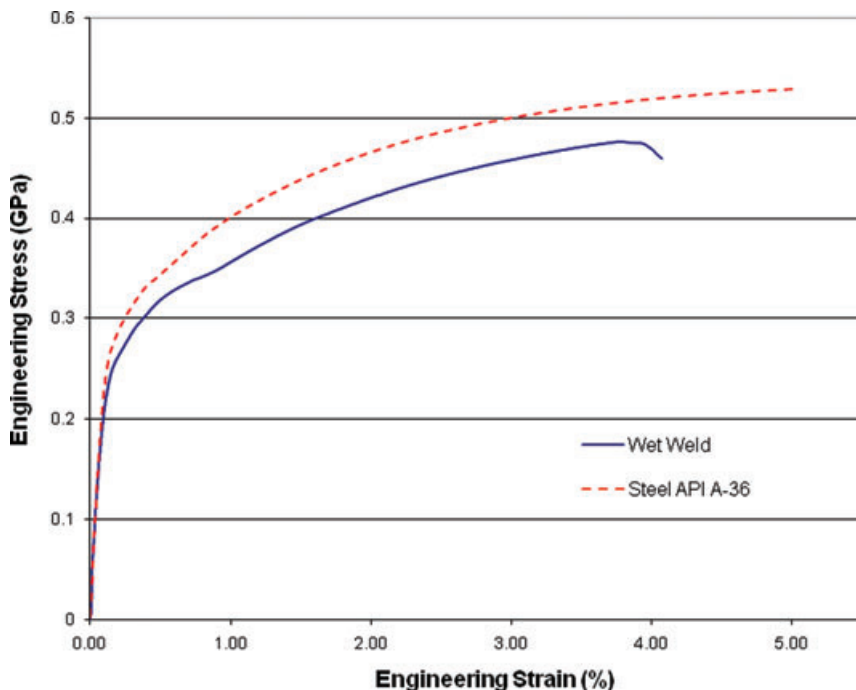


Fig. 5 Engineering stress–strain curves from tensile tests of ASTM-A36 and a wet welded specimen.

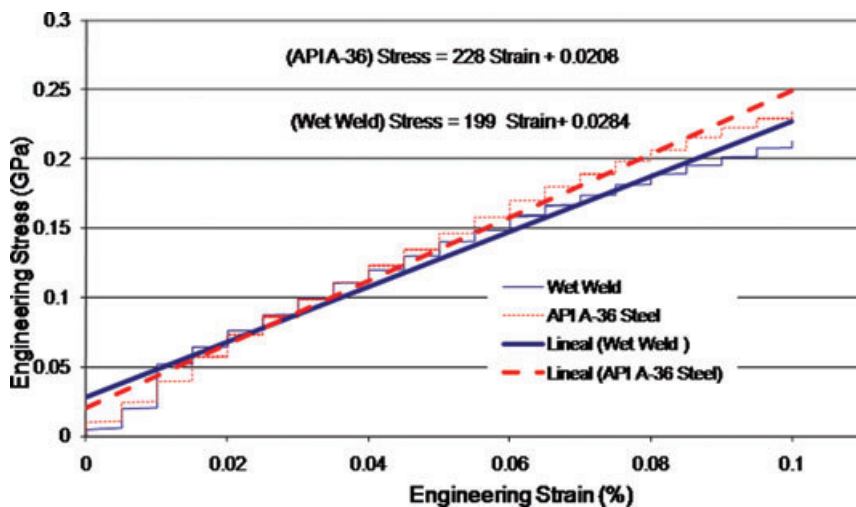


Fig. 6 Linear range of stress–strain curves.

Crack initiates at the location of highest stress, which for the as grinded condition occurs at the bottom of the groove or at both ends of the groove where the groove reaches the plate surface. Occurrence of one or the other case would depend on the groove geometry; the second case is known as short repair.² Wet weld stress–strain properties were considered for the fracture mechanics analysis where the stress distribution through the thickness is used to estimate the fatigue life.

Stress distribution was obtained from a T-butt finite element analysis where a fatigue crack was removed by

grinding and the groove was filled with wet weld. A finite element analysis of a fatigue crack repaired T-butt was produced; the model represents the case where a fatigue crack was removed by grinding a groove of radius R and the groove was filled with wet weld (see Fig. 7).

Experimentation on T-butts welded plate specimens has been used extensively to explain fatigue behaviour of more complex welded structures. Testing T-butt specimens was considered convenient because it is more economical than on full scale tubular connections. Although particular stress distributions found in tubular connections are

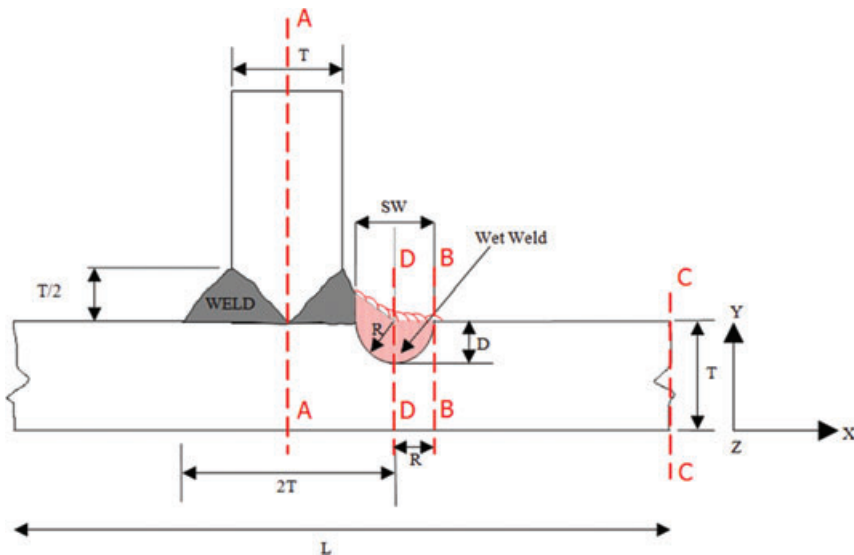


Fig. 7 T-butt model and crack repair geometry for stress analysis.

not reproduced when testing on T-butt specimens, extrapolation of the results to tubular welded connections is possible and is based on extrapolation of the Y factor determined for fatigue cracked repaired T-butt plates to tubular joints to estimate fatigue lives by fracture mechanics procedures. The extrapolation of Y from plates is a normal procedure for the determination of Y for tubular joints. In fact, the majority of the theoretical Y equations for tubular joints were developed from plates and then affected by a moment release procedure.¹² The moment release procedure is used to consider the so-called load shedding effect present during crack growth in tubular joints; this effect is not present in crack growth of plates. The load shedding effect is based on the observation that in circular sections as the crack grows through the thickness, the bending moment decreases while the membrane force remains constant. Therefore, the bending stress has to be corrected by a reduction function known as moment release, as proposed by Aaghakouchak *et al.*¹²

In Fig. 7, the shaded area at the weld toe is the groove filled with wet weld where the crack was removed. The wet weld stress properties used in the finite element model are those obtained from Figs 5 and 6. The base metal is ASTM A-36 steel. To optimize the time of analysis, model symmetry was taken into account and it was only modelled from section A-A to the right hand side; boundary conditions were implemented along section A-A where x, y and z displacements were constrained and rotations freed. Bending stress along sections B-B and D-D by application of stress along section C-C was computed using the ANSYS software package for finite element analysis. Section B-B is located at the intersection of the groove with the plate surface, and this is at a distance R from the weld toe as indicated in Fig. 7. According to Fig. 7, T-butt and

Table 1 T-butt and repair dimensions used for FEA models

Model	T (mm)	SW (mm)	L (mm)	R (mm)	D (mm)
1	20	8	400	4	4
2	20	8	400	4	8

repair dimensions considered for the finite element analysis (FEA) are given in Table 1. Repair geometry shown in Fig. 7 corresponds to model 1 dimensions according to Table 1; repair dimensions for model 2 produce a 'U' shaped groove repair with vertical walls, because D is deeper than R having its centre located below the weld toe along section D-D.

Stress concentration factors (SCF) computed from FEA of model 1 according to Table 1 are shown in Fig. 8. In this figure, SCF distributions through the thickness are calculated for the following conditions: as welded (unrepaired), grinded up to depth $D = 4$ and groove filled with wet weld (repaired) at sections D-D and B-B. The flat plate condition is included only for comparison purposes. SCF in Fig. 8 for sections D-D or B-B is the ratio of top surface stress/nominal stress, where the nominal stress considered for this study is the plate bottom surface stress at section D-D or B-B, because weld toe effect is negligible at the bottom surface of the plate; computed stresses were produced by bending loading in all cases. SCF is defined as the ratio of FEA calculated stress/FEA nominal calculated stress, where the nominal stress is a stress unaffected by any stress concentration.

It can be seen from Fig. 8 that at the weld toe, section D-D, for the depth range $0.1 < x/T < 1.0$, the as welded and grinded $D = 4$ + wet weld filled groove SCF distributions

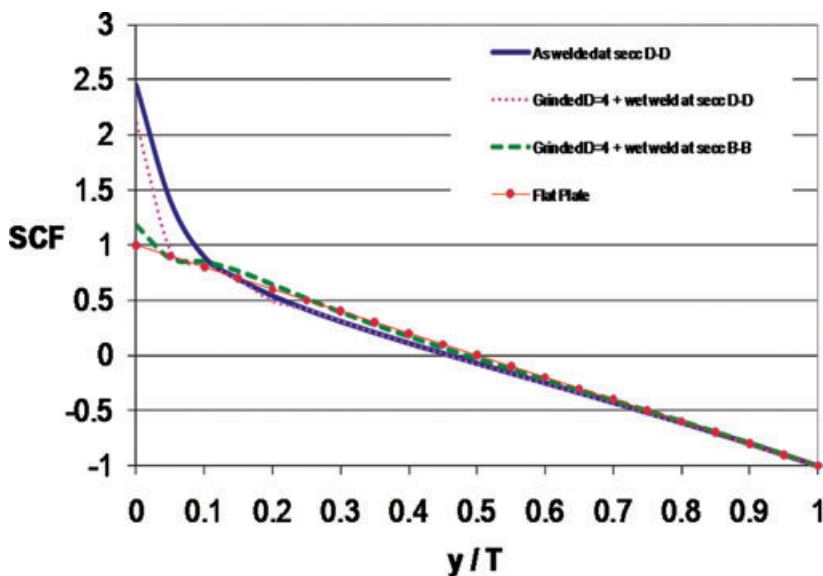


Fig. 8 SCF through the thickness for various conditions.

are the same. For depth range $0 < x/T < 0.1$ the deviation is due to the elasticity modulus difference, because weld shape and its dimensions remained identical in the FEA model for the as-welded and grinded models. This effect would increase if wet weld quality was lower than the experimentally tested. It is worth highlighting that the only difference between the as welded and the grinded $D = 4+$ wet weld groove filled models is the elasticity modulus value; $E_{\text{wet weld}} = 199 \text{ GPa}$ is 13% less than $E_{\Delta-36} = 228 \text{ GPa}$. Fig. 8 also shows that at section B-B for depth range $0.1 < x/T < 1.0$, the flat plate condition and the grinded $D = 4+$ wet weld filled groove SCF distributions are the same because weld toe effect is negligible at section B-B, $\text{SCF} = 1.2$.

It is widely known that the fatigue process has three stages: initiation, propagation and failure and fracture mechanics is only applicable for fatigue life estimation in the propagation stage. Thus, performing the fracture mechanics procedure described in Rodríguez-Sánchez *et al.* (2005)¹¹ for fatigue life estimation of the as-welded and grinded $D = 4+$ wet weld filled leads to similar results because stress distribution through the thickness for both cases is similar. Additionally, fatigue initiation which is highly dependent on surface conditions and which could make a difference between the as-welded and grinded $D = 4+$ wet weld filled cannot be estimated by fracture mechanics, thus it is worth considering experimental fatigue testing for its assessment.

The analysis of model 2 according to Table 1, T-butt as-welded and grinded $D = 8+$ wet weld showed a similar trend of SCF stress distributions through the thickness as described previously for model 1, thus SCF stress distributions for model 2 do not provide additional in-

formation for the study and are not presented in this work.

As has been mentioned previously, the repair method by filling the groove with wet weld and the as-welded condition would have a similar fatigue life during crack propagation as they have similar through-thickness stress distribution. Thus, it has been considered that to make a difference in the fatigue initiation stage, weld toe profiling can be implemented to reduce the weld toe SCF after wet welding and in addition if equipment is available, inducing compressive residual stresses to inhibit fatigue crack initiation is also an option; following sections explain these procedures.

WELD TOE PROFILING TO EXTEND THE FATIGUE INITIATION STAGE

Once wet welding has been used to fill the groove produced during crack removal, weld toe profiling has been considered in this study because the grinding tool is available as it could be also used to remove the crack (see Fig. 9).¹³ Weld toe profiling can improve fatigue life by a factor of 2 approximately by extending the crack initiation stage. Weld profiling has the purpose to produce a smooth transition between the weld and the plate or pipe repaired. This practice has demonstrated fatigue life extension of welded components, as such the American Bureau of Shipping S-N curves allow a credit of 2.2 on fatigue life when suitable toe grinding and NDE are provided. A robust review of the weld toe grinding effects on fatigue life extension is given in Rodríguez-Sánchez *et al.* (2008).¹

INDUCING RESIDUAL STRESSES BY PEENING FOR FATIGUE LIFE EXTENSION

Peening is the process of impacting a metal surface with hard objects causing plastic deformation on the surface. The impact objects can be hard small particles, a bunch of needles or even a simple hammer and the process would be known as shot peening, needle peening or hammer peening, respectively.

The mechanisms of fatigue improvement using peening are:

- Cold work
- Residual compressive stress.

The cold work process is used in the industry to improve the strength of metals by changing the metallurgical conditions of the surface resulting in an increased surface hardness and refined grain structure. With the increased hardness, the brittleness is also expected to increase; consequently there is a limit to which cold working may be applied without danger of fracture.

The residual compressive stress is probably the most important benefit of peening in terms of fatigue improvement. Residual stress is produced because the surface layer of material is deformed beyond its yield point by peening; however, it cannot deform freely as the material underneath is not affected by the peening and therefore has not been plastically deformed. So, a compressive residual stress is developed in the surface material due to the constraint imposed by the deeper layers.¹⁴

It has been found by researchers that the fatigue improvement by peening is mainly due to the residual compressive stress rather than due to the cold work hardening process. Occasional high tensile loads, such as many components experience in service, reduce the beneficial effects

of peening because plastic deformation resulted at points of high stress concentration when the loading is applied.

A residual compressive stress reduces the effective range of fatigue stress, reduces crack growth and can even stop cracks from growing completely. However, there are still difficulties in making quantitative predictions of the effect on fatigue life as a result of a particular peening process. Fracture Mechanics procedures have not been easily applied for peened components; moreover, peening has a greater effect on the crack initiation phase where fracture mechanics cannot be applied. Peening leaves a surface far from being smooth which may cause crack starting points.

The following rules of thumb are recommended for the application of shot peening but the concept can be extended for other methods of peening. If the component under consideration is achieving a reversed bending endurance limit close to 0.5 of the tensile strength in steels or 0.25 in other alloys, further improvement by peening is unlikely. The maximum residual compressive stress induced by shot peening is approximately 60% of the ultimate tensile strength in compression; this ratio is common to all metallic materials.¹⁴

The general conclusion on the behaviour of cracks growing from a peened surface in fatigue is that surface effects, which may be regarded as minute cracks, already exist in the surface but that their initial growth rate is considerably slower than that of cracks which are eventually initiated in an as-welded (unpeened) surface.

EXPERIMENTAL FINDINGS ON THE INDUCTION OF RESIDUAL STRESSES

Although, underwater shot peening for the improvement of fatigue crack resistance has not been used in practice, it was considered convenient to include it in this study because other applications of shot blasting such as marine growth removal are currently in use in underwater

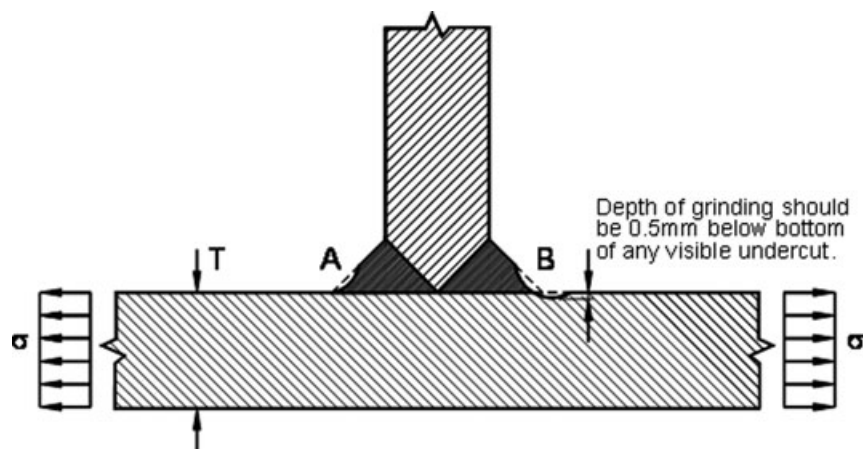


Fig. 9 Weld toe profiling to improve fatigue life.¹³

conditions. Hence, adjustments to currently used techniques based on shot blasting suggest that shot peening in underwater conditions might be possible. Hammer and needle peening have been used in underwater conditions proving its effectiveness inducing residual stresses; however its application into narrow grooves as in geometries presented in Table 1 appear complicated. It was decided to test shot peening in this work because it is a technique widely used in air conditions for residual stress induction and has the feasibility that the shots can reach the bottom of the groove for the geometries presented in this work.

Two T-butt welded specimens as in Fig. 7 having both an edge repair D4R2 (repair of constant section all across the specimen width) machined in as-welded condition were fatigue tested. Specimen UPD4R2 was tested after machining the edge repair and no subsequent treatment was applied. Specimen LPD4R2 was shot peened after the edge repair was machined. The purpose for testing these two identical shaped specimens was to determine the benefit of compressive residual stresses induced by shot peening on the fatigue life of repaired specimens. Both specimens were tested until failure and multiple cracking and coalescence was observed in the bottom of the edge repair.

With the application of equipment such as the Alternate Current Potential Drop (ACPD) which is able to provide crack growth measurements, the crack growth rate per cycle (da/dN) can be determined experimentally and knowing the fatigue constants of the material (C and m), it is possible to determine the stress intensity factor from Paris law expressed in Eq. (1).¹⁵

$$\Delta K = \left(\frac{1}{C} \frac{da}{dN} \right)^{\frac{1}{m}}. \quad (1)$$

On the other hand, the stress intensity factor range ΔK in repaired welded joints can be described by Eq. (2).

$$\Delta K = Y \Delta \sigma \sqrt{\pi a}. \quad (2)$$

Equation (2) is a general expression that can be applied to any crack geometry and loading mode by considering the corresponding Y factor. From observation of Eqs (1) and (2), the Y factor value has a direct effect in the stress intensity factor and this one in the crack growth rate. Y factor for the case of the crack geometries present in welded joints varies as a function of parameters such as plate width, crack geometry, stress field, geometrical discontinuities and structural restraints.

For the calculation of the fatigue life of an offshore crack repaired welded joint by crack removal, the Y factor should include the particular characteristics of the crack growing in the repaired notch and propagating through the thickness of the welded member under the membrane

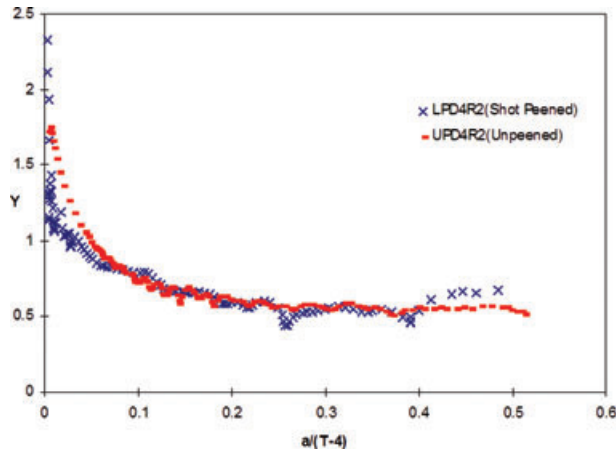


Fig. 10 Experimental Y factors for edge crack repaired specimens in unpeened and peened conditions.

and bending stresses produced by the wave loading on the structure.

Fig. 10 shows experimental Y factors for the edge repaired specimens UPD4R2 and LPD4R2 in unpeened and peened conditions, respectively; it can be observed that the unpeened curve is smoother than that for the peened specimen in the range $0 < a/(T-4) < 0.08$; this may be explained by a multiple crack initiation effect, possibly caused by the mildly rough surface left by the shot particles. Another observation from the same figure is obtained considering the point where the two curves intersect which is at $a/(T-4) = 0.08$ being $T = 30$ mm for these specimens; at this point the crack is 2 mm deep; this coincides with the approximate thickness of the residual stress compressive layer. This could be indicating the sensitivity of ACPD to residual stress.

Fig. 10 compares the experimentally determined Y factors for an unpeened and lightly peened specimens and shows in general a lower value of Y for the peened specimen in the range $0 < a/(T-4) < 0.08$. This finding could mean that peening reduced the crack growth rate in this region. However, because the Y values are only slightly lower for the peened specimen, it has to be considered that other factors such as the crack aspect ratio or the accuracy of the measurement technique may have been involved that affected the Y values. It is, for example, possible that the presence of residual stress and its relaxation as the crack grows could have had an influence on the ACPD readings. Therefore, it is not possible to draw a firm conclusion from the experimental data obtained from only two specimens.

GENERAL GUIDELINES TO IMPLEMENT THE REPAIR PROCEDURE

The proposed fatigue crack repair procedure initiates removing the crack by grinding it out. To decrease the

contribution of crack propagation, this work also proposed filling the grinded groove with wet weld.

Grinding can be performed either by burr grinding or by disc cutting. The use of disc grinding is discouraged because grinding marks could become crack initiators. However, fatigue initiation for the proposed procedure does not rely on the surface finish left after grinding out the crack, because wet welding erases the grinding marks.

Wet welding can be performed by using E6013 rutile grade electrodes with alloying additions. These electrodes can produce acceptable wet welds for the conditions where cracks typically occur in fixed and floating offshore structures for the oil industry. These locations are in shallow waters or nearby the splash zone, respectively.

To delay fatigue initiation, it has been proposed in this work to perform weld toe profiling to produce a smooth transition from the wet weld to the plate. This practice does not increase the repair complexity because the same grinding tool used for crack removal can be used for weld toe profiling after wet welding. Attention should be paid to the force control on the grinding tool to avoid burr or disc skipping on the plate surface.

Finally, as it was experimentally tested and results presented in this work, induction of compressive residual stresses on the repaired surface can improve the resistance against fatigue initiation; this practice should be recommended as optional because its benefits could be erased by an overloading which for the case of offshore structures is highly possible under storm conditions.

CONCLUSIONS

A crack repair procedure based on crack removal by grinding, subsequent filling of the produced groove with wet welding and weld toe profiling with an optional induction of compressive residual stresses on the surface has been proposed to reinstate as-welded fatigue life.

Wet welding technology has improved considerably in recent years. Techniques required for performing the proposed crack repair procedure are of common use in the offshore oil industry, thus the proposed procedure which combines grinding, wet welding and shot peening is feasible for industrial application.

The proposed procedure can reinstate the original fatigue life of a crack repaired joint regardless of crack depth before repair. Fatigue initiation for the proposed procedure does not rely on the surface finish left after grinding out the crack, because wet welding erases the grinding marks. Use of weld toe profiling after wet welding is recommended. An extensive testing program should be performed before the proposed procedure is industrially used, the collected data would support its effectiveness.

It is a common practice to determine Y factor data from T-butt specimens and extrapolate it to tubular joints by

incorporating the load shedding effect. Thus, conclusions presented in this work can be applicable to offshore platforms.

Effectiveness of the proposed procedure does not rely on a complete removal of the crack as in the case of crack repair by grinding removal leaving an empty groove. An effective option to assure that crack propagation is halted, even if the crack is not totally removed due to crack detection capabilities of the inspection equipment, is by fusing the crack tip when melting the bottom of the groove during wet weld deposition.

REFERENCES

- 1 Rodríguez-Sánchez, J. E., Rodríguez-Castellanos, A., Carabajal-Romero, M. and Ayala-Uraga, E. (2009). Controlled weld toe profiles for fatigue life extension of T-Butt joints: an application to FSOs & FPSOs. *Int. J. Offshore Mech. Arctic Eng.* **131**, 1–8.
- 2 Rodriguez-Sánchez, J. E., Dover, W. D. and Brennan F. P. (2004). Application of short repairs for fatigue life extension. *Int. J. Fatigue* **26**, 413–420.
- 3 Suga, Y. and Hasui, A. (1986). On formation of porosity in underwater weld metal. *Int. Inst. Weld.* **IX**, 1388–1386.
- 4 Liu S. and Rowe M (2002). Progress in underwater wet welding, The Quintessential SMA Consumables. *ASM International Conference on Trends on Welding Research, Pine Mountain, Georgia*.
- 5 Perez Guerrero, F (2007). The mechanism of porosity formation in underwater steel welds using SMAW process. Ph.D. Thesis, Colorado School of Mines.
- 6 Liu, S. and Perez, F (2007). *Phase III Joint Research Program between MMS and IMP Underwater Wet Welding for Offshore Structures and Pipelines in the Gulf of Mexico: Enhanced Reliability and Integrity of Underwater Wet Welds*. Final report.
- 7 Liu, S. and Perez, F. (2004). *Joint Research Program between MMS and IMP Underwater Wet Welding for Offshore Structures and Pipelines in the Gulf of Mexico: Process Maturation and Technology Transfer*. Final report.
- 8 Matlock, D. K., Edwards, G. R., Olson, D. L. and Ibarra, J (1983). An evaluation of the fatigue behavior in surface, habitat, and underwater wet welds. *International Institute of Welding Conference, Trondheim, Norway*. 303–310.
- 9 Ibarra, S., Liu S. and Olson, D. L (1995). Underwater wet welding of steel. *Weld. Res. Coun. Bull.* **401**, 1–39.
- 10 Perez-Guerrero, F. and Liu, S (2007). Explaining porosity formation in underwater wet welds. *26th International Conference on Offshore Mechanics and Arctic Engineering, American Society of Mechanical Engineers*.
- 11 Rodríguez-Sánchez, J. E., Dover, W. D., Brennan, F. P. and Rodríguez-Castellanos, A. (2005). Fracture mechanics analysis of fatigue crack repaired joints. *Int. J. Offshore Mech. Arctic Eng.* **127**, 182–189.
- 12 Aaghakouchack, A.A., Glinka, G. and Dharmavasan, S. (1989). A load shedding model for fracture mechanics analysis of fatigue cracks in tubular joints. *OMAE 89 Conference*.
- 13 NORSO standard N-004 Rev. 2, October 2004.
- 14 Marsh, K. J. (1993). *Shot Peening: Techniques and Applications*. Engineering Materials Advisory Services Ltd.
- 15 Paris, P. C. and Erdogan, F. (1963). A critical analysis of crack propagation laws. *Trans. ASME, J. Basic Eng.* **85**, 528.

REHABILITATION AND REPAIR OF WELDED ELEMENTS AND STRUCTURES BY ULTRASONIC PEENING



Y.
Kudryavtsev^{1a}



J.
Kleiman¹



A.
Lugovskoy²



L.
Lobanov³



V.
Knysh³



O.
Voitenko³



G.
Prokopenko⁴

¹ Integrity Testing Laboratory Inc. (Canada)

² Atoll (Ukraine)

³ Paton Welding Institute (Ukraine)

⁴ Institute of Metal Physics (Ukraine)

E-mail: ^a ykudryavtsev@itlinc.com

ABSTRACT

The Ultrasonic Peening (UP) is the most efficient technique for increasing the fatigue life of welded elements as compared to such existing improvement treatments as grinding, TIG-dressing, shot peening, hammer peening, etc. The results of experimental investigation of the efficiency of UP for rehabilitation and repair of welded elements and structures with the goal of preventing the origination and propagation of fatigue cracks are considered in this document. UP treatment was applied to large-scale welded specimens in as-welded condition, after 50 % of expected fatigue life and after repair of fatigue cracks. Also, different techniques for restraining and repair of fatigue cracks were analyzed and compared: overloading; drilling of the crack tips; drilling of the crack tips with installation of high strength bolts; local explosive treatment; local heat treatment; welding with and without UP of weld toe zones. As an example, the practical application of UP for rehabilitation and repair of welded elements of highway and railway bridges are also discussed.

IIW-Thesaurus keywords: Bridges; Combined processes; Fatigue life; Fatigue tests; Peening; Reference lists; Repair; Railways; Roads; Structures; Ultrasonic processing; Welded joints; Work hardening.

1 INTRODUCTION

Ultrasonic Peening (UP) is a leading technology in the application of High Power Ultrasound (HPU) for fatigue life improvement of welded components and structures [1-4]. The UP technology is based on more than 30 years of extensive research and development by an international group of experts in the use of HPU for industrial applications. One of the first publications on this topic can be attributed to Prof. G. Prokopenko and his colleagues as early as 1974 [5]. During the different stages of its development, the UP process was also known as ultrasonic treatment (UT) [5-7], ultrasonic impact technique/technology/treatment (UIT) [8-10] or ultrasonic impact peening (UIP) [11-12]. A brief histori-

cal review of UP development is provided in IIW Document XIII-2010-04 [1].

The most recent design of the UP equipment is based on "Power on Demand" concept. Using this concept, the power and other operating parameters of the UP equipment are adjusted to produce the necessary changes in residual stresses, stress concentration and mechanical properties of the surface layers of materials to attain the maximum possible increase in fatigue life of welded structures. The basic UP system is suitable for most fatigue improvement applications with the power consumption of 300-500 watts. More powerful UP systems can be designed and produced for special applications. Basic UP systems for manual and robotic applications are shown on Figure 1.

The degree of fatigue strength improvement due to post-weld treatment depends on the mechanical properties of the base material, the geometry of the welded joint, the parameters of cyclic loading and other factors. This is

Doc. IIW-1806-07 (ex-doc. XIII-2076-05) recommended for publication by Commission XIII "Fatigue of welded components and structures".



Figure 1 – Basic UP systems for manual (left) and robotic (right) applications

particularly the case when UP treatment is applied. In order to improve the effectiveness of the UP treatment with respect to minimum time-, labour- and power-consumption a software package for "Optimum Application of Ultrasonic Peening" has been developed. This software tool is based on an original predictive model that considers the above mentioned variables [1].

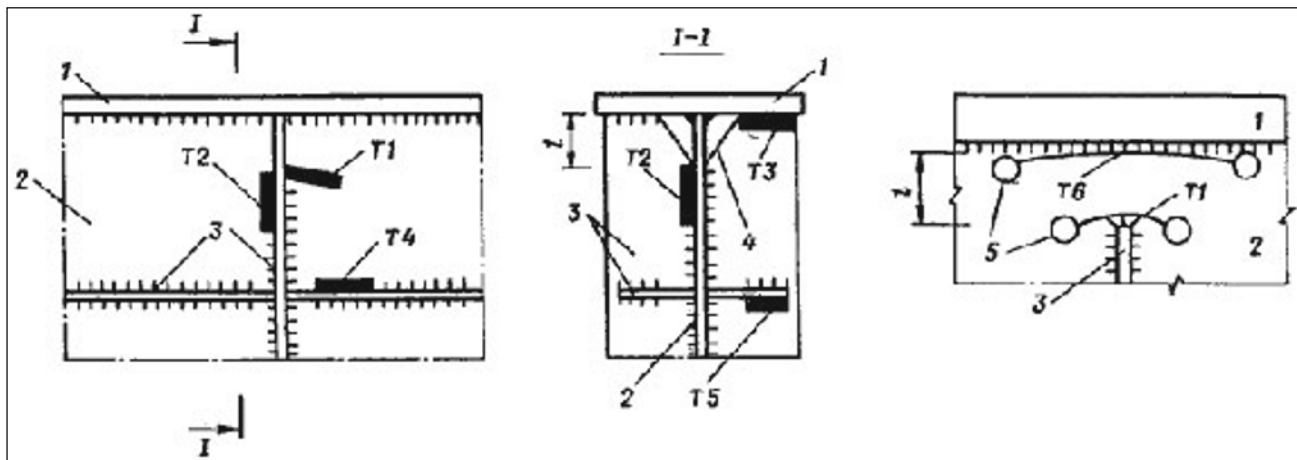
The UP technology has been applied successfully for the fatigue life improvement of different machine parts and welded structures in a number of different industries including: Railway and Highway Bridges, Shipbuilding, Construction Equipment, Mining, Automotive and Aerospace.

The current paper reports the results of an experimental investigation of the efficiency of UP for the rehabilitation and repair of welded elements and structures with the goal of preventing the initiation and propagation of fatigue cracks. The UP treatment was applied to large-scale welded specimens in the as-welded condition, after 50 % of expected fatigue life and after the repair of

fatigue cracks. Also, the efficiency of using the UP treatment in repair of fatigue cracks was assessed in comparison with other techniques. The following techniques for retarding the growth of fatigue cracks were considered; overloading; hole drilling of the crack tips; hole drilling of the crack tips combined with the installation of high strength bolts; local explosive treatment; local heat treatment; welding without and with UP treatment of weld toe zones. As an example, the practical applications of UP for rehabilitation and repair of welded elements of highway and railway bridges are also considered in this document.

2 APPLICATION OF UP FOR REHABILITATION OF WELDED ELEMENTS AND STRUCTURES

One example of the effective application of UP is the fatigue life improvement of welded joints of highway and railway bridges. Published reports and direct observations of welded bridges have shown that the typical zones of fatigue crack initiation are the ends of vertical welded stiffeners [8], i.e., crack types T1 and T2 in Figure 2. The effectiveness of applying UP for the prevention of fatigue crack initiation and retarding propagation in such locations was studied experimentally using fatigue testing of large-scale welded samples, see Figure 3. Fatigue testing showed that UP could prevent the initiation of fatigue cracks for these types of welded details for the studied cyclic loading conditions. It was shown that UP treatment of the weld toe over a length of about 100 mm from the end zones of the welded stiffeners could produce a significant increase of the fatigue strength of this welded detail and could eliminate the initiation of fatigue cracks. Figure 3 shows the zone of crack initiation in un-treated test specimens and the UP treated areas for improved test specimens. The UP treatment of weld toe produced an easily visible groove [8, 9].



a) Railway bridge

b) Railway bridge

c) Highway bridge

T1-T6 - Zones of fatigue crack initiation

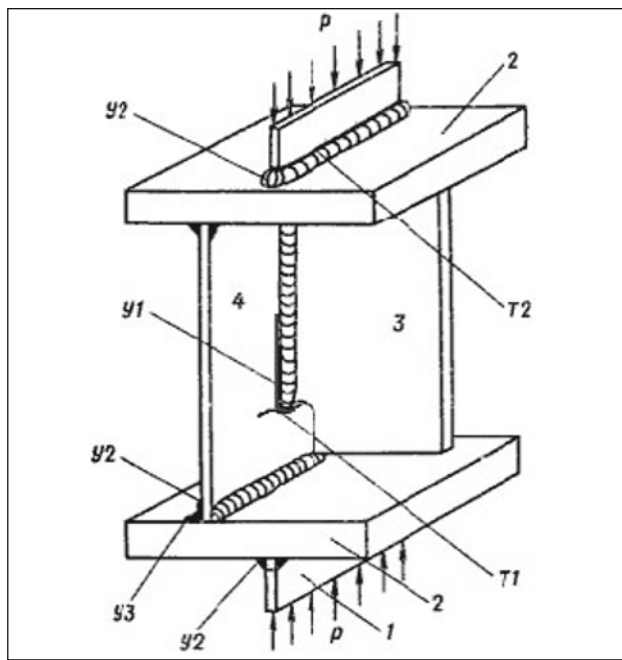
1, 2, and 3 - Upper flange, web and stiffeners of the bridge span

4 - Openings in the stiffener

5 - Holes produced to prevent the propagation of fatigue cracks

1 - Zone of local bending of the web [8]

Figure 2 – Schematic presentation of the location of fatigue cracks in welded elements of bridges



T1 - Zone of fatigue cracks initiation

Y1 - Zone of UP treatment

3 - Welded stiffener

4 - Web

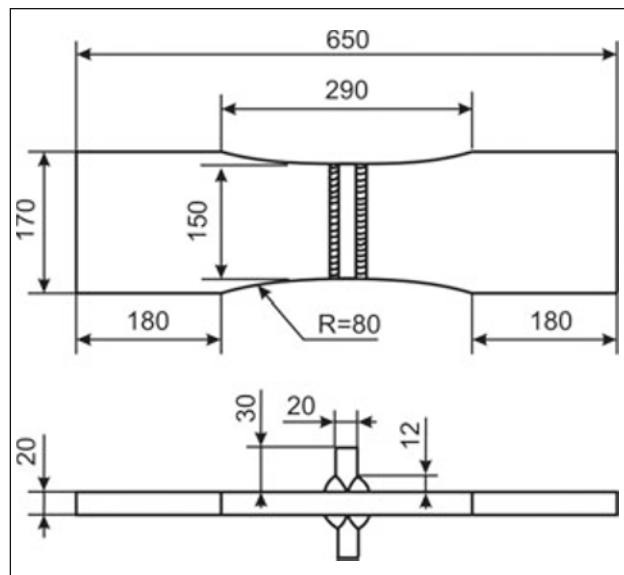
Figure 3 – Drawing of welded sample imitating the attachment of the vertical stiffener to the web for fatigue testing in as-welded condition and after UP [8]

Effectiveness of UP applied after 50 % of expected fatigue life of welded elements

Virtually all previous test programs using UP were intended to demonstrate the efficiency of the technology for new welded constructions. Previous tests illustrated that UP could be effectively applied for the prevention of fatigue crack initiation in new welded bridges. However, there was also a need to investigate the effectiveness of the method for bridges already in service. The goal was to examine the effectiveness of UP when applied to bridge details already exposed to cyclic loading conditions corresponding to several years in service. This section describes fatigue testing of welded details when UP treatment was applied after 50 % of the expected fatigue life of welded elements in the as-welded condition.

Three series of large-scale welded samples were subjected to fatigue testing to evaluate the effectiveness of UP application to the existing welded structures:

1. in as welded condition,
2. UP was applied before fatigue testing,
3. UP was applied after fatigue loading with the number of cycles corresponding to 50 % of the expected fatigue life of samples in as-welded condition.



(Dimensions in mm)

Figure 4 – General view of welded sample for fatigue testing

The general view of welded sample for fatigue testing is shown on Figure 4.

Mechanical properties and chemical composition of base material are presented in Tables 1 and 2.

All welded samples were tested at stress ratio $R = 0$ ($\Delta\sigma = \sigma_{max}$). The results of the fatigue testing are presented in Figure 5.

As can be seen from Figure 5, the UP produced a significant increase in the fatigue strength of the welded joints for both series of UP treated samples. The increase in the mean fatigue strength (at $N = 2 \cdot 10^6$ cycles) of the welded samples was 49 % (from 119 MPa to 177 MPa) for UP treated samples before fatigue loading and was 66 % (from 119 MPa to 197 MPa) for samples treated with UP after fatigue loading corresponding to 50 % of the expected fatigue life of the samples in as-welded condition. The resulting increase in fatigue life due to UP treatment was a factor of 5-10 times depending on the level of applied loading. With reference to Figure 5, the higher increase of fatigue life of UP treated welded elements for fatigue curve #3 could be explained by a more beneficial redistribution of residual stresses and/or "healing" of fatigue damaged material by UP in comparison with the fatigue curve #2. Additional research work is now in progress to explain this and similar results.

Table 1 – Mechanical properties of base material

σ_y MPa	σ_u MPa	δ %	ψ %
260	465	37.6	63

Table 2 – Data on chemical composition of base material

%							
C	Si	Mn	S	P	Cr	Ni	Cu
0.210	0.205	0.52	0.019	0.007	0.04	0.04	< 0.01

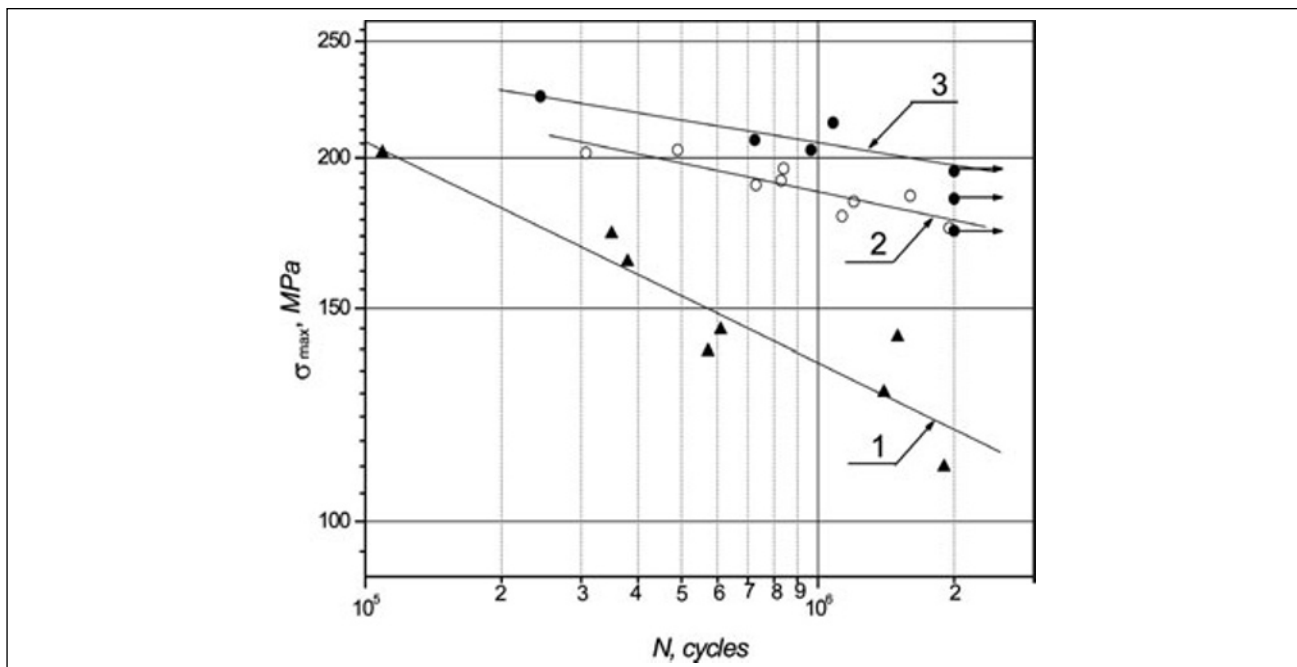


Figure 5 – Fatigue curves of welded samples (transverse non-load-carrying attachment):

1 – in as welded condition, 2 – UP was applied before fatigue testing,

3 – UP was applied after fatigue loading with the number of cycles corresponding to 50 % of expected fatigue life of samples in as-welded condition

In cases where experimental data is lacking for specific materials, loading conditions or joints improved by UP, the improvement factors described in IIW recommendations on fatigue life improvement of welded elements for different peening techniques [13, 14] can be applied to estimate the expected increase of fatigue strength of welded elements by UP. This benefit factor is 1.3 for steels with the yield strength less than 355 MPa, and 1.6 – for steels with the yield strength of more than 355 MPa. The benefit factor for aluminium alloys is 1.6. This factor could be applied to increase the limit stress range (at 2·10⁶ cycles) of UP treated welded element. A benefit factor of, for instance 1.3, corresponds to a 2.2 times increase in fatigue life of the welded element [13, 14].

3 APPLICATION OF UP FOR REPAIR OF FATIGUE CRACKS IN WELDED ELEMENTS AND STRUCTURES

In the previous section it was shown that UP treatment is an effective way for rehabilitation of welded structures. Throughout this document, rehabilitation is defined as the prevention of possible fatigue crack initiation in existing welded structures that are in service. The UP could also be effectively used during the repair of fatigue cracks.

The results of experimental investigation of the efficiency of traditional and advanced techniques for fatigue life improvement of structural elements with fatigue cracks are considered in this chapter. Large-scale specimens containing fatigue cracks were subjected to further

fatigue testing after a number of fatigue crack restraining and repair techniques were applied. These techniques included: overloading, drilling of the crack tips, drilling of the crack tips combined with the installation of high strength bolts, local explosive treatment, local heat treatment, repair welding with and without UP of weld toe zones.

A number of large scale specimens, see Figure 6, with observable fatigue cracks were subjected to further fatigue loading both without any repair and using one of the previously mentioned repair procedures. In all cases the cyclic loading was zero-to-tension ($R = 0$) with the maximum stress of 155 MPa. The fatigue testing of large scale specimens showed that the repair of fatigue crack by welding with the subsequent UP treatment provided longest fatigue life in comparison with other ways to prolong the service life of structural elements with fatigue cracks. The results of fatigue testing of specimens with cracks subjected to the above-mentioned improvement techniques are summarized in Figure 7. This figure shows the number of fatigue cycles to complete separation of the test pieces following the repair procedure.

A predictive model and software for fatigue assessment of welded elements with cracks in the as-welded condition and after the application of common improvement techniques based on the introduction of beneficial compressive residual stresses in the zone of crack tip have been developed and experimentally verified [15]. In some specimens and real welded structures the residual stresses were measured by non-destructive ultrasonic method [16, 17]. This information was further used to compute of the effect of compressive residual stresses on fatigue crack propagation.

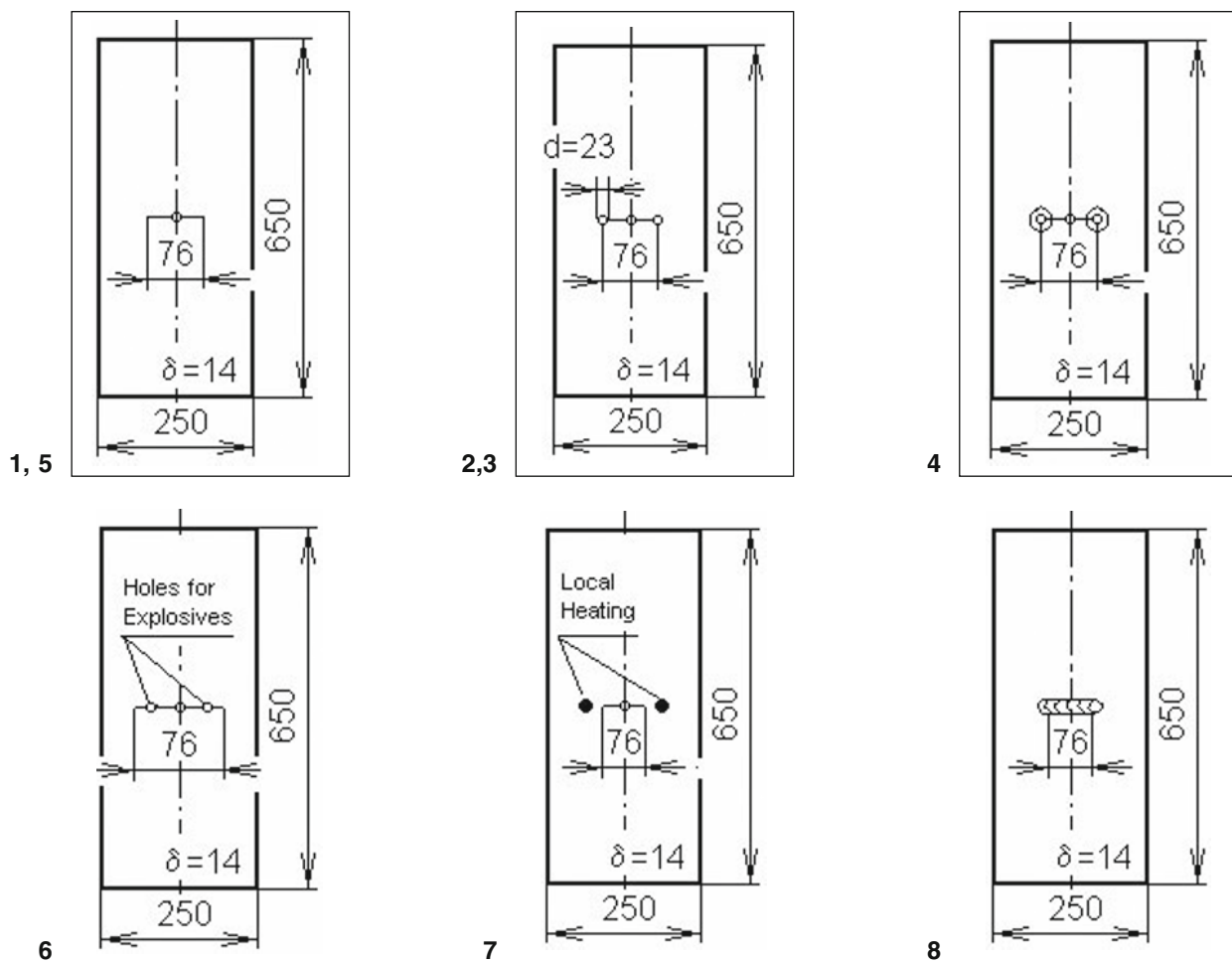
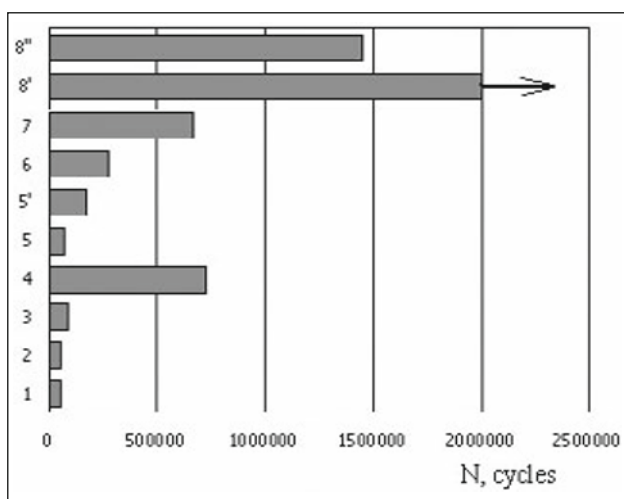


Figure 6 – Drawings of specimens with fatigue cracks for further fatigue testing at the following conditions: 1 - initial condition (no repair), 2, 3 - drilling of the crack tips with and without cold working, 4 - drilling of the crack tips combined with installation of high strength bolts, 5 - overloading, 6 - local explosive treatment, 7 - local heat treatment, 8 - welding with and without UP of weld toe zones



1 - Initial condition, 2 and 3 - Drilling of the crack tips with and without cold working, 4 - Drilling of the crack tips with installation of high strength bolts, 5 - Overloading (yield strength), 5' - Overloading (0.7 yield strength), 6 - Local explosive treatment, 7 - Local heat treatment, 8'' - Repair by welding without UP, 8' - Repair by welding with UP treatment of the weld toe zones, 8 - Repair by welding with UP treatment of the weld toe zones

Figure 7 – Comparison of the efficiency of different techniques of restraining and repair of fatigue cracks

4 EXAMPLES OF PRACTICAL APPLICATION OF UP FOR REHABILITATION AND REPAIR OF WELDED STRUCTURES

4.1 Rehabilitation: prevention of fatigue crack initiation

Based on the fatigue data and the solution described in Chapter 2, UP was applied during the rehabilitation of welded elements of a highway bridge over the Ohio River in the USA, see Figures 8 and 9. The bridge was constructed about 30 years ago. The welded details of the bridge did not have macroscopic fatigue cracks. The motivation for application of the UP for fatigue life improvement of this bridge was the fatigue cracking in welded elements of another bridge of approximately the same age and design. The stages of preparation for UP treatment of the bridge and the process of UP treatment of one of the welded vertical stiffeners are shown on Figures 8 and 9. More than two thousand welded details of the bridge structure that were considered to be fatigue critical were UP treated. The total length weld toe treated using UP treated was about 500 meters.



**Figure 8 – Ultrasonic Peening of a welded bridge:
Preparation for UP treatment
(Two UP Systems/Lifts)**



**Figure 9 – Ultrasonic Peening of a welded bridge:
UP of the end of one of welded vertical stiffeners**

4.2 Repair of fatigue crack

During the regular inspection of the railway bridge over Dnepr River in Ukraine, a fatigue crack was found in one of the welds of the bridge span. The fatigue crack was located in the weld connecting the upper flange and the web. The length of the crack was about 1 meter. The location of fatigue crack in welded element of bridge span is shown on Figure 10.

The fatigue crack was repaired using standard welding procedures. To prevent possible recurrence of fatigue cracks at the same location, the repaired zone was UP treated. The process of UP treatment of repaired zone in welded element of bridge span is shown on Figures 10 and 11.

5 CONCLUSIONS

The effectiveness of Ultrasonic Peening for repair and rehabilitation of fatigue loaded welded structures had been studied using large-scale laboratory specimens and has been applied to in-service bridge structures. The following conclusions can be made.

1. Ultrasonic Peening is a relatively new and promising technique for fatigue life improvement that could be effi-

ciently used for rehabilitation and repair of welded elements and structures.

2. The application of Ultrasonic Peening for treatment of welded elements of existing structures provides, practically, the same increase in fatigue life of welded elements that could be achieved by treatment after/during construction.
3. The results of fatigue testing of large-scale specimens showed that the welding and subsequent application of Ultrasonic Peening provides the highest endurance of specimens with fatigue cracks as compared with other considered techniques for fatigue life improvement.
4. The modern equipment for Ultrasonic Peening could be efficiently applied for rehabilitation and repair of welded elements of highway and railway bridges and other areas.

REFERENCES

- [1] Kudryavtsev Y., Kleiman J., Lobanov L., Knysh V., Prokopenko G.: Fatigue life improvement of welded elements by Ultrasonic Peening, International Institute of Welding, IIW Document XIII-2010-04, 2004, 20 p.



Figure 10 – Photo showing the location of fatigue crack in welded element of bridge span and application of UP during the repair of crack



Figure 11 – Enlarged view of the zone of repair (welding + UP treatment) of fatigue crack in welded element of bridge span

- [2] Kudryavtsev Y., Kleiman J., Prokopenko G., *et al.*: Effect of Ultrasonic Peening on microhardness and residual stress in materials and welded elements, X International Congress and Exposition on Experimental and Applied Mechanics, Costa Mesa, California USA, June 7-10 2004, (on CD).
- [3] Kudryavtsev Y., Kleiman J., Prokopenko G., *et al.*: Computerized complex for Ultrasonic Peening of parts and welded elements, 32nd Annual Ultrasonic Industry Association Symposium, New York, NY, USA, October 21-23 2002 (on CD).
- [4] Kudryavtsev Y., Kleiman J., Prokopenko G., *et al.*: Mechanism and efficiency of Ultrasonic Peening in fatigue improvement, SEM Annual Conference & Exposition on Experimental and Applied Mechanics, Milwaukee, Wisconsin, USA, June 10-12 2002, (on CD).
- [5] Polozky I., Nedoseka A., Prokopenko G., *et al.*: Relieving of welding residual stresses by ultrasonic treatment, Paton Welding Journal, 1974, No. 5., pp. 74-75 (in Russian).
- [6] Krivko V., Prokopenko G.: Ultrasonic treatment of welded joints, Welding Production, 1979, No. 5, pp. 32-33 (in Russian).
- [7] Mikheev P., Nedoseka A., Parkhomenko A., *et al.*: Efficiency of ultrasonic treatment application for increase of fatigue strength of welded joints, Paton Welding Journal, 1984, No. 3, pp. 4-7.
- [8] Kudryavtsev Y., Korshun V., Kuzmenko A.: Improvement of fatigue life of welded joints by the ultrasonic impact treatment, Paton Welding Journal, 1989, No. 7. pp. 24-28.
- [9] Kudryavtsev Y., Mikheev P., Korshun V.: Influence of plastic deformation and residual stresses, created by ultrasonic impact treatment, on the fatigue strength of welded joints, Paton Welding Journal, 1995, No. 12, pp. 3-7.
- [10] Trufiakov V., Mikheev P., Kudryavtsev Y., Statnikov E.: Ultrasonic impact treatment of welded joints, International Institute of Welding, IIW Document XIII-1609-95, 1995.
- [11] Trufyakov V., Mikheev P., Kudryavtsev Y., Reznik D.: Ultrasonic impact peening treatment of welds and its effect on fatigue resistance in air and seawater, Proceedings of the Offshore Technology Conference, OTC 7280, 1993, pp. 183-193.
- [12] Trufyakov V., Mikheev P., Kudryavtsev Y., Reznik D.: Fatigue endurance of welded joints, Residual stresses and fatigue improvement treatments, Ship Structure Symposium "93", Arlington, Virginia, USA, November 16-17 1993, pp. N1-N14.
- [13] Haagensen P., Maddox S.: IIW Recommendations on post weld improvement of steel and aluminium structures, International Institute of Welding, IIW Doc. XIII-1815-00, 2000.
- [14] Hobbacher A.: Recommendations for fatigue design of welded joints and components, International Institute of Welding, IIW Doc. XIII-1965-03/XV-1127-03, 2003.
- [15] Kudryavtsev Y., Kleiman J., Knysh V., Mikheev P.: Fatigue life improvement of structural elements with fatigue cracks, SEM Annual Conference & Exposition on Experimental and Applied Mechanics, Milwaukee, Wisconsin, USA, June 10-12 2002 (on CD).
- [16] Kudryavtsev Y., Kleiman J., Gushcha O.: Ultrasonic measurement of residual stresses in welded railway bridge, Structural Materials Technology: An NDT Conference, Atlantic City, NJ, February 28-March 3 2000, pp. 213-218.
- [17] Kudryavtsev Y., Kleiman J., Gushcha O., *et al.*: Ultrasonic technique and device for residual stress measurement, SEM International Congress and Exposition on Experimental and Applied Mechanics, Costa Mesa, California, USA, June 7-10 2004 (on CD).



Short communication

Repairing large cracks and reversing fatigue damage in structural metals

Charles R. Fisher^a, Hunter B. Henderson^b, Michael S. Kesler^b, Pingping Zhu^c, Glenn E. Bean^d, M. Clara Wright^e, John A. Newman^f, L. Catherine Brinson^g, Oscar Figueroa III^h, Michele V. Manuel^{i,*}

^a Naval Surface Warfare Center – Carderock Division, 9500 MacArthur Blvd, West Bethesda, MD 20817, USA

^b Oak Ridge National Laboratory, 1 Bethel Valley Rd, Oak Ridge, TN 37830, USA

^c Fiat-Chrysler Automobiles, 800 Chrysler Dr, Auburn Hills, MI 48326, USA

^d The Aerospace Corporation, 2310 E. El Segundo Blvd, El Segundo, CA 90245, USA

^e NASA – John F. Kennedy Space Center, Kennedy Space Center, FL 32899, USA

^f NASA – Langley Research Center, 1 NASA Dr, Hampton, VA 23666, USA

^g Northwestern University, 2145 Sheridan Road, Tech A214, Evanston, IL 60208, USA

^h University of Florida, 100 Rhines Hall, PO Box 116400, Gainesville, FL 32611, USA

ⁱ University of Florida, 100 Rhines Hall, PO Box 116400, Gainesville, FL 32611, USA

ARTICLE INFO

Article history:

Received 16 November 2017

Received in revised form 29 June 2018

Accepted 8 July 2018

Keywords:

Self-healing

Thermodynamics

Design

Metal-matrix composite

Shape-memory alloy

ABSTRACT

Self-healing materials represent a paradigm shift from traditional materials development, enabling intrinsic repair of functionality (such as strength) after a catastrophic failure as opposed to part replacement. Several healing mechanisms have been demonstrated in polymeric and ceramic materials, but few in metallic systems. This study demonstrates a **novel liquid-assisted self-healing metal-matrix composite (MMC)** designed to be capable of over 90% strength recovery after a healing cycle. The aluminum (Al)-based matrix is reinforced with continuous nickel-titanium (NiTi) shape-memory alloy (SMA) reinforcements. Using a tailored heat treatment for healing, a paired effect of crack closure from the SMA reinforcement and partial liquefaction of the matrix occurs. These effects result in a compressive force across the crack surface, and, coupled with increased diffusion rates from the liquefied matrix, produces consolidation and healing in the composite structure. This work provides experimental and computational evidence for the healing mechanism under both tensile and fatigue conditions.

© 2018 The Authors. Published by Elsevier Ltd. This is an open access article under the CC BY license (<http://creativecommons.org/licenses/by/4.0/>).

1. Introduction

Self-healing materials can be considered biomimetic, replicating the way biological systems are able to restore functionality after a catastrophic failure. While self-healing polymers and ceramics have been described extensively in the literature, the development of self-healing metallic systems has been inhibited by several factors: increased healing activation energy, small atomic volume for crack filling, and slow diffusion rates when healing using solid-state mechanisms [1]. Despite these difficulties, there is a need for materials that have self-healing capability with higher strength and toughness in structural applications where metals are traditionally used. A structural self-healing metal would be particularly advantageous in applications where part replacement is difficult or impossible. Other applications include components that are challenged by infrequent service, require high reliability, or operate in

remote conditions. Self-healing MMCs with the ability to repeatedly heal could also benefit traditional applications where the higher initial cost of a material would be offset by decreased repair costs over time.

Only a few mechanisms of self-healing in metals have been proposed, with liquid-assisted healing considered a prime candidate for recovery from large-scale material failure. This mechanism is based on a thermodynamics-driven design methodology first described by Olson [2–4], and consists of a metallic matrix reinforced by longitudinal shape memory alloy (SMA) wires to form a composite. This matrix is designed to possess semi-solid character at elevated temperatures, allowing the material to form a liquid phase that facilitates healing.

The damage and healing cycle of the self-healing composite involves careful interaction between the metallic matrix and SMA reinforcement with temperature, as illustrated in Fig. 1. After damage occurs and a crack propagates through the MMC, load is transferred from the matrix alloy to the crack-bridging SMA reinforcement. These reinforcements remain intact while accommodating strain due to their shape memory effect [5]. To recover

* Corresponding author.

E-mail address: mmanuel@mse.ufl.edu (M.V. Manuel).

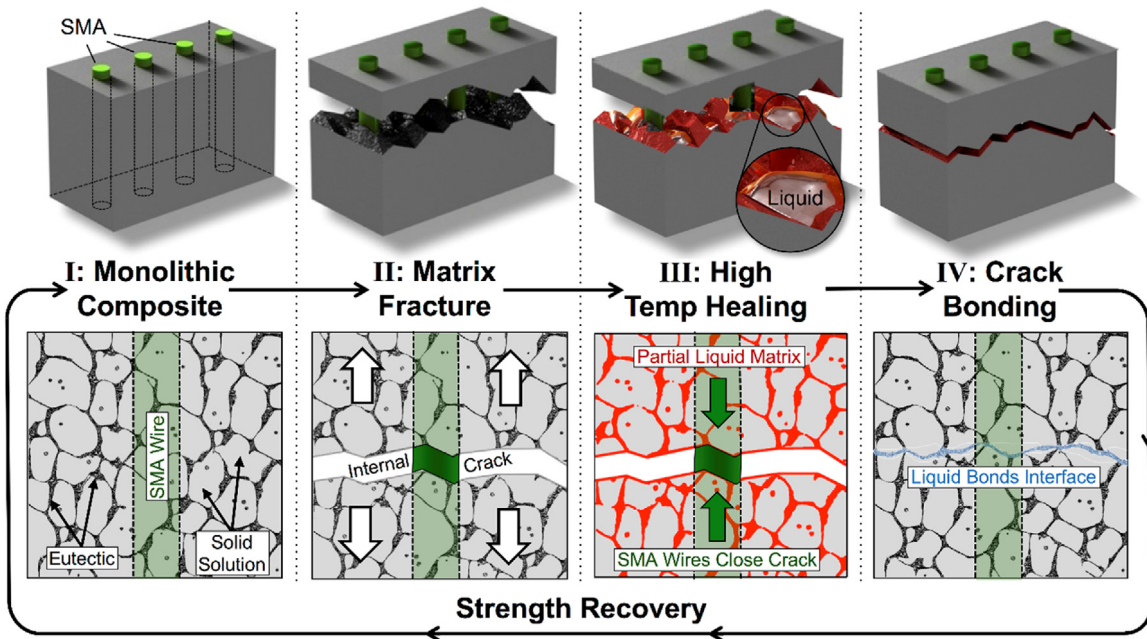


Fig. 1. The healing cycle for liquid-assisted self-healing metal-matrix composites. The system consists of a metallic matrix with a eutectic micro-constituent shown in black and reinforcing SMA wires shown in green (I). After catastrophic failure, the SMA wires deform to bridge the crack (II). To heal the sample, a high temperature healing treatment is initiated, during which the eutectic component melts and SMA wires close the crack (III). During cooling, the eutectic component freezes, welding the crack surfaces and eliminating the crack (IV). (For interpretation of the references to color in this figure legend, the reader is referred to the web version of the article.)

the damage, the MMC is heated above the SMA's austenite start (A_s) temperature. This initiates shape recovery of the SMA, pulling the crack together as the SMA reinforcements return to their initial length. Concurrently, the increased temperature causes softening and liquefaction of the eutectic micro-constituent in the matrix, which enables the recovery of plastic strain in the matrix as well as crack filling. Combined with the crack closure force provided by the SMA reinforcement completely reverting to their original length, the MMC welds itself together and, upon cooling, results in a solidified composite able to realize its pre-cracked, original strength.

2. Self-healing MMC design

To demonstrate the self-healing effect in a structural alloy, the aluminum–silicon (Al–Si) system was used as the matrix. Si additions to Al decrease eutectic temperature and provide increased castability [6], while the eutectic microstructure of the Al–Si enables reliable equilibrium partial-liquid heat treatment. Alloys with a Si content below 3 wt% Si additions are prone to hot-shortness during casting [7], so an Al–3 at.% Si (3.1 wt% Si) was selected. Using the PANDAT thermodynamic software system [8], a temperature of 592 °C for Al–3Si was calculated to yield 20% liquid and 80% solid, a combination which has been found to maintain structural stability throughout an elevated temperature healing cycle while possessing enough liquid phase to enable healing [9,10].

3. Tensile strength recovery

To fabricate the composite for tension experiments, liquid Al–3Si was cast over continuous NiTi SMA wire reinforcements into a dog bone shaped graphite mold. Each composite had three parallel SMA wires along the tensile axis, resulting in 2 vol% SMA reinforcement. Subsequently, each specimen was heat treated at the healing temperature (592 °C) for 24 h to stabilize the microstructure, then mechanically tested in tension. Tensile tests of three individual composite specimens resulted in average values of 39.4 MPa

for 0.2% offset yield strength (σ_y), 93.6 MPa for ultimate tensile strength (UTS), and 3.9% for strain to failure. After inducing matrix failure, each specimen was put through the 592 °C, 24 h healing cycle and tested again in tension. Post-healing, the composites possessed an average strength recovery of 91.6% compared to the initial test (see Healing efficiency model in Section 7). Fig. 2A shows before and after healing mechanical testing data, with corresponding optical images of the fractured area within each tensile specimen. It should be noted that all cracks extended through the entire cross-section of each composite specimen. A representative video of the healing heat-treatment for an Al–3Si matrix reinforced with 2 vol% NiTi SMA wires, showing both shape recovery and partial matrix liquefaction to enable healing, is presented as Movie S1.

Fig. 2B is a schematic of how each composite constituent component behaves prior to failure. Since the reinforcement is in the form of longitudinal fibers, strain is assumed to be equivalent between the Al–3Si matrix and SMA reinforcement before cracks form in the matrix. Since the SMA deforms by detwinning to the same strain as when the matrix fails and cracks, these quantities are nearly equivalent. Thus, in the absence of wire prestrain, a certain amount of matrix plasticity is required for the crack to be clamped by the SMA wires. Conversely, the matrix should not be more ductile than the recoverable strain of the SMA. A highly plastic matrix would strain the SMA reinforcement beyond its recoverable strain, reducing shape recovery capability. These results show that extensive damage can be reversed in a structural materials system given a compatible mechanical response between the matrix and reinforcement.

4. Computational simulation of crack closure

To gain more insight into the mechanics of crack closure and healing, a finite element (FE) approach [11] was used with the post-crack condition as a starting point. The initial conditions of the model are as follows. First, the SMA reinforcements are given a 6% pre-strain, which is elongation of the SMA prior to matrix cracking (due to matrix plasticity). The reinforcements were fixed to the

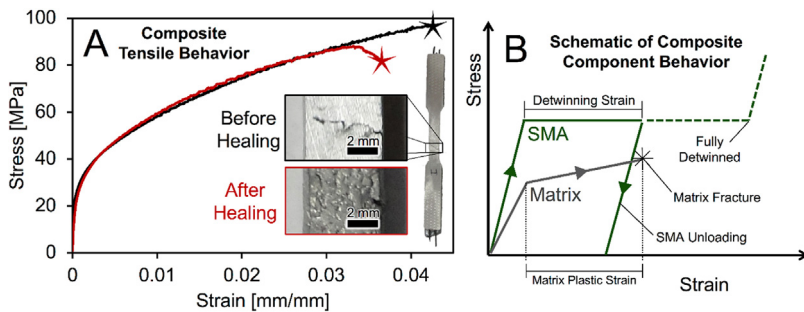


Fig. 2. (A) Mechanical test information for an Al-3Si/SMA longitudinally-reinforced composite. Note the inset macro-images correspond to the before and after healing heat treatment of a crack along the dog bone-shaped specimen. (B) Schematic of constituent component (SMA reinforcement and matrix) mechanical behavior internal stress as a function of applied strain. Note that plastic strain in the matrix and detwinning strain in the SMA reinforcement before failure are roughly equivalent.

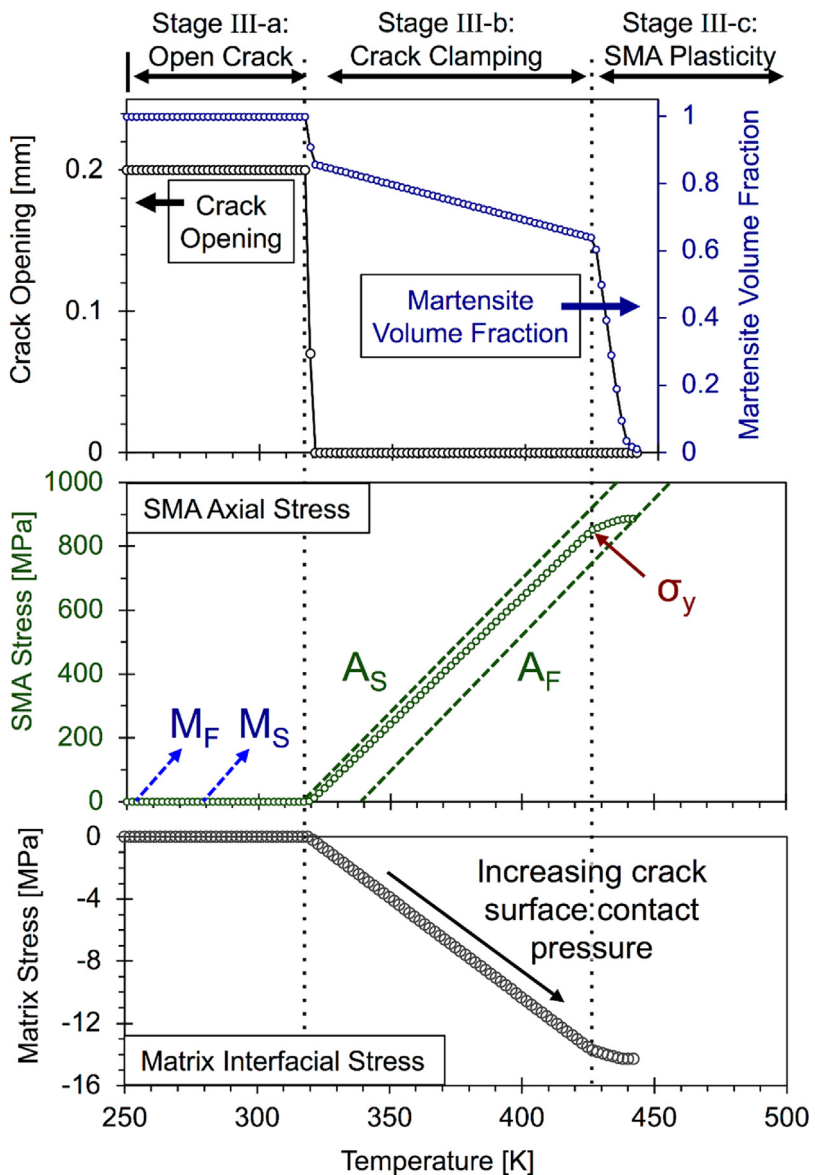


Fig. 3. Finite element simulation of the crack closure process (Stage III from Fig. 1) as a function of temperature, with crack opening, martensite volume fraction, and SMA and Al-3Si matrix stress displayed. As the sample is heated, an austenitic phase transformation in the wires closes the crack and initiates crack surface contact pressure that increases with temperature. Note that the stress in the SMA is tensile (positive) and the stress on the matrix interface is compressive (negative).

Al-3Si matrix at both ends (i.e., axial displacement at each composite end is uniform), while otherwise fully debonded along the length of the reinforcement. Lastly, the initial gap is set at 0.2 mm in the center of the 30 mm long matrix, equivalent to the cracks

exhibited by the experimental tension specimens. The composite responded to heating in three stages of behavior, as shown in Fig. 3. In the figure, M_S , M_F , A_S , A_F , and σ_y represent the SMA martensite and austenite start and finish temperatures and yield stress,

respectively. In Stage III-a, from 250 K to 318 K (-23°C to 45°C), no movement occurs. In Stage III-b, the SMA begins to transform from martensite to austenite and quickly closes the gap in the matrix. As temperature is further increased, more martensite transforms and the stress in the SMA reinforcement increases, illustrating the crack clamping mechanism. Note that the transformation temperatures are a function of stress. In Stage III-c, the SMA reaches the temperature dependent yield stress and begins to accommodate strain by slip, and the transformation to austenite completes. The transformation of the matrix to partial liquid above the eutectic temperature of 850 K (577°C) is not included in the model, but the remaining clamping force ensures that the interface would remain in contact to bond effectively.

This modeling effort illustrates the need for pre-strained SMA reinforcements to enable crack closure and healing in the MMC through a crack clamping mechanism. Without the pre-strain in the SMA reinforcements, the sample would experience crack closure but no crack clamping force (as illustrated by the increase in the crack surface contact pressure in Fig. 3). The compressive force helps to ensure adequate contact between the crack faces and facilitates healing efficacy. Overall, investigations found the elevated temperature compressive strength of the matrix, the bond strength between the matrix and SMA reinforcements, and the ductility of the composite material play a major role in determining self-healing capabilities as these factors affect the amount of strain imparted on the SMA reinforcements and directly relates to the recovery force during healing.

5. Fatigue life recovery

In Al alloys, especially for aerospace and space applications, material failure is most likely to occur from fatigue [12]. Therefore, to investigate the healing mechanism in a more representative

failure condition, fatigue testing was conducted on Al-3Si reinforced with NiTi SMA reinforcements using middle tension [M(T)] fatigue crack growth rate tests. The results from M(T) fatigue testing can be seen in Fig. 4. On the scale in Fig. 4B and C, 0 mm represents the center of the sample and 12 mm represents the outer edge. In all four tests, the crack length decreased as a result of the healing cycle, as the matrix bonded to itself, and the crack growth rate decreased after healing. The micrographs in Fig. 4D–G show that upon initial testing, cracking propagates mostly intergranular, following the eutectic regions (matching the failure path seen in tensile testing), while after healing the crack path becomes more tortuous. Since the preferential crack propagation path in Al-3Si is along the brittle eutectic, microstructural modification, such as morphology changes and growth, during the healing treatment redirects the crack path and thus the sample exhibits a toughening behavior. These early tests indicate that, in addition to the strength recovery after catastrophic failure previously discussed, the healing cycle is also effective at repairing fatigue damage and thus may be beneficial in extending fatigue life.

6. Conclusion and future work

These initial investigations into an Al-3Si matrix reinforced with 2 vol% NiTi SMA wires resulted in 91.6% healing efficiency on average under tensile conditions, and showed promise for healing fatigue cracks. While the overall strength of the tested MMCs is below industry standards for cast aluminum alloys, the methodology of liquid-assisted self-healing MMC design is applicable to other metallic systems outside of Al-Si. Any system exhibiting a solid + liquid region at a temperature which will not adversely affect the thermal properties of SMA wires has self-healing potential. Future designs will seek to improve strength to that of

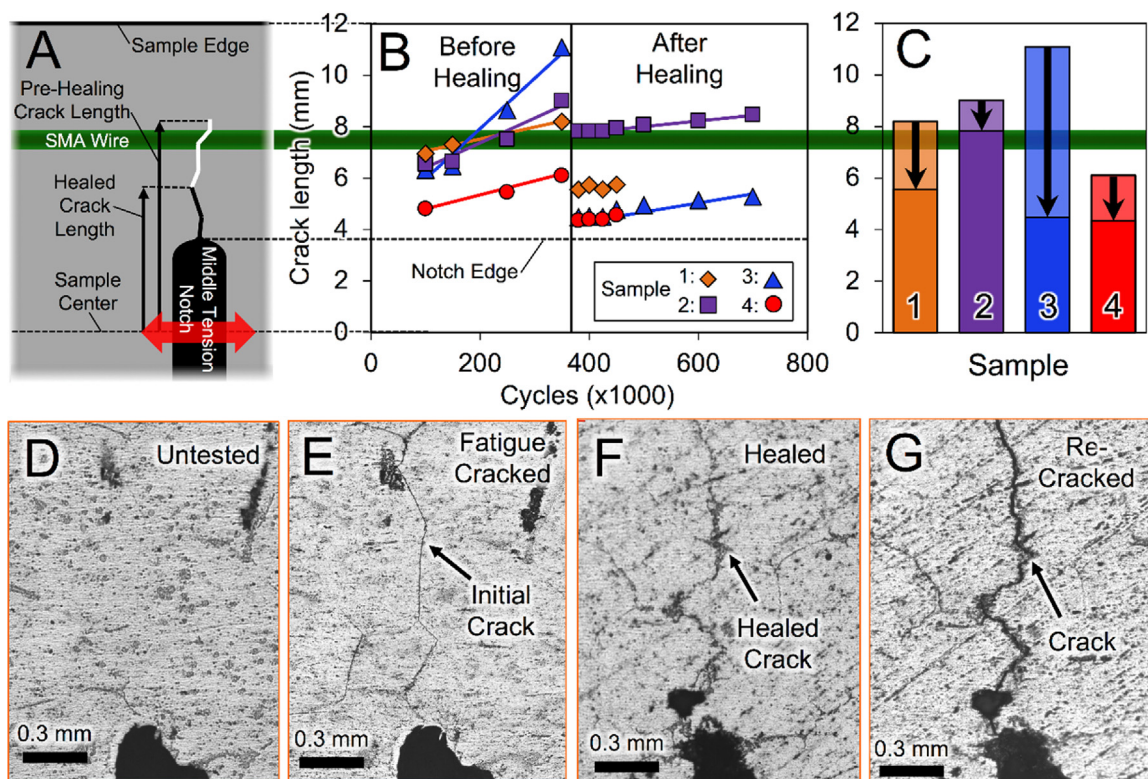


Fig. 4. (A) Schematic of area of interest in the M(T) notch specimens, (B) fatigue data showing decreased crack growth rate relative the location of the embedded SMA reinforcement, (C) crack length before and after healing. Micrographs of a (D) untested specimen, (E) post-fatigue cracking, (F) post-healing, and (G) after a second M(T) fatigue test.

commercial Al alloys while maintaining the high healing efficiency found in the Al–Si composite system. These structural materials could be incorporated into a number of technologies in the future, where functionality can be restored after a loss of mechanical integrity.

7. Experimental

7.1. Preparation of composite

A master alloy was prepared by melting Al (shot, 99.99%, Alfa Aesar) and Si (lump, 99.9999%, Alfa Aesar) at 850 °C until a liquid solution and casting into a graphite mold. Appropriate amounts of this master alloy and Al to obtain an Al-3 at.% Si alloy were melted at 750 °C until a liquid solution. A graphite mold coated with boron-nitride with custom designed ends to hold wires was heated to 350 °C with the NiTi wires (Ni-49.3 at.% Ti, Ø = 0.87 mm, Memry Corporation) already aligned. The Al–Si melt was poured over the NiTi wires and allowed to cool. The composite was heat-treated at 592 °C for 24 h to set the post-heal microstructure. The matrix composition was confirmed via inductively coupled plasma atomic emission spectroscopy (ICP-AES). Each healing cycle was performed by vacuum encapsulating the composite in a Pyrex tube and heat-treating at 592 °C for 24 h.

7.2. Tensile testing

Specimens were fabricated according to the sub-size tensile specimen dimensions in ASTM E8M: Standard Test Methods for Tension Testing of Metallic Materials [13]. Tensile testing was completed on an Instron 5582 mechanical testing machine at a strain rate of 1.0%/min. Strain was measured with an extensometer (Model 3542, Epsilon Technology Corporation) attached to the gauge area.

7.3. Fatigue testing

Four middle tension [M(T)] fatigue crack growth rate specimens were fabricated with geometry based on ASTM E647: Standard Test Method for Measurement of Fatigue Crack Growth Rates [14]. Fatigue testing was completed on an MTS 321.12 hydraulic load frame in strain control, with maximum stress of 80% yield strength (32 MPa), stress ratio $R=0.1$, and frequency of 80 Hz. Pre-cracks were initiated at a central machined notch and all tests were halted at 350,000 cycles. Subsequently, each M(T) specimens underwent a healing cycle of 24 h at 592 °C before being re-tested. Crack size was measured optically from the center of each M(T) specimen.

7.4. Healing efficiency model

The healing efficiency of a composite was determined by comparing the ultimate tensile strength (UTS) of the virgin composite against the post-heal UTS of the same specimen via the following Eq. (1):

$$\frac{UTS_{virgin}}{UTS_{healed}} \times 100\% = \% \text{ Healed} \quad (1)$$

Supporting information

Supplementary Movie S1 of the healing during heat-treatment is available.

Acknowledgements

The authors would like to thank our funding partners at the Florida Space Grant Research program (NNX10AM01H), National Science Foundation (CMMI-0824352) and the National Aeronautics and Space Administration (NNX12AQ42G, NNX13AR53A, and NNX12AP71A).

Appendix A. Supplementary data

Supplementary data associated with this article can be found, in the online version, at [doi:10.1016/j.apmt.2018.07.003](https://doi.org/10.1016/j.apmt.2018.07.003).

References

- [1] S. Van der Zwaag, N.H. van Dijk, H.M. Jonkers, S.D. Mookhoek, W.G. Sloof, Self-healing behaviour in man-made engineering materials: bioinspired but taking into account their intrinsic character, *Philos. Trans. R. Soc. A* 367 (2009) 1689–1704.
- [2] G.B. Olson, Computational design of hierarchically structured materials, *Science* 277 (1997) 1237–1242.
- [3] G.B. Olson, Designing a new material world, *Science* 288 (2000) 993–998.
- [4] G.B. Olson, Beyond discovery: design for a new material world, *CALPHAD* 25 (2001) 175–190.
- [5] C.M. Wayman, T.W. Duerig, An introduction to martensite and shape memory, in: T.W. Duerig, K.N. Melton, D. Stockel, C.M. Wayman (Eds.), *Engineering Aspects of Shape Memory Alloys*, Butterworth-Heinemann, United Kingdom, 1990, pp. 3–20.
- [6] A.M. Russell, K.L. Lee, *Structure–Property Relations in Nonferrous Metals*, John Wiley and Sons, Inc., New Jersey, 2005.
- [7] P.H. Jennings, A.R.E. Singer, W.I. Pumphrey, Hot-shortness of some high-purity alloys in the systems Al–Cu–Si and Al–Mg–Si, *J. Am. Inst. Met.* 74 (1948) 227–248.
- [8] S.L. Chen, F. Zhang, S. Daniel, F.Y. Xie, X.Y. Yan, Y.A. Chang, R. Schmid-Fetzer, W.A. Oates, Calculating phase diagrams using Pandat and PanEngine, *J. Mater.* 53 (2003) 48–51.
- [9] M.V. Manuel, Principles of self-healing in metals and alloys: an introduction, in: S.K. Ghosh (Ed.), *Self-Healing Materials: Fundamentals, Design Strategies, and Applications*, Wiley-VCH, Weinheim, Germany, 2009.
- [10] M.V. Manuel, G.B. Olson, Biologically inspired self-healing metals, in: N. aan Zee (Ed.), *Proc. 2nd Int. Conf. on Self-Healing Mater.*, Springer, New York, 2009.
- [11] P. Zhu, Z. Cui, M.S. Kesler, J.A. Newman, M.V. Manuel, M.C. Wright, L.C. Brinson, Characterization and modeling of three-dimensional self-healing shape memory alloy-reinforced metal-matrix composites, *Mech. Mater.* 103 (2016).
- [12] R.J. Wanhill, Fatigue crack initiation in aerospace aluminum alloys, components, and structures, in: N. aan Zee (Ed.), *Proc. 1st Int. Conf. on Self-Healing Mater.*, Springer, New York, 2007.
- [13] ASTM E8M-04, 2004, Standard Test Methods for Tension Testing of Metallic Materials [Metric], ASTM International, West Conshohocken, PA, 2004 www.astm.org.
- [14] ASTM E647-15e1, Standard Test Method for Measurement of Fatigue Crack Growth Rates, ASTM International, West Conshohocken, PA, 2015 www.astm.org.